universität wien

DISSERTATION

Titel der Dissertation

Functional Analysis of Conserved Motifs in Two Mg^{2+} Transporting Channels: ScMrs2p and TmCorA

Verfasserin

Mag. Soňa Svidová

angestrebter akademischer Grad

Doktorin der Naturwissenschaften (Dr.rer.nat.)

Wien, 2011

Studienkennzahl lt. Studienblatt:	A 091 441
Dissertationsgebiet lt. Studienblatt:	Genetik/Mikrobiologie
Betreuerin / Betreuer:	Prof. Dr. Kristina Djinovic-Carugo

Table of contents

1.1. Summary

Thermotoga maritima CorA and *Saccharomyces cerevisiae* Mrs2 proteins are members of a large CorA/Mrs2/Alr1 protein superfamily of Mg^{2+} uptake systems. The conservation of the primary sequence in this family is relatively low, with the exception of the characteristic Y/F-G-M-N signature motive or presence of bulky hydrophobic amino acids in the predicted gate region of both proteins. In order to investigate the role of these conserved sequences, I present mutational studies of the Leu294 residue in the gate region of TmCorA and the highly conserved G-M-N motive of ScMrs2.

The Leu294 residue in the cytoplasmic neck of the TmCorA is considered to be the main gate for Mg^{2+} transport. I created three mutations at this position: aspartic acid, glycine and arginine. In the Leu294Asp and Leu294Gly mutant I observed a defect in the closing of the pore. In the Leu294Arg mutant not just the gating, but also the regulation of Mg^{2+} uptake was affected. These results confirmed the importance of the Leu294 for gating of Mg^{2+} transport and also show the influence of the charge and structural features of the amino acids on the gating mechanism.

The G-M-N motive at the end of the first transmembrane of ScMrs2 was considered to be essential for the protein function and already a single mutation in this region completely abolished Mg^{2+} transport.

I performed random mutagenesis of all three amino acids at once and obtained a considerable amount of mutants, which retained different levels of Mg^{2+} transport activity, in all cases significantly lower then in the wild-type ScMrs2. Sequence analysis showed the highest Mg^{2+} uptake levels in case of a hydrophilic amino acid on the first position, and a hydrophobic amino acid on position 3 and vice versa. Further analysis of the mutants showed changed ion selectivity to Mn^{2+} and Zn^{2+}, caused probably by blockage of the channel. From these we can conclude, that the G-M-N motif is important, but not essential for the ScMRS2 mediated Mg^{2+} uptake and it seems to be part of the ion selectivity filter.

1.2. Zusammenfassung

Thermotoga maritima Cora und *Saccharomyces cerevisiae* Mrs2 Proteine sind Mitglieder einer großen CorA/Mrs2/Alr1 Protein Superfamilie der Mg^{2+} Transport-Systeme. Die Konservierung der primären Sequenz in dieser Familie ist relativ gering, mit Ausnahme des Y / F-G-M-N Motivs oder der großen hydrophoben Aminosäuren in dem vermutlichen Gate-Bereich beider Proteine. Um die Rolle dieser konservierten Sequenzen zu untersuchen, präsentiere ich Mutationsstudien des Leucines 294 im Gate-Bereich von TmCorA und des hoch konservierten G-M-N Motivs von ScMrs2.

Das Leu294 im Grenzbereich zwischen Membrane und Cytoplasma im TmCorA Protein gilt als Gate für Mg^{2+} Transport. Ich habe drei Mutationen an dieser Position geschaffen: Asparaginsäure, Glycin und Arginin. In der Leu294Asp und Leu294Gly Mutante beobachtete ich einen Defekt in der Schließung der Pore. In der Leu294Arg Mutante war nicht nur das Gating, sondern auch die Regulation des Mg^{2+}-Transportes betroffen. Diese Ergebnisse bestätigen die Bedeutung der Leu294 fürs Gating von Mg^{2+} Transport und zeigen auch den Einfluss von der Ladung und von den strukturellen Eigenschaften der Aminosäuren auf den Gating-Mechanismus. Das G-M-N Motiv am Ende der ersten Transmembrandomäne des ScMrs2 galt für die Funktion des Proteins als notwendig und bereits eine einzige Mutation in dieser Region schaffte den Mg^{2+}-Transport völlig ab. Ich führte Random-mutagenese aller drei Aminosäuren auf einmal durch und erhielt eine beträchtliche Menge an Mutanten, die unterschiedliche Mg^{2+}-Transportaktivität aufwiesen, in allen Fällen geringer als in dem Wildtyp-ScMrs2. Die Sequenzanalyse zeigte die höchste Mg^{2+} Transportaktivität im Falle einer hydrophilen Aminosäur auf der ersten Position, und einer hydrophoben Aminosäure an Position 3 und umgekehrt. Die weitere Analyse der Mutanten zeigte veränderte Ionen Selektivität zu Mn^{2+} und Zn^{2+}, verursacht wahrscheinlich durchs Blocken des Kanals. Aus diesen Ergebnissen schließe ich, dass das G-M-N Motiv wichtig, aber nicht notwendig, für den ScMRS2 vermittelten Mg^{2+}-Transport, und es scheint ein Teil des Ionen-Selektivitätsfilter zu sein.

2. Introduction

2.1. The chemical and biological importance of magnesium

Magnesium is the most abundant divalent cation within the cells. It plays an important role in many metabolic processes. Mg^{2+} acts as cofactor for hundreds of enzymes, influences DNA and protein synthesis, in mitochondria, it is a key factor fot ATP synthesis, it is important as signaling molecule, by binding to RNAs and many proteins it also contributes to establishing and maintaining physiological structures, stabilizing membranes and active conformations of macromolecules, it modulates membrane transport of other ions (like Ca^{2+}, Na^{+}, K^{+}) and intracellular Mg^{2+} concentration has an inverse correlation with blood pressure (Gunther, 1993; Huang, et al., 1995; Maguire and Cowan, 2002; Romani, 2007; Romani and Scarpa, 1992; Sperrazza and Spremulli, 1983; Sternberg, et al., 1995; Touyz, 2006; Whelton and Klag, 1989).

Cellular Mg^{2+} concentrations are in the millimolar range (~15 to 20 mM) (Beeler, et al., 1997; Beeler, et al., 1994; Graschopf, et al., 2001; Romani and Scarpa, 1992). The majority of Mg^{2+} in the cell is bound to ligands, there is only a small fraction of up to 5% left in a free ionized state (Romani and Scarpa, 1992; Romani and Scarpa, 2000).

Magnesium has the smallest ionic radius (0.65 Å) among the major biological cations but at the same time the largest hydration radius (4.76 Å), which means a 400-fold change in the volume between these two states, whereas for example in the case of potassium the volume changes only 4-fold (Moomaw and Maguire, 2010). This, coupled with the slower exchange rate of solvent waters around the hydrated Mg^{2+}, means difficulties of binding of these cation to proteins and other biological molecules. For example, an Mg^{2+} transport protein must first recognize the hydrated cation, interact with it, be able to remove the hydration shell and pass the dehydrated ion into the transport pathway across the membrane. This procedure is probably the same for all cation transporters, but in the case of an Mg^{2+} transporter this task is far harder than for the other cation transport systems because of the big volume change and relatively strong interactions of Mg^{2+} with the water molecules of the hydration shell (Maguire and Cowan, 2002). The coordination number and solvent exchange rate for Mg^{2+} may also determine its biochemical functions. Mg^{2+} is invariably hexacoordinated - six water

molecules are required to complete the hydration sphere, whereas Ca^{2+} is more promiscuous and can adopt 6, 7, or 8 coordinate bonding arrangements. The coordination sphere of Mg^{2+} is much more constrained than the one of Ca^{2+} (Maguire and Cowan, 2002).

Interactions of magnesium with its interaction partners can take place through the water shell (outer-sphere chemistry) or with the cation itself (inner-sphere-chemistry).

Interaction with enzymes and other proteins can be mediated by inner or outer sphere coordination to alter the conformation of enzymes or the participation in the chemistry of the catalytic reaction. However, since magnesium binds its water shell much stronger than other ions, it is probably rarely fully dehydrated during binding with the ligand. This means that a potential water molecule associated with magnesium can be more important for the reactions than the ion itself.

2.2. Magnesium transport systems

Cellular Mg^{2+} homeostasis involves systems facilitating influx and others that mediate extrusion of the ion. The channel forming proteins, or associated proteins, limit ion fluxes by opening or closing the channels and keep the intracellular or intra-organellar concentrations within ranges required for physiological processes.

Mg^{2+} influx is an electrogenic process driven by the inside negative membrane potential. Using various genetic approaches, two classes of cellular Mg^{2+} channel proteins have been identified and characterized: the large heterogeneous CorA/Mrs2/Alr1 protein superfamily, found in prokaryotes, eukaryotic organisms, as well as plants (Gardner, 2003; Graschopf, et al., 2001; Knoop, et al., 2005; Kolisek, et al., 2003; Wachek, et al., 2006; Weghuber, et al., 2006) and the TRPM6 / TRPM7 family of the mammalian plasma membrane (Schlingmann and Gudermann, 2005; Schmitz, et al., 2003). CorA/Mrs2/Alr1 protein superfamily members are high-affinity Mg^{2+} uptake systems enabling growth of the cells even in very low external Mg^{2+}concentrations. Mutants lacking these systems can not survive without being provided with high external Mg^{2+} concentrations.

Extrusion of Mg^{2+} occurs against the electrochemical gradient. It is mediated by exchange against H^+, Na^+, or other ions and driven by their inside-directed gradients (Dai, et al., 2001; Romani and Scarpa, 2000).

2.2.1. Magnesium transport in Bacteria

The first genes involved in Mg^{2+} transport in bacteria were reported by Smith and Maguire in 1998. In Prokaryotes there are three classes of proteins mediating magnesium transport: CorA, MgtA/B and MgtE. CorA and MgtE are widespread amongst both Eubacteria and Archaea, the MgtA/B type is found primarily in Eubacteria (Maguire, 2006).

CorA - the major Mg^{2+} uptake system in E. coli and S. thyphimurium

The CorA system is the major magnesium uptake system in *E. coli* and *S. thyphimurium.* Previous investigations showed that it is essential for bacterial growth (Webb, 1966) but standard rich media provide sufficient magnesium concentrations for growth (Smith and Maguire, 1998). CorA was primarily identified by its ability to mediate the influx of Co^{2+}, which is toxic for the cells at high concentrations. The CorA gene encodes a constitutively expressed 37 kDa integral membrane protein (Smith, et al., 1993) and is widely distributed amongst Eubacteria and Archaea. The sequence homologies rang from 98% between the *E. coli* CorA and that of *S. thyphimurium* to 15-20% between more distantly related species (Kehres, et al., 1998).

Table 1 lists the transport kinetics of the CorA Mg^{2+} transport system (Gibson, et al., 1991; Hmiel, et al., 1986; Snavely, et al., 1989).

	Mg^{2+}	**Co^{2+}**	**Ni^{2+}**
K_m (µM)	15	30	240
V_{max} (pmol/min/10^8 cells	250	500	360

CorA also mediates influx of Ni^{2+} and Co^{2+} (Grubbs, et al., 1989; Smith, et al., 1993; Snavely, et al., 1989), but uptake of these ions under physiological conditions is very unlikely as the K_a values (see Table I) are in a range where concentrations would be already toxic for bacteria.

Transport activity of the CorA protein can be selectively inhibited by cation hexaamines that imitate the fully hydrated Mg^{2+} cation (Kucharski, et al., 2000). This could be the evidence for the hypothesis that initial interaction with the transporter occurs with a fully hydrated magnesium ion, which is then dehydrated to pass through the pore and afterwards hydrated again. This hypothesis is supported by the results of a mutational analysis done by Moomaw and Maguire, which suggest that the initial interaction takes place between the extracellular loop of CorA and a hydrated Mg^{2+} cation (Moomaw and Maguire, 2010).

The CorA - mediated ion flux is driven by the inside negative membrane potential and in physiological terms therefore constitutes a uniport (Froschauer, et al., 2004; Smith and Maguire, 1998; Szegedy and Maguire, 1999).

In the last years three crystal structures of *Thermotoga maritima* CorA have been published (Eshaghi, et al., 2006; Lunin, et al., 2006; Payandeh and Pai, 2006). All showed that the transporter exists in a pentameric form and consists of a cytosolic funnel shaped part, linked to the transmembrane region by long α7 helices (stalk helices) (Fig. 1a, b).

The big cytosolic part of each monomer is built by a seven-stranded parallel, antiparallel ß-sheet (ß 1-7) sandwiched between two sets of α-helices (α1, α2, α3 and α4, α5, α6). The pore is formed by the trans-membrane part of the α7 helices, which connect the cytosolic part with the membrane, and surrounded by the α8 trans-membrane helices (the second transmembrane helices), which anchor the complex in the membrane and end in a highly conserved positively charged motif (KKKKWL) called “basic sphincter”).

The α7 helix includes the highly conserved ^{311}Y-G-M-N-F^{315} signature sequence at its end (Kehres, et al., 1998). This sequence, virtually found in all CorA homologues, was considered to be essential for the transport function and even conservative single mutations at these positions were not tolerated and resulted in almost complete loss of transport activity. The main-chain carbonyls of the Y-G-M-N motif are exposed into the central part of the pore entrance on the periplasmic side and are probably part of a polar strip suited for interacting with cations (Eshaghi, et al., 2006). Lunin et al. proposed that the ring of five Asn314 side chains of the G-M-N motif periplasmic entrance of the pore blocks ion movement and plays a role in the initial dehydration of the Mg^{2+} ions. The Asn 314 ring appears to be held in conformation by an aromatic stacking interaction between Tyr 311 of one monomer and Phe 315 of an adjacent monomer (Y and F of the conserved YGMNF sequence) (Lunin, et al., 2006). The G-M-N motif has been shown to be critical for protein function, because even

conservative single point mutations completely abolish Mg^{2+} transport (Payandeh, et al., 2008; Szegedy and Maguire, 1999).

TM1 and TM2 are connected by a short extracellular loop of only seven amino acids which immediately follows the YGMNF sequence. This loop always contains significant surplus of negatively charged aminoacids in those CorA family members known to transport Mg^{2+} and is probably responsible for initial binding of the hydrated Mg^{2+} (Lunin, et al., 2006) and acceleration of the dehydration process (Moomaw and Maguire; Moomaw and Maguire, 2010).

In the cytoplasmic neck of the pore a hydrophobic ring is created by residues Leu294 and Met291, surrounded by the aforementioned basic sphincter (Fig. 1c). This concentration of positive charges and the significant conservation of the bulky hydrophobic residues at positions 291 and 294 in the CorA protein family is considered to be of high importance for gating of the transporter. Opening and closing of the gate is regulated by interaction of the Mg^{2+} ion with a divalent cation sensing site (DCS), placed between Asp89 in the α3 helix in the N-terminal part of one monomer and Asp253 of the α7 helix of the adjacent monomer (Eshaghi, et al., 2006; Lunin, et al., 2006; Payandeh and Pai, 2006) (Fig. 1b) and a second potential DCS site, involving residues Glu88 and Asp175, which was identified by Eshaghi et al. (Eshaghi, et al., 2006) and Payandeh et al. (Payandeh and Pai, 2006) (Fig. 1b).

As mentioned above, the cytosolic part is shaped like a funnel. It shows the lowest sequence conservation among CorA transporters. The inner wall of the funnel is lined with rings of negatively charged or hydroxyl-bearing residues. Similar arrangement of charged residues can be found also in other cation channels and may act as an electrostatic sink to increase the local ion concentration (Doyle, et al., 1998).

The predicted secondary structure of CorA orthologues agrees quite well with the crystal structure of the *T. maritima* CorA. This fact allows predicting also the structure of other members of the CorA/Mrs2/Alr1 protein superfamily.

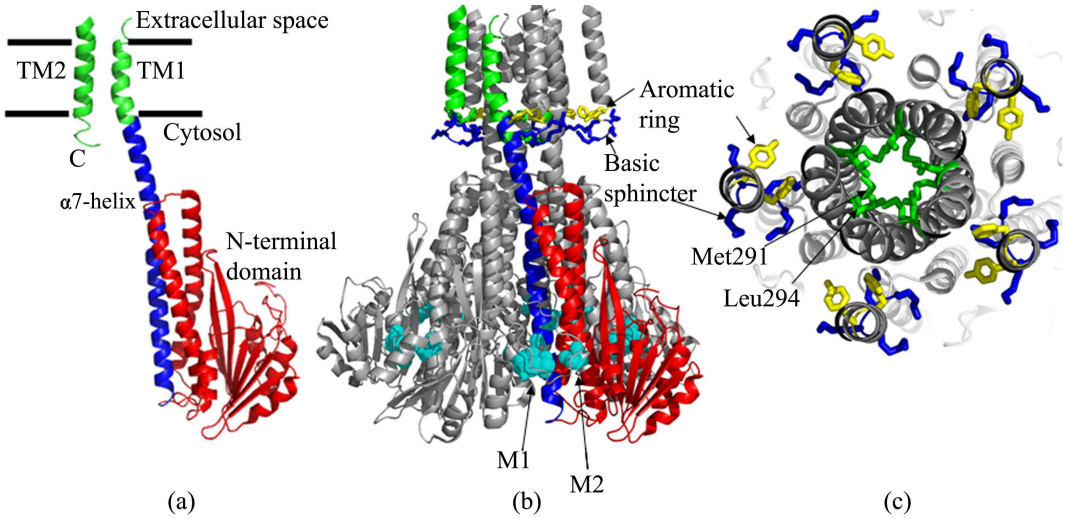

Figure 1.: Structure of the TmCorA Mg^{2+} transporter. (a) single monomer: green - transmembrane domains TM1 and TM2, blue - α7 helix, red - N-terminal domain. (b) side view of the hompentamer: cyan - DCS sites M1 and M2. (c) view from the top: blue - basic sphincter, yellow - aromatic ring, green - the gate forming residues Leu294 and Met291.

2.2.2. Magnesium transport in yeast

Genetic screens led to the identification of two distant homologues of the CorA protein in the yeast *Saccharomyces cerevisiae*, Alr1p (MacDiarmid and Gardner, 1998) and Mrs2p (Bui *et al*., 1999). The ScAlr1p forms the major pore for Mg^{2+} influx in the plasma membrane (Graschopf *et al*., 2001) and ScMrs2p is located in the inner membrane of the mitochondria. While Alr1p related proteins are restricted to lower eukaryotes, Mrs2p related proteins are present by nearly all eukaryotic genomes sequenced up today. Homologues of Mrs2p are found in mitochondria of yeast and plants as well as of mammalia. In plants Mrs2-related proteins not only found in mitochondria, but also in plasma, chloroplast and mitochondrial membranes (Gebert, et al., 2009; Schock, et al., 2000).

The sequence variation within the CorA-Mrs2-Alr1 protein superfamily is very high. The only common features are the presence of two predicted transmembrane (TM) domains near the C-terminus, which are separated by a short loop preceded by a F/Y-G-M-N motif at the end of first TM domain. The long N- and short C-terminal sequences of the CorA, Mrs2 and Alr1 subfamilies are variable in size and have no conserved sequence motifs were found. The conclusion that members of these subfamilies are functional orthologs is based on the fact, that CorA, Mrs2 and Alr1 mediate influx of Mg^{2+} into cells or mitochondria (Smith and Maguire, 1998; Liu *et al*., 2002; Kolisek *et al*., 2003), that CorA can partially substitute for

either Mrs2 or for Alr1 when expressed in yeast (Bui *et al*., 1999; Graschopf *et al*., 2001) and Mrs2 can substitute for CorA when expressed in *Salmonella typhimurium* (Svidova, et al., 2011).

Bacterial CorA as well as yeast Mrs2 and Alr1 has been shown to form homo-oligomeric (tetra- or pentameric) complexes in the membranes (Kolisek, et al., 2003; Sponder, et al., 2010; Warren, et al., 2004).

ScMrs2p mediates Mg^{2+} uptake into mitochondria

The *Saccharomyces cerevisiae MRS2* encodes an integral protein of the inner mitochondrial membrane with a molecular weight of 54 kDa. The gene was originally identified as suppressor of group II intron RNA splicing defects (Koll, et al., 1987). Group II introns are magnesium dependent ribozymes catalyzing a splicing (Ostersetzer, et al., 2005) and Mrs2p was found to be a magnesium selective channel responsible for maintaining proper Mg^{2+} levels in mitochondria (Gregan, et al., 2001b).

Yeast cells lacking *MRS2* are respiratory deficient but viable, when provided with fermentable substrates. They exhibit a growth defect on non-fermentable substrates (so called petite phenotype).

ScMrs2p is a distant relative of the bacterial Mg^{2+} transporter CorA. This transporter family exhibits virtually no conservation regarding the primary sequence (Gardner, 2003; Knoop, et al., 2005) with the exception of the characteristic Y/F-G-M-N signature motive, the surplus of negatively charged amino acid in the following loop and presence of bulky hydrophobic amino acids in the predicted gate region. Furthermore, the two trans-membrane domains near the C-terminus and two α-helices in the large N-terminal part (Bui, et al., 1999) are common structural features of these proteins. Studies done in the lab of R.J. Schweyen revealed that Mrs2 plays a role in ion transport into mitochondria and could be functionally replaced by CorA (Bui, et al., 1999) and vice versa.

Mrs2p-mediated Mg^{2+} transport was extensively studied using the Mg^{2+} sensitive, fluorescent dye Mag-Fura 2, where it was shown that ScMrs2p mediates a rapid, highly regulated Mg^{2+} uptake into mitochondria. Basal mitochondrial magnesium concentrations are in a range of 0.5-0.8 mM in yeast cells cultured in standard medium. Isolated mitochondria respond within

seconds to a rise in the external magnesium concentration with a rapid increase of the mitochondrial free Mg^{2+} concentration (150 µM s^{-1}). The driving fore for this Mg^{2+} influx via Mrs2 is the strong (inside negative) membrane potential of –130 to -160 mV (Kolisek, et al., 2003). The high conductance of ~150 pS characterizes Mrs2p as a channel (Kolisek, et al., 2003). ScMrs2p is also able to mediate Ni^{2+} transport, but with a 3.5-fold smaller conductance (~45 pS) than Mg^{2+}, whereas it is not permeable for Ca^{2+}, Mn^{2+} or Co^{2+}. Additionally, suppression of Mg^{2+} currents in the presence of Co^{2+} was observed suggesting Co^{2+} to interact with the pore (Schindl, et al., 2007).

As noted above, the F/Y-G-M-N motif at the C-terminal end of the first transmembrane helix is the signature sequence of the CorA/Mrs2/Alr1 protein superfamily. The G-M-N motif has been shown to be critical for protein function, because even conservative single point mutations completely abolish Mg^{2+} transport. This was confirmed on ScMrs2p (Kolisek, et al., 2003) its yeast homologue ScLpe10p (Sponder, et al., 2010) and its bacterial homologue CorA (Payandeh, et al., 2008; Szegedy and Maguire, 1999) where single mutations of the G-M-N motif were introduced, suggesting that this sequence might be critical for positioning the periplasmic loop, which is probably responsible for initial binding of the hydrated Mg^{2+} (Lunin, et al., 2006) and acceleration of the dehydration process (Moomaw and Maguire, 2010).

ScLpe10p modulates the function of ScMrs2p

The genome of *Saccharomyces cerevisiae* encodes a homologue of Mrs2p, which has 32% sequence identity with the MSR2 gene. It is known as *LPE10*. Furthermore chemical cross-linking experiments (Kolisek, et al., 2003) and blue-native PAGE (Weghuber, unpublished data) provided evidence that Mrs2p is able to form high molecular weight complexes (possibly tetramers or pentamers), which is also consistent with the data obtained from analysis of the CorA crystal structure (Lunin, et al., 2006).

The *LPE10* gene encodes a 47kDa protein with two trans-membrane domains. It posses the Y/F-G-M-N sequence at the end of the first trans-membrane domain which, is a characteristic feature for magnesium transporters of the CorA/Mrs2/Alr1 protein superfamily. Unlike Mrs2p, Lpe10p does not posses an extension of the highly positively charged C-terminal sequence (Gregan, et al., 2001a), which seems to be unique for Mrs2p. Like Mrs2p it is

located in the inner mitochondrial membrane and has been reported to be involved in Mg^{2+} uptake as well, but the mode of action remains undefined (Gregan, et al., 2001a).

Disruption of the *LPE10* gene causes similar phenotype as disruption of *MRS2*: a growth defect on non-fermentable substrates (*petite* phenotype) (Gregan, et al., 2001a), loss of Mg^{2+}influx into mitochondria, comparable to *MRS2* deletion, and in addition a 30% decrease of the mitochondrial membrane potential (driving force for Mrs2p-mediated Mg^{2+} uptake into mitochondria), which was not observed in mitochondria from *mrs2Δ* cells (Sponder, et al., 2010). Addition of the K^+/H^+ exchanger nigericin, which artificially increases the mitochondrial membrane potential (Nowikovsky, et al., 2007), leads to restoration of Mg^{2+}-influx into mitochondria from *lpe10*Δ cells, but not into the double deletion *mrs2*Δ, *lpe10*Δ strain (Sponder, et al., 2010). This, together with mutational analysis of Lpe10p and domain swaps between Mrs2p and Lpe10p indicates that the maintenance of the mitochondrial membrane potential and Mg^{2+}influx are functionally separated (Sponder, et al., 2010).

Despite of the similar phenotype of the *mrs2Δ* and *lpe10Δ*, both proteins cannot substitute for each other and expression of one of the proteins in the *mrs2*Δ, *lpe10*Δ background is not sufficient for fully restore growth. The growth defect of the *lpe10Δ* strain can be partially restored by low-copy (but not upon high-copy) expression of Mrs2p. In contrast high-copy expression of Lpe10p is needed for partial complementation of the *mrs2Δ* caused growth defect. In an *mrs2Δ lpe10Δ* double disruptant only the high-copy expression of Mrs2p weakly restores growth (Sponder, et al., 2010). These data suggest that expression levels of these to proteins are crucial for the formation of a functional channel.

In vitro chemical cross-linking assays and Blue-Native gel-electrophoresis experiments revealed homo-oligomeric Lpe10-complexes similar to those formed by Mrs2p (Kolisek, et al., 2003) and interaction of Lpe10p with the Mrs2-containing channel complex (Sponder, et al., 2010).

Single channel recordings on giant lipid vesicles with over-expressed ScLpe10p isolated from *mrs2*Δ, *lpe10*Δ cells showed that Lpe10p it self cannot mediate Mg^{2+}influx into mitochondrial. In contrary, the conductance of the Mrs2-channel was strongly decreased, when Lpe10p and Mrs2p were co-expressed (Sponder, et al., 2010). It seems that Lpe10p plays an important role in the formation of the mitochondrial Mg^{2+}-channel resulting in hetero-oligomerisation of Mrs2p and Lpe10p and thus a modulation of the Mrs2-mediated Mg^{2+} influx into mitochondria.

3. Results

3.1. Publication I

Functional analysis of the conserved hydrophobic gate region of the magnesium transporter CorA

Soňa Svidová [a], Gerhard Sponder [a], Rudolf J. Schweyen [a,†], Kristina Djinović-Carugo [b,c,*]

Biochimica et Biophysica Acta 1808 (2011) 1587–1591

[a] Department of Microbiology, Immunobiology and Genetics, Max F. Perutz Laboratories, University of Vienna, Dr. Bohrgasse 9/4, A-1030 Vienna, Austria

[b] Department for Structural and Computational Biology, Max F. Perutz Laboratories, University of Vienna, Campus Vienna Biocenter 5, A-1030 Vienna, Austria

[c] Department of Biochemistry, Faculty of Chemistry and Chemical Technology, University of Ljubljana, Ljubljana, Slovenia

[*] Corresponding author.

Authors' contributions to the manuscript

As the first author of this article, I prepared the manuscript. I designed the primers and performed the random PCR mutagenesis in the gate region of TmCorA, performed the complementation assays on solid media, growth curves, Mg^{2+} uptake measurements and PAGE and western blotting. I analyzed most of the data and merged data for the manuscript.

Biochimica et Biophysica Acta 1808 (2011) 1587–1591

Contents lists available at ScienceDirect

Biochimica et Biophysica Acta

journal homepage: www.elsevier.com/locate/bbamem

Functional analysis of the conserved hydrophobic gate region of the magnesium transporter CorA

Soňa Svidová [a], Gerhard Sponder [a], Rudolf J. Schweyen [a,†], Kristina Djinović-Carugo [b,c,*]

[a] Department of Microbiology, Immunobiology and Genetics, Max F. Perutz Laboratories, University of Vienna, Dr. Bohrgasse 9/4, A-1030 Vienna, Austria
[b] Department for Structural and Computational Biology, Max F. Perutz Laboratories, University of Vienna, Campus Vienna Biocenter 5, A-1030 Vienna, Austria
[c] Department of Biochemistry, Faculty of Chemistry and Chemical Technology, University of Ljubljana, Ljubljana, Slovenia

ARTICLE INFO

Article history:
Received 1 September 2010
Received in revised form 23 October 2010
Accepted 26 October 2010
Available online 11 November 2010

Keywords:
CorA
Magnesium transport
Hydrophobic gate
Thermotoga maritima

ABSTRACT

The Leu294 residue in the cytoplasmic neck of *Thermotoga maritima* CorA is considered to be the main gate for Mg^{2+} transport. We created three site-directed mutants at this position: in the Leu294Asp and Leu294Gly mutants we observed a defect in closing of the pore, while in the Leu294Arg mutant not only gating, but also the regulation of Mg^{2+} uptake was affected. Our results confirmed the importance of the Leu294 for gating of Mg^{2+} transport and in addition revealed the influence of the charge and structural features of the amino acid residues on the gating mechanism.

1. Introduction

Magnesium transporters of the CorA family are widely distributed amongst Eubacteria and Archaea. The CorA gene encodes a constitutively expressed integral membrane protein [1]. Previous investigations showed that it is essential for bacterial growth [2] but standard rich media provide sufficient magnesium concentrations for growth [3].

In the last years three crystal structures of *Thermotoga maritima* CorA have been published [4–6]. All showed that the transporter exists in a pentameric form, consisting of a cytosolic funnel shaped part, linked to the transmembrane region by long α7 helices (Fig. 1a, b). The pore is formed by the first trans-membrane helices and surrounded by the second trans-membrane helices, which anchor the complex in the membrane and end in a highly conserved positively charged motif (KKKKWL) called "basic sphincter". In the cytoplasmic neck of the pore a hydrophobic ring is created by residues Leu294 and Met291, surrounded by the aforementioned basic sphincter (Fig. 1c). This concentration of positive charges and the significant conservation of the bulky hydrophobic residues at positions 291 and 294 in the CorA protein family is considered to be of high importance for gating of Mg^{2+} ions. Opening and closing of the gate is most probably regulated by interaction of the Mg^{2+} ion with a divalent cation sensing site (DCS), placed between Asp89 in the α3 helix in the N-terminal part of one monomer and Asp253 of the α7 helix of the adjacent monomer [4–6] (Fig. 1b). A second DCS site, involving residues Glu88 and Asp175, was identified by Eshaghi et al. [5] and Payandeh et al. [6] (Fig. 1b).

The exact gating mechanism of the TmCorA transporter could not been revealed yet. It has been proposed that binding of the Mg^{2+} ions to the DCS sites evokes a structural rearrangement of the cytosolic domain causing positively charged residues of the basic sphincter to close the pore by drawing the negative charges away from the middle of the pore, and thereby preventing the positively charged Mg^{2+} ion to pass. Removal of Mg^{2+} from the DCS sites would cause a movement of the N-terminal domain, resulting in drawing the basic sphincter away from the neck of the pore and allowing the Mg^{2+} ion to pass [4]. According to the recently performed 110-ns molecular-dynamics simulations, based on the CorA structures published by Eshaghi et al. [5] and Payandeh et al. [8], the binding or unbinding of Mg^{2+} ions to the DCS sites evokes structural rearrangements of the cytosolic domains and the α7 helices transmit these changes to the gate region causing closing or widening of the pore [7].

Leu294 in the hydrophobic ring is the critical residue for Mg^{2+} gating. It creates a strong energetic barrier for ion permeation and probably controls the movement of Mg^{2+} ions indirectly through the movement of water. According to Payandeh et al. [8], not only an energetic, but also a mechanic barrier can influence the uptake of Mg^{2+} and "opening sensitivity" of the transporter. To investigate this hypothesis in more detail, this mutational study was focused on Leu294 which was mutated to 15 different amino acids using random PCR mutagenesis. After a preliminary screen, three of these mutants representing different types of amino acids: positively charged hydrophilic arginine, negatively charged hydrophilic aspartic acid and small neutral glycine, were chosen for closer investigations.

* Corresponding author. Campus Vienna Biocenter 5, A-1030 Vienna, Austria. Tel.: +43 1 4277 52203/52201; fax: +43 1 4277 9522.
E-mail address: kristina.djinovic@univie.ac.at (K. Djinović-Carugo).
† Deceased on 15th of February 2009.

0005-2736/$ – see front matter © 2010 Elsevier B.V. All rights reserved.
doi:10.1016/j.bbamem.2010.10.017

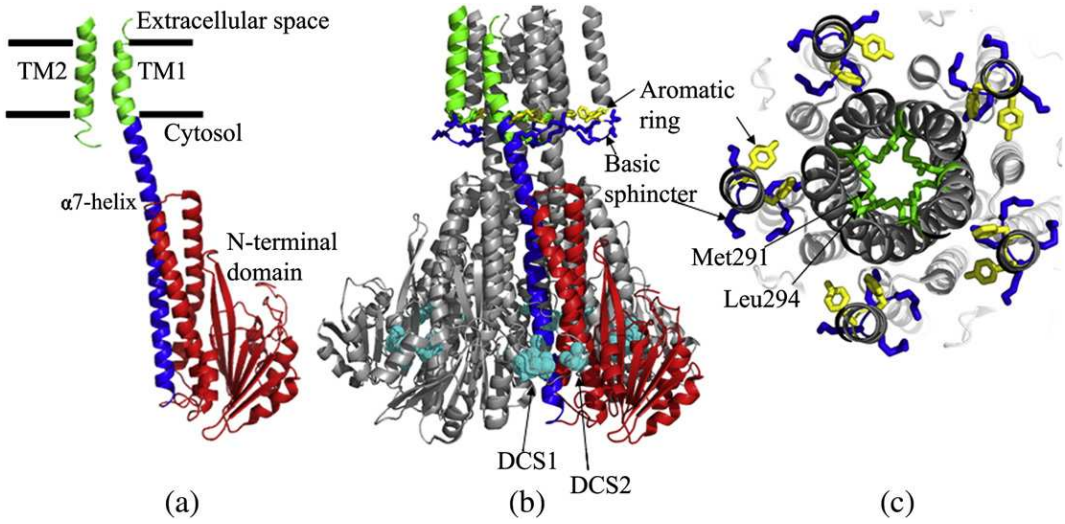

Fig. 1. Structure of the TmCorA Mg^{2+} transporter. (a) Single monomer: green — transmembrane domains TM1 and TM2, blue — α7 helix, red — N-terminal domain. (b) Side view of the homopentamer: cyan — DCS sites 1 and 2. (c) View from the top: blue — basic sphincter, yellow — aromatic ring, green — the gate forming residues Leu294 and Met291.

2. Materials and methods

2.1. Bacterial strains, growth media and genetic procedures

Salmonella enterica serovar Typhimurium strain LB5010 was used as wild-type reference.

Salmonella enterica serovar Typhimurium strain MM281 (DEL485 (leuBCD)mgtB::MudJ;mgtA21::MudJ;corA45::mudJ;zjh1628::Tn10 (cam) Cam^R, Kan^R, Mg^{2+} dependent) was kindly provided by M.E. Maguire. It lacks all major magnesium transport systems *CorA*, *MgtA* and *MgtB* and requires Mg^{2+} concentrations in millimolar range for growth.

Strains were grown in LB medium (10 g tryptone, 5 g yeast extract, 10 g NaCl per liter) with ampicillin (100 μg/ml). MM281 required addition of 10 mM $MgCl_2$.

LB plates contained 2% Difco™ Agar Noble, minimizing possible Mg^{2+} contamination.

2.2. Plasmid constructs

The *Thermotoga maritima* CorA coding sequence was kindly provided by S. Eshaghi and used as template for PCR. The sequence was amplified using the following primers: TmCorwoSfw 5′-CGCGGATCCGAGGAAAA-GAGGCTGTCTGC-3′ and TmCorrev 5′-TCCCCCGGGTCACAGC-CACTTCTTT-TTCTTG-3′. The 1035 bp PCR product was cut with BamHI and SmaI restriction enzymes and cloned into the pQE80L vector with an IPTG-inducible promoter.

2.3. Random PCR mutagenesis

In order to introduce various amino acid substitutions in CorA, an overlap extension PCR according to Pogulis et al. [9] was used.

Random mutagenesis of the Leu294 amino acid with the mutagenic forward primer 5′-GCGGTCTTCTTGATGTGTACCTTTCGAGTGTAAGTAA-CAAAACAAACGAAGTGATGAAGGTGNNNACCATCATAGCG-3′ and the reverse primer 5′-CGCTATGATGGTNNNCACCTTCATCACTTCGTTTG-TTTTGTTACTTACACTCGAAAGGTACACATCAAGAA-GACCGC-3′ was performed with mutagenic PCR according to standard protocols. PCR product was cut with BamHI and PstI restriction enzymes and cloned into a BamHI and PstI digested pQE CorA construct. Correctly ligated constructs were identified by deletion of the BsaBI restriction site in the CorA gene, resulting in a silent mutation from a thymine to a cytosine. No additional mutations were found by sequencing.

2.4. Complementation assays on solid media

The CorA, MgtA, MgtB deletion strain MM281 was transformed with pQE80L constructs harbouring TmCorA or mutated versions thereof. Single colonies were inoculated in LB medium containing 10 mM $MgCl_2$ and grown over night. The cultures were washed twice with 0.7% saline, adjusted to an OD_{600} of 0.1, and diluted 1:10, 1:100 and 1:1000 and spotted on LB plates containing 100 mM $MgCl_2$ or on standard LB plates, both supplemented with different IPTG concentrations (0; 0.01; 0.1 mM). The cultures were incubated for 24 h at 37 °C.

2.5. Growth curves

Overnight cultures of MM281 cells transformed with the aforementioned plasmid constructs were grown in LB medium with 10 mM $MgCl_2$, washed twice with LB and inoculated to an OD_{600} of 0.1 into liquid LB medium containing different concentrations of $MgCl_2$ and IPTG.

2.6. Measurement of Mg^{2+} uptake by spectrofluorometry

For these measurements cells were grown in low-phosphate LB medium in order to minimize complexation of Mg^{2+} by an excess of phosphate, which might cause variation in Mg^{2+} concentration. The measurements have been performed as described previously [10].

2.7. PAGE and western blotting

Overnight cultures of MM281 cells transformed with the aforementioned plasmid constructs were washed twice with LB medium and diluted in fresh LB + Amp medium to an OD_{600} of 0.1. Expression was induced by adding 0.05 mM IPTG for 3 h. Equivalents of 3 ml culture with an OD_{600} of 0.5 were taken. The cell pellet was resuspended in 20 μl SDS-Laemmli buffer and 20 μl 8 M Urea and sonicated for 5 s. After 15 min centrifugation at 13,000 rpm, equal volumes of supernatant were loaded on 10% SDS/polyacrylamide gels, blotted and labelled with an antiserum against the 6xHis tag (Qiagen).

3. Results

There are several hydrophobic constrictions along the TmCorA ion conduction pathway. The narrowest one is formed by the highly conserved residues Leu294 and Met291 [4–6]. They are considered to

be part of the potential "hydrophobic gate" [4,8]. To verify this hypothesis our mutations targeted the Leu294, we analysed mutants containing three different residues: positively charged arginine, negatively charged aspartic acid and small glycine.

3.1. Effect of positive charge at position 294 on gating of CorA: Leu294Arg mutant

In the growth complementation assay the Leu294Arg mutant showed similar growth as the wild-type TmCorA on plates without $MgCl_2$ and with different IPTG concentrations, which means, that the change from hydrophobic leucine to the hydrophilic, positively charged arginine does not cause a dramatic change in the protein function (Fig. 2). While on plates containing 100 mM $MgCl_2$ and 0.1 mM IPTG the wild-type TmCorA exhibited a growth defect, probably caused by Mg^{2+} overdose, the Leu294Arg mutant was still able to grow indicating decreased transport efficiency of this mutant (Fig. 2).

Mg^{2+} uptake measurements of the Leu294Arg mutant showed slower Mg^{2+} influx and lower steady-state values (~80% of wild-type values) (Fig. 3) suggesting that (i) the pore of the transporter is smaller than in wild-type TmCorA; (ii) the sensitivity of CorA to Mg^{2+} or the regulation of opening and closing of the pore was affected.

The growth curves of cells transformed with TmCorA Leu294Arg mutant (Fig. 4a, b, c) support these hypotheses. In liquid medium supplemented with 0.05 mM IPTG the cells grew much slower than those with wild-type TmCorA (Fig. 4b), while the shapes of the curves remained similar, pointing to a lower Mg^{2+} transport capacity of this mutant. The same was true for cells growing in medium with 0.05 mM IPTG and 3 mM $MgCl_2$ (Fig. 4c). We did not observe any indications of Mg^{2+} overdose, not even after 11 hour incubation (results not shown), suggesting that closing of the transporter remained tightly regulated. In medium without $MgCl_2$ the cells with Leu294Arg mutant were unable to grow, exactly like those with wild-type TmCorA (Fig. 4a).

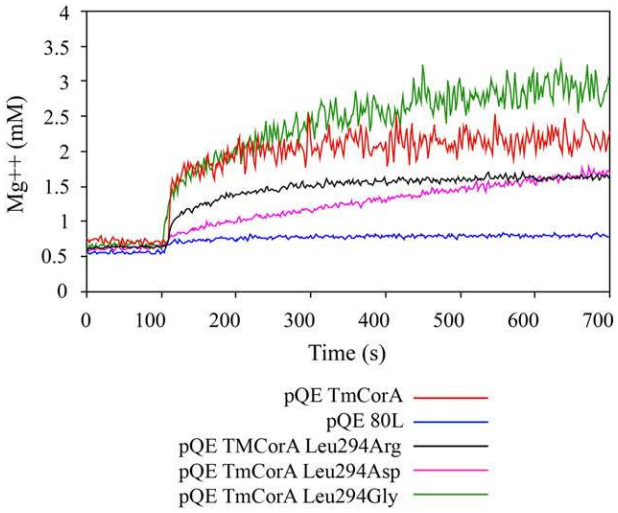

Fig. 3. Representative recordings of Mg^{2+} uptake. *S. typhimurium* strain MM281 which lacks all three known magnesium transport systems was transformed with plasmids indicated. The representative recordings show changes in fluorescence intensity of Mag-Fura-2 monitored over 10 min time after adding 10 mM $MgCl_2$. The pQE TmCorA and pQE80L empty constructs served as positive and negative control.

3.2. Effect of negative charge at position 294 on gating of CorA: Leu294Asp mutant

Cells transformed with TmCorA Leu294Asp mutant showed a growth defect on medium containing 0.1 mM IPTG as well as on media containing 0.1 mM IPTG and 100 mM $MgCl_2$ in the growth complementation assay (Fig. 2). This suggests either a higher Mg^{2+}

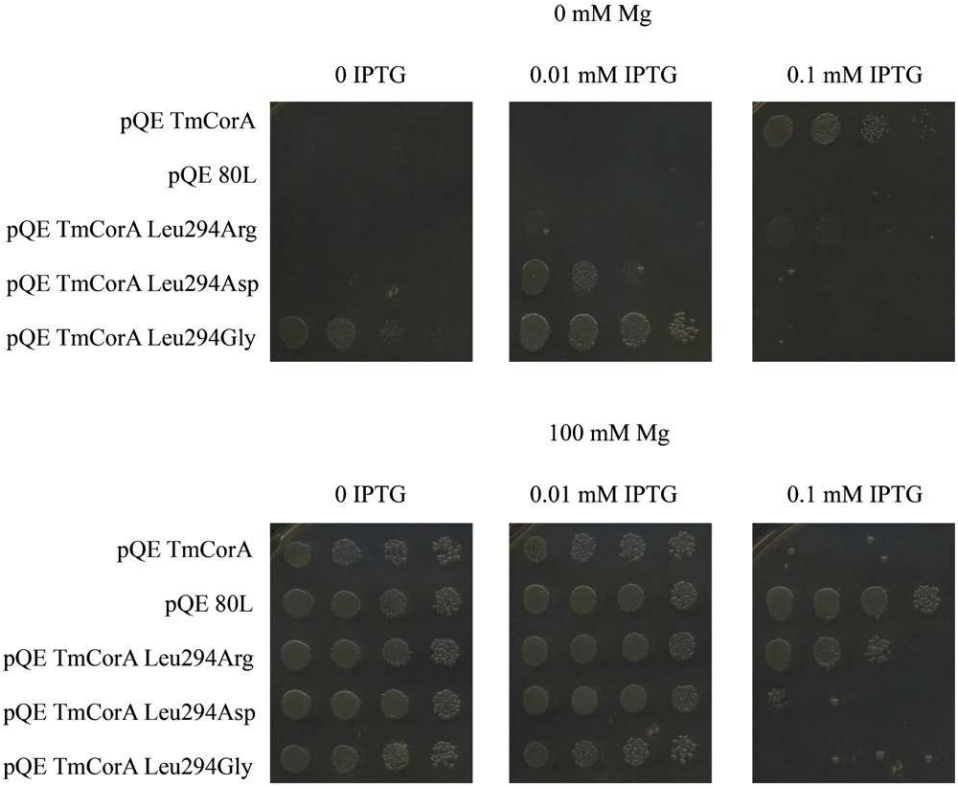

Fig. 2. Growth complementation assay of the gating mutants. *S. typhimurium* strain MM281 which lacks all three known magnesium transport systems was transformed with plasmids indicated. The pQE TmCorA and pQE80L empty constructs served as positive and negative control.

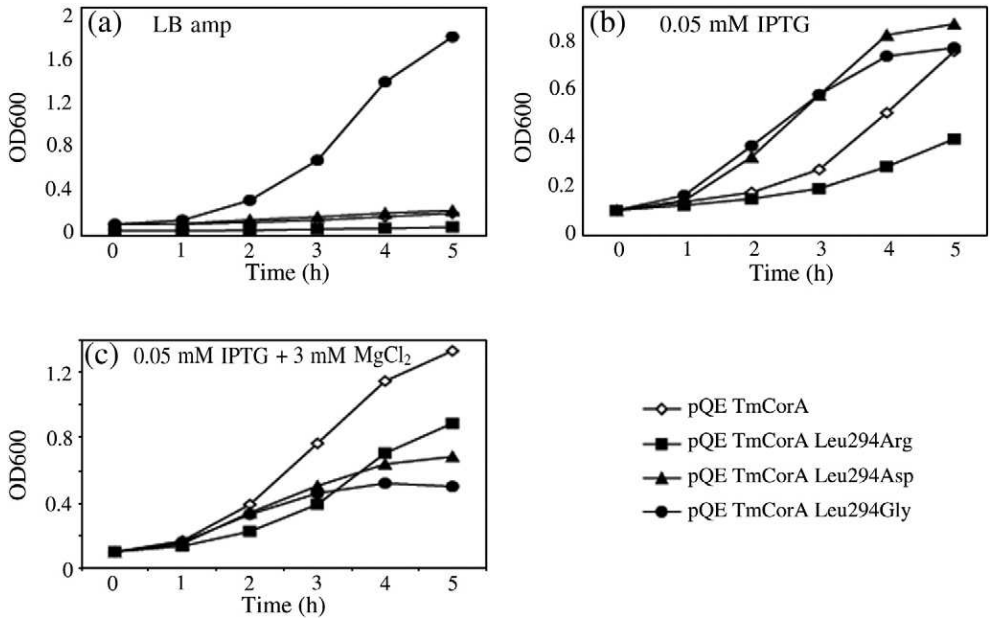

Fig. 4. Effect of gating mutations in different liquid medium. Growth curves of the *S. typhimurium* strain MM281 which lacks all three known magnesium transport systems, transformed with plasmids indicated. Cells were grown over night in LB amp medium containing 10 mM $MgCl_2$. Cultures were diluted to an OD_{600} of 0.1 and grown over 5 h. The data were averaged from three independent experiments.

transport capacity, which might be caused by a defect in the regulation process of the opening and closing of the channel or in the closing itself, leading to Mg^{2+} overdose during the 24 hour incubation and consequently to a toxic effect of this protein at high expression levels.

Mg^{2+} uptake of Leu294Asp mutant increased slowly and did not reach a steady-state level within a time period of 600 s (Fig. 3), suggesting that the pore is neither completely open nor can it close properly, causing slow, constant Mg^{2+} uptake, leading finally to a Mg^{2+} overdose. This mutation apparently causes a defect in the regulation of opening and closing or/and in the closing process itself, which was corroborated by the growth curves (Fig. 4a, b, c): neither cells transformed with the TmCorA nor cells transformed with the Leu294Asp mutant were able to grow in medium without $MgCl_2$ (Fig. 4a). In medium containing 0.05 mM IPTG we observed rapid growth but after 4 h a steady-state phase was reached, probably due to a Mg^{2+} overdose (Fig. 4b). In medium containing 0.05 mM IPTG and 3 mM $MgCl_2$ the shape of the Leu294Asp mutant growth curve differed from that of the wild-type TmCorA: the mutant cells grew significantly slower, reaching only an OD_{600} of 0.6 (~50% of the wild-type CorA) (Fig. 4c), which indicates a Mg^{2+} overdose caused by the constant Mg^{2+} uptake depicted in Fig. 3.

3.3. Effect of removal of side chain at position 294 on gating of CorA: Leu294Gly mutant

As expected, the Leu294Gly mutant was even more Mg^{2+} sensitive than the Leu294Asp variant. The cells did not grow on plates containing 0.1 mM IPTG suggesting a defect in the closing and/or in the regulation of the transporter and the growth on plates containing 0.01 mM IPTG points to a higher Mg^{2+} uptake capacity compared to the wild-type TmCorA (Fig. 2). In case of the Leu294Gly mutant the cells also grew on plates without additional $MgCl_2$ or IPTG (Fig. 2) which might be due to not tight enough regulation of the used plasmid, leading to leaky expression of the CorA gene in the absence of IPTG. This was tested by determination of expressed CorA levels using western blots (Fig. 6). The low expression level of the wild-type TmCorA protein was not sufficient to provide cells with enough Mg^{2+} in a low Mg^{2+} medium, but in the case of the Leu294Gly mutant cells are able to take up enough Mg^{2+} to survive. This observation supports the suggested increased Mg^{2+} transport ability of the Leu294Gly mutant, which was also observed in Mg^{2+} uptake measurements (Fig. 3). The Mg^{2+} influx was as fast as in cells transformed with wild-type TmCorA, but it did not reach a steady-state, which indicates a defect in the closing of the transporter.

In liquid medium containing 0.05 mM IPTG we observed fast growth of the Leu294Gly cells, followed by a steady-state after 4 h (Fig. 4b). In medium supplemented with 0.05 mM IPTG and 3 mM $MgCl_2$ the cells stopped to grow already after 3 h, reaching only ~40% of the wild-type level, and contrary to the wild-type cells, they began to die (Fig. 4c). This effect can be related not only to an increased Mg^{2+} transport ability but also to a closing defect of the transporter. Increased Mg^{2+} transport ability of the Leu294Gly mutant (Fig. 3) allowed growth of the cells also in medium without any supplements (Fig. 4a), suggesting eminent structural changes caused by this mutation.

In order to confirm that the higher Mg^{2+} uptake capacity of this mutant is due to the Leu294Gly mutation, we used Co(III)hexamine, a known blocker of the CorA transporter [8,11,12]. We compared the wild-type *Salmonella typhimurium* strain LB5010, which has all major Mg^{2+} uptake systems (CorA, MgtA, MgtB) with strain MM281 deficient for these genes, transformed with wild-type TmCorA and with TmCorA Leu294Gly mutant. In liquid LB medium (Fig. 5) strain LB5010 grew fast, whereas strain MM281 containing the Leu294Gly mutation showed reduced growth, and strain MM281 with wild-type TmCorA did not grow at all. After addition of 3 mM Co(III)hexamine, growth of LB5010 cells and MM281 cells containing wild-type TmCorA remained unchanged, whereas growth of MM281 cells with the Leu294Gly mutation was completely inhibited proving that growth of cells under low Mg^{2+} conditions is the result of this mutation.

4. Discussion

Gating of the TmCorA magnesium transporter is a complex process, involving several events resulting in structural rearrangements of the pentamer: binding of Mg^{2+} ions to the regulatory DCS site(s) with consequent rearrangements of α-helices in the N-terminal domain, the pore-forming α7 helices and the basic sphincter are considered to lead collectively to conformational changes in the gating region. Leu294 lies

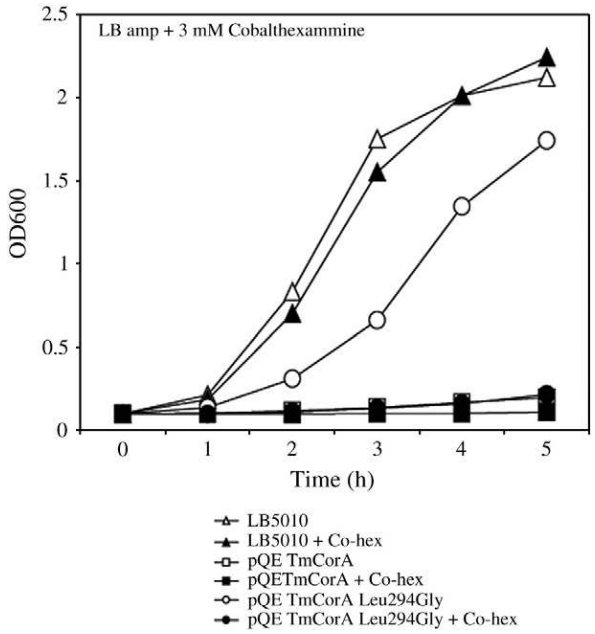

Fig. 5. Effect of Co(III)hexamine, inhibitor of the CorA-mediated magnesium transport. Growth curves of the *S. typhimurium* strains LB5010 (wild-type strain) transformed with pQE80L parental vector and MM281 (*corAΔ*, *mgtAΔ*, *mgtBΔ*) transformed with pQE80 TmCorA and pQE80 TmCorA L294G in the presence or absence of cobalt hexamine. The data were averaged from three independent experiments.

in the 15 Å long region termed MM stretch (spanning residues Met291 to Met301) proposed to play a central role in controlling the ionic conduction profile by representing both a steric as well as an electrostatic bottleneck for Mg^{2+} translocation [7]. This region involves a series of hydrophobic residues among which Leu at position 294 plays a critical role in the gating process. The effects of the Leu294 mutation to Asp and Gly may be mechanistically and structurally explained by local structural and electrostatic changes due to introduction of a negatively charged or a small amino acid residue with no side chain.

In case of glycine, the absence of the side chain could on one hand cause a wider opening of the pore and on the other impair its complete closing. This is in agreement with results of Payandeh et al. [8], who showed that exchange of Leu294 to a hydrophobic amino acid with a smaller side chain (Ile, Val or Ala) results in an increased ability of cells to grow on media supplemented with low $MgCl_2$ concentrations.

In case of introduction of an aspartic acid at position 294, the negatively charged side chains coming from five protomers repulse each other and thereby maximise the distance between them, leading to the incapacity of the transporter to properly close and to maintain a stable magnesium concentration in the cell. Furthermore, slow magnesium uptake of this mutant indicates that Mg^{2+} ions are probably trapped in the ring of negative charges.

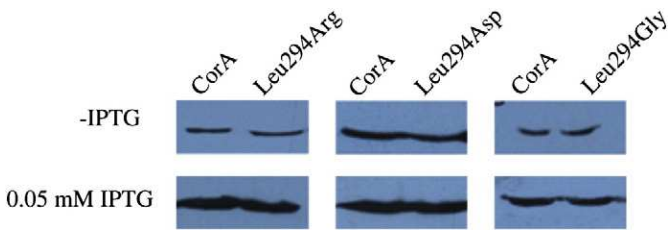

Fig. 6. Western blot analysis of whole cell samples. *S. typhimurium* strain MM281 which lacks all three known magnesium transport systems was transformed with plasmids indicated. The synthesis of CorA protein and variants thereof was induced by addition 0.05 mM IPTG for 3 h.

The effects observed with the Leu294Arg mutant cannot only be explained by local changes. Concentration of positively charged arginine residues in this region might have two opposite effects: repulsion of the positively charged residues causing a local structural distortion, and/or repulsion of the Mg^{2+} ion and hindering its passing through the pore. Both effects can explain the slow-down of Mg^{2+} transport, but not the low steady-state values observed in Mg^{2+} uptake measurements, which indicate a change in the regulation of Mg^{2+} influx. According to Payandeh et al. a valine mutation at position 294 can alter Mg^{2+}-binding properties of the transporter [8]. Due to the distance of ~65 Å between the Leu294 and the DCS sites a direct interaction seems impossible. Since the loss of Mg^{2+} ions from DCS sites can induce conformational rearrangements of the magnesium-binding domains, transmitted to the gate region by the α7 helices and leading to changes allowing ions to pass through [7,8], also a reverse process might be possible. Certain mutations in the gate region may evoke structural rearrangements of the α7 helices leading to conformational changes in the DCS sites, resulting in their changed affinity to Mg^{2+} ions.

5. Concluding remarks

In summary, we confirmed the importance of the Leu294 as a mechanical barrier to Mg^{2+} permeation. We furthermore propose an additional function of this residue in the regulation of Mg^{2+} uptake. Since Mg^{2+} transport involves multiple coordinated structural movements, further structural and functional analyses will be required to fully understand the molecular basis of this process.

Acknowledgements

We thank Michael Maguire (Case Western Reserve University) for providing the *Salmonella typhimurium* strains MM281 and LB5010 and Said Eshaghi (Karolinska Institute, Sweden) for providing the TmCorA coding sequence. We also thank Elisabeth Froschauer, Muhammad Bashir Khan and Oliviero Carugo (Univ. of Pavia, Italy and Max F. Perutz Laboratories, Austria) for fruitful discussions.

This work was supported by WWTF (LS05021) and FWF (P20141).

References

[1] R.L. Smith, J.L. Banks, M.D. Snavely, M.E. Maguire, Sequence and topology of the CorA magnesium transport systems of *Salmonella typhimurium* and *Escherichia coli*. Identification of a new class of transport protein, J. Biol. Chem. 268 (1993) 14071–14080.
[2] M. Webb, The utilization of magnesium by certain Gram-positive and Gram-negative bacteria, J. Gen. Microbiol. 43 (1966) 401–409.
[3] R.L. Smith, M.E. Maguire, Microbial magnesium transport: unusual transporters searching for identity, Mol. Microbiol. 28 (1998) 217–226.
[4] V.V. Lunin, E. Dobrovetsky, G. Khutoreskaya, R. Zhang, A. Joachimiak, D.A. Doyle, A. Bochkarev, M.E. Maguire, A.M. Edwards, C.M. Koth, Crystal structure of the CorA Mg2+ transporter, Nature 440 (2006) 833–837.
[5] S. Eshaghi, D. Niegowski, A. Kohl, D. Martinez Molina, S.A. Lesley, P. Nordlund, Crystal structure of a divalent metal ion transporter CorA at 2.9 angstrom resolution, Science 313 (2006) 354–357.
[6] J. Payandeh, E.F. Pai, A structural basis for Mg2+ homeostasis and the CorA translocation cycle, EMBO J. 25 (2006) 3762–3773.
[7] N. Chakrabarti, C. Neale, J. Payandeh, E.F. Pai, R. Pomes, An iris-like mechanism of pore dilation in the CorA magnesium transport system, Biophys. J. 98 (2010) 784–792.
[8] J. Payandeh, C. Li, M. Ramjeesingh, E. Poduch, C.E. Bear, E.F. Pai, Probing structure–function relationships and gating mechanisms in the CorA Mg2+ transport system, J. Biol. Chem. 283 (2008) 11721–11733.
[9] R.J. Pogulis, A.N. Vallejo, L.R. Pease, In vitro recombination and mutagenesis by overlap extension PCR, Meth. Mol. Biol. 57 (1996) 167–176.
[10] E.M. Froschauer, M. Kolisek, F. Dieterich, M. Schweigel, R.J. Schweyen, Fluorescence measurements of free [Mg2+] by use of mag-fura 2 in *Salmonella enterica*, FEMS Microbiol. Lett. 237 (2004) 49–55.
[11] L.M. Kucharski, W.J. Lubbe, M.E. Maguire, Cation hexaammines are selective and potent inhibitors of the CorA magnesium transport system, J. Biol. Chem. 275 (2000) 16767–16773.
[12] M. Kolisek, G. Zsurka, J. Samaj, J. Weghuber, R.J. Schweyen, M. Schweigel, Mrs2p is an essential component of the major electrophoretic Mg2+ influx system in mitochondria, EMBO J. 22 (2003) 1235–1244.

3.2. Publication II

Mutational analysis of functional domains in Mrs2p, the mitochondrial Mg^{2+} channel protein of *Saccharomyces cerevisiae*

Julian Weghuber, Frank Dieterich, Elisabeth M. Froschauer, Soňa Svidová and Rudolf J. Schweyen

FEBS Journal 273 (2006) 1198–1209

Max F. Perutz Laboratories, Department of Genetics, University of Vienna, Austria

Authors' contributions to the manuscript

I performed site directed mutagenesis in the loop region of MRS2 and prepared and cloned the mutants J10 and J11. I performed the complementation assays on solid media and Mg^{2+} uptake measurements with this mutants and PAGE and western blotting for all mutants used in this study. I also analyzed the data for J10 and J11 mutants.

the FEBS Journal

Mutational analysis of functional domains in Mrs2p, the mitochondrial Mg^{2+} channel protein of *Saccharomyces cerevisiae*

Julian Weghuber, Frank Dieterich, Elisabeth M. Froschauer, Sona Svidovà and Rudolf J. Schweyen

Max F. Perutz Laboratories, Department of Genetics, University of Vienna, Austria

Keywords
gain-of-function; mag-fura 2; Mg^{2+}; mitochondria; mutagenesis

Correspondence
R.J. Schweyen, Max F. Perutz Laboratories, Department of Genetics, University of Vienna, Dr. Bohrgasse 9, 1030, Austria
Fax: +43 14277 9546
Tel: +43 14277 54604
Email: rudolf.schweyen@univie.ac.at

(Received 29 November 2005, revised 20 January 2006, accepted 27 January 2006)

doi:10.1111/j.1742-4658.2006.05157.x

The nuclear gene *MRS2* in *Saccharomyces cerevisiae* encodes an integral protein (Mrs2p) of the inner mitochondrial membrane. It forms an ion channel mediating influx of Mg^{2+} into mitochondria. Orthologues of Mrs2p have been shown to exist in other lower eukaryotes, in vertebrates and in plants. Characteristic features of the Mrs2 protein family and the distantly related CorA proteins of bacteria are the presence of two adjacent transmembrane domains near the C terminus of Mrs2p one of which ends with a F/Y-G-M-N motif. Two coiled-coil domains and several conserved primary sequence blocks in the central part of Mrs2p are identified here as additional characteristics of the Mrs2p family. Gain-of-function mutations obtained upon random mutagenesis map to these conserved sequence blocks. They lead to moderate increases in mitochondrial Mg^{2+} concentrations and concomitant positive effects on splicing of mutant group II intron RNA. Site-directed mutations in several conserved sequences reduce Mrs2p-mediated Mg^{2+} uptake. Mutants with strong effects on mitochondrial Mg^{2+} concentrations also have decreased group II intron splicing. Deletion of a nonconserved basic region, previously invoked for interaction with mitochondrial introns, lowers intramitochondrial Mg^{2+} levels as well as group II intron splicing. Data presented support the notion that effects of mutations in Mrs2p on group II intron splicing are a consequence of changes in steady-state mitochondrial Mg^{2+} concentrations.

Magnesium transport into mitochondria plays an important role in the cellular Mg^{2+} homeostasis and in the regulation of cellular and mitochondrial functions [1]. Physiological studies indicated that mitochondrial uptake of Mg^{2+} is an electrogenic process, driven by the inside negative membrane potential. But proteins involved in this process remained unknown and mitochondrial Mg^{2+} influx was suggested to occur via nonspecific leak pathways rather than specific transport proteins [2].

This laboratory identified the *MRS2* gene of the yeast *Saccharomyces cerevisiae* as encoding a mitochondrial protein (Mrs2p) involved in Mg^{2+} influx [3]. It was found to be an integral protein of the inner mitochondrial membrane, distantly related to the ubiquitous bacterial Mg^{2+} transport protein CorA and the yeast plasma membrane Mg^{2+} transport protein Alr1p [4]. This CorA-Mrs2-Alr1 superfamily of proteins is characterized by the presence of two adjacent transmembrane domains (TM-A, TM-B) near their C terminus and a short conserved primary sequence motif (F/Y-G-M-N) at the end of TM-A.

Members of the Mrs2p subfamily exhibit considerable sequence similarity. Mammals contain a single *MRS2* gene and its protein (hsMrs2p) is located in mitochondria [5]. The yeast genome contains two genes

Abbreviations
ARM, arginine-rich motif; CRB, conserved residue block; TM, transmembrane.

of this subfamily (*MRS2*, *LPE10*), while plants encode up to 15 variants of Mrs2p, located either in mitochondria, in the plasma membrane or in other cellular membranes [6].

The *S. cerevisiae* protein Mrs2p has been shown to mediate Mg^{2+} influx into mitochondria. Overexpression of the protein was found to increase Mg^{2+} influx into isolated mitochondria, while deletion of the *MRS2* gene nearly abolished it [7]. Single channel patch-clamping revealed the presence of a Mg^{2+} selective channel of high conductance. This channel is made up of a homo-oligomer of Mrs2p (J. Weghuber, R. Schindl, C. Romain & R.J. Schweyen, unpublished data).

In the absence of Mrs2p, yeast cells are respiration deficient, but viable when provided with fermentable substrates (*petite* phenotype). Mitochondria of mutant yeast cells lacking Mrs2p retain a low capacity Mg^{2+} influx system whose molecular identity remains to be determined. Although Mg^{2+} influx mediated by this system is comparatively slow (5–10× less than Mrs2p mediated influx), its activity leads to steady state Mg^{2+} concentrations $[Mg^{2+}]_m$ of about half of those of Mrs2p wild-type mitochondria [7] (J. Weghuber, R. Schindl, C. Romain & R.J. Schweyen, unpublished data).

Except for the presence of two adjacent TM domains and the F/Y-G-M-N motif, there is little sequence similarity among members of the CorA-Alr1-Mrs2 superfamily of proteins. Members of the Mrs2 subfamily, however, have several conserved regions with charged amino acid residues. Upon random and site-directed mutagenesis we isolated and characterized mutants with reduced Mg^{2+} influx into mitochondria (loss-of-function) or with improved influx (gain-of-function).

Results

Sequence conservation in Mrs2 proteins

Figure 1 exhibits a sequence alignment of ScMrs2, its only human homologue HsMrs2 and AtMrs2–11, its closest relative among the series of plant homologues [6]. Like other proteins of the CorA-Mrs2-Alr1 superfamily, these three proteins have two predicted transmembrane domains (TM-A, TM-B) near the C terminus. The short sequence connecting TM-A and TM-B has a surplus of negatively charged amino acids, notably two glutamic acid residues at positions +5 and +6 C terminal to the conserved F/Y-G-M-N motif, while the sequences C terminal to TM-B contains a surplus of positively charged residues, mostly arginines. This distribution of charges favours an orientation of the Mrs2 proteins with the N and C termini (positive) on the inner side and the TM-A-TM-B connecting sequence on the (negative) outer side of the membrane [8]. In fact, this topology has been experimentally determined for ScMrs2 [3].

The most N-terminal and C-terminal sequences of Mrs2 proteins are variable in length and exhibit little sequence similarity. Their central part, in contrast, exhibits a significant degree of sequence conservation among the three proteins shown in Fig. 1 and also when larger numbers of Mrs2-type proteins are compared. Secondary structure analysis of this part revealed high probability for extended alpha-helical regions (not shown). The COILS program predicts two coiled-coil regions (CC1, CC2) (Fig. 1). While the probability for CC1 and its position relative to conserved residues vary to some extent between sequences compared, CC2 starts with a block of conserved residues and is separated from TM-A by about 20 residues with some sequence conservation (conserved residue block; CRB-5) (Fig. 1).

Gain-of-function alleles

Overexpression of Mrs2p has previously been shown to suppress RNA splicing defects of mitochondrial group II introns in yeast [9]. Later this suppressor effect was also observed with certain mutant alleles of the *MRS2* gene expressed at standard levels [10,11]. These gain-of-function mutations were found to be clustered in the central part of the gene (Fig. 1) and mostly resulted in single amino acid substitutions within or next to conserved sequences of the Mrs2 protein family (Fig. 1). Those conserved sequences are highlighted in Fig. 1 and marked CRB-3, CRB-4 and CC2. Mrs2p sequence alignments marked three further conserved sequences (CRB-1, CRB-2 and CRB-5), which were not affected by the gain-of-function mutants studied.

Using random PCR mutagenesis of the central part of Mrs2p (aa 180–340) we continued the search for gain-of-function mutants. Two single base pair substitutions (*mrs2-J7* and *mrs2-J8*) and one double mutation (*mrs2-J9*) were identified (Fig. 1), which suppressed the *mit- M1301* mutation if expressed from a low-copy plasmid (Fig. 2A). Restoration of growth on YPdG was highly significant, but not as good as observed with the best suppressor (*MRS2-M9*) of the previously studied series [11] (data not shown).

Interestingly, these mutants are located in a block of conserved amino acid residues at the start of the second coiled-coil domain (CC2), which is conserved among the Mrs2-CorA protein family (Fig. 1). Analysis of this coiled-coil region in Mrs2-HA-J7, Mrs2-HA-J8 and Mrs2-HA-J9 mutant proteins (COILS program on

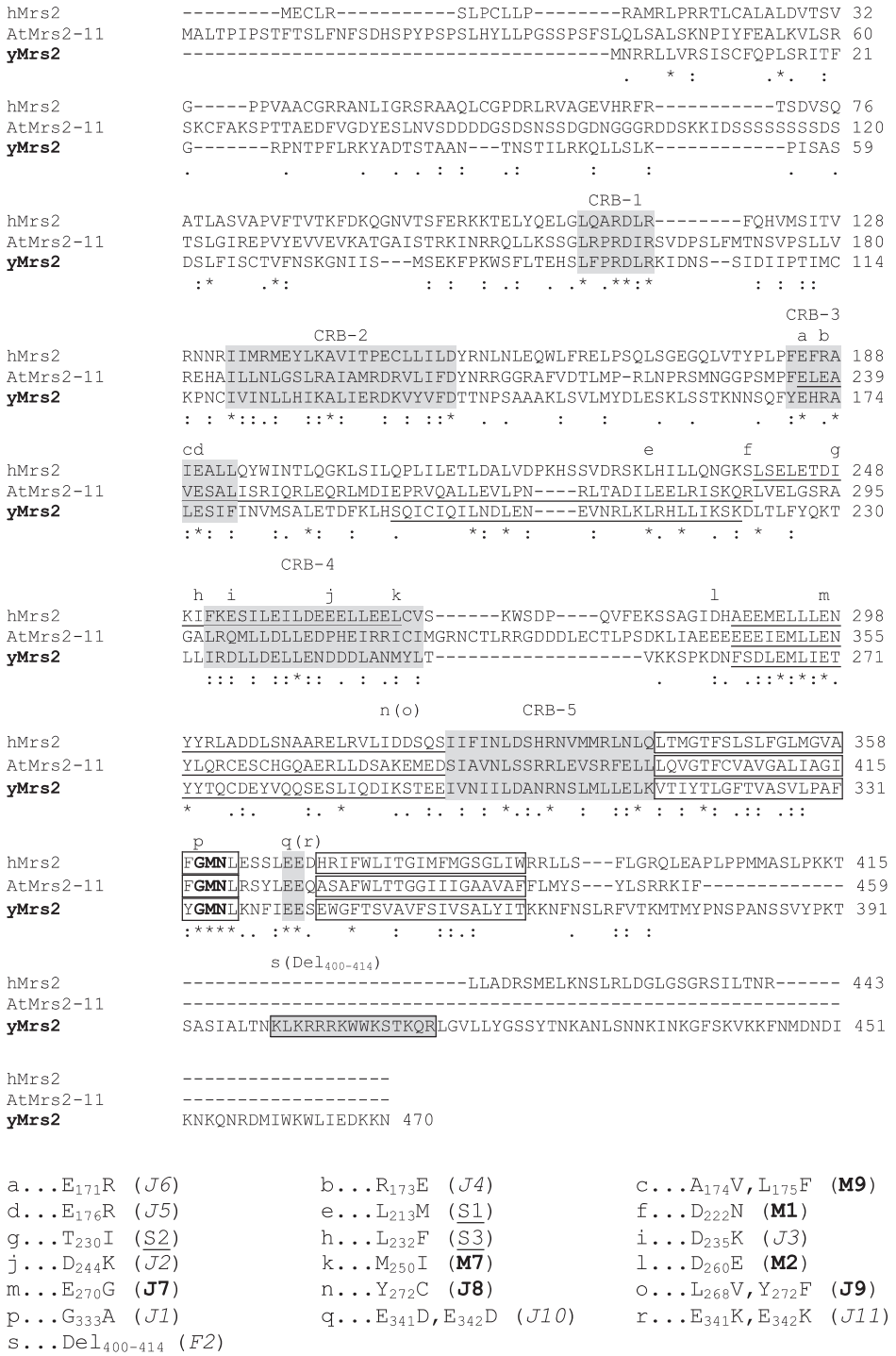

a...$E_{171}R$ (*J6*) b...$R_{173}E$ (*J4*) c...$A_{174}V, L_{175}F$ (**M9**)
d...$E_{176}R$ (*J5*) e...$L_{213}M$ (S1) f...$D_{222}N$ (**M1**)
g...$T_{230}I$ (S2) h...$L_{232}F$ (S3) i...$D_{235}K$ (*J3*)
j...$D_{244}K$ (*J2*) k...$M_{250}I$ (**M7**) l...$D_{260}E$ (**M2**)
m...$E_{270}G$ (**J7**) n...$Y_{272}C$ (**J8**) o...$L_{268}V, Y_{272}F$ (**J9**)
p...$G_{333}A$ (*J1*) q...$E_{341}D, E_{342}D$ (*J10*) r...$E_{341}K, E_{342}K$ (*J11*)
s...$Del_{400-414}$ (*F2*)

Fig. 1. Sequence alignment of HsMrs2, AtMrs2 and ScMrs2 proteins and mutations in ScMrs2. Predicted transmembrane domains are boxed; * indicates identical residues; : indicates conservative substitution; . indicates semiconservative substitutions. The sequence of a motif conserved in all putative magnesium transporters, G-M-N, is indicated in boldface. Predicted coiled-coil regions are underlined, five regions with conserved amino acid residues (CRB-1–5; conserved residue block) are shaded grey. A region of positively charged amino acid residues of ScMrs2p (ARM) is boxed and shaded light grey. All mutations of ScMrs2p previously described or studied in this work are marked a–s and base changes as well as allele designations are given below the figure. Mutations obtained by random mutagenesis are indicated in bold, those created by site-directed mutagenesis in italic; the J series and the F2 mutation were generated during this work, while M and S mutations have been previously reported by Gregan *et al.* [11] and by Schmidt *et al.* [10], respectively.

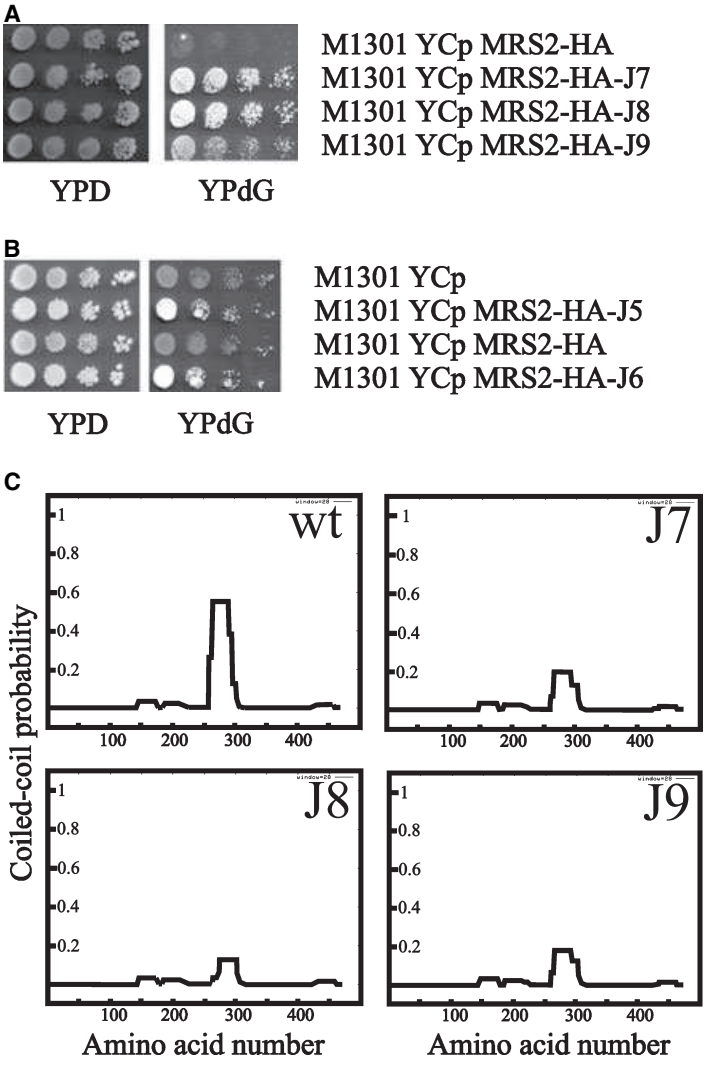

Fig. 2. Suppressors of the mitochondrial *mit-M1301* intron mutation. (A,B) Yeast *MRS2* cells with the mitochondrial intron mutation *M1301* were transformed either with the empty low-copy plasmid YCp111, with this plasmid expressing the wild-type *MRS2*-HA gene, or the gain-of-function mutant alleles MRS2-HA-J5 and -J6 (B), or MRS2-HA-J7 to -J9 (A). Serial dilutions of transformants were spotted on fermentable (YPD) and nonfermentable (YPdG) substrates and grown for 3 or 6 days, respectively. (C) Probability for predicted coiled-coil domains of wild-type Mrs2p and mutant Mrs2-variants (-J7, -J8, -J9). Prediction was performed with the COILS program available on http://www.ch.embnet.org (window width set at 28).

http://www.ch.embnet.org) revealed that all three mutations led to a similar decrease of the coiled-coil probability from 0.65 (wild-type Mrs2p) to 0.15–0.2 (Fig. 2C).

Out of a series of site-directed mutations two were found to result in a gain-of-function phenotype. Mrs2-J5 and -J6 have single amino acid substitutions reversing charges from positive to negative (Glu176Arg and Glu171Arg) in CRB-3. When expressed from a low-copy vector (YCp) in a mit^{+} strain they showed near normal growth on YPdG medium (data not shown). Suppression of the mit^{-} *M1301* phenotype was comparable to that of the randomly generated gain-of-function mutations (Fig. 2A and B).

Loss-of-function alleles

Mrs2-HA-J2, J3 and J4 were site-directed mutations resulting in single amino acid substitutions reversing charges (Asp244Lys, Asp235Arg and Arg173Glu, respectively). When expressed from a low copy number vector (YCp) all of them caused as loss of complementation of the *mrs2*Δ mutant phenotype. Two mutants (-J3 and -J4) showed a significant restoration of growth on nonfermentable YPG medium if expressed from a high-copy vector (YEp) (Fig. 3).

A fundamental feature of Mrs2p is the existence of two transmembrane-domains and a short connecting sequence of about 7–8 amino acids. This is supposed to be the only part of the protein located in the intermembrane space of yeast mitochondria [3,8]. The sequence contains a surplus of positively charged amino acids. Many Mrs2 proteins, e.g. ScMrs2, HsMrs2 and AtMrs2–11 (Fig. 1) have two Glu residues at position +5 and +6 relative to the F/Y-G-M-N motif. The negative charges might play a role as topogenic signals for Mrs2p membrane

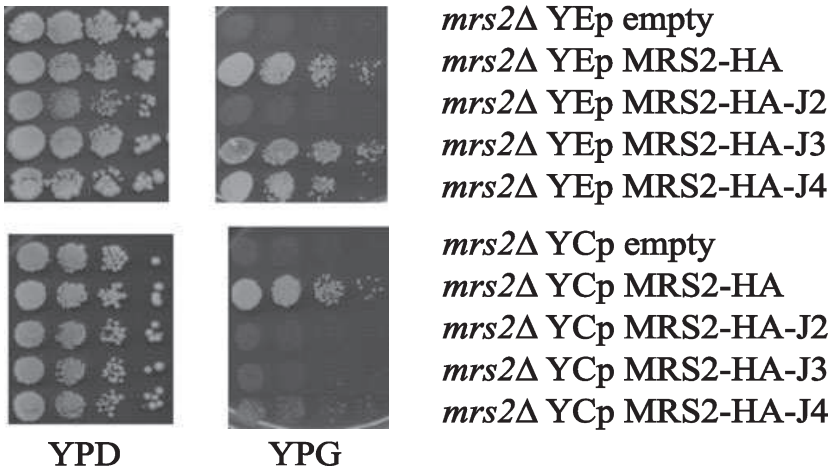

Fig. 3. Growth phenotypes of loss-of-function *mrs2* mutants. Mutant *mrs2*Δ cells were transformed with empty vectors YCp111 or YEp351, with those vectors harboring the wild-type MRS2-HA allele or mutant loss-of-function alleles -J2, -J3 or -J4. Serial dilutions of cells were spotted on fermentable (YPD) and nonfermentative (YPG) medium and grown for 3 or 6 days, respectively.

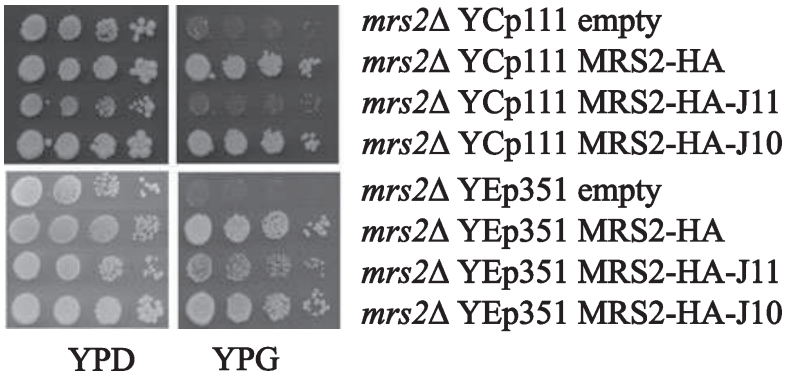

Fig. 4. Growth phenotypes of mutants with amino acid substitutions in the TM-A/TM-B connecting loop.Site-directed mutagenesis was used to obtain mutations -J10 and -J11 of the *MRS2* gene resulting in substitution of the two neighbouring glutamic acid residues at positions 5 and 6 of the connecting loop by two aspartic acid or two lysine residues, respectively. Serial dilutions of the *mrs2*Δ mutant transformed with either the empty plasmid YEp351 or this plasmid with the MRS2-HA-J10 and -J11 genes were spotted on fermentable (YPD) and nonfermentable (YPG) media as indicated and grown at 28 °C for 3 or 6 days, respectively.

insertion and for attracting Mg^{2+} to the pore of the channel.

We performed site-directed mutagenesis substituting Glu341 and Glu342 by two Asp residues (*mrs2-J10*, conservative mutation) or by Lys residues (*mrs2-J11*, replacing two negative charges by positive ones). Expression of Mrs2-J10 fully complemented the *mrs2*Δ growth defect when expressed either from a low-copy or a high-copy vector. In contrast, expression of Mrs2-J11 did not significantly complement the *mrs2*Δ growth defect when expressed from a low-copy plasmid, while it restored growth weakly when overexpressed (Fig. 4). Immunoblotting (Fig. 5) revealed that the Mrs2-J10 and Mrs2-J11 mutant proteins were expressed at a level slightly reduced compared to the one of wild-type Mrs2p in mitochondria. As revealed from proteinase K treatment of mitoplasts mutant Mrs2-J11 appeared to be properly inserted into the inner membrane (data not shown). This excluded the possibility that reduced activity of J11 was caused by reduced expression or stability of the protein or its misorientation in the membrane due to changes in topogenic signals. Accordingly, the amino acids Glu341-Glu342 *per se* appear not to be of critical importance, but the presence of negative charges is relevant for full Mrs2p function.

Effects of loss-of-function and gain-of-function mutations on Mg^{2+} influx into isolated mitochondria

Using the Mg^{2+} sensitive dye mag-fura 2 entrapped in isolated mitochondria we have previously shown that free ionized matrix Mg^{2+} ($[Mg^{2+}]_m$) rapidly increases upon elevating the external Mg^{2+} concentration ($[Mg^{2+}]_e$). This increase in $[Mg^{2+}]_m$ essentially has

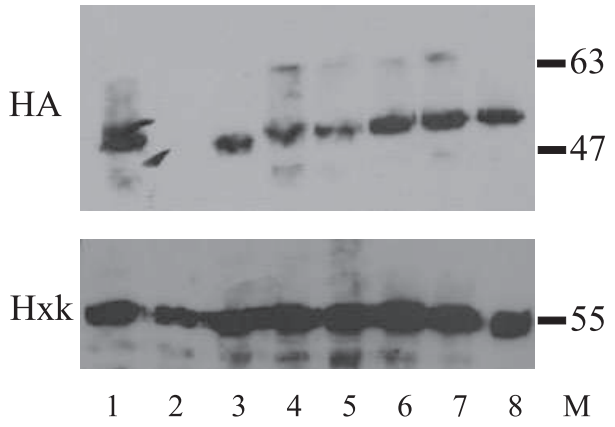

Fig. 5. Western blot analysis of wild-type and mutant Mrs2-HA products. Isolated mitochondria of *mrs2*Δ mutant cells transformed with YEp351 MRS2-HA (lane 1), the empty YEp351 plasmid (lane 2), or the mutant alleles -F2, -J11, -J10, -J4, -J3, -J2 (lane 3–8) were separated by SDS/PAGE and analysed by immunoblotting with an HA or hexokinase antiserum, respectively.

been shown to reflect influx of Mg^{2+} driven by the inside negative membrane potential of mitochondria. Mitochondria of *mrs2*Δ mutant cells were found to lack this rapid increase in $[Mg^{2+}]_m$, while overexpression of Mrs2p considerably stimulated it, but without changing the steady state $[Mg^{2+}]_m$ reached after this rapid influx [7]. We have used this technique to determine changes of Mg^{2+} influx into mitochondria of the mutants described here.

Figure 6A presents results on Mg^{2+} influx into mitochondria mediated by loss-of-function *mrs2* alleles (*mrs2-J2, -J3, -J4*) in an *mrs2*Δ strain. Addition of Mg^{2+} to 1 mM, 3 mM and 9 mM $[Mg^{2+}]_e$ did not result in a rapid, stepwise increase of $[Mg^{2+}]_m$ as it was mediated by wild-type Mrs2p. Instead, $[Mg^{2+}]_m$ increased slowly over extended periods of time and stayed far below values reached by mitochondria expressing wild-type Mrs2p. Values mediated by allele Mrs2-HA-J2 were lowest, and similar to that of mitochondria lacking Mrs2p (*mrs2*Δ mutant). These findings correlate with the growth of cells expressing the loss-of-function alleles in an *mrs2*Δ strain (Fig. 3), since Mrs2-HA-J2 did not support growth, while Mrs2-HA-J3 and Mrs2-HA-J4 did so when expressed from a multicopy vector.

Mitochondria expressing the loop mutant Mrs2-HA-J10 protein expressed in an *mrs2*Δ strain exhibited Mg^{2+} influx and steady state $[Mg^{2+}]_m$ similar to mitochondria expressing the wild-type Mrs2p from the same vector (Fig. 6B). Mitochondria with the loop mutant protein Mrs2-HA-J11 had slightly reduced $[Mg^{2+}]_m$-values at resting condition (nominally Mg^{2+} free). Response to increased $[Mg^{2+}]_e$ was low, and final $[Mg^{2+}]_m$ stayed far below the one observed in wild-type mitochondria. Thus, growth of *mrs2-J10* and *mrs2-J11* mutant cells on nonfermentable substrates (cf. Figure 1) and their capacity of Mg^{2+} influx correlated well.

Mitochondria of all gain-of function mutants showed rapid Mg^{2+} influx essentially like wild-type mitochondria, but with a tendency to last a bit longer and thus to reach moderately elevated $[Mg^{2+}]_m$-values. Two representative curves obtained with mitochondria of the previously isolated mutants *MRS2-M7* and *MRS2-M9* [11] are shown in Fig. 6C. Elevated $[Mg^{2+}]_m$-values were most significant with $[Mg^{2+}]_e$ of 1 mM, which is close to physiological $[Mg^{2+}]$ of the cell cytoplasm, and mitochondria of the gain-of-function mutant showing strongest growth on YPG (*MRS2-M9*) [11] also showed highest steady state $[Mg^{2+}]_m$.

Ariginine rich motif of Mrs2p is not essential for the splicing of group II introns

The crucial role of Mrs2p in splicing of mitochondrial group II introns has been described previously [9,10], and work from this laboratory concluded that it would be carried out indirectly through the establishment of $[Mg^{2+}]_m$ permissive for RNA splicing [7,11]. However, direct interaction of Mrs2p with the intron RNA has also been invoked as contributing to group II intron splicing [10]. These authors noted a C-terminal, matrix-located cluster with a high occurrence of positively charged amino acid residues (residues 400–414), a so-called arginine-rich motif (ARM), and pointed to its possible role as an RNA binding domain [10]. The ARM is not conserved in the F/Y-G-M-N protein family (cf. Figure 1). In this work, we created an *MRS2* mutant named *mrs2-F2,* which lacks the ARM sequence. We expressed this mutant Mrs2 protein from a low-copy (YCp) and a high-copy (YEp) vector in an *mrs2*Δ mutant strain either containing (DBY747 long) or lacking (DBY747 short) mitochondrial group II introns [9]. Mrs2-HA-F2 complemented the *mrs2*Δ strain only poorly when expressed from a YCp vector, but efficiently when overexpressed, indicating that the mutant protein has retained some activity (Fig. 7A). Growth of the *mrs2*Δ cells without and with the mutant Mrs2-F2p expressing plasmid was slightly better in the intron-less background. The amount of Mrs2-HA-F2 protein expressed from a YEp vector (Fig. 5) consistently appeared to be somewhat lower than that of wild-type Mrs2p. Splicing of the mitochondrial group II intron *bI1* in *mrs2*Δ cells expressing Mrs2-HA or Mrs2-HA-F2 from a high-copy vector or a low-copy vector was analysed by RT/PCR involving

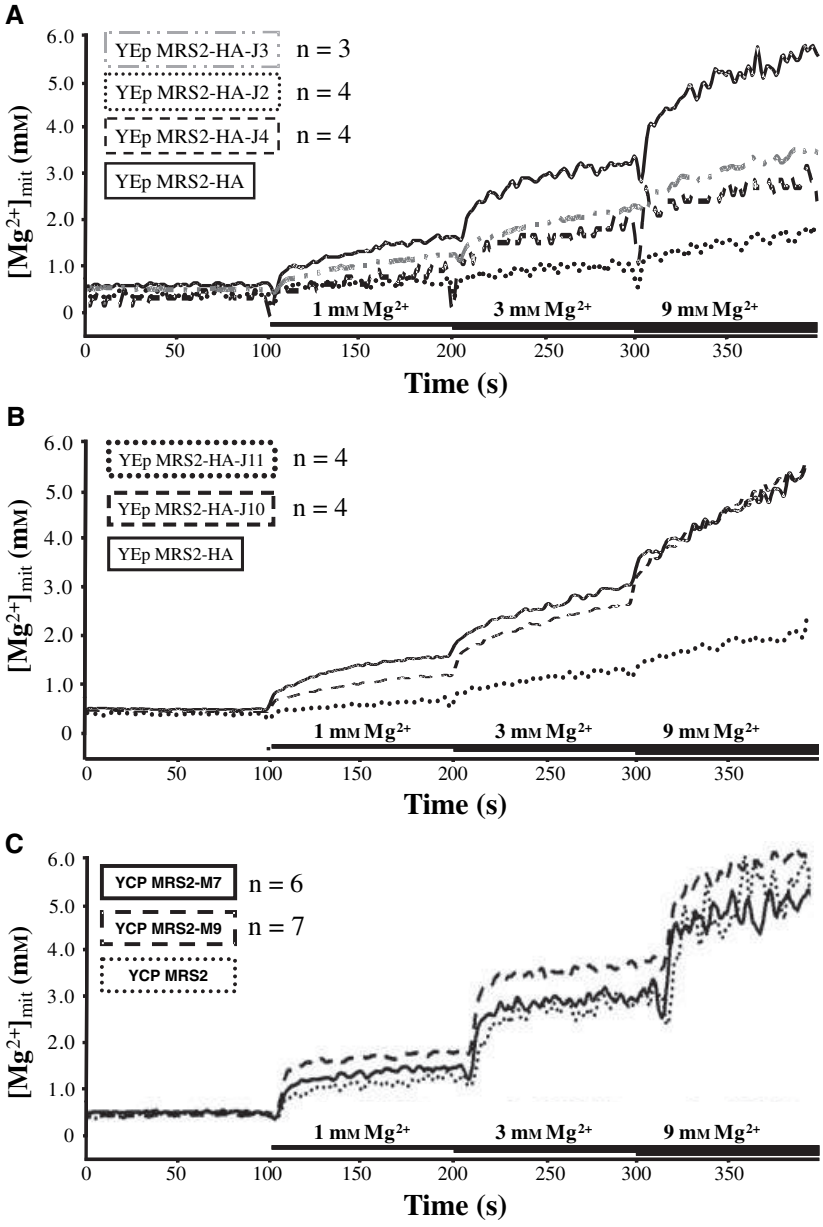

Fig. 6. Mg^{2+} influx into isolated mitochondria with point mutations in the *MRS2* gene. Mutant *mrs2*Δ cells were transformed with wild-type or mutant *MRS2* alleles expressed from YEp351 or YCp33. Isolated mitochondria were loaded with the Mg^{2+} sensitive dye mag-fura 2 and intramitochondrial free Mg^{2+} concentrations $[Mg^{2+}]_m$ were determined in nominally Mg^{2+} free buffer or upon addition of Mg^{2+} to the buffer to final $[Mg^{2+}]_e$ concentrations given in the figures. (A) Loss-of-function mutants *mrs2*-HA-J2, -J3 and -J4 and (B) *mrs2* loop mutants J10 and J11 expressed from the multicopy vector YEp351 in an *mrs2*Δ strain. (C) *MRS2* gain-of-function mutants *MRS2M7* and *-M9* expressed from the low-copy vector YCp33 in an *mrs2*Δ strain. Out of several repeated experiments (numbers given in the figure) representative curves are presented.

three primers, leading to the amplification of cDNAs complementary to pre-mRNA and mRNA [11]. Upon ectopic expression of wild-type Mrs2p, either from a low- or a high-copy vector in *mrs2*Δ cells, cDNAs representing mature mRNA only were detected. In the absence of Mrs2p as well as in the presence of the ARM-deleted Mrs2-HA-F2 protein from a YCp vector we observed abundant RT/PCR products representing pre-mRNA (Fig. 7B). Accordingly, deletion of the ARM motif directly or indirectly resulted in the inhibition of *bI1* RNA splicing. In contrast, upon ectopic expression of the ARM-deleted Mrs2-HA-F2 protein from a YEp vector we observed exclusively cDNA representing mature mRNA, indicating efficient restoration of RNA splicing. We also investigated the influx of Mg^{2+} into mitochondria isolated from *mrs2*Δ cells expressing the Mrs2-HA-F2 mutant protein from a low-copy (YCp) or a multicopy vector (YEp) by using the Mg^{2+} sensitive dye mag-fura 2. Mg^{2+} influx rates and saturation levels upon addition of 1, 3 and 9 mM $[Mg^{2+}]_e$ of mitochondria isolated from *mrs2*Δ mutant cells transformed with MRS2-HA-F2 were in the range of those determined for multicopy expression of wild-type Mrs2p. In contrast, expression of Mrs2-HA-F2 from a low-copy vector did not restore the rapid influx of Mg^{2+} into mitochondria (Fig. 7C).

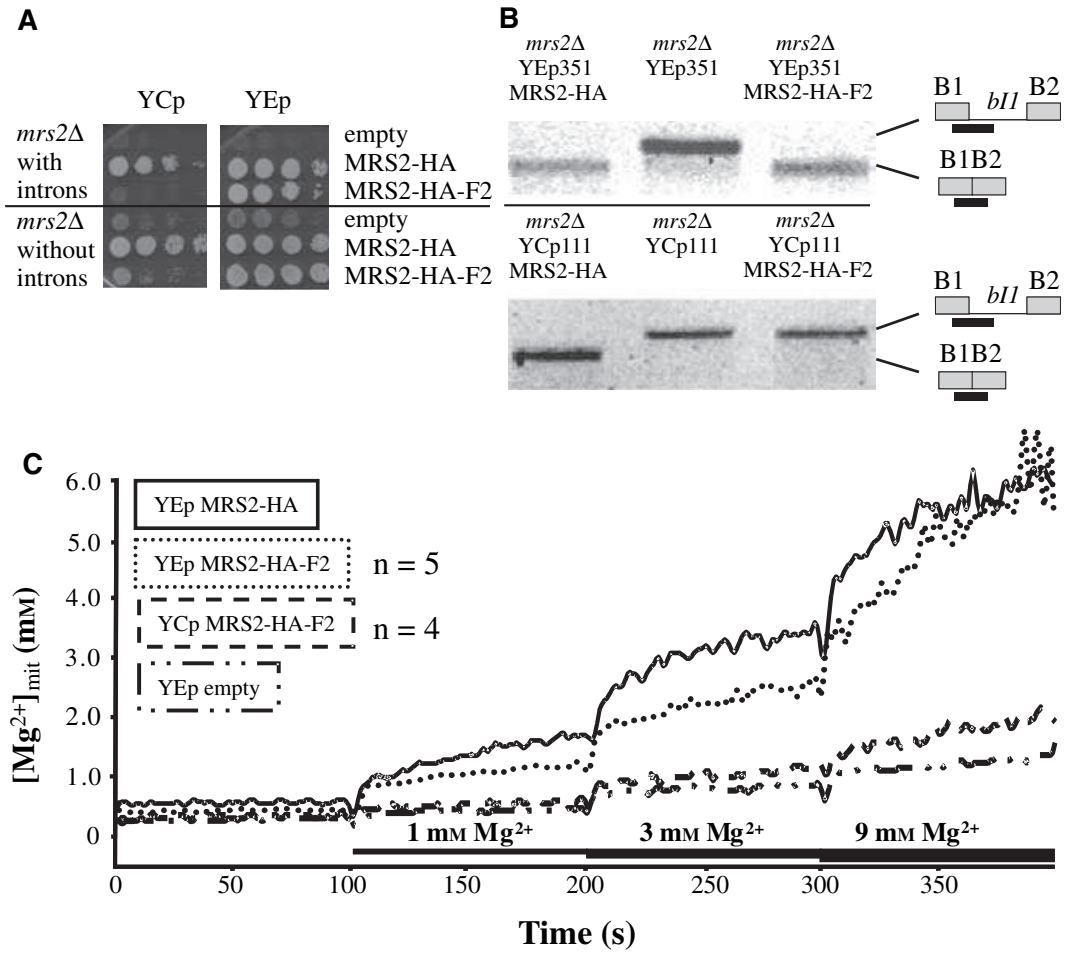

Fig. 7. Phenotypes associated with deletion of arginine-rich motif (ARM) of Mrs2p. (A) Growth phenotypes on nonfermentable media of *S. cerevisiae mrs2*Δ cells with and without mitochondrial introns expressing different *MRS2* alleles. Serial dilutions of yeast cultures were spotted onto YPG media as indicated and grown at 28 °C for 6 days. Strain genotypes are shown on the left, plasmids used are shown above and plasmid-expressed *MRS2* alleles are shown on the right . YCp, low-copy vector YCp111; YEp, high-copy vector YEp351. (B) Splicing of group II intron *bI1* in *S. cerevisiae*. Mitochondrial RNA was isolated from *S. cerevisiae mrs2*Δ cells carrying either an empty vector (YEp351/YCp111) or expressing wild-type MRS2-HA or the MRS2-HA-F2 mutant from the same plasmids. Splicing of group II intron *bI1* was analysed by RT/PCR involving primer pairs amplifying either a 494-bp product or a 404-bp product complementary to the B1–bI1 junction of pre-RNA or B1–B2 mRNA, respectively. (C) Effects on Mg^{2+} influx into isolated mitochondria from *mrs2*Δ mutant cells transformed with YEp351 MRS2-HA, YEp351 MRS2-HA-F2, YCp111 MRS2-HA-F2 or the empty plasmid. Out of several repeated experiments (numbers given in the figure) representative curves are presented.

Taken together, deletion of the ARM motif of Mrs2p led to a significant reduction in Mg^{2+} influx into mitochondria, in RNA splicing and in growth on nonfermentable substrate when the mutant protein was expressed at a low level. Yet overexpression of the Mrs2-HA-F2 protein essentially compensated for its reduced activity.

Discussion

Sequence analysis of Mrs2 homologues from various eukaryotes revealed the presence of stretches with conserved amino acids in the central part of Mrs2 proteins (Fig. 1). We defined five sequence blocks containing various charged amino acid residues (CRB-1–5). Three of them (CRB-3–5) are in the vicinity of two putative coiled-coil domains, which suggests that they may participate together with the coiled-coil domains in folding of the N-terminal half of Mrs2p oligomers.

The functional importance of this central part of Mrs2p is underlined by mutational studies. Mutants selected after random mutagenesis to restore splicing of mitochondrial group II intron splice defects ([10,11]

and this study) all cluster in this part of Mrs2p. Most of these mutations affect sequences of CRBs or sites adjacent to them. Some of them also change the prediction probability for coiled-coils. These point mutations as well as two deletion and insertion mutations in putative coiled-coil sequences (J. Weghuber, R. Schindl, C. Romain & R.J. Schweyen, unpublished data) were found to cause slightly increased steady-state $[Mg^{2+}]_m$. These data thus confirm our previous findings that suppression of group II intron splice defects correlates with a mutational increase in Mrs2p-mediated $[Mg^{2+}]_m$ [7,11].

They further point to a prominent role of the central part of Mrs2p in Mg^{2+} homeostasis control. We propose that the two predicted coiled-coil domains and adjacent conserved sequences either are involved in oligomerization of the Mrs2p channel protein or in forming structures participating in the gating of this channel. Possibly they contribute to both functions. The coiled-coil consensus motif contains charged residues at position *e* and *g* of the heptad repeat [12]. Conserved charged residues right before these domains may be required to initiate formation of coiled-coil structures [13,14]. An apparent feature of Mrs2 proteins is the constant distance between the predicted second coiled-coil domain CC2 and the first transmembrane domain TM-A as well as a considerable degree of sequence conservation in the 20 amino acids separating these two domains. Placed directly at the inner side of the membrane this sequence is expected to be of particular importance for channel function.

It is worth noting that the conserved sequences in the central part of Mrs2p are highly charged. Their vicinity to predicted coiled-coil domains may position them in a way that they can contribute to the formation of higher order structures of the Mrs2p part on the inner side of the membrane, which may contribute to the proposed opening/closing of the channel.

The Mrs2 sequence C-terminal to the TM domains is highly variable in length and lacks obviously conserved primary sequence elements. A generally conserved feature is a surplus of positive charges, which may constitute topogenic signals for the orientation of this part of Mrs2p towards the matrix side of the membrane [15]. Yeast Mrs2p has a particularly long C-terminal sequence (Fig. 1). This includes an ARM, which previously has been invoked to directly interact with Mrs2p in group II intron splicing [10]. But none of the randomly generated gain-of-function mutations, which were selected as suppressing splice defects, affected any sequence in the C-terminal part of Mrs2p [10,11]. Also, mutant mitochondria with a deletion of ARM (MRS2-HA-F2 allele) as studied here showed a correlation between Mg^{2+} steady state levels and group II intron RNA splicing activity. Both activities were considerably reduced when Mrs2-HA-F2 was expressed from a low-copy vector, while they were near normal when expressed from a high copy number vector (Fig. 7B and C). Effects of this deletion on growth of yeast cells were similar in strains containing mitochondrial group II introns and in strains lacking these introns. Accordingly, the ARM deletion has a primary effect on the activity of Mrs2p-mediated Mg^{2+} uptake. The observed correlation between $[Mg^{2+}]_m$ and group II intron splicing is consistent with our notion of a dependence of RNA splicing on $[Mg^{2+}]_m$ [11]. Yet our data do not rigorously exclude a role of the ARM sequence on splicing independent of its role on Mg^{2+} uptake.

Most Mrs2 proteins with experimentally shown Mg^{2+} transport activity have two glutamic acid residues in the short loop connecting the two TM domains (Fig. 1). This loop is supposed to be the only part of the protein located in the intermembrane space and the negative charged residues within this loop were characterized as a topogenic signal for the correct integration of the protein into the inner-mitochondrial membrane [3,8]. Substitution of these glutamic acids by lysines (positively charged) resulted in a complete loss of mitochondrial Mg^{2+} uptake whereas substitution by aspartic acids (negatively charged) had no measurable effect. Although amounts of the mutant proteins were found to be somewhat reduced, its insertion into the inner mitochondrial membrane appeared to be normal indicating that the two Glu residues are not of particular importance for the topology of Mrs2p. Other topogenic signals, e.g. the high positive charge of the C-terminal sequence may suffice to orient Mrs2p in the inner mitochondrial membrane. We propose that the Glu residues in the external loop of Mrs2p are essential to attract positively charged Mg^{2+} ions to the entrance of the Mrs2 channel.

Experimental procedures

Yeast strains, growth media and genetic procedures

The yeast *S. cerevisiae* DBY747 wild-type strain (long/short), the isogenic *mrs2*Δ deletion strain (DBY *mrs2-1*, long/short) and the DBY747 *M1301* strain have been described previously [9,16,17]. Yeast cells were grown in rich medium (yeast extract peptone dextrose, Becton Dickinson Austria GmbH, Schwechat, Austria) with 2% glucose as a carbon source to stationary phase.

Plasmid constructs

The construct YEp351 MRS2-HA [16] was digested with *Pae*I and *Sac*I and the MRS2-HA insert was cloned into an empty YCp111 vector digested with the same enzymes resulting in the construct YCp111 MRS2-HA.

The wild-type *MRS2* gene and *MRS2* gain-of-function mutants (*MRS2-M7* and *MRS2-M9*) expressed from the low-copy vector YCp33 have been previously described [11].

In order to introduce various protein substitutions and deletions of Mrs2p, overlap extension PCR according to Pogulis *et al.* [18] was used. Mutated amino acids, primers, and restriction enzymes for cloning and verification are given in Table 1. No additional mutations were found by sequencing. The constructs expressing mutant Mrs2p variants from the YEp351 vector were cut with *Pae*I and *Sac*I and cloned into an empty YCp111 vector digested with the same enzymes resulting in the constructs YCp111 MRS2-HA-J2, YCp111 MRS2-HA-J3, YCp111 MRS2-HA-J4, YCp111 MRS2-HA-J5, YCp111 MRS2-HA-J6, YCp111 MRS2-HA-J10 and YCp111 MRS2-HA-J11.

To create an in-frame deletion of amino acids 400–414 covering the ARM of Mrs2p, overlap extension PCR using the primer pairs as indicated in Table 1 was performed. The PCR product was cloned via *Xho*I and *Sac*I digestion into the YCp111 MRS2-HA construct leading to YCp111 MRS2-HA-F2. YEp351 MRS2-HA-F2 was generated via *Bsm*I–*Nde*I cloning of the deletion-carrying MRS2-HA-F2 fragment of YCp111 MRS2-HA-F2 into YEp351MRS2-HA. The introduced mutation referred as *mrs2-F2* was verified by restriction analysis and sequencing.

Random PCR mutagenesis

Random mutagenesis of the central part of the *MRS2* gene with the mutagenic forward primer 5′-TACGCGTCGAC AGTATTTTCATCAACGTAATGAGC-3′ and the reverse primer 5′-CCGCCACTGAAGTAAACCCC-3′ was performed with mutagenic PCR using high $MgCl_2$ and $MnCl_2$ according to standard protocols. PCR products were cut with *Sal*I and *Bsm*I and cloned into a *Xho*I and *Bsm*I digested YCp111 MRS2-HA construct. Correctly ligated constructs were identified by deletion of the *Xho*I restriction site of the *MRS2* gene, resulting in a conservative mutation from Glu176 to aspartic acid. A total of 306 constructs identified this were pooled and transformed into the DBY747 M1301 strain. The growth of transformants on nonfermentable glycerol medium detected three mutants with increased suppression of the *M1301* intron mutation, referred as *mrs2-J7* (Glu270 to glycine), *mrs2-J8* (Tyr272 to cysteine) and *mrs2-J9* (Tyr272 to phenylalanine and Leu268 to valine), which were identified by sequencing.

Table 1. Mutated amino acids, primers and restriction enzymes used for cloning and verification. Primer A, 5′-GTTGTCCTCCACCAAGAATAACTCTC-3′; primer B, 5′-CCGCCACTGAAG TAAACCCC-3′; primer C, 5′-GTTGTCCTCCACCAAGAATAACTCTC-3′; primer D, 5′-GACCATGATTACGAATTCGAGCTCG-3′; primer E, 5′-GACCATGATTACGAATTCGAGCTCG-3′.

Name	Bases mutated	Amino acids mutated	Mutagenic forward primer	Mutagenic reverse primer	Forward/ reverse primer	Cloning sites
mrs2-J6	511, 512	Glu171 to Arg	5′-CAAGAATAACTCTCAA TTTTACAGGCATAGAGCCCTCGAAAGT-3′	5′-ACTTTCGAGGGCTCGA TATGCCTGTAAAATTGAGAGTTATTCTTG-3′	A/B	*Pst*I, *Bsm*I; verification: *Xho*I
mrs2-J5	526, 527	Glu176 to Arg	5′-ACGAGCATAGAGCC	5′-CATAACGTTGATGA	A/B	*Pst*I, *Bsm*I; verification: *Psp1406*I
mrs2-J2	730, 732	Asp244 to Lys	CTCAGGAGTATTTTCATCAACGTTATG-3′ 5′-GAGATCCATTAGATGAACTATTAGAAAAC AAAGATGATTTAGCAAACATGTACTTGACA-3′	AAATACTCCTGAGGGCTCTATGCTCGT-3′ 5′-TGTCAAGTACATGTTTGCTAAATCATCTTTGTTT TCTAATAGTTCATCTAATGGATCTC-3′	A/B	*Xho*I, *Bsm*I; verification: *Bgl*II
mrs2-J3	703, 704	Asp235 to Arg	5′-CTTTTTACCAAAA AACTTTATTGATTAGA CGT CTATTAGATGAACTATTAGAAAACGACG-3′	5′-CGTCGTTTTCTAATAGTTCATCTAATAGACGTCT AATCAATAAAGTTTTTTGGTAAAAAAG-3′	A/B	*Xho*I, *Bsm*I; verification: *Bsa*HI
mrs2-J4	517, 518	Arg173 to Glu	5′-ATAACTCTCAATTTTACGAGCATGAAGCCCTC GAAAGTATTTTCATC-3′	5′-GATGAAAATACTTTCGAGGGCTTCATGCTCGTAA AATTGAGAGTTAT-3′	A/B	*Pst*I, *Bsm*I; verification: *Xho*I
mrs2-F2		Deletion 400–414 CAG-3′	5′-GCCCTGACAAATTTG GGAGTGCTACTTTATGGCTG-3′	5′-GTAGCACTCCCAAATTTGTCAGGGCAATAGACG	C/D	*Xho*I, *Sac*I
mrs2-J11	1021, 1024 and 1026	Glu341 + Glu342 to Lys	5′-GCATTTTATGGTATGAATTTAAAGAATTTCATC AAGAAAAGTGAATGGG-3′	5′-CCCATTCACTTTTCTTGATGAAATTCTTTAAAT TCATACCATAAAAATGC-3′	A/E	*Xho*I, *Nde*I; verification: *Bsm*I
mrs2-J10	1023, 1026	Glu341 + Glu342 to Asp	5′-GCATTTTATGGTATGAATTTAAAGAATTTCATC GACGACAGTGAATGGG-3′	5′-CCCATTCACTGTCGTCGATGAAATTCTTTAAATT CATACCATAAAATGC-3′	A/E	*Xho*I, *Nde*I verification: *Bsm*I

RT/PCR assays

Total cellular RNA was isolated by extraction with Total RNA isolation Kit (Promega GmBH, Mannheim, Germany). RT/PCR was performed with 200–300 ng RNA, avian myeloblastosis virus reverse transcriptase and *Tfl* DNA polymerase (Promega) according to the manufacturer's protocol. In order to amplify exon *B1*–exon *B2* and exon *B1*–intron *bI1* junctions of the mitochondrial *COB* transcript, three oligonucleotide primers B1 (5′-AGTGA ATAGTTATATTATTGATTCACC-3′ 5′exon), B2 (5′-AT AACTAGTGCACCTCAATGTGAC-3′ 3′ exon), and bI1 (5′-ATTACTAATAATGCATGTCTAATTAGG-3′, intron bI1) were added simultaneously at concentration of 285 pmol (B1), 6 pmol (B2) and 130 pmol (bI1). Sizes of expected products were 494 bp for the exon–intron junction of pre-mRNA (B1 + bI1) and 404 bp for the exon–exon junction of mRNA (B1 + B2).

Isolation of mitochondria and measurement of $[Mg^{2+}]_m$ by spectrofluorometry

The isolation of mitochondria by differential centrifugation and the ratiometric determination of intramitochondrial Mg^{2+} concentrations ($[Mg^{2+}]_m$) dependent on various external concentrations ($[Mg^{2+}]_e$) has been performed as previously reported [7].

PAGE and western blotting

Mitochondria were isolated from an *mrs2*Δ yeast strain expressing the MRS2-HA, MRS2-HA-J2, F2, J3, J4, J10 or J11 constructs from a YEp351 multicopy vector. Thiry micrograms of mitochondrial preparations were mixed with loading buffer containing β-mercaptoethanol and samples were heated to 80 °C for 4 min before loading on SDS/polyacrylamide gels. Mrs2-HA protein-containing bands were visualized by use of an anti-HA serum (Covance Inc., Princeton, NJ, USA).

Computer analysis

Prediction of coiled-coil regions of Mrs2p and Mrs2 gain-of-function mutants from protein sequence was performed with the COILS program available on http://www.ch.embnet.org. Sequence alignment of various Mrs2 homologues was carried out by using the CLUSTALW program on http://www.ebi.ac.uk/clustalw/.

References

1 Romani AM & Scarpa A (2000) Regulation of cellular magnesium. *Front Biosci* **5**, 720–734.

2 Jung DW, Panzeter E, Baysal K & Brierley GP (1997) On the relationship between matrix free Mg2+ concentration and total Mg2+ in heart mitochondria. *Biochim Biophys Acta* **1320**, 310–320.

3 Bui DM, Gregan J, Jarosch E, Ragnini A & Schweyen RJ (1999) The bacterial magnesium transporter CorA can functionally substitute for its putative homologue Mrs2p in the yeast inner mitochondrial membrane. *J Biol Chem* **274**, 20438–20443.

4 Graschopf A, Stadler J, Hoellerer M, Eder S, Sieghardt M, Kohlwein S & Schweyen RJ (2001) The yeast plasma membrane protein Alr1p controls Mg^{2+} homeostasis and is subject to Mg^{2+} dependent control of its synthesis and degradation. *J Biol Chem* **276**, 16216–16222.

5 Zsurka G, Gregan J & Schweyen RJ (2001) The human mitochondrial Mrs2 protein functionally substitutes for its yeast homologue; a candidate magenesium transporter. *Genomics* **72**, 158–168.

6 Knoop V, Groth-Malonek M, Gebert M, Eifler K & Weyand K (2005) Transport of magnesium and other divalent cations: evolution of the 2-TM-GxN proteins in the MIT superfamily. *Mol Gen Genomics* **23**, 1–12.

7 Kolisek M, Zsurka G, Samaj J, Weghuber J, Schweyen RJ & Schweigel M (2003) Mrs2p is an essential component of the major electrophoretic Mg^{2+} influx system in mitochondria. *EMBO J* **17**, 1235–1244.

8 Baumann F, Neupert W & Herrmann JM (2002) Insertion of bitopic membrane proteins into the inner membrane of mitochondria involves an export step from the matrix. *J Biol Chem* **277**, 21405–21413.

9 Wiesenberger G, Waldherr M & Schweyen RJ (1992) The nucelar gene MRS2 is essential for the excision of group II introns from yeast mitochondrial transcripts in vivo. *J Biol Chem* **267**, 6963–6969.

10 Schmidt U, Maue I, Lehmann K, Belcher SM, Stahl U & Perlman PS (1998) Mutant alleles of the MRS2 gene of yeast nuclear DNA suppress mutations in the catalytic core of a mitochondrial group II intron. *J Mol Biol* **282**, 525–541.

11 Gregan J, Kolisek M & Schweyen RJ (2001) Mitochondrial magnesium homeostasis is critical for group II intron splicing in vivo. *Genes Dev* **15**, 2229–2237.

12 Arndt KM, Pelletier JN, Müller KM, Plückthun A & Alber T (2002) Comparison of in vivo selection and rational design of heterodimeric coiled coils. *Structure* **10**, 1235–1248.

13 Kammerer RA, Schulthess T, Landwehr R, Lustig A, Engel J, Aebi U & Steinmetz MO (1998) An autonomous folding unit mediates the assembly of two-stranded coiled coils. *Proc Natl Acad Sci USA* **95**, 13419–13424.

14 Frank S, Lustig A, Schulthess T, Engel J & Kammerer RA (2000) A distinct seven-residue trigger sequence is indispensable for proper coiled-coil formation of the human macrophage scavenger receptor

oligomerization domain. *J Biol Chem* **275**, 11672–11677.
15 Neupert W (1997) Protein import into mitochondria. *Annu Rev Biochem* **66**, 863–917.
16 Koll H, Schmidt C, Wiesenberger G & Schmelzer C (1987) Three nuclear genes suppress a yeast mitochondrial splice defect when present in high copy number. *Curr Genet* **12**, 503–509.
17 Gregan J, Bui DM, Pillich R, Fink M, Zsurka G & Schweyen RJ (2001) The mitochondrial inner membrane protein Lpe10p, a homologue of Mrs2p, is essential for magnesium homeostasis and group II intron splicing in yeast. *Mol Gen Genet* **264**, 773–781.
18 Pogulis RJ, Vallejo AN & Pease LR (1996) In vitro recombination and mutagenesis by overlap extension PCR. *Methods Mol Biol* **57**, 167–176.

3.3. Publication III:

Effect of mutations in the conserved GMN motif on ion transport and selectivity in the yeast magnesium transporter Mrs2p

Soňa Svidova[1], Gerhard Sponder[1], Muhammad Bashir Khan[3], Rudolf J. Schweyen[1†], Oliviero Carugo[2], Kristina Djinović-Carugo[3,4*]

Manuscript in revision in Biochimica et Biophysica Acta

[1]Department of Microbiology, Immunobiology and Genetics, Max F. Perutz Laboratories, University of Vienna, Vienna, Austria
[2]Department of General Chemistry, University of Pavia, Pavia, Italy
[3]Department of Structural and Computational Biology, Max F. Perutz Laboratories, University of Vienna, Vienna, Austria
[4]Department of Biochemistry, Faculty of Chemistry and Chemical Technology, University of Ljubljana, Ljubljana, Slovenia
[*]Corresponding author

Authors' contributions to the manuscript

As the first author of this article, I prepared the manuscript. I designed the primers and performed the random PCR mutagenesis in the GMN region of ScMrs2, the preliminary screen for viable mutants in bacteria, complementation assays on solid media in bacteria. I cloned the selected mutants into yeast vectors and performed Mg^{2+} uptake measurements in isolated mitochondria and PAGE and western blotting. I analyzed most of the data and merged data for the manuscript.

Effect of mutations in the conserved GMN motif on ion transport and selectivity in the yeast magnesium transporter Mrs2p

Soňa Svidová[1], Gerhard Sponder[1], Muhammad Bashir Khan[3], Rudolf J. Schweyen[1†], Oliviero Carugo[2], Kristina Djinović-Carugo[3,4*]

[1]Department of Microbiology, Immunobiology and Genetics, Max F. Perutz Laboratories, University of Vienna, Vienna, Austria

[2]Department of General Chemistry, University of Pavia, Pavia, Italy

[3]Department of Structural and Computational Biology, Max F. Perutz Laboratories, University of Vienna, Vienna, Austria

[4]Department of Biochemistry, Faculty of Chemistry and Chemical Technology, University of Ljubljana, Ljubljana, Slovenia

*Correspondence address: Campus Vienna Biocenter 5, A-1030 Vienna, Austria

Phone: +43-1-4277-52203/52201

Fax: +43-1-4277-9522

E-mail: kristina.djinovic@univie.ac.at

†Deceased on 15th of February 2009

Abstract

The highly conserved G-M-N motif of the CorA-Mrs2-Alr1 family of Mg^{2+} transporters has been proven to be essential for Mg^{2+} transport. We performed random mutagenesis of the G-M-N motif of *Saccharomyces cerevisiae* Mrs2p, and an unbiased genetic screen. We obtained a large number of mutants still capable of Mg^{2+} transport, albeit below the wild-type level, as assessed by measurements of Mg^{2+} influx into isolated mitochondria. Growth complementation assays in the presence of different concentrations of divalent cations (Ca^{2+}, Co^{2+}, Mn^{2+} and Zn^{2+}), revealed some mutants with reduced growth in the presence of Mn^{2+} and Zn^{2+} ions. We hereby conclude that the G-M-N motif can be partially replaced by certain combinations of amino acids. We show that it plays a role in ion selectivity, together with the flanking negatively charged loop at the entrance of the channel, to which selectivity filter function has primarily been assigned.

Keywords: magnesium transport, Mrs2, G-M-N motif, *Saccharomyces cerevisiae*, mitochondria

1. Introduction

As the most abundant divalent cation within cells, magnesium is required for numerous cellular functions, including coordination to nucleotide triphosphates, membrane stability, regulation of gene transcription, DNA replication, enzyme catalysis, and protein synthesis [1; 2; 3; 4; 5]. Maintenance of Mg^{2+} concentrations within a certain range is therefore critical for cell viability. Cellular membranes are impermeable to divalent cations, which necessitates transmembrane channels or carriers that allow Mg^{2+} to pass through in a controlled manner.

Members of the large, heterogeneous CorA/Mrs2/Alr1 protein superfamily, found in prokaryotes, eukaryotic organisms, as well as in plants are high-affinity Mg^{2+} uptake systems enabling growth of bacterial and yeast cells even in very low external Mg^{2+} concentrations [6; 7; 8; 9; 10; 11]. Mutants lacking these transporters cannot survive without being provided with high external Mg^{2+} concentrations [7; 9; 12].

The *MRS2* gene encodes a 54 kDa integral protein of the inner mitochondrial membrane (Mrs2p). Yeast cells lacking *MRS2* are respiratory deficient and therefore exhibit a growth defect on non-fermentable substrates ("*petite* phenotype") [13; 14; 15]. Besides Mrs2p, *S. cerevisiae* expresses a homologous protein known as Lpe10p/Mfm1p, essential for magnesium homeostasis and group II intron splicing in yeast [16]. Deletion of *LPE10*/*MFM1* also results in a "*petite* phenotype" [17] and in a considerable reduction of the mitochondrial membrane potential ($\Delta\Psi$) [18].

Mrs2p is a distant relative of the bacterial Mg^{2+} transporter CorA, which three-dimensional crystal structure has already been solved [19; 20; 21]. Conservation of the primary sequences in the CorA/Mrs2/Alr1 protein superfamily is in the range of 15-20% [6; 8]. Despite of the low primary sequence homology there are several structurally conserved features, in particular the two α-helices (termed "willow helices") in the large N-terminal part and two trans-membrane helices (TM1, TM2) near the C-terminus

connected by a short conformationally flexible loop (Figure 1) [17]. The sequence G-M-N, a motif at the end of TM1 and the presence of bulky hydrophobic amino acids in the predicted gate region at the intracellular/intramitochondrial end of the pore are the only universally conserved features, indicating an essential role for the function of these proteins [19; 20; 21].

Mrs2p-mediated Mg^{2+} transport has been extensively studied using the Mg^{2+} sensitive, fluorescent dye mag-fura-2, where it was shown that Mrs2p mediates rapid, highly regulated Mg^{2+} uptake into mitochondria [9]. Isolated mitochondria respond within seconds to a rise in the external magnesium concentration with a rapid increase of the mitochondrial free Mg^{2+} concentration (150 µM s^{-1}) [9]. The high conductance of ~150 pS obtained in patch-clamp recordings, characterizes Mrs2p as a channel [22] and preliminary data on the Mrs2p homologue, *Salmonella typhimurium* CorA, suggest a similarly high conductance [23]. The assumption of a common mechanism of Mg^{2+} transport for Mrs2p and CorA is supported by the fact that Mrs2p can be functionally replaced by CorA [17] and *vice versa* (this study). Furthermore, Mg^{2+} transport is in both cases inhibited by cobalt(III)-hexaammine, an analogue for the hydrated Mg^{2+} ion [22; 24; 25].

Mrs2p is able to mediate Ni^{2+} transport, albeit with a 3.5-fold lower conductance (~45 pS) compared to Mg^{2+}, whereas it is not permeable for Ca^{2+}, Mn^{2+} or Co^{2+} [22]. Additionally, suppression of Mg^{2+} currents in the presence of Co^{2+} was observed suggesting Co^{2+} to interact with the pore [22]. This is different to *S. typhimurium* CorA and yeast Alr1p for which transport of Ni^{2+} as well as of Co^{2+} has been reported [6; 24].

The G-M-N motif has been shown to be critical for the function of CorA and even conservative single point mutations completely abolish Mg^{2+} transport [26; 27]. This was also confirmed for Mrs2p where single mutations in the G-M-N motif were introduced [9]. This suggests that this sequence is indispensable for the function, possibly through suitably positioning the

periplasmic loop implicated in initial binding of the hydrated Mg^{2+} [19] and in assisting in the dehydration process [23].

The crystal structure of *Thermotoga maritima* CorA revealed that main-chain carbonyl groups of the G-M-N motif are exposed into the center of the pore entrance on the periplasmic side and form a polar strip suited for interaction with cations [20]. Lunin et al. proposed that the ring of five Asn314 side chains of the G-M-N motif in the CorA pentamer at the periplasmic entrance occlude the pore in the closed state [19].

In order to further investigate the importance and role of the G-M-N motif we performed random PCR mutagenesis on the G-M-N triplet to obtain mutants harbouring all possible amino acid combinations and identified those still capable of transporting Mg^{2+}. The active mutants were further characterized using *in vivo* and *in vitro* studies showing that the G-M-N motif can be in part functionally replaced by certain combinations of amino acids. Our results corroborate the notion that this motif plays an important role in ion selectivity.

2. Materials and Methods

2.1 Yeast and bacterial strains, growth media and genetic procedures

2.1.1 Bacterial cells

Escherichia coli DH10B F^- endA1 recA1 galE15 galK16 nupG rpsL ΔlacX74 Φ80lacZΔM15 araD139 Δ(ara,leu)7697 mcrA Δ(mrr-hsdRMS-mcrBC) λ^-

Salmonella enterica serovar Typhimurium transmitter strain LB5010: metA22 metE551 ilv-452 leu-3121 trpC2 xyl-404 galE856 hsdL6 hsdSA29 hsdSB121 rpsL120 H1-b H2-e, n, x flaA66 nml (-) Fel-2(-).

Salmonella enterica serovar Typhimurium strain MM281 DEL485 (leuBCD)mgtB::MudJ;mgtA21::MudJ;corA45::mudJ;zjh1628::Tn10(cam).

Cam^R, Kan^R, Mg^{2+} dependent) was kindly provided by M.E. Maguire. It lacks all three major magnesium transport systems *CorA, MgtA* and *MgtB* and therefore requires medium containing Mg^{2+} concentrations in the millimolar range.

Salmonella enterica serovar Typhimurium strain MM 1927 DEL485 (leuBCD);mgtB::MudJ;mgtA21::MudJ;corA45::mudJ;zjh1628::Tn10(cam) CamR, Kan^R, pALTER-CorA (AmpR).

Strains were grown in LB medium (1% tryptone, 0.5% yeast extract, 1% NaCl) with ampicillin (100 µg/ml). MM281 required addition of 10 mM $MgCl_2$. LB plates contained 2% Difco Agar Noble minimizing possible Mg contamination.

2.1.2 Yeast cells

The yeast *S. cerevisiae* DBY747 *mrs2*Δ deletion strain (DBY mrs2-1, short) has been described previously [13; 14; 15]. Yeast cells were grown in rich medium (1% yeast extract, 2% peptone) with 2% glucose as a carbon source (YPD) [11].

2.1.3 Plasmid constructs

The construct YEp351 MRS2-HA was described previously [17].

For cloning of *MRS2* into the vector pGEX-3X with IPTG-inducible promoter the primers M2GEXfw: 5'-CGCGGATCCCCAATCGGCGTCTCCTGG-3' and MRS2HiXrev: 5'-TGCTCTAGATCAATGGTGATGGTGATGG-3' were used. The resulting PCR fragment was cloned into the vector via BamHI and XbaI restriction sites.

2.1.4 Random PCR mutagenesis

In order to introduce various amino acid substitutions in Mrs2p, overlap extension PCR according to Pogulis et al. [28] was used. No additional mutations were found by sequencing.

Random mutagenesis of the GMN motif of *MRS2* was performed with the mutagenic forward primer 5'-GCATCTGTTCTGCCGGCGTTCTATNNNNNNNNNTTAAAGAATTTCATCGAGGAGAGTG -3' and the reverse primer 5'-CACTCTCCTCGATGAAATTCTTTAANNNNNNNNNATAGAACGCCGGCAGAACAGATGC -3' according to standard protocols.

PCR products were digested with XhoI and EcoRI and cloned into an XhoI and EcoRI digested pGEX-MRS2 construct. For transformation into the DH10B *Escherichia coli* strain standard calcium chloride method was used. Correctly ligated constructs were identified by deletion of the BsmI restriction site of the *MRS2* gene, resulting in a silent mutation from an adenine to a guanine.

2.2 Identification of tolerated substitutions

A total of 45,600 constructs were pooled and transformed into the *S. typhimurium* transmitter strain LB5010. A total of 46,848 construct were pooled and transformed into the *S. typhimurium* strain MM281, plated on LB plates supplemented with 10 mM $MgCl_2$ and replicaplated on LB plates containing 0.05 mM IPTG to induce protein expression. 49 mutants able to grow on this medium were sequenced. No additional mutations were found by sequencing.

2.3 Serial dilutions

For serial dilutions on plates, cells were grown in liquid LB medium containing 10 mM $MgCl_2$ at 37℃ over night, washed twice with LB medium, ad justed to an A_{600} of 1 and diluted to an A_{600} 0.1, 0.01 and 0.001. Serial dilutions were spotted onto LB medium plates containing different concentrations of $MgCl_2$, IPTG, $MnCl_2$ or $ZnCl_2$ and incubated for 24 h.

2.4 Isolation of mitochondria and measurement of changes in the intramitochondrial Mg^{2+} concentrations by spectrofluorimetry

Isolation of mitochondria by differential centrifugation and ratiometric determination of intramitochondrial Mg^{2+} concentrations ($[Mg^{2+}]_m$) dependent

on various external concentrations ($[Mg^{2+}]_e$) was performed as previously reported [9].

3. Results and discussion

3.1 Screening of triple G-M-N mutants

According to the studies of Szegedy and Maguire [26] and of Kolisek et al. [9], single amino acid substitutions in the G-M-N motif of CorA or Mrs2p are sufficient to abolish Mg^{2+} transport. Since single conservative mutations in the G-M-N motif are poorly tolerated, we performed a triple site random mutagenesis screen in order to address the question whether any other amino acid combination can substitute for this unique and universally conserved motif.

Since large-scale isolation of mitochondria from yeast is extremely time consuming and thus not suitable for high throughput analyses, we decided to develop a bacterial system for screening for functional G-M-N mutants. Based on the fact, that Mrs2p can be functionally replaced by its bacterial homologue CorA [17], we assumed that Mrs2p expressed in the *S. typhimurium* strain MM281 depleted of all major Mg^{2+} transport systems (CorA, MgtA and MgtB), could complement the Mg^{2+} transport deficiency. *S. typhimurium* strain MM1927 lacking the magnesium uptake systems MgtA and MgtB and over-expressing only CorA was used as the positive control. As depicted in Figure 2, growth of MM281 cells was only supported at a high magnesium concentration of 10 mM. MM281 cells expressing Mrs2p virtually grew like MM1927 also without addition of external $MgCl_2$. This experiment clearly proved the ability of Mrs2p to complement the *corAΔmgtAΔmgtBΔ* induced Mg^{2+} deficiency of strain MM281 and enabled us to investigate our G-M-N mutants of Mrs2p in bacteria.

After transforming the mutant library into strain MM281**,** we replicaplated the transformants on LB plates without additional Mg^{2+} but

supplemented with 0.05 mM IPTG to induce protein expression. These conditions restrict growth exclusively to mutants still able to transport Mg^{2+}.

We obtained a considerable amount of mutants able to grow without additional Mg^{2+} supplementation. 62 mutants were sequenced, 7 of which contained the G-M-N motif itself (showing the functional dominance of this sequence), while 55 contained mutations of the G-M-N motif, 6 of which appeared twice, resulting in 9 different mutations. These 49 mutants were analyzed further using a growth complementation assay on plates supplemented with different IPTG concentrations to investigate, how their Mg^{2+} transport ability differs from wild-type Mrs2p. The assays were scored with four symbols “+” for cells able to grow at all four dilution steps, while “-” represents no growth at all on the plate (Tab. 1).

Bacterial cells transformed with wild-type *MRS2* were able to grow on plates with only 0.03 mM IPTG. In contrast, the analyzed mutants exhibited only poor growth at this IPTG concentration or did not grow at all. Upon stronger expression (IPTG concentrations of 0.035 – 0.05 mM) viability and growth of most of the mutants improved (Tab. 1). These results indicate that several G-M-N triple mutants still exhibited Mg^{2+} transport albeit at lower efficiency than wild-type Mrs2p.

3.2 Sequences of the functional mutants

The prominent feature of the amino acid sequences of the functional mutants is their divergence from the canonical G-M-N motif. A glycine at the first position is observed only twice (4%), a methionine appears twice (4%) at the second position, and in only one case there is an asparagine at the third position. The only mutant resembling the wild type protein is characterized by the presence of a G-T-N tripeptide instead of G-M-N.

Interestingly, about 80% of the functional mutants have a positively charged residue at the G-M-N motif. In 59% of the cases this occurs at the first position, in 18% of the cases at the second position, and only in 4% of the cases at the third position. However, the co-presence of two positively

charged amino acids is uncommon (only in about 10% of the cases). There is only one evident correlation between two positions: in the 59% of the cases in which the first position is occupied by a positively charged residue, a small and hydrophobic amino acid (Val, Ile or Leu) occupies the third position.

In contrast, few negatively charged residues are observed in the functional mutants, i.e. only six times at the first position and twice at the other two positions. No other clear trends were observed.

In a previous mutation analysis of the G-M-N motif of *S. typhimurium* CorA, none, even the most conservative single mutations (A-M-N, G-A-N, G-C-N, G-I-N, G-M-A, G-M-L, G-M-Q) were tolerated [26]. A mutational study of Mrs2p performed by Kolisek et al. [9] also confirmed the importance of the G-M-N motif: mutation to A-M-N reduced Mg^{2+} uptake to the level of the *mrs2*Δ mutant. These findings are in agreement with our results, as neither these mutants nor any other single point mutation - with the exception of the rather poorly growing G-T-N mutant - were found amongst the functional mutants, which are notably diverse from the native motif G-M-N. It might be hypothesised that while single mutations within the canonical G-M-N motif are evolutionary not tolerated by Nature, multiple adjacent mutations, though unlikely to occur in Nature, result in functional molecules.

3.3 The effect of mutations of the G-M-N sequence on cation selectivity of Mrs2p

We performed a growth complementation assay on plates containing 0.05 mM IPTG and different concentrations of divalent cations (Ca^{2+}, Co^{2+}, Mn^{2+} and Zn^{2+}), known substrates of the yeast plasma membrane Mg^{2+} uptake system Alr1p, a homologue of Mrs2p [29]. We selected 10 mutants for this assay (Tab. 2, 3), in which we examined if the presence of the aforementioned divalent cations in the growth medium influenced cell growth compared to wild-type Mrs2p.

Seven of the chosen mutants had a positively charged amino acid (K, R, H) at the first position and a small, hydrophobic residue at the third position (like 35% of the mutants of Table 1). The last three mutants did not fit in the pattern “positively charged – X – hydrophobic”, and were chosen as representatives of well (R-A-W), medium (R-R-T) and poorly (R-V-H) complementing mutant variants.

In case of Ca^{2+} and Co^{2+} we did not observe any difference (results not shown) in the growth complementation assay compared to plates not supplemented with cations, suggesting that no transport or blockage of the channel by these ions occurred. In a study employing patch clamp electrophysiology on giant lipid vesicles fused with inner-mitochondrial membranes, Mrs2p was permeable for Mg^{2+} and Ni^{2+} but not for Ca^{2+}, Mn^{2+} or Co^{2+}. However, suppression of Mg^{2+} currents in the presence of Co^{2+} was observed [22]. In our case no effect of Co^{2+} was observed, both on wild-type Mrs2p and on the investigated mutants. This might be due to different techniques used: patch-clamp recordings on single ion channels allow very precise measurements of the ion currents and tight control of ionic conditions on both sides of the channel which is not possible in a growth complementation assay on plates. Furthermore, ion concentrations used in the patch-clamp experiments were much higher (~ 1000x in this case) than concentrations used *in vivo,* and as a consequence*,* we cannot properly compare the results of the growth complementation assay and the patch-clamping experiments.

The tested concentrations of $MnCl_2$ reduced growth of all mutants, whereas growth of cells harboring wild-type *MRS2* remained unaffected. The negative effect of $MnCl_2$ increased with increasing concentrations of the cation (Table 2). Furthermore, the growth defect was differently pronounced in the mutants: the top three least affected are characterized by positively charged residues at the first and the second position (K-R-L; R-R-T), while the two most affected mutants carry Arg at the first, and Leu at the third position (R-Q-L; R-V-L) (Table 2).

The effect of $ZnCl_2$ was similar to $MnCl_2$, however the growth defect of the mutants was slightly less pronounced (Table 3). The three least affected and the two most affected mutants were the same as those identified in the Mn^{2+} assay.

The R-V-H, R-A-W and R-R-T mutants do not significantly differ from the “positively charged - X - hydrophobic” set, suggesting that the absence of a hydrophobic amino acid at the third position does not critically affect ion selectivity, when combined with a small hydrophobic or positively charged residue on the second place.

Amongst the reasons for the manganese and zinc dependent negative effects on growth complementation assays, it is possible to hypothesize that both Mn^{2+} and Zn^{2+} either cross the channel and enter into the cells or block the entrance of the pore, stopping the flux of Mg^{2+}. Both explanations might be coherent with the experimental observation that increasing cation concentrations correlate with negative effects on cell growth. However, it is impossible to determine exactly the underlying mechanism of the negative effects, given the comparable ionic radii of Mg^{2+}, Mn^{2+} and Zn^{2+} (0.72 Å, 0.82 Å, 0.75 Å, respectively) and the consequent similarity between the hexa-aquaions [30]. It is on the other hand clear that Mn^{2+} and Zn^{2+} did not affect growth of cells hosting wild type Mrs2, suggesting that the G-M-N motif is involved in ion selectivity.

Apart from the size of the hydrated and non-hydrated ions, the water exchange rate of the hydrated ion appears to be an important parameter for the transport activity of the channel. Mg^{2+} has a very slow water exchange rate of 10^5 s^{-1} compared to Mn^{2+} and Zn^{2+} for which exchange rates are at least one to two orders of magnitude higher [31]. The incoming Mg^{2+} ion has to be at least partially dehydrated to enter the channel. The sequence G-M-N and the loop residues might generate a unique structural environment specially suited for the interaction and dehydration of Mg^{2+}. Consequently, alterations of the G-M-N motif could lead to a more or less productive

interaction with ions different from Mg^{2+} and thereby alter the selectivity of the channel.

3.4 Mg^{2+} influx into isolated mitochondria

In order to directly investigate Mg^{2+} influx into isolated mitochondria of selected mutants we used the Mg^{2+}-sensitive dye mag-fura-2 (Figure 3). The mutants were selected on the basis of good (R-M-V, R-F-V, R-C-V), medium (R-Q-L) or poor (R-V-H) growth complementation capacity in *S. typhimurium* strain MM281 (Table 1). After addition of $MgCl_2$ to a concentration of 1 mM Mg^{2+} a lack of the characteristic rapid Mg^{2+} influx [9] was observed in most mutants, together with significantly lower steady-state Mg^{2+} levels (Figure 3). The only exception was the R-Q-L mutant, which lacked rapid Mg^{2+}influx, but finally reached a mitochondrial Mg^{2+} concentration comparable to the wild-type level during the subsequent 100 seconds. After addition of $MgCl_2$ to the final concentration of 3 mM Mg^{2+}, we observed Mg^{2+} influx in all mutants, however, it did not reach the final steady-state level of wild-type Mrs2p. The differences between mutants were minimal, with the exception of the R-Q-L mutant**,** which reached almost wild-type Mg^{2+} levels. At the same time this mutant was found amongst the variants exhibiting the strongest growth reduction on plates supplemented with Mn^{2+} and Zn^{2+}. This mutation strongly affected ion selectivity but at the same time had only a minor effect on the conductivity of the channel for Mg^{2+}, implying that ion conduction and ion selectivity are two independent processes.

These results show that all investigated mutants maintained a certain ability to transport Mg^{2+} in *S. typhimurium* cells (Table 1) and mutants R-V-H, R-M-V, R-F-V, R-C-V and R-Q-L also in yeast mitochondria (Figure 3), albeit in both systems the transport activity was significantly decreased compared to the wild type protein.

4. Conclusions

The asparagine residues of the G-M-N motif have been proposed to block the entrance of the channel in the closed conformation [19; 23]. Furthermore, this

motif has been implicated in suitably orienting the flexible, negatively charged loop at the mouth of the pore for interaction with the hydrated magnesium ion. The loop connecting TM1 and TM2 appears to form the initial interaction site for hydrated Mg^{2+} and likely participates in the dehydration process of the ion required prior to its entrance into the pore of the channel [23]. The high conductance of Mrs2p [22] and CorA [23] channels were proposed to be based on a mechanism which involves electrostatic interactions of the loop residues with the hydration shell of Mg^{2+} and not with the ion itself [23].

Our study on the G-M-N motif identified viable triple mutants hosting a positively charged residue primarily on the first but also on the third position. At a first glance, the presence of positively charged residues in functional mutants might seem counterintuitive as these mutations could in fact hinder the transport of Mg^{2+} ions by electrostatic repulsion. However, since it is structurally unfeasible for all three amino acid residues of the motif to be in direct contact with the ion [27], it is plausible to envisage that these residues form a structural motif critical for ion uptake, which can be partially accomplished by different amino acid combinations, eventually leading to a functionally equivalent structure.

In order to assess the impact of mutations in the G-M-N motif on the selectivity of Mrs2p, we performed growth complementation assays on plates supplemented with different cations (Ca^{2+}, Co^{2+}, Mn^{2+} and Zn^{2+}). Our results show that mutations in the G-M-N motif lead to reduced growth of the cells in presence of Mn^{2+} and Zn^{2+} while Ca^{2+} and Co^{2+} did not influence their viability. This can take place *via* two possible competitive mechanisms: (i) Mn^{2+} and Zn^{2+} are transported through the pore and the growth defect is caused by Mn^{2+}/Zn^{2+} overdose, or (ii) Mn^{2+} and Zn^{2+} ions are trapped and block the channel for Mg^{2+} transport causing in this way the growth defect by Mg^{2+} deficiency.

In summary we conclude that despite its high degree of conservation, the G-M-N motif can be functionally replaced by certain combinations of amino acid residues. Most frequently a positively charged residue in the first

and a hydrophobic residue in the third position were found in functional mutants. Our studies suggest that the G-M-N motif plays a role in ion selectivity, being therefore part of the selectivity filter together with the flanking negatively charged loop, at the entrance of the Mrs2p channel. The concurrent involvement of the G-M-N motif in the gating process and in ion selectivity as well, might be the molecular basis for its universal conservation throughout the phyla.

5. Acknowledgements

We thank Michael Maguire (Case Western Reserve University) for providing the *Salmonella typhimurium* strains MM281. We thank Elisabeth Froschauer (Max F. Perutz Laboratories, Univ. Vienna, Austria) for fruitful discussions. Rainer Schindl, Julian Weghuber and Christoph Romanin (Univ. Linz, Austria) are kindly acknowledged for critical reading of the manuscript.MBK, GS, SS were recipients of a PhD fellowship from FWF (P20141) and from WWTF (LS05021). MBK was partially supported by the University of Vienna funds. The BIN-III initiative of the Austrian GEN-AU for financial support is acknowledged.

6. **References**

[1] J.A. Cowan, Metallobiochemistry of magnesium. Coordination complexes with biological substrates: site specificity, kinetics and thermodynamics of binding, and implications for activity. Inorg. Chem. 30 (1991) 2740- 2747.

[2] J.A. Cowan, Metal Activation of Enzymes in Nucleic Acid Biochemistry. Chem Rev 98 (1998) 1067-1088.

[3] J.A. Cowan, T. Ohyama, K. Howard, J.W. Rausch, S.M. Cowan, and S.F. Le Grice, Metal-ion stoichiometry of the HIV-1 RT ribonuclease H domain: evidence for two mutually exclusive sites leads to new mechanistic insights on metal-mediated hydrolysis in nucleic acid biochemistry. J Biol Inorg Chem 5 (2000) 67-74.

[4] C.E. Dann, 3rd, C.A. Wakeman, C.L. Sieling, S.C. Baker, I. Irnov, and W.C. Winkler, Structure and mechanism of a metal-sensing regulatory RNA. Cell 130 (2007) 878-92.

[5] G.J. Quigley, M.M. Teeter, and A. Rich, Structural analysis of spermine and magnesium ion binding to yeast phenylalanine transfer RNA. Proc Natl Acad Sci U S A 75 (1978) 64-8.

[6] R.C. Gardner, Genes for magnesium transport. Curr Opin Plant Biol 6 (2003) 263-7.

[7] A. Graschopf, J.A. Stadler, M.K. Hoellerer, S. Eder, M. Sieghardt, S.D. Kohlwein, and R.J. Schweyen, The yeast plasma membrane protein Alr1 controls Mg2+ homeostasis and is subject to Mg2+-dependent control of its synthesis and degradation. J Biol Chem 276 (2001) 16216-22.

[8] V. Knoop, M. Groth-Malonek, M. Gebert, K. Eifler, and K. Weyand, Transport of magnesium and other divalent cations: evolution of the 2-TM-GxN proteins in the MIT superfamily. Mol Genet Genomics 274 (2005) 205-16.

[9] M. Kolisek, G. Zsurka, J. Samaj, J. Weghuber, R.J. Schweyen, and M. Schweigel, Mrs2p is an essential component of the major electrophoretic Mg2+ influx system in mitochondria. EMBO J 22 (2003) 1235-44.

[10] M. Wachek, M.C. Aichinger, J.A. Stadler, R.J. Schweyen, and A. Graschopf, Oligomerization of the Mg2+-transport proteins Alr1p and Alr2p in yeast plasma membrane. FEBS J 273 (2006) 4236-49.

[11] J. Weghuber, F. Dieterich, E.M. Froschauer, S. Svidova, and R.J. Schweyen, Mutational analysis of functional domains in Mrs2p, the mitochondrial Mg2+ channel protein of Saccharomyces cerevisiae. FEBS J 273 (2006) 1198-209.

[12] S.P. Hmiel, M.D. Snavely, J.B. Florer, M.E. Maguire, and C.G. Miller, Magnesium transport in Salmonella typhimurium: genetic characterization and cloning of three magnesium transport loci. J Bacteriol 171 (1989) 4742-51.

[13] H. Koll, C. Schmidt, G. Wiesenberger, and C. Schmelzer, Three nuclear genes suppress a yeast mitochondrial splice defect when present in high copy number. Curr Genet 12 (1987) 503-9.

[14] G. Wiesenberger, M. Waldherr, and R.J. Schweyen, The nuclear gene MRS2 is essential for the excision of group II introns from yeast mitochondrial transcripts in vivo. J Biol Chem 267 (1992) 6963-9.

[15] J. Gregan, M. Kolisek, and R.J. Schweyen, Mitochondrial Mg(2+) homeostasis is critical for group II intron splicing in vivo. Genes Dev 15 (2001) 2229-37.

[16] J. Gregan, D.M. Bui, R. Pillich, M. Fink, G. Zsurka, and R.J. Schweyen, The mitochondrial inner membrane protein Lpe10p, a homologue of Mrs2p, is essential for magnesium homeostasis and group II intron splicing in yeast. Mol Gen Genet 264 (2001) 773-81.

[17] D.M. Bui, J. Gregan, E. Jarosch, A. Ragnini, and R.J. Schweyen, The bacterial magnesium transporter CorA can functionally substitute for its putative homologue Mrs2p in the yeast inner mitochondrial membrane. J Biol Chem 274 (1999) 20438-43.

[18] G. Sponder, S. Svidova, R. Schindl, S. Wieser, R.J. Schweyen, C. Romanin, E.M. Froschauer, and J. Weghuber, Lpe10p modulates the activity of the Mrs2p-based yeast mitochondrial Mg2+ channel. FEBS J 277 3514-25.
[19] V.V. Lunin, E. Dobrovetsky, G. Khutoreskaya, R. Zhang, A. Joachimiak, D.A. Doyle, A. Bochkarev, M.E. Maguire, A.M. Edwards, and C.M. Koth, Crystal structure of the CorA Mg2+ transporter. Nature 440 (2006) 833-7.
[20] S. Eshaghi, D. Niegowski, A. Kohl, D. Martinez Molina, S.A. Lesley, and P. Nordlund, Crystal structure of a divalent metal ion transporter CorA at 2.9 angstrom resolution. Science 313 (2006) 354-7.
[21] J. Payandeh, and E.F. Pai, A structural basis for Mg2+ homeostasis and the CorA translocation cycle. EMBO J 25 (2006) 3762-73.
[22] R. Schindl, J. Weghuber, C. Romanin, and R.J. Schweyen, Mrs2p forms a high conductance Mg2+ selective channel in mitochondria. Biophys J 93 (2007) 3872-83.
[23] A.S. Moomaw, and M.E. Maguire, Cation selectivity by the CorA Mg2+ channel requires a fully hydrated cation. Biochemistry 49 5998-6008.
[24] R.L. Smith, and M.E. Maguire, Microbial magnesium transport: unusual transporters searching for identity. Mol Microbiol 28 (1998) 217-26.
[25] L.M. Kucharski, W.J. Lubbe, and M.E. Maguire, Cation hexaammines are selective and potent inhibitors of the CorA magnesium transport system. J Biol Chem 275 (2000) 16767-73.
[26] M.A. Szegedy, and M.E. Maguire, The CorA Mg(2+) transport protein of Salmonella typhimurium. Mutagenesis of conserved residues in the second membrane domain. J Biol Chem 274 (1999) 36973-9.
[27] J. Payandeh, C. Li, M. Ramjeesingh, E. Poduch, C.E. Bear, and E.F. Pai, Probing structure-function relationships and gating mechanisms in the CorA Mg2+ transport system. J Biol Chem 283 (2008) 11721-33.
[28] R.J. Pogulis, A.N. Vallejo, and L.R. Pease, In vitro recombination and mutagenesis by overlap extension PCR. Methods Mol Biol 57 (1996) 167-76.
[29] C.W. MacDiarmid, and R.C. Gardner, Overexpression of the Saccharomyces cerevisiae magnesium transport system confers resistance to aluminum ion. J Biol Chem 273 (1998) 1727-32.
[30] R.D. Shannon, Revised Effective Ionic Radii and Systematic Studies of Interatomic Distances in Halides and Chalcogenides.
Acta Crystallographica A32 (1976) 751-76.
[31] M.E. H. Diebler, G. Ilgenfritz, G. Maab, R. Winkler, Kinetics and Mechanism of Reactions of Main Group Metal Ions with Biological Carriers. Appl. Chem.
20 (1969) 93-115.

Table 1

S. typhimurium strain MM281 was transformed with plasmids indicated, serially diluted and replicaplated on plates with increasing IPTG concentrations. The number of "+" symbols corresponds to the number of dilution steps exhibiting growth.

Sequence	0.03 mM IPTG	0.035 mM IPTG	0.04 mM IPTG	0.045 mM IPTG	0.05 mM IPTG
G-M-N	++++	++++	++++	++++	++++
R-F-V*	+	++++	++++	++++	++++
R-I-L	+	++++	++++	++++	++++
R-M-V	+	++++	++++	++++	++++
R-Q-I	+	++++	++++	++++	++++
R-Q-L*	+	++++	++++	++++	++++
R-V-L*	+	++++	++++	++++	++++
L-R-C	++	+++	+++	++++	++++
R-A-W	+	++++	+++	++++	++++
R-V-M	+	++++	+++	++++	++++
I-R-I	++	+++	++	++++	++++
K-A-I	-	++++	+++	++++	++++
K-R-L	-	++++	+++	++++	++++
R-F-I	+	++++	+++	++++	+++
R-V-I	+	++++	+++	++++	+++
R-N-L	-	+++	+++	++++	++++
R-P-L	+	+++	+++	++++	+++
C-F-L	++	++	++	+++	++++
R-G-F	+	+++	+++	+++	+++
R-S-V	+	+++	+++	++++	++
R-C-V	-	++	++	++++	++++
F-R-L*	+	++	++	+++	+++
D-F-G	+	++	+	+++	+++
K-A-M	-	++	++	+++	+++
R-F-Y	+	++	++	+++	++
R-R-T	-	++	++	+++	+++
V-R-A	+	++	++	++	+++
V-R-C	+	++	++	++	+++
D-F-P*	+	++	+	++	+++
E-F-P	+	++	++	++	++
K-H-V	-	++	++	+++	++
E-Q-V	+	++	+	++	++
G-D-M	+	++	+	++	++
K-Y-I	-	++	++	++	++
R-T-Y	-	++	++	++	++
E-F-A	+	+	+	++	++
G-T-N	+	+	+	++	++
K-M-L	-	++	+	++	++
P-D-L*	-	+	++	++	++
R-F-Q	-	++	+	++	++
R-V-H	-	+	+	+++	++
R-Y-S	-	++	++	++	+
R-F-S	-	+	+	++	++
T-S-E	+	+	+	+	++
E-S-K	-	+	+	++	+
F-R-E	-	+	+	++	+
K-I-T	-	+	+	++	+
P-N-V	-	+	+	+	+
P-R-L	-	+	+	+	+
P-T-L	-	-	-	+	+

* Mutants which appeared two times.

Table 2

S. typhimurium strain MM281 was transformed with plasmids indicated, serially diluted and replicaplated on plates with 0.05 mM IPTG and different $MnCl_2$ concentrations. The number of "+" symbols corresponds to the number of dilution steps exhibiting growth.

Sequence	0 mM $MnCl_2$	0.01 mM $MnCl_2$	0.1 mM $MnCl_2$
G-M-N	++++	++++	++++
K-R-L	++++	+++	++
R-A-W	++++	+++	++
R-R-T	+++	+++	++
K-A-I	++++	++	+
R-M-V	++++	++	+
R-C-V	++++	+	+
R-F-V	++++	+	+
R-Q-L	++++	+	+
R-V-L	++++	+	+
R-V-H	++	++	+

Table 3

S. typhimurium strain MM281 was transformed with plasmids indicated, serially diluted and replicaplated on plates with 0.05 mM IPTG and different $ZnCl_2$ concentrations. The number of "+" symbols corresponds to the number of dilution steps exhibiting growth.

Sequence	0 $ZnCl_2$	0.01 mM $ZnCl_2$	0.1 mM $ZnCl_2$
-	-	-	-
G-M-N	++++	++++	+++
K-R-L	++++	+++	++
R-R-T	+++	+++	++
R-A-W	++++	++	+
K-A-I	++++	++	+
R-C-V	++++	++	+
R-F-V	++++	++	+
R-M-V	++++	++	+
R-Q-L	++++	++	+
R-V-L	++++	++	+
R-V-H	++	++	++

Figure 1 Schematic representation of the Mrs2p pentamer.
Position of the G-M-N motif at the end of the TM1 helix is marked, together with TM1 and N- and C- termini of subunits. Flexible loop connecting TM1 and TM2 is depicted in red.

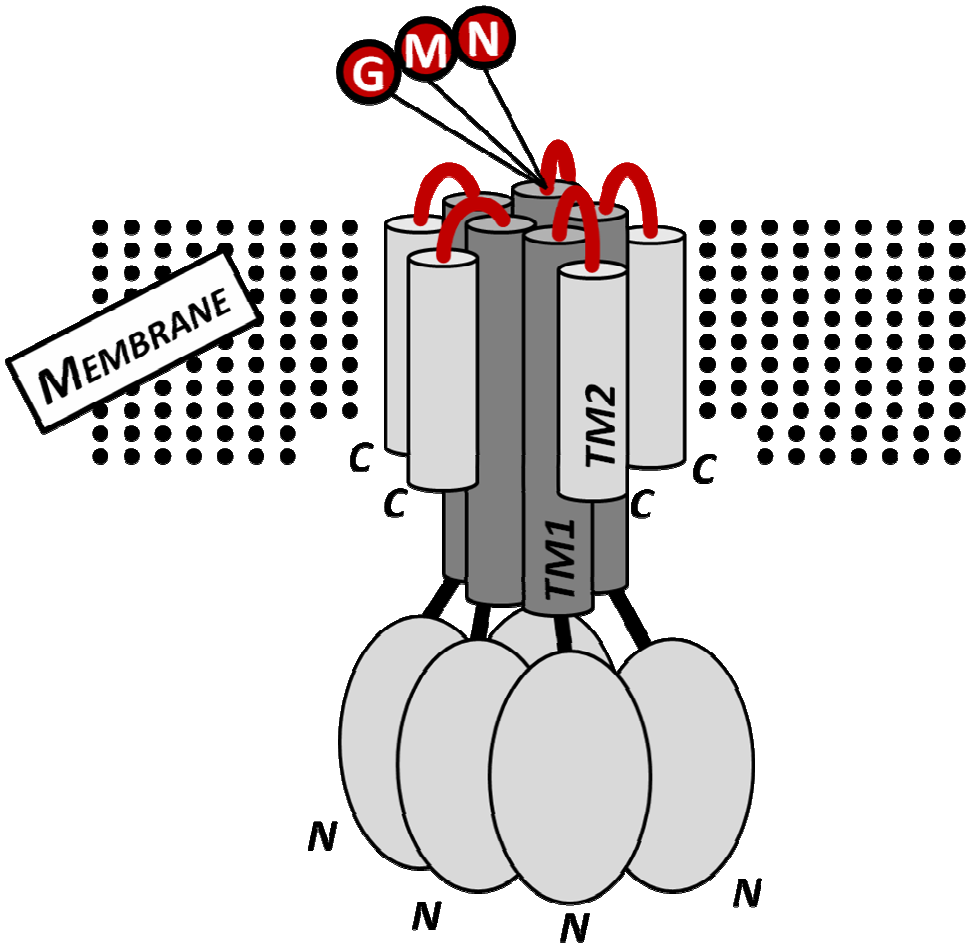

Figure 2 Growth complementation assay of the MM281 mutant strain by Mrs2p. Over night cultures of MM1927 and MM281 were transformed with plasmids indicated, serially diluted and spotted on LB medium plates with 10 mM magnesium chloride or 0.05 mM and 0.025 mM IPTG concentrations and incubated on 37℃ for 24 hours.

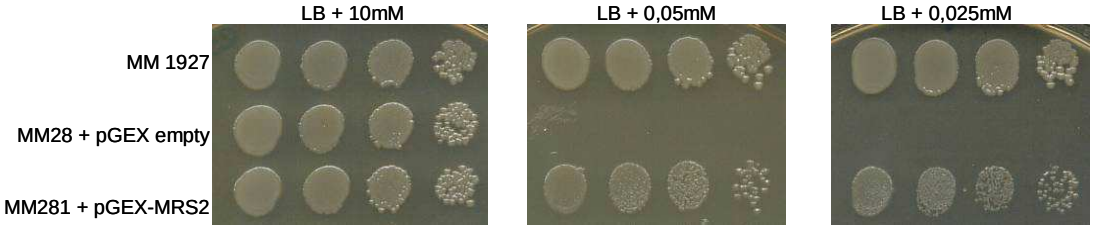

Figure 3 Representative recordings of [Mg^{2+}] uptake.
S. cerevisiae strain DBY747 *mrs2*Δ was transformed with the indicated plasmids and mitochondria were isolated. The representative recordings show changes in fluorescence intensity of mag-fura-2 monitored over 300 seconds after step-wise addition of $MgCl_2$.

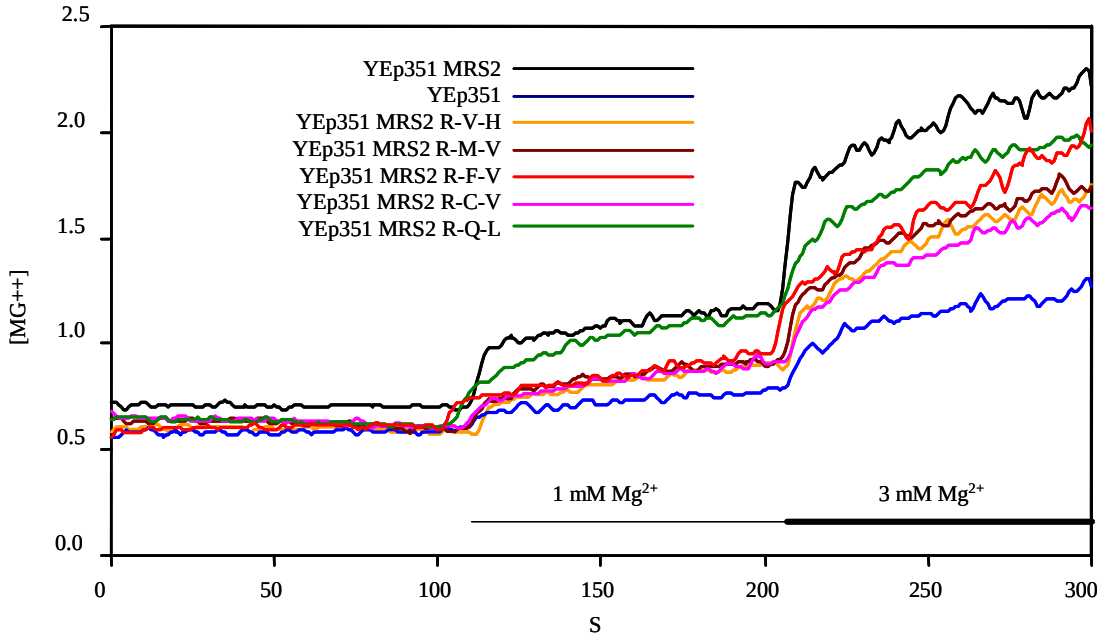

3.4. Publication IV

Structural and Functional Characterization of the N-Terminal Moiety of Yeast Mg^{2+} Transporter Mrs2

Muhammad Bashir Khan[1], Gerhard Sponder[2], Björn Sjöblom[1], Soňa Svidová[2], Rudolf J. Schweyen[2†], Oliviero Carugo[3], and Kristina Djinović-Carugo[1,4,*]

Manuscript in preparation for Journal of Molecular Biology

[1]Department for Structural and Computational Biology, Max F. Perutz Laboratories, University of Vienna, Vienna, Austria

[2]Department of Microbiology, Immunobiology and Genetics, Max F. Perutz Laboratories, University of Vienna, Vienna, Austria

[3]Department of Chemistry, University of Pavia, Pavia, Italy

[4]Department of Biochemistry, Faculty of Chemistry and Chemical Technology, University of Ljubljana, Ljubljana, Slovenia

[*]Corresponding author

Authors' contributions to the manuscript

I designed the primers for the mutational analysis of ScMrs2, performed the site-directed mutagenesis, clone the mutants into yeast vectors and took part on the Mg^{2+} uptake measurements in isolated mitochondria.

Structural and Functional Characterization of the N-Terminal Moiety of Yeast Mg^{2+} Transporter Mrs2

Muhammad Bashir Khan[1], Gerhard Sponder[2], Björn Sjöblom[1], Soňa Svidová[2], Rudolf J. Schweyen[2†], Oliviero Carugo[3], and Kristina Djinović-Carugo[1,4,*]

[1]Department for Structural and Computational Biology, Max F. Perutz Laboratories, University of Vienna, Vienna, Austria

[2]Department of Microbiology, Immunobiology and Genetics, Max F. Perutz Laboratories, University of Vienna, Vienna, Austria

[3]Department of Chemistry, University of Pavia, Pavia, Italy

[4]Department of Biochemistry, Faculty of Chemistry and Chemical Technology, University of Ljubljana, Ljubljana, Slovenia

*Correspondence e-mail: kristina.djinovic@univie.ac.at

† Deceased in February 2009

ABSTRACT

Eukaryotic Mrs2 transporters are distantly related to the major bacterial Mg^{2+} transporter CorA and the eukaryotic Alr1, located in the plasma membranes of lower eukaryotes. All Mrs2 proteins are functional pentamers composed of large soluble N-terminal domains and 2 adjacent transmembrane helices, followed by a variable C-terminal region. Here we report a functional and structural analysis of the regulatory N-terminal domain of Mrs2 from the inner mitochondrial membrane of *Saccharomyces cerevisiae* by crystallography, genetics, biochemistry and fluorescence spectroscopy. By analytical gel filtration and dynamic light scattering, the N-terminal domain of Mrs2 forms a homopentamer in low-salt solutions. Structural analysis showed that the fold of the N-terminal domain bears differences compared with the prokaryotic CorA counterpart, and suggested residues that form hydrophobic gates and the putative magnesium sensing site**.** Functional analysis of the candidate gating mutants in isolated mitochondria confirmed the involvement of the identified amino acids in gating. We further functionally examined the exceptionally long C-terminus of *S. cerevisiae* Mrs2, in particular, a positively charged stretch in the C-terminal region concerning its function in the transporter regulation.

Keywords: amino-terminal domain / structural biology / eukaryotic magnesium transporter / hydrophobic gates / Mrs2

\body

Magnesium ion, Mg^{2+}, is essential for many biochemical processes and remains the only major biological ion whose mechanism of transport is still not fully understood. It is present at 15–25 mM in prokaryotic and mammalian cells (1-3). Mg^{2} mediates the stabilization of macromolecules during binding to nucleotides and is a cofactor for many enzymes. By regulating the activities of ion channels and transporters, Mg^{2+} also influences cell volume and signalling processes (2, 3). In the cytosol, the majority of Mg^{2+} is bound to adenosine-5'-triphosphate (ATP) and other phosphonucleotides. In all cells, Mg^{2+} is an essential structural element for ribosomes and membranes. In prokaryotes, Mg^{2+} is an important regulatory signal that is essential for virulence (1, 4-6). Balancing Mg^{2+} levels is vital for normal cellular function. Homeostasis is maintained by a delicate balance of transport activities across the plasma and organelle membranes.

The CorA family mediates Mg^{2+} uptake in most prokaryotes and is the most extensively studied set of magnesium transporters. Mrs2 family of transporters constitute the major mitochondrial Mg^{2+} uptake system in yeast, plants, and mammals (7-10) and are essential for mitochondrial biogenesis (11). Mrs2 transporters are distantly related to the CorA, as well as to the Alr1 family, which is restricted to lower eukaryotes where it forms the principal Mg^{2+} uptake system in the plasma membrane. Although the sequences of the CorA-Mrs2-Alr1 superfamily are extremely divergent, they appear to exploit the membrane potential in driving Mg^{2+} uptake (8, 12). Furthermore, some of these transporters can partially functionally replace each other, which strongly suggests that they are homologues (7, 9, 13, 14).

3 crystal structures (at 2.9, 3.7, and 3.9 Å resolution) (1, 6, 15) of *Thermatoga maritima* CorA (Tm-CorA) and the structure of the soluble cytoplasmic domain of the *Vibrio parahemolyticus* zinc transporter ZntB (Vp-ZntB) (at 1.9 Å resolution) have revealed homopentameric assemblies (16). The subunits are composed of 2 transmembrane α-helices (TM1, TM2) and an

intracellular N-terminal moiety that forms a funnel in the functional pentamer. Two divalent cation sensing (DCS) sites that regulate the opening and closing of the transporter have been mapped to the N-terminal domain of CorA (1, 6, 15, 17).

The cation selectivity of CorA and Mrs2 is attributed to the signature motif G-M-N (18, 19), that lies at the end of the TM1 α-helix at the outer surface of the membrane. Together with the successive negatively charged loop, the G-M-N motif has been implicated in the binding and dehydration of magnesium hexaaqua ions (1, 6, 15). Residue Asn314 of the G-M-N motif at the external entrance to the pore and a pair of hydrophobic rings that are formed by Met291 and Leu294 were hypothesized to be involved the gating of the channel (1, 6, 15). It has been recently reported by Yu Xia et al. that Tm-CorA preferentially transports Co^{2+} and not Mg^{2+} (20).

Mechanisms by which the conductance of the bacterial transporter Tm-CorA is regulated have been proposed (1, 6, 15, 17): in the absence of sufficient intracellular Mg^{2+} levels, Mg^{2+} ions bound between monomers are released, causing the N-terminal domains of the protomers to move as a rigid body, whereas the willow helices (2 antiparallel helices at the N-terminus) rearrange with respect to each other and relative to the stalk helix (the pore-forming helix). These actions create a torque along the stalk helix. The torque propagates to the hydrophobic gates (Met291 and Leu294) and activates the periplasmic gate residue Asn314 through interaction of the cytoplasmic N-terminus (acidic residues) and the positively charged C-terminal basic sphincter. This activation impinges on the Asn314 residue through movement of TM2 and the MPEL motif (in the loop that connects TM1 and TM2), allowing Mg^{2+} ion to flow through (1, 17).

The low sequence homology between eukaryotic Mrs2 transporters and the prokaryotic Tm-CorA transporter, or any other protein with a known structure,

renders it difficult to infer structure and function of Mrs2 accurately based on prokaryotic homologues. Here we report the crystal structure of the N-terminal domain of the yeast (*Saccharomyces cerevisiae*) mitochondrial magnesium transporter Mrs2 at 1.28 Å resolution and functional characterization of selected residues that are critical for magnesium transport.

RESULTS AND DISCUSSION

Ionic strength modulates oligomeric state of $Mrs2_{48-308}$

Based on our study (21), we designed a stable Mrs2 construct (48–308), denoted $Mrs2_{48-308}$ (this construct was termed $Mrs2_{16-276}$ in our previous publication, wherein the mitochondrial targeting sequence was not included in the numbering), which included the entire regulatory N-terminal domain of Mrs2. By analytical size exclusion chromatography, $Mrs2_{48-308}$ behaves as a monomer in high-ionic-strength buffers and as a homopentamer in low-ionic-strength buffers (Figure S1). The circular dichroism (CD) spectrum of $Mrs2_{48-308}$ showed minima at 208 and 219 nm, typical for a protein that is rich in α-helices (Figure S2).

Dynamic light scattering (DLS) was used to assess the monodispersity of the protein in solution: a monomodal distribution with a polydispersity of 5% was observed, and the gyration radius was estimated to be 4.2 nm in high-ionic-strength buffers. Under low-ionic-strength conditions, the protein solution exhibited polydispersity of about 25% and a radius of gyration of 14 nm, which are consistent with the analytical size exclusion chromatography findings. These data suggest that our construct is autonomously folded into the native conformation in solution and that the protein solution is monomeric at high ionic strengths and pentameric at low ionic strengths.

Overall structure of $Mrs2_{48-308}$ versus those of prokaryotic magnesium and zinc transporters

A monomer of $Mrs2_{48-308}$ was crystallized in the orthorhombic space group $P2_12_12_1$, and its structure solved by experimental phasing, exploiting the anomalous signals of sulphur (21). The overall organizations of prokaryotic (Tm-CorA) and eukaryotic ($Mrs2_{48-308}$) magnesium transporters are similar (Figure 1C and D). Each subunit can be divided into an N-terminal alpha/beta domain that is followed by an alpha domain. Whereas the former is a compact alpha-beta-alpha sandwich, the latter forms a triple coiled-coil, the end of which enters the membrane with a TM helix (Figure 1C).

While the coiled-coil domains in Tm-CorA and $Mrs2_{48-308}$ are nearly identical, the N-terminal domains differ notably (Figure 1C and D). The central beta sheet is formed by 7 strands in Tm-CorA versus 6 strands in $Mrs2_{48-308}$. Whereas the last 4 strands (termed C1–C4 in the Figure 1D) are topologically identical in both proteins and form a series of 3 beta hairpins, the first 2 beta strands differ topologically. The alpha helix that follows the N2 strand, and the entire N3 strand are missing in $Mrs2_{48-308}$, rendering the eukaryotic protein smaller than its prokaryotic counterpart. Although this disparity appears to have arisen due to deletion during molecular evolution, we cannot reject other hypotheses. However, it is clear that any structural alignments of these structural moieties will be misleading, because Tm-CorA and Mrs2 adopt different folds.

The relatively long α5 and α6 helices, which extend toward the membrane, are called ‘willow’ helices in Tm-CorA, “as they hang down like the branches of a weeping willow tree” and harbor many glutamic and aspartic acid residues in the tip region (1). For $Mrs2_{48-308,}$ α5 and α6, corresponding to the willow helices of Tm-CorA, contain 3 acidic residues compared with 10 in Tm-CorA. In Tm-CorA, there is also an extended loop between C2 and C3 that protrudes like the willow helices toward the membrane surface. The tip of this loop in Tm-CorA has a very high density of aspartic and glutamic acid residues (22). In contrast, the C2 and

C3 strands of $Mrs2_{48-308}$ are shorter, and the loop that intercalates between them does not protrude toward the willow helices nor does it harbour any acidic residues (Figure 1C and D).

To determine the structural neighbours of $Mrs2_{48-308}$, we used the web-based Dali server (23), which identified the following structures that had Z-scores greater than 9: (i) *Thermotoga maritima* divalent metal ion transporter Tm-CorA (PDB code 2IUB); (ii) *Vibrio parahaemolyticus RIMD* cytoplasmic domain of zinc transporter Vp-ZntB (PDB code 3CK6); (iii) *Dictyostelium discoideum* STAT protein, (PDB code 1UUS); and (iv) *Escherichia coli* Pore-forming toxins (PDB code 2WCD). The latter two hits clearly have molecular functions different from Mrs2 and CorA. All of these structures have low sequence similarity with *S. cerevisiae* Mrs2, and only the metal ion transporter Tm-CorA was identified in a BLAST search (24) against the Mrs2 sequence.

Detailed structural comparisons (Text S1) clearly demonstrates that the prokaryotic proteins Tm-CorA and Vp-TntB are structurally more similar to each other than to the eukaryotic protein $Mrs2_{48-308}$. Vp-ZntB also contains a mixed 7-stranded beta-sheet that is clearly similar to that of Tm-CorA but differs from the 6-stranded sheet of $Mrs2_{48-308}$. Moreover, we hypothesize that the structural variability between the 3 proteins is related to the different states (open/closed) of the ion channel/transporter, which are reflected in the reorientation of the coiled-coil moiety (see below) and influenced by cation concentrations.

A structure-based sequence alignment (SBSA) (manually corrected) between $Mrs2_{48-308}$ and Tm-CorA together with the analysis of the Mrs2 pentamer model identified important residues involved in the formation of hydrophobic gates and in propagation of magnesium across the ion conduction pathway in Mrs2-type transporters (Figure 1B).

Model of $Mrs2_{48-308}$ funnel

To generate a model of the pentameric funnel from the monomeric $Mrs2_{48-308}$ structure, we superimposed $Mrs2_{48-308}$ onto the helical domains of Tm-CorA and Vp-ZntB. The maximum diameter of the funnel, based on Tm-CorA is 106 Å, and the residues at the C-terminus of the stalk helix (forming the wall of the funnel) clash at the tips (Figure 2C and D). This phenomenon might be attributed to the structure of Tm-CorA, which has been reported in a closed conformation, whereas monomeric $Mrs2_{48-308}$ is more relaxed and might reflect an open conformation of the transporter.

In a functional pentamer, each protomer makes contacts with 2 adjacent molecules. Our structural analysis of the $Mrs2_{48-308}$ funnel model, based on the Tm-CorA structure, shows 5 hydrogen bonding interactions and 1 salt bridge. The residues involved in the formation of the salt bridge are Glu295 of one and Lys291 of an adjacent protomer. The interacting residues belong to the α7 stalk helix of a subunit, the α7 stalk helix of the adjacent subunit, and the tip of the α5 and α6 willow helices.

Conversely, the funnel model that is based on Vp-ZntB has a maximum diameter of 102 Å and reveals no clash of the C-termini - further evidence that the Vp-ZntB is likely in an open conformation. A structural analysis of the funnel model of $Mrs2_{48-308}$ shows that the interface between the α7 stalk helix of a protomer and the α5 and α6 willow helices of an adjacent protomer, comprises 2 hydrogen bonds and 1 salt bridge. The residues involved in the formation of the salt bridge are Lys221 of a protomer and Glu205 of an adjacent protomer.

In contrast, there are 8 hydrogen bonds and 8 salt bridges in the funnel domain of the Vp-ZntB (PDB code 3CK6) transporter and 16 hydrogen bonds and 15 salt bridges in Tm-CorA (PDB code 2BBJ). Although the stereochemistry of the interface of the $Mrs2_{48-308}$ funnel was not optimized, the presence of remarkably fewer hydrogen bonds and salt bridges compared with Tm-CorA and

Vp-ZntB might explain the higher sensitivity of $Mrs2_{48-308}$ to elevated salt concentrations.

Analysis of the electrostatic surface potential of the structure of $Mrs2_{48-308}$ showed that the α7 helices, forming the inner wall of the pentameric funnel, are lined along their lengths with negatively charged or hydroxyl-bearing residues (Figure 2A and B). Such an arrangement exists in other monovalent cation (KcsA) and divalent cation (CorA, ZntB) channels and were proposed to constitute an electrostatic sink that increases local ion concentrations (25).

Putative magnesium-sensing sites in Mrs2

Two divalent cation binding sites - termed “divalent cation sensor” (DCS) sites - have been identified at the protomer-protomer interface in the funnel of Tm-CorA (1, 6, 15, 17). Whereas the first binds cations directly through the 2 carboxylates of Asp89 and Asp253, the second, comprising Glu88, Asp175, Asp253, and His257, binds them indirectly by coordinating hydrated metal cations. According to a model of the regulation of Tm-CorA, a torque is generated at the bottom of the stalk helix (α7) by releasing bound magnesium from magnesium-binding sites and propagates toward the hydrophobic gate (1, 6, 15, 17).

Based on a structural comparison between Tm-CorA and our model of the $Mrs2_{48-308}$ funnel, we identified the candidate the amino acid residues that could form a DCS site in Mrs2 that corresponds to DSC1 of Tm-CorA: Asp97 from one subunit and Glu270 from an adjacent subunit (Figure 2C and D, Figure 3D). By sequence alignment of eukaryotic Mrs2 homologues, Asp97 and Glu270 are highly conserved throughout the entire family, and equivalent residues exist in the prokaryotic CorA family (Figure 1B). In $Mrs2_{48-308}$, Glu270 lies in the N-terminus of α7, corresponding to Asp253 in Tm-CorA (Figure 3A and C); Asp97 is located in the α3 helix, corresponding to Asp89 of Tm-CorA (Figure 3A and B). In this structural analysis, we could not confidently identify the residues that constitute the second DCS site.

In the initial crystallization conditions of $Mrs2_{48-308}$ no magnesium was present, but we obtained crystals with 1.5 mM magnesium chloride and 1.5 mM cobalt chloride. The structures of $Mrs2_{48-308}$ in magnesium, cobalt, and nickel-soaked crystals and magnesium and cobalt co-crystals did not reveal bound metal ions and were essentially identical to the native crystal structure in the absence of exogenous divalent cations, showing that the addition of magnesium in the crystal environment did not change the structure of the native protein. The absence of cations bound to the monomeric $Mrs2_{48-308}$ is in agreement with the notion that the DCSs are composed of ligands from adjacent subunits in the pentamer, implying that a single subunit cannot bind divalent ions with high affinity.

Effect of metal ions on protease susceptibility of pentameric $Mrs2_{48-308}$

Payandeh at al. showed that cations in the protomer interface stabilize Tm-CorA but are not required to maintain its pentameric state (Payandeh & Pai, 2006). Furthermore, they demonstrated that Tm-CorA becomes resistant to trypsin in a divalent cation-dependent manner, wherein the presence of ions renders the conformation trypsin-resistant, presumably reflecting the closed state of the channel. To determine whether $Mrs2_{48-308}$ undergoes conformational changes in function of divalent cations, we performed the protease susceptibility assay in the presence and absence of magnesium and cobalt ions.

Prior to this experiment, $Mrs2_{48-308}$ was dialyzed against a low-ionic-strength buffer to induce the formation of functional pentamers and subsequently incubated with various concentrations of magnesium, cobalt, EDTA and trypsin. In the presence of EDTA, the protein was protected from protease digestion. Conversely, only high concentrations of cobalt rendered $Mrs2_{48-308}$ less susceptible to trypsin cleavage, whereas the presence of magnesium did not, irrespective of incubation time (Figure S4). The reactions were performed at 4°C and 37°C for 4 and 15 hours.

These results suggest that Mrs2 adopts 2 distinct conformations in a magnesium-dependent manner, wherein the closed conformation (in the presence of magnesium) appears to be more susceptible to protease cleavage compared to the open conformation (in the presence of EDTA). This differential susceptibility compared with Tm-CorA implicates distinct conformations and distinct conformational changes in the N-terminal domains of the 2 types of transporters. Differences between the folds of the 2 domains might explain the varying responses and patterns with regard to protease susceptibility.

Hydrophobic gates in Mrs2

In Tm-CorA Met291 and Leu294 form the main hydrophobic gates by creating a strong energetic barrier to ion permeation (1, 26). The gate residues in Tm-CorA are positioned at the membrane/cytoplasmic interface, with Met291 being cytoplasmic and Leu294 membrane embedded (1).

As no 3-dimensional structure of full-length Mrs2 is available, we generated the Mrs2 pentamer, including the transmembrane helices, starting from the funnel model and extended the sequence in the alignment and in the model (by homology modelling) to the C-terminal TM1 and TM2 α-helices. Inspection of sequence alignment (Figure 1B) showed that eukaryotic magnesium transporters consistently display a three amino acid insertion after position corresponding to Met291 in prokaryotic transporters, extending in this way the helix α7.

In searching for gating residues in Mrs2 corresponding to Met291 and Leu294 in Tm-CorA, we imposed 2 criteria: (i) involvement in formation of a constriction in the pore; (ii) mitochondrial matrix location for the first gating residue and membrane embedded location for the second position.

By analysis of the pentameric Mrs2 model, the narrowest constriction of the pore lay at residue Met309 (Figure 3F), corresponding to the hydrophobic

gate residue Met291 in Tm-CorA (Figure 3E). By TMpred analysis (Online server Prediction of Transmembrane Regions and Orientation http://www.ch.embnet.org/software/TMPRED_form.html) of the primary sequence of *S. cerevisiae* Mrs2, the first transmembrane helix comprises residues Val315 to Leu336, while Met309 is predicted to be located in the matrix. Further, by sequence alignment of members of the eukaryotic Mrs2 family, Met309 is highly conserved (Figure 1B), and we named it Gate 1.

The second narrowest opening, which we termed Gate 2, occurred at Val315, corresponding to Leu294 in Tm-CorA (Figure 3E and F). TMpred analysis predicts Val315 to be in a transmembrane helix. Sequence alignment of eukaryotic Mrs2 homologues revealed that Val315 is less conserved than Met309, with the bulkier phenylalanine and smaller valine present in some sequences (Figure 1B).

Functional analysis of selected mutants

To validate the candidate residues that were identified in our structural analysis to be involved in magnesium sensing and the formation of hydrophobic gates, we performed a functional and mutational analysis of these residues. Further, we examined the role of positively charged residues at the C-terminus in transport activity and regulation of Mrs2.

DCS mutants

According to our structural analysis, Asp89 and Asp253, which form the primary cation-sensing site in Tm-CorA, in Mrs2 correspond to Asp97 and Glu270 in Mrs2. In Tm-Cor, mutations in the first DCS site alter the transport of Mg^{2+} by Tm-CorA (17).

To assay the function of Asp97 in the regulation of the transporter, we performed site-directed mutagenesis, changing Asp97 to Ala, Phe, and Trp. We intentionally did not choose a positively charged mutation, because Payandeh et

al reported that salt bridge across the first DCS site can partially maintain TmCorA in a closed or inactive conformation (17). The resulting mutants expressed in *S. cerevisiae,* did not exhibit notable growth defects on non-fermentable carbon sources (Figure 4A). Accordingly, no significant differences in Mg^{2+} uptake between wild-type Mrs2 and the mutant proteins in isolated mitochondria were observed (Figure 4B).

Based on the high conservation of Asp97 throughout the Mrs2 subfamily, the lack of effect is noteworthy and implies that the sensing of magnesium, which is exerted by several residues in the two DCS sites cannot be abrogated by a mutation of a single residue in Mrs2. Large hydrophobic residues at the Asp97 location were predicted to disrupt metal binding as well as to perturb domain closure or packing within the funnel. The weak effect of bulky amino acid residue on growth on non-fermentable carbon sources may be explained by local structural rearrangements, allowing for conformational changes upon transporter closure.

Gating mutants

The candidate Gate 1 and 2 residues (Met309 and Val315) were mutated to 3 amino acids with disparate properties with regard to size and charge - the small glycine, the negatively charged glutamic acid, and the bulky phenylalanine. The effects of these mutations were monitored by growth complementation assays and using mag-fura-2 measurements of Mg^{2+} influx into mitochondria.

Deletion of *MRS2* causes a growth defect on non-fermentable carbon sources and abolishes Mg^{2+} influx into mitochondria (8, 27). Strain DBY747 *mrs2*Δ was transformed with the high-copy number vector YEp351 or with the centromeric plasmid YCp22, harbouring the mutated *MRS2* variants, and as controls, the wild-type *MRS2* and the empty vector. In growth tests, all 3 mutations at Met309 location impaired growth on non-fermentable carbon sources, indicating that they had a considerable effect on magnesium

homeostasis in mitochondria. The Met309Gly mutant had the most dramatic effect (Figure 5A, B).

The greatest decrease in magnesium uptake was observed in the Met309Phe variant (Figure 5B), which is attributed to its bulky side chain, narrowing the pore at this position. The Met309Gly mutant effected the highest degree of deregulation with regard to the gating of the channel. The exchange of Met309 for Gly resulted in a considerably stronger influx compared with the wild-type protein and significantly elevated the final steady-state magnesium concentrations (Figure 5B). Particularly strong uptake was observed after the initial addition of magnesium, and plateau levels were less pronounced compared with the wild-type control (Figure 5B). The transporter was able to close the ion conduction pathway to a limited extent (Figure 5B), suggesting that in the Met309Gly mutant, the pore is wide and cannot close properly due to the absence of the glycine side chain. An effect similar to that of Met309Gly mutant was observed for Met309Glu, which displayed higher final steady-state magnesium levels compared with wild-type (Figure 5B). This effect was most likely by forming a negatively charged ring in the pentamer, and eliciting more robust transport due to increased electrostatic attraction of the magnesium ion.

Substitution of Gate 2 residue Val315 to Glu and Phe had no significant effects on growth on non-fermentable carbon sources (Figure 6A). Consistent with this result, Mg^{2+} uptake was less affected by mutations compared with Gate 1 mutants at position 309. Mg^{2+} uptake by the Glu mutant was comparable with that of wild-type Mrs2. The bulky Phe residue was well tolerated and did not impair ion conduction to such an extent that led to a substantial reduction in magnesium uptake (Figure 6B). This is not surprising, as this residue is found at position 315 also in some naturally occurring sequences, suggesting that a bulkier residue can be accommodated at this location (Figure 1B). As expected, the Val315Gly mutation reduced growth (Figure 6A), which was though less pronounced than in the Met309Gly mutant (Figure 5A). Based on the mag-fura-2

measurements, this effect was caused by greater magnesium uptake due to a widening of the channel at this position (Figure 6B).

Taken together the above observations confirm the residue Met309 as Gate 1, equivalent to Met291 in Tm-CorA, but leave some uncertainty as to Val315 residue being Gate 2. The less pronounced constriction together with natural amino acid variability at this location may be the basis for good tolerance of the mutations. Nevertheless, it needs to be kept in mind that the homology models have their limitations, in particular, when it comes to accommodation of insertions or deletions. Based on the amino acid sequence alignment (Figure 1B) highly conserved Leu313 could be an alternative candidate for Gate 2, although it is not positioned inside the pore in the homology model.

Function of the Mrs2 C-terminus

Tm-CorA has a highly conserved, positively charged sequence at the C-terminus termed the basic sphincter. It lies at the level of the hydrophobic gate of the pore and was proposed to be important for transporter function, by drawing negative charges away from the middle of the pore and preventing passage of the charged Mg^{2+} cations (1, 6, 28). The combination of the positive potential field of the ring of lysine residues in the basic sphincter and the hydrophobic barrier of the gate creates an effective impediment to the passage of positively charged Mg^{2+} ions in the closed state. In the open state, the negatively charged willow helices pull the positive charge of the basic sphincter away from the central axis of the pore, allowing the passage of magnesium (1, 6, 15).

C-termini of the Mrs2 family members vary in length and are nearly devoid of conserved primary sequence motifs. The only conserved feature is a surplus of positively charged residues (Table S1). On average, 20% of residues in the C-terminus of the Mrs2 family have a positive charge, which may collectively have the same function as the basic sphincter in Tm-CorA.

Yeast Mrs2 has a 107-amino-acid-long C-terminal with in total 24 positively charged residues, amongst which there is a KRRRK stretch (402–406) that is not conserved in the Mrs2 family. This positively charged sequence was deleted in a previous study, reducing Mg^{2+} uptake when expressed from a low-copy vector. In contrast, overexpression of this mutant nearly restored Mg^{2+} uptake to wild-type levels (28). To obtain better insight into the function of the KRRRK stretch, we reversed the charge of this sequence by introducing negatively charged Glu residues at these positions. The resulting mutant permitted good growth on non-fermentable carbon sources, expressed from the centromeric plasmid YCp22 or when overexpressed (Figure 7A). Mg^{2+} uptake capacity was moderately increased in this mutant.

To further investigate the function of the C-terminus, we removed the C-terminal region of Mrs2 after residue Thr376. Notably, truncation of the entire C-terminus impeded the growth of cells on non-fermentable carbon sources (Figure 7A), consistent with the strong reduction in Mg^{2+} transport, based on mag-fura-2 measurements in isolated mitochondria (Figure 7B).

Taken together, the small, non-conserved, positively charged stretch alone (KRRRK, 402-406) does not appear to be critical for Mrs2 function. A highly negatively charged cluster at this position encloses the ion conduction pathway and generates a more active transporter without impairing its regulation (Figure 7B). Conversely, complete truncation of the C-terminus (deletion of 94 residues at the C-terminus), impairs transport, suggesting that the electrostatic potential that results from the overall surplus of positively charged residues in the C-terminus of Mrs2 has a similar function as the basic sphincter in Tm-CorA.

Conclusions

This study provides the first molecular view of the regulatory N-terminal moiety of a eukaryotic magnesium transporter Mrs2 from *S. cerevisiae*. Together with structure-based mutagenesis and functional analysis *in vivo*, the study

provides insight into gating and regulation of Mrs2. The study identified candidate residues implicated in divalent cation binding, residues involved in formation of the hydrophobic gate, and showed that the entire C-terminal region acts as the basic sphincter. Our observations suggest a higher degree of regulation of the Mrs2 transporter compared with CorA; i.e. the high inside negative membrane potential of mitochondria attracts the positively charged Mg^{2+} ion, requiring fine and stringent control of transport at more than one site of the ion conduction pathway to ensure normal mitochondrial function.

MATERIALS AND METHODS

Protein expression and purification

Details on cloning and purification were reported earlier (21). The mitochondrial matrix domain of *Saccharomyces cerevisiae* was cloned from genomic DNA into pETM-11 vector (EMBL Hamburg) with a tobacco etch virus (TEV) cleavable N-terminal His_6-tag. The recombinant protein was over expressed in BL-21 star (DE3) at 21 °C, in the presence of 0.025 mg/ml of kanamycin and induced by 0.5 mM isopropyl β-D-thiogalactopyranoside (IPTG). Cells were sonicated in a suitable buffer. The supernatant after centrifugation was applied onto a 5 ml Ni–NTA agarose column (Qiagen). The N-terminal His_6-tag was cleaved using TEV. After the TEV cleavage, the protein was reapplied on a Ni-NTA column, followed by Resource Q column, and HiLoad 26/60 Superdex 200 (GE Healthcare) size exclusion chromatography.

Protein purity and monodispersity controls

The purity of the protein solution used for the crystallization experiments was evaluated by SDS-PAGE analysis and showed a single band of apparent molecular weight of about 30 kDa. Dynamic light scattering (DLS) was used to assess the monodispersity of the protein solution: a monomodal distribution with a polydispersity of 5% was observed and the gyration radius was estimated to be 4.2 nm, suggesting that the protein solution was homogenous and monomeric.

Circular dichroism (CD) spectroscopy in the far ultraviolet wavelength range showed that the protein is rich in alpha helical content.

Analytical gel filtration chromatography

Analytical gel filtration chromatography on $Mrs2_{48-308}$ was performed at 4 °C, using the construct eluted as a monomer from Superdex 200 10/300 column (Amersham Biosciences), after dialyzing the protein against low ionic salt and run on an analytical gel filtration 200 10/300 column in 15 mM Tris-Hcl (pH 8.0), 15mM NaCl. The protein eluted as a pentamer.

Crystallization

Details on crystallization conditions were reported earlier (21). Initial crystallization screening conditions obtained from the sparse matrix screen from MembFac kits and Hampton Research were optimized by hanging drop at 22 °C. Magnesium and cobalt-soaked crystals were obtained by soaking the native crystal with 1-5 mM magnesium chloride and 5 mM cobalt chloride in the crystallization drops. Co-crystals with magnesium or cobalt were grown by vapor diffusion at 22 °C in a solution containing 2.8 mg/ml protein, 22% v/v ethylene glycol 56 mM Na/K phosphate pH 6.3, 1.5 mM magnesium chloride, or cobalt chloride. Crystals were flash-frozen in a solution containing 30% v/v ethylene glycol 56 mM Na/K phosphate pH 6.3 and mounted on loops at 100 K prior to data collection.

Data collection, structure solution and refinement

$Mrs2_{48-308}$ X-ray diffraction data sets were collected at 100 K in a cold nitrogen stream using various beamlines at ESRF or Microstar rotating anode at 1.54 Å. The crystals of $Mrs2_{48-308}$ diffracted to 1.83 Å resolution on an in-house source and to 1.28 Å at ESRF. Detail of the data collection, statistics and processing were reported earlier (21). Crystallographic data collected in-house were processed (integrated and scaled) with the Proteum2 software suite (Bruker AXS Inc.), while the synchrotron data sets were processed using XDS (30). The

structure of $Mrs2_{48-308}$ was solved, using a highly redundant data set collected on an in-house source by the single-wavelength anomalous dispersion method (SAD) exploiting the Mrs2 native sulphur (S) atoms for phasing using SHELXD (31). After finding the S atoms, heavy atom refinement and density modification were performed using autoSHARP (32). The electron density map obtained from autoSHARP was traced by ARP/wARP (33, 34), which fitted 243 out of 261 amino acid residues in three different chains with R_{work}/R_{free} = 0.21/0.30. The structure refinement yielded final R_{work} and R_{free} values of 0.193 and 0.243, respectively. This model contains 258 amino-acid residues and 432 water molecules. Two complete data sets at 1.42 Å and 1.28 Å were collected at ESRF ID14-1, processed individually using XDS. The data sets were then scaled together using SCALA. The structure from S-SAD data was further refined against the merged 1.28 Å data sets using REFMAC5 and phenix. The final model contains 261 amino acid and 392 water and five ethylene glycol molecules with a R_{work} and R_{free} of 0.169 and 0.204 respectively. Details on the refinement statistics are shown in Table S2.

Miscellaneous

The SBSA were made by SHEBA (Structural Homology by Environment-Based Alignment) (35). For the SBSA, the structures $Mrs2_{48-308}$ and Tm-CorA were first aligned by SHEBA. The two aligned sequences were then aligned with randomly selected sequences of ten eukaryotic and ten prokaryotic magnesium channels using the profile alignment features of ClustalX2 (36).

Manual adjustments were applied to further improve alignments. Sequence identity and conservation were determined using the Lalign web-server (37) and ESPript (Gouet et al, 2003), respectively. Protein Homology/analogY Recognition Engine (phyre) (http://www.sbg.bio.ic.ac.uk/~phyre) was used for homology modeling of the transmembrane portion of Mrs2 (38).

Protease susceptibility assay

For 50 ml reaction volumes, stock solutions were prepared to obtain the final concentration desired upon dilution: 39 ml of protein (2.5 mg/ml), 1µl of trypsin (10 mg/ml; Sigma), and 10µl of 0-100 mM of metal solution. Reaction solutions were mixed and equilibrated at 4°C for 20 min. Trypsin was then added, and reactions were incubated at 4° or 37°C for the desired times. After adding 50 ml of SDS–PAGE sample buffer, samples were boiled and run immediately on 15% SDS–PAGE gels. In order to rule out the possibility of trypsin inhibition, controls were performed on the test protein bovine serum albumin (BSA) over the full range of conditions.

Yeast strains, growth media and genetic procedures

S. cerevisiae strain DBY747 and the isogenic deletion strain *mrs2*Δ have been described previously (13, 27). Yeast cells were grown in YPD (1% yeast extract, 2% peptone, 2% glucose) to stationary phase. For growth tests on solid media, yeast cells were grown in YPD over night, washed with dH_2O and spotted in ten-fold dilutions on YPD or YPG (1% yeast extract, 2% peptone, 3% glycerol) and incubated at 28°C for 2 (YPD) or 6 days (YPG).

Plasmid constructs

The plasmid Yep351-*MRS2*-HA (Bui 1999) was used as the template in overlap extension PCR. Mutagenic forward and reverse primers are reported in Text S2.

Verification of positive clones was performed by restriction analysis of the introduced EcoRI (Met309 and Val315) or AvaI (Asp97) sites (underlined). All restriction sites were introduced by silent mutations. No additional mutations were found by sequencing of the complete ORF.

PCR fragments were digested with XbaI and SmaI and cloned in the vector Yep351-MRS2-HA and YCp22-MRS2-HA digested with the same enzyme

combination. To create the C-terminal truncation of *MRS2*, the primer MRS2Mcsfw and the reverse primer MRS2 CutCterm rev: GCGCGCGTCGACCGGTCATCTTTGTCAC were used. The XbaI/SalI digested PCR fragment was cloned in vector Yep351 and YCp22. For the substitution of the positive amino acid stretch by negatively charged amino acid residues in the KRRRK/E mutant the mutagenic primers MRS2 KRRRK/E fw: **5'-** GCGTCTATTGCCCTGACAAATAAACTAGAAGAGGAAGAGGAATGGTGGAAG TCAACCAAGCAGCGG-3' and MRS2 KRRRK/E rev: 5'-CCGCTGCTTGGTTGACTTCCACCATTCCTCTTCCTCTTCTAGTTTATTTGTCA GGGCAATAGACGC-3' were used with the above mentioned primers in overlap extension PCR. Positive clones were verified by the introduced HincII restriction site (underlined).

Isolation of mitochondria and measurement of $[Mg^{2+}]_m$ by spectrofluorimetry

Isolation of mitochondria and the ratiometric determination of intramitochondrial Mg^{2+} concentrations ($[Mg^{2+}]_m$) dependent on various external concentrations ($[Mg^{2+}]_e$) were performed as reported previously (8).

ACKNOWLEDGMENTS

We acknowledge the ESRF, Grenoble for the provision of synchrotron radiation. MBK, GS, SS were recipients of a PhD fellowship from FWF (P20141) and from WWTF (LS05021). MBK was partially supported by the University of Vienna funds. We also acknowledge The BIN-III imitative of the Austrian GEN-AU for financial support. The coordinates of the $Mrs2_{48-308}$ have been deposited in Protein Data Bank (PDB) under the accession code 3RKG.

CONFLICT OF INTEREST

The authors declare that they have no conflict of interest.

REFERENCES

1. Lunin VV*, et al.* (2006) Crystal structure of the CorA Mg2+ transporter. *Nature* 440(7085):833-837.

2. Mobasheri A*, et al.* (1998) Ion transport in chondrocytes: membrane transporters involved in intracellular ion homeostasis and the regulation of cell volume, free [Ca2+] and pH. *Histol Histopathol* 13(3):893-910.
3. Ikari A*, et al.* (2008) TRPM6 expression and cell proliferation are up-regulated by phosphorylation of ERK1/2 in renal epithelial cells. *Biochem Biophys Res Commun* 369(4):1129-1133.
4. Papp-Wallace KM*, et al.* (2008) The CorA Mg2+ channel is required for the virulence of Salmonella enterica serovar typhimurium. *J Bacteriol* 190(19):6517-6523.
5. Garcia Vescovi E, Soncini FC, & Groisman EA (1996) Mg2+ as an extracellular signal: environmental regulation of Salmonella virulence. *Cell* 84(1):165-174.
6. Eshaghi S*, et al.* (2006) Crystal structure of a divalent metal ion transporter CorA at 2.9 angstrom resolution. *Science* 313(5785):354-357.
7. Zsurka G, Gregan J, & Schweyen RJ (2001) The human mitochondrial Mrs2 protein functionally substitutes for its yeast homologue, a candidate magnesium transporter. *Genomics* 72(2):158-168.
8. Kolisek M*, et al.* (2003) Mrs2p is an essential component of the major electrophoretic Mg2+ influx system in mitochondria. *EMBO J* 22(6):1235-1244.
9. Li L, Tutone AF, Drummond RS, Gardner RC, & Luan S (2001) A novel family of magnesium transport genes in Arabidopsis. *Plant Cell* 13(12):2761-2775.
10. Schock I*, et al.* (2000) A member of a novel Arabidopsis thaliana gene family of candidate Mg2+ ion transporters complements a yeast mitochondrial group II intron-splicing mutant. *Plant J* 24(4):489-501.
11. Walker GM, Birchandersen A, Hamburger K, & Kramhoft B (1982) Magnesium-Induced Mitochondrial Polymorphism and Changes in Respiratory Metabolism in the Fission Yeast, Schizosaccharomyces Pombe. (Translated from English) *Carlsberg Research Communications* 47(4):205-214 (in English).
12. Froschauer EM, Kolisek M, Dieterich F, Schweigel M, & Schweyen RJ (2004) Fluorescence measurements of free [Mg2+] by use of mag-fura 2 in Salmonella enterica. *FEMS Microbiol Lett* 237(1):49-55.
13. Bui DM, Gregan J, Jarosch E, Ragnini A, & Schweyen RJ (1999) The bacterial magnesium transporter CorA can functionally substitute for its putative homologue Mrs2p in the yeast inner mitochondrial membrane. *J Biol Chem* 274(29):20438-20443.
14. Kehres DG & Maguire ME (2002) Structure, properties and regulation of magnesium transport proteins. *Biometals* 15(3):261-270.
15. Payandeh J & Pai EF (2006) A structural basis for Mg2+ homeostasis and the CorA translocation cycle. *EMBO J* 25(16):3762-3773.
16. Tan K*, et al.* (2009) Structure and electrostatic property of cytoplasmic domain of ZntB transporter. *Protein Sci* 18(10):2043-2052.

17. Payandeh J*, et al.* (2008) Probing structure-function relationships and gating mechanisms in the CorA Mg2+ transport system. *J Biol Chem* 283(17):11721-11733.
18. Kehres DG, Lawyer CH, & Maguire ME (1998) The CorA magnesium transporter gene family. *Microb Comp Genomics* 3(3):151-169.
19. Worlock AJ & Smith RL (2002) ZntB is a novel Zn2+ transporter in Salmonella enterica serovar Typhimurium. *J Bacteriol* 184(16):4369-4373.
20. Xia Y*, et al.* (2011) Co2+ selectivity of Thermotoga maritima CorA and its inability to regulate Mg2+ homeostasis present a new class of CorA proteins. *Journal of Biological Chemistry*.
21. Khan MB, Sjoblom B, Schweyen RJ, & Djinovic-Carugo K (2010) Crystallization and preliminary X-ray diffraction analysis of the N-terminal domain of Mrs2, a magnesium ion transporter from yeast inner mitochondrial membrane. *Acta Crystallogr Sect F Struct Biol Cryst Commun* 66(Pt 6):658-661.
22. Maguire ME (2006) The structure of CorA: a Mg(2+)-selective channel. *Curr Opin Struct Biol* 16(4):432-438.
23. Holm L & Sander C (1996) Mapping the protein universe. *Science* 273(5275):595-603.
24. Altschul SF, Gish W, Miller W, Myers EW, & Lipman DJ (1990) Basic local alignment search tool. *J Mol Biol* 215(3):403-410.
25. Roux B & MacKinnon R (1999) The cavity and pore helices in the KcsA K+ channel: electrostatic stabilization of monovalent cations. *Science* 285(5424):100-102.
26. Svidova S, Sponder G, Schweyen RJ, & Djinović-Carugo K (2010) Functional analysis of the conserved hydrophobic gate region of the magnesium transporter CorA. *Biochim Biophys Acta* 1808:1587–1591.
27. Wiesenberger G, Waldherr M, & Schweyen RJ (1992) The nuclear gene MRS2 is essential for the excision of group II introns from yeast mitochondrial transcripts in vivo. *J Biol Chem* 267(10):6963-6969.
28. Weghuber J, Dieterich F, Froschauer EM, Svidova S, & Schweyen RJ (2006) Mutational analysis of functional domains in Mrs2p, the mitochondrial Mg2+ channel protein of Saccharomyces cerevisiae. *FEBS J* 273(6):1198-1209.
29. Baumann F, Neupert W, & Herrmann JM (2002) Insertion of bitopic membrane proteins into the inner membrane of mitochondria involves an export step from the matrix. *J Biol Chem* 277(24):21405-21413.
30. Kabsch W (1988) Automatic-Indexing of Rotation Diffraction Patterns. (Translated from English) *Journal of Applied Crystallography* 21:67-71 (in English).
31. Uson I & Sheldrick GM (1999) Advances in direct methods for protein crystallography. *Curr Opin Struct Biol* 9(5):643-648.
32. Vonrhein C, Blanc E, Roversi P, & Bricogne G (2007) Automated structure solution with autoSHARP. *Methods Mol Biol* 364:215-230.

33. Morris RJ, Perrakis A, & Lamzin VS (2003) ARP/wARP and automatic interpretation of protein electron density maps. *Methods Enzymol* 374:229-244.
34. Joosten K*, et al.* (2008) A knowledge-driven approach for crystallographic protein model completion. *Acta Crystallogr D Biol Crystallogr* 64(Pt 4):416-424.
35. Jung J & Lee B (2000) Protein structure alignment using environmental profiles. *Protein Eng* 13(8):535-543.
36. Larkin MA*, et al.* (2007) Clustal W and Clustal X version 2.0. *Bioinformatics* 23(21):2947-2948.
37. Pearson WR (1991) Searching protein sequence libraries: comparison of the sensitivity and selectivity of the Smith-Waterman and FASTA algorithms. *Genomics* 11(3):635-650.
38. Kelley LA & Sternberg MJ (2009) Protein structure prediction on the Web: a case study using the Phyre server. *Nat Protoc* 4(3):363-371.

FIGURE LEGENDS

Figure 1 Structure-based sequence alignment of $Mrs2_{48-308}$ and its closest structural homologue Tm-CorA and comparison of their folds. (A) A schematic view of the domain structure of Mrs2 (B) Structure-based sequence alignment of $Mrs2_{48-308}$ and Tm-CorA (PDB code 2IUB). The first two sequences belonging to the structures of $Mrs2_{48-308}$ and Tm-CorA are followed by ten sequences of eukaryotic Mrs2 and ten sequences of prokaryotic CorA transporters from different species. Identical residues between Mrs2 and Tm-CorA transporters are in red. The gaps due to residues omitted from the sequence alignment are represented by two solid black lines. The sequences of the two phyla are separated by horizontal black solid line. The sequence identity between the prokaryotic species used in the alignment is about 53% while between eukaryotic species is about 52%. The conserved signature sequence GMN is boxed. Residues of the putative magnesium binding site in eukaryotes, i.e. Asp97 and Glu270, are boxed and are denoted by + and × symbols. The prokaryotic magnesium binding site formed by Asp89 and Asp253 is boxed and denoted by = and # symbols in the sequence alignment. The residue involved in the formation of an Asp ring is boxed and represented by * symbol. The residues involved in the hydrophobic gate formation, i.e. Met309, Val315 in case of Mrs2 transporter and Met291, Leu294 in case of Tm-CorA transporter are boxed and are denoted by G1 and G2 in the sequence alignment (representing Gate 1 and Gate 2), respectively. The secondary structure derived from $Mrs2_{48-308}$ is shown above the sequence. The residues embedded in the first transmembrane helix (TM1) are represented by black solid line (C) The structures of the soluble moiety of Tm-CorA and Mrs2 contain a C-terminal triple coiled-coil (magenta), which continues into the membrane (not shown), and an N-terminal alpha/beta/alpha domain (green). (D) The N-terminal domains of Tm-CorA and $Mrs2_{48-308}$ are different. While the last four beta strands (C1-C4, yellow) are topologically identical, there are three N-terminal beta strands in Tm-CorA and two in Mrs2 (N1 and N2, magenta) and three in Tm-CorA (N1-N3, magenta). The helix, which

is intercalated between the second and the third strand, of Tm-CorA is missing in $Mrs2_{48-308}$.

Figure 2 Structural features of $Mrs2_{48-308}$ and the funnel model. (A) $Mrs2_{48-308}$ is represented as ribbon and the side chains of the negatively charged or hydroxyl bearing residues of helix α7, making the inner side of the pore, are represented as stick. (B) Electrostatic surface potential analysis of Mrs2, generated by APBS. Views are from the helix forming the inner wall of the funnel (*red*, negatively charged; *blue*, positively charged; *white*, uncharged). The red arrow shows the gradual increase of negative charge from top to bottom (C) Side view of the pentamer funnel model of the inner soluble domain of Mrs2 based on Tm-CorA. (D) Bottom view of the pentamer funnel model, highlighting the putative magnesium binding site (red). All structural figures were created with Pymol (http://www.pymol.org/).

Figure 3 Putative magnesium binding site in $Mrs2_{48-308}$ and the hydrophobic gate residues in Mrs2 and Tm-CorA. (A) Superposition of $Mrs2_{48-308}$ (blue) and Tm-CorA (cyan) soluble domains showing the magnesium binding site of Tm-CorA and the putative magnesium binding site of $Mrs2_{48-308}$. The colored boxes (panels B and C) show the residues involved in magnesium sensing. (B) The magnesium binding residue Asp89 of Tm-CorA and the corresponding putative magnesium binding residue Asp97 of $Mrs2_{48-308}$. (C) The magnesium binding residue Asp253 of Tm-CorA and the corresponding putative magnesium binding residue Glu270 of $Mrs2_{48-308}$. (D) Putative magnesium binding pocket featuring Asp97 from one monomer (blue) and Glu270 from an adjacent subunit (cyan) in a proposed functional funnel model. (E) Top view of CorA (PDB code 2IUB) showing the hydrophobic gate residues Met291 and Leu294 (red). (F) Top view of the model of Mrs2 transporter showing the putative hydrophobic Gate 1 residues Met309 and Gate 2 residues Val315 (red).

Figure 4 Mutation of Asp97 of a putative Mg^{2+} binding site in Mrs2 does not influence the regulation of the transporter. (A) Growth phenotypes of *Saccharomyces cerevisiae* strain DBY747 *mrs2*Δ expressing *MRS2* variants harbouring mutations in the D97 site from high-copy number vector YEp351 or low copy vector YCp22. Serial dilutions of yeast cultures were spotted on fermentable (YPD) or non-fermentable (YPG) plates and incubated at 28°C for 3 or 6 days, respectively. (B) $[Mg^{2+}]_e$-dependent changes in $[Mg^{2+}]_m$ in DBY 747 *mrs2*Δ mitochondria expressing *MRS2* or the mutant variants were determined. Representative curve traces of four individual measurements are shown.

Figure 5 Mutations in the hydrophobic Gate 1 (M309) of Mrs2 impairs growth on non-fermentable carbon sources and alters the transport activity of the channel. (A) Growth phenotypes of *Saccharomyces cerevisiae* strain DBY747 *mrs2Δ* expressing wild-type *MRS2* and the corresponding *MRS2* mutant variants from high-copy number vector YEp351 or low copy vector YCp22. Serial dilutions of the different strains were spotted on fermentable (YPD) and non-fermentable (YPG) substrates and grown for three or six days, respectively. (B) $[Mg^{2+}]_e$-dependent changes in $[Mg^{2+}]_m$ in mitochondria of *mrs2*Δ *cells*, and cells expressing WT *MRS2* or the mutant variants. Isolated mitochondria were loaded with the Mg^{2+}-sensitive dye mag-fura-2 and changes in the intramitochondrial free Mg^{2+} concentration upon addition of Mg^{2+} to the nominally Mg^{2+}-free buffer, as indicated in the figure, were determined. Representative recordings of four individual measurements are shown.

Figure 6 Characterization of mutants in the hydrophobic gate 2 of Mrs2. (A) Serial dilutions of DBY747 WT and DBY747 *mrs2*Δ cells transformed with the vectors Yep351 and YCp22 expressing *MRS2* or different mutant variants for V315 were spotted on fermentable (YPD) or non-fermentable (YPG) plates and incubated at 28°C for 3 or 6 days, respectively. (B) $[Mg^{2+}]_e$-dependent changes in $[Mg^{2+}]_m$ in mitochondria of DBY 747 *mrs2*Δ cells expressing WT *MRS2* or mutant

variants of V315. Representative curve traces of three individual measurements are shown.

Figure 7 Characterization of the Mrs2 C-terminus. (A) Phenotypes associated with charge reversion of the KRRRK stretch and truncation of the C-terminus after Thr376. Serial dilutions of yeast cultures were spotted on fermentable (YPD) or non-fermentable (YPG) plates and incubated at 28°C for 3 or 6 days, respectively. (B) $[Mg^{2+}]_e$-dependent changes in $[Mg^{2+}]_m$ in DBY 747 *mrs2*Δ mitochondria expressing the KRRRK/E mutant or the *MRS2* variant with a C-terminal truncation. Representative curve traces of four individual measurements are shown.

Figure 1 Structure-based sequence alignment of $Mrs2_{48-308}$ and its closest structural homologue Tm-CorA and comparison of their folds.

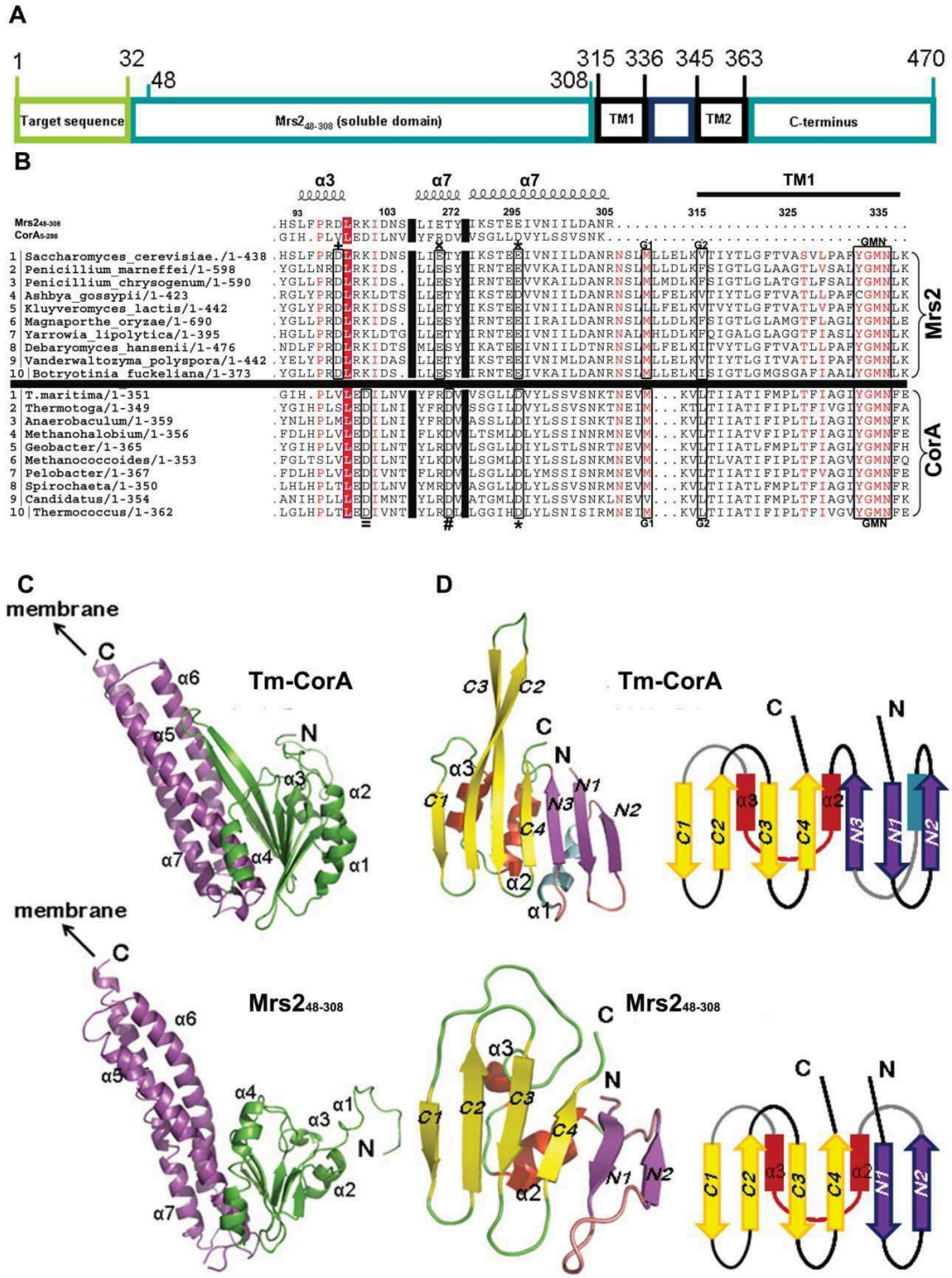

Figure 2 Structural features of $Mrs2_{48-308}$ and the funnel model.

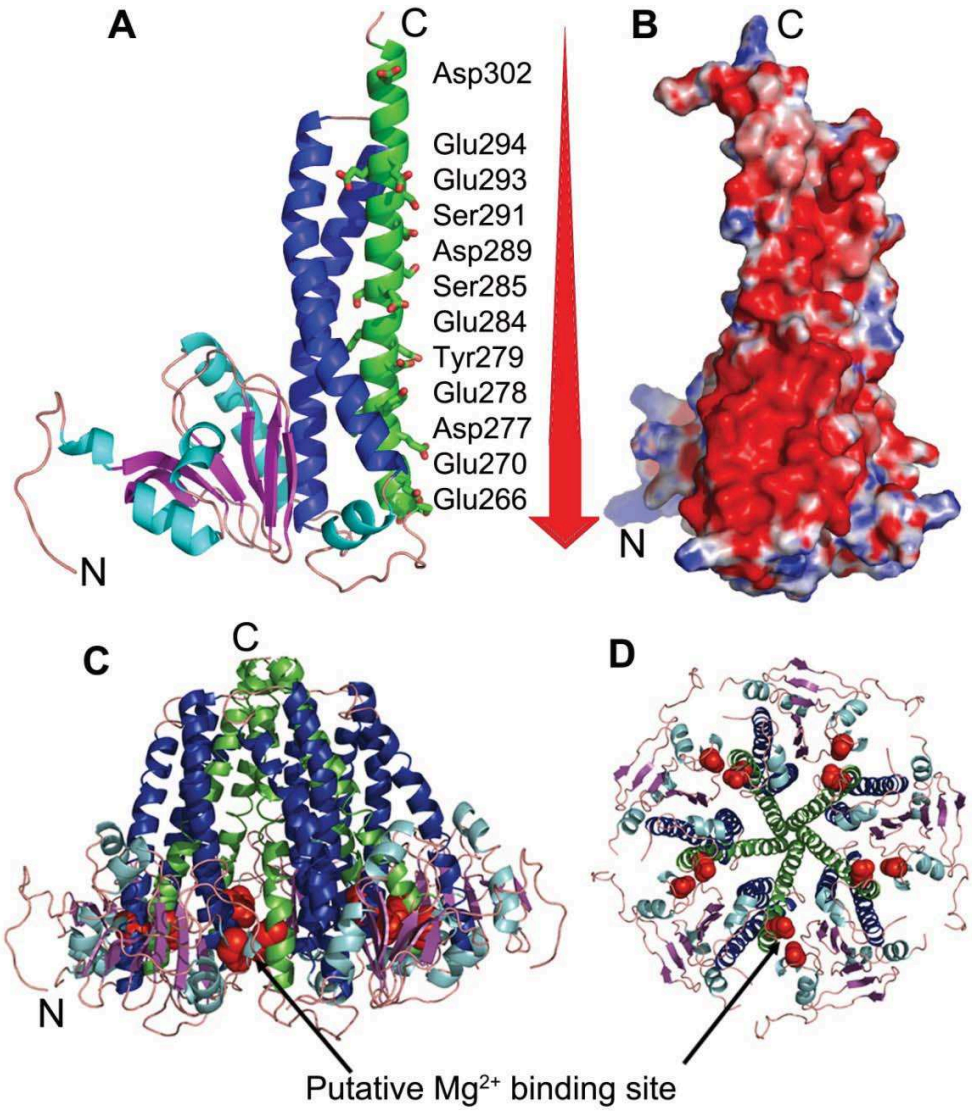

Figure 3 Magnesium binding site in $Mrs2_{48-308}$ and hydrophobic gate residues in Mrs2 and Tm-CorA.

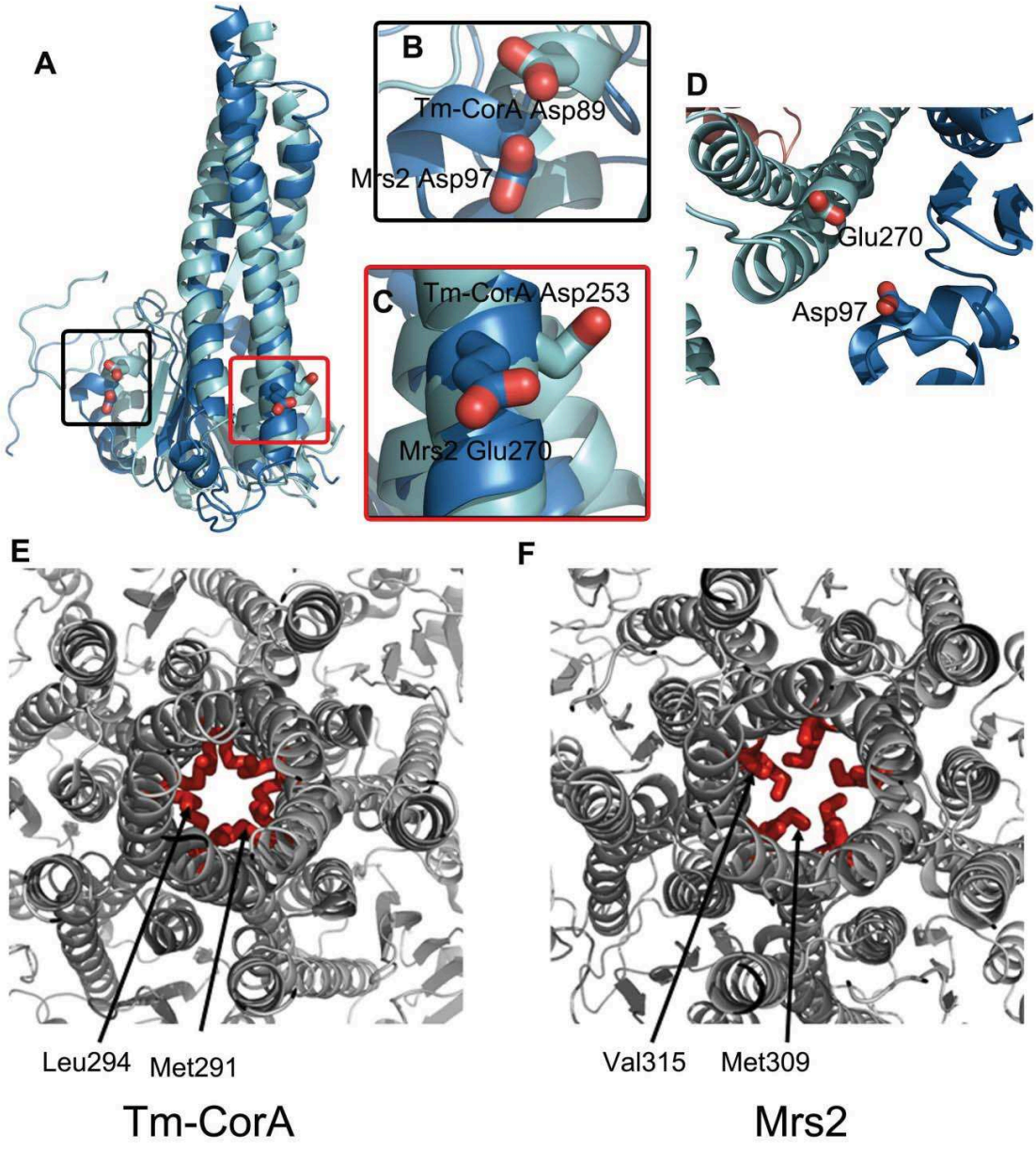

Figure 4 Mutation of Asp97 in putative Mg^{2+} binding site in Mrs2.

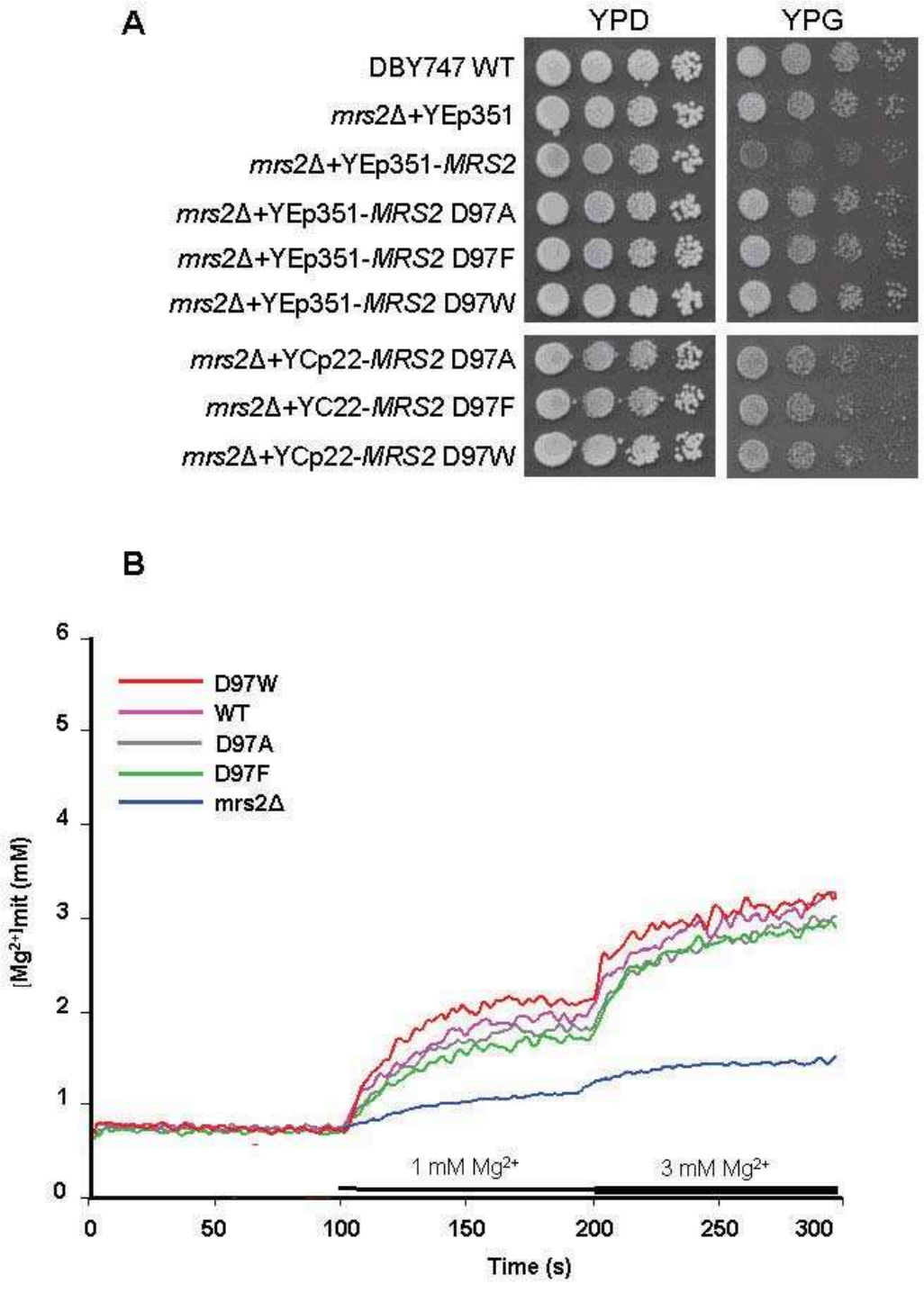

Figure 5 Mutations in the hydrophobic Gate 1 (Met309) of Mrs2.

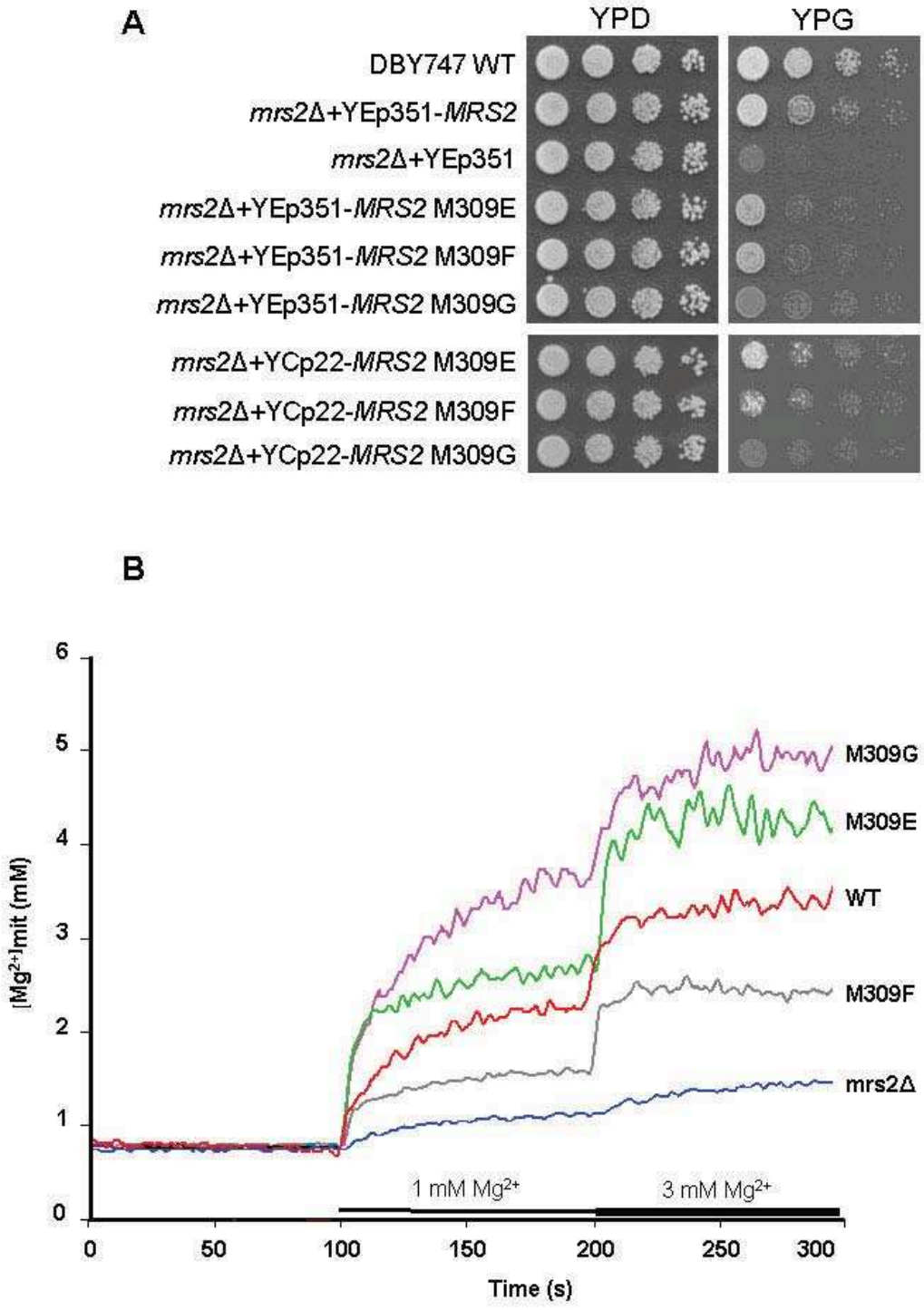

Figure 6 Characterization of mutants in the hydrophobic Gate 2 of Mrs2.

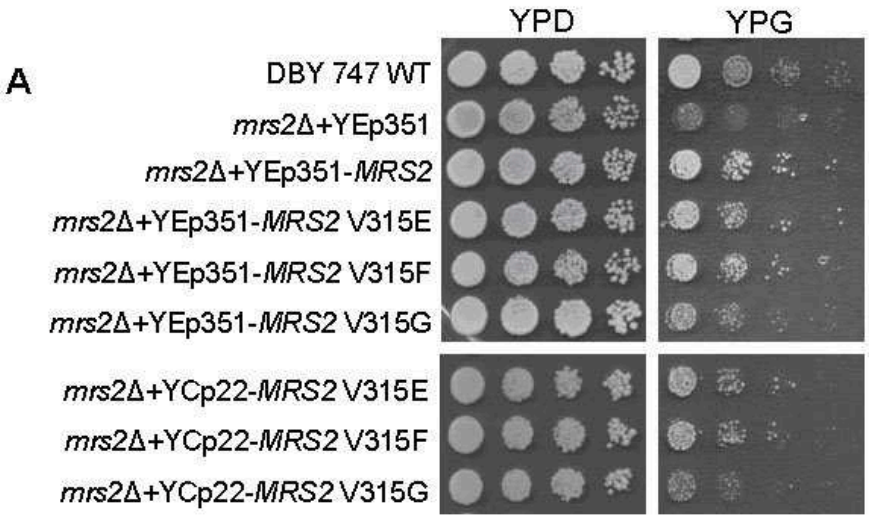

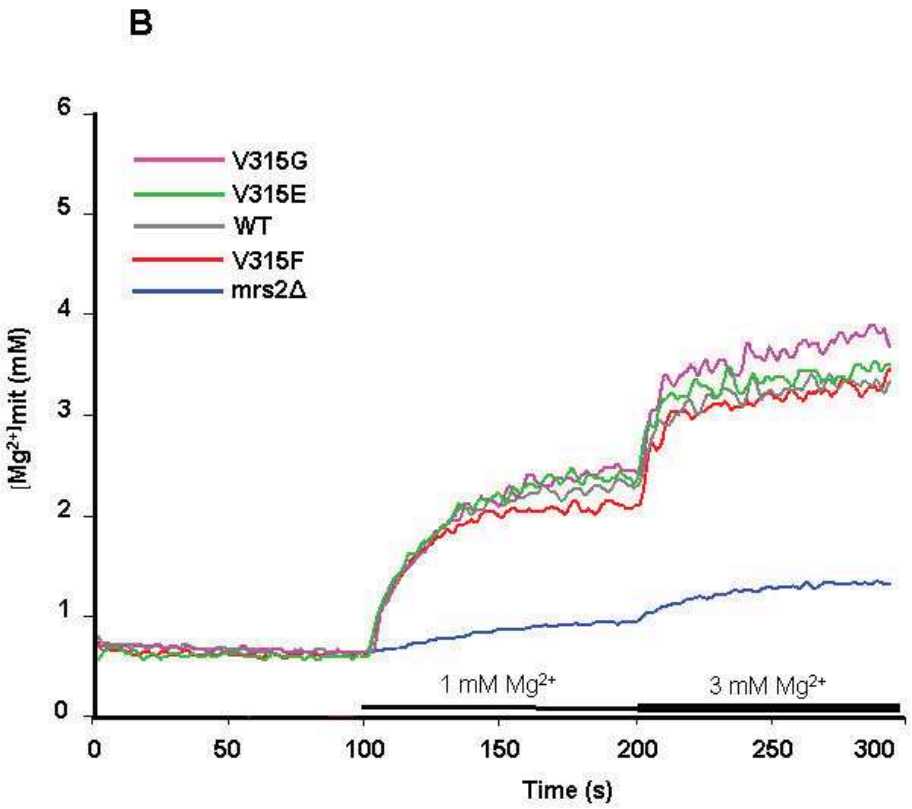

Figure 7: Characterization of the Mrs2 C-terminus.

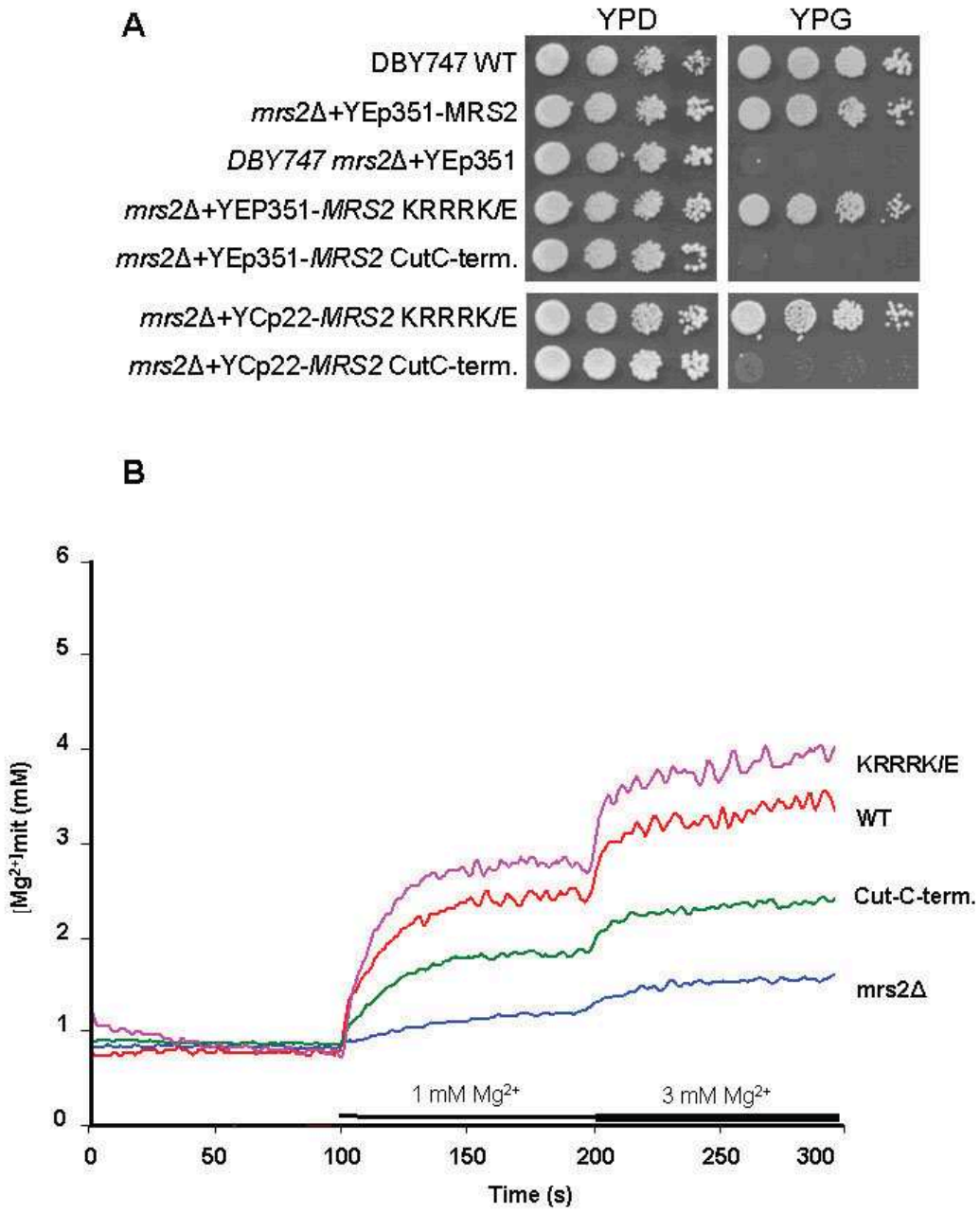

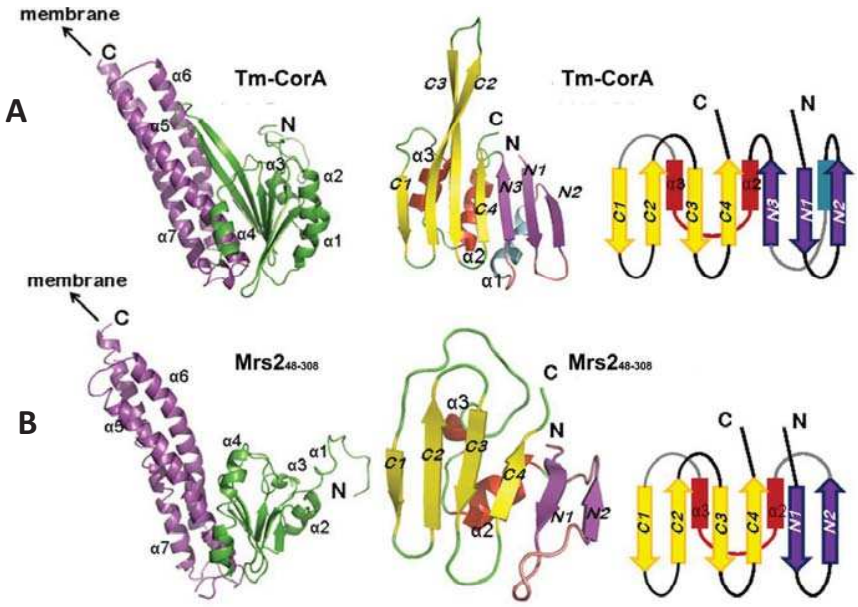
A
membrane
C
α6
α5
α7
α4
α3
α2
α1
N
Tm-CorA
C3
C2
C
N
α3
C1
C4
N1
N3
N2
α2
α1
Tm-CorA
C
N
C1
C2
C3
C4
N3
N1
N2
B
membrane
C
α6
α5
α7
α4
α3
α1
α2
N
Mrs2 48-308
C
α3
N
C1
C2
C3
C4
α2
N1
N2
Mrs2 48-308
C
N
C1
C2
C3
C4
N1
N2

3.5. Publication V

A Root-Expressed Magnesium Transporter of the MRS2/MGT Gene Family in Arabidopsis thaliana Allows for Growth in Low-Mg^{2+} Environments

Michael Gebert,[a] KarolineMeschenmoser,[a] SoňaSvidová ,[b] JulianWeghuber,[b] Rudolf Schweyen,[b,1] Karolin Eifler,[a] Henning Lenz,[a] Katrin Weyand,[a] and Volker Knoop [a,2]

The Plant Cell, Vol. 21: 4018–4030,

[a] Institut fuer Zelluläre und Molekulare Botanik, Universität Bonn, D-53115 Bonn, Germany
[b] Vienna Biocenter, Abteilung fuer Mikrobiologie und Genetik, A-1030 Wien, Austria

Authors' contributions to the manuscript

I performed the functional complementation and Mg^{2+} uptake measurements in the yeast mitochondria, performed PAGE and western blotting on yeast mitochondria, analyzed the data from these experiments and participated partly in the preparation of the manuscript.

The Plant Cell, Vol. 21: 4018–4030, December 2009, www.plantcell.org

A Root-Expressed Magnesium Transporter of the *MRS2/MGT* Gene Family in *Arabidopsis thaliana* Allows for Growth in Low-Mg^{2+} Environments [W]

Michael Gebert,[a] Karoline Meschenmoser,[a] Soňa Svidová,[b] Julian Weghuber,[b] Rudolf Schweyen,[b,1] Karolin Eifler,[a] Henning Lenz,[a] Katrin Weyand,[a] and Volker Knoop[a,2]

[a] Institut für Zelluläre und Molekulare Botanik, Universität Bonn, D-53115 Bonn, Germany
[b] Vienna Biocenter, Abteilung für Mikrobiologie und Genetik, A-1030 Wien, Austria

The *MRS2/MGT* gene family in *Arabidopsis thaliana* belongs to the superfamily of CorA-MRS2-ALR-type membrane proteins. Proteins of this type are characterized by a GMN tripeptide motif (Gly-Met-Asn) at the end of the first of two C-terminal transmembrane domains and have been characterized as magnesium transporters. Using the recently established mag-fura-2 system allowing direct measurement of Mg^{2+} uptake into mitochondria of *Saccharomyces cerevisiae*, we find that all members of the *Arabidopsis* family complement the corresponding yeast *mrs2* mutant. Highly different patterns of tissue-specific expression were observed for the MRS2/MGT family members in planta. Six of them are expressed in root tissues, indicating a possible involvement in plant magnesium supply and distribution after uptake from the soil substrate. Homozygous T-DNA insertion knockout lines were obtained for four members of the *MRS2/MGT* gene family. A strong, magnesium-dependent phenotype of growth retardation was found for *mrs2-7* when Mg^{2+} concentrations were lowered to 50 μM in hydroponic cultures. Ectopic overexpression of *MRS2-7* from the cauliflower mosaic virus 35S promoter results in complementation and increased biomass accumulation. Green fluorescent protein reporter gene fusions indicate a location of MRS2-7 in the endomembrane system. Hence, contrary to what is frequently found in analyses of plant gene families, a single gene family member knockout results in a strong, environmentally dependent phenotype.

INTRODUCTION

Magnesium is essential for a vast number of fundamental biochemical processes in all living cells. For example, Mg^{2+} ions are involved in the interaction of the ribosome subunits, are the counter-ions of ATP and the central ions in chlorophylls, and act as cofactors in numerous enzymes, most notably those involved in nucleotide metabolism (Maguire and Cowan, 2002) and photosynthetic carbon fixation (Lilley et al., 1974; Marschner, 2002). The Mg^{2+} ion has a unique physico-chemistry: of all biologically relevant cations, it has the smallest ionic radius, yet the largest hydration shell. This results in a 400-fold difference in volume between the hydrated and nonhydrated states. Accordingly, the proteins for the transport of magnesium across biological membranes likewise appear to be unique in nature (Shaul, 2002; Gardner, 2003; Moomaw and Maguire, 2008).

Best studied among the membrane transport systems for Mg^{2+} are the bacterial CorA proteins, which were named after the cobalt resistance phenotype observed in the respective bacterial mutants (Kehres et al., 1998; Moncrief and Maguire, 1999; Niegowski and Eshaghi, 2007). CorA proteins are characterized by a unique topology of two closely spaced, C-terminal transmembrane (TM) domains, the first of which invariably ends with a GMN (Gly-Met-Asn) tripeptide motif. The crystal structure of the *Thermotoga maritima* CorA protein has recently been determined (Eshaghi et al., 2006; Lunin et al., 2006; Payandeh and Pai, 2006). These studies have shown that CorA assembles as a pentamer protein complex in which the respective first TM domains of each protein subunit line the channel's pore within the membrane, while the five N termini form a large, cone-shaped funnel inside the cell.

Homologous proteins of the CorA type can be identified in all domains of life: in archaea, in eubacteria, and in all kingdoms of eukaryotes (Knoop et al., 2005). The best studied of the eukaryotic CorA homologs is the yeast Mrs2p protein, which is located in the inner mitochondrial membrane and was named for the impaired mitochondrial RNA splicing phenotype of mutants that was initially observed (Wiesenberger et al., 1992; Bui et al., 1999; Gregan et al., 2001a; Kolisek et al., 2003; Weghuber et al., 2006; Schindl et al., 2007). Structural and functional CorA/MRS2 homologs in the yeast plasma membrane are the ALR proteins, named for the aluminium resistance phenotype of mutants that initially led to their identification (MacDiarmid and Gardner, 1998; Graschopf et al., 2001; Liu et al., 2002; Lee and Gardner, 2006; Wachek et al., 2006). Only single, mitochondrial CorA-type homologs are identified in metazoan genomes, and the human homolog has been shown to complement the yeast *mrs2* mutant (Zsurka et al., 2001).

[1] Rudolf Schweyen passed away on February 15, 2009.
[2] Address correspondence to volker.knoop@uni-bonn.de.
The author responsible for distribution of materials integral to the findings presented in this article in accordance with the policy described in the Instruction for Authors (www.plantcell.org) is: Volker Knoop (volker.knoop@uni-bonn.de).
[W] Online version contains Web-only data.
www.plantcell.org/cgi/doi/10.1105/tpc.109.070557

In plants, CorA homologs have been identified as members of extended gene families. In *Arabidopsis thaliana*, this gene family has 10 members, and the family was initially named At MRS2 (Schock et al., 2000), and alternatively At MGT (Li et al., 2001) for magnesium transport. In the studies cited above, several members of the CorA-MRS2-ALR superfamily (or 2-TM-GMN-type proteins; Knoop et al., 2005) were shown to complement respective mutants across wide phylogenetic distances to varying degrees, indicating structural and functional homology in spite of low overall sequence similarities (except for the conserved GMN motif).

The extension of the *MRS2*/*MGT* gene families in plants may on the one hand be explained by adapting an evolutionary very old invention to the many different membrane systems of the plant cell. Indeed, the most distant and phylogenetic basal gene family member *MRS2-11*/*MGT10*, for example, could be localized to the chloroplast (Drummond et al., 2006). On the other hand, because land plants are sessile organisms that cannot actively choose between alternative environments, they may require a larger range of magnesium transport functionality (e.g., in adapting to Mg^{2+} availability in the soil).

Given the diversity of the *MRS2*/*MGT* gene family, it is fundamental to clearly evaluate the individual capacities for magnesium transport and the tissue-specific expression patterns. The recently established method of directly measuring the uptake of magnesium using the fluorescent magnesium binding dye, mag-fura-2, has motivated us to study all members of the plant family. Here, we used the mag-fura-2 system (Kolisek et al., 2003) to characterize the transport properties of the whole gene family via heterologous expression in the yeast *mrs2* mutant.

Fusions of the β-glucuronidase (GUS) reporter gene to the promoter region of each *MRS2*/*MGT* gene were tested to investigate whether tissue- or organ-specific expression patterns are present in *Arabidopsis*. The physiological functions of MRS2/MGT proteins were addressed by characterizing gene knockout mutants. Viable homozygous knockout lines were raised for four genes of the family. No significant phenotypes were observed for single-gene knockouts (KOs) of three genes (*MRS2-1*, *MRS2-5*, and *MRS2-10*). Likewise, no impairment of plant growth and development was observed for two double KO lines that were created (*mrs2-1 mrs2-5* and *mrs2-5 mrs2-10*), even in spite of strong and overlapping gene expression early in seedling development. However, when substrate magnesium supply was lowered to 50 μM Mg^{2+}, we found a strong magnesium-dependent phenotype in planta for three independent single-gene KOs of the root-expressed *MRS2-7* gene. This KO mutant phenotype of *mrs2-7* is complemented and overcompensated with a cauliflower mosaic virus (CaMV) 35S promoter–driven *MRS2-7* construct, which additionally leads to an increase in biomass accumulation under magnesium-limiting conditions when compared with wild-type *Arabidopsis*.

RESULTS

Ancestry of the Plant *MRS2*/*MGT* Gene Family

The *Arabidopsis MRS2* gene family was originally described as encompassing 10 genomic loci, including one presumptive pseudogene, *MRS2-9* (Schock et al., 2000). A nearly simultaneous report of the gene family (Li et al., 2001) introduced the alternative *MGT* nomenclature and left the *MRS2-9* pseudogene unaccounted for but added a member with more distant similarity, *MGT10*, now also referred to as *MRS2-11* (Drummond et al., 2006). The complete rice (*Oryza sativa*) genome sequence allows comparative inferences concerning differential diversification of the gene family in this monocot compared with the dicot *Arabidopsis*. The members of the At *MRS2*/*MGT* gene family have their counterparts in nine proteins encoded in the genome of rice (Figure 1).

Five clades of *Arabidopsis MRS2*/*MGT* genes were observed (Figure 1), and for these we here suggest labels A through E, with characteristic intron insertion sites for each type of gene. We found that all 12 introns in *MRS2-11* (and its rice ortholog Os03g48000) are unique to clade A as can be inferred from different intron phases of closely spaced introns for which we suggest a nomenclature (see Supplemental Figure 1 online). Only clades B through E share three ancient introns in phase 0, which are occasionally lost later in evolution of the gene family (Figure 1).

Complementation of the Yeast *mrs2* Mutant

Given that *MRS2-1*, the founding member of the *Arabidopsis* gene family, was initially characterized by its ability to complement the yeast *mrs2* mutant when targeted to mitochondria (Schock et al., 2000), we reasoned that other members of the gene family would behave similarly, if possibly to differing degrees. Accordingly, we have now cloned a series of constructs containing the core coding regions of all *MRS2* genes (except for the pseudogenes *MRS2-8* and *MRS2-9*). These constructs were fused to the yeast Mrs2p mitochondrial targeting sequence and are driven from the native yeast *MRS2* promoter in the vector YEp351.

Complementation of the *mrs2* respiratory deficiency is easily monitored by restoration of the growth defect on nonfermentable medium with glycerol as the main carbon source (YPdG). Growth of yeast transformants containing *Arabidopsis* constructs was indistinguishable from growth of the yeast *mrs2* mutant transformed with the native Mrs2p coding sequence or the empty vector on nonselective YPD medium, indicating that these constructs do not interfere with yeast metabolism (Figure 2, left panels). We found that members of the *MRS2* gene family were able to complement the *mrs2* phenotype to similar degrees (Figure 2, right panels). MRS2-6 reconstituted growth to the highest level among the *Arabidopsis* proteins but was clearly less efficient compared with wild-type Mrs2p.

Mg^{2+} Transport Measurements

The molecular analysis of *mrs2* complementation using MRS2-1 showed that splicing of mitochondrial group II introns was restored (Schock et al., 2000). This phenomenon is now known to be an indirect effect through providing appropriate Mg^{2+} levels for group II intron ribozyme function in the yeast mitochondria (Gregan et al., 2001b). An indication for a direct involvement of MRS2-1 in mitochondrial Mg^{2+} uptake, however, had been obtained through measurements of mitochondrial magnesium

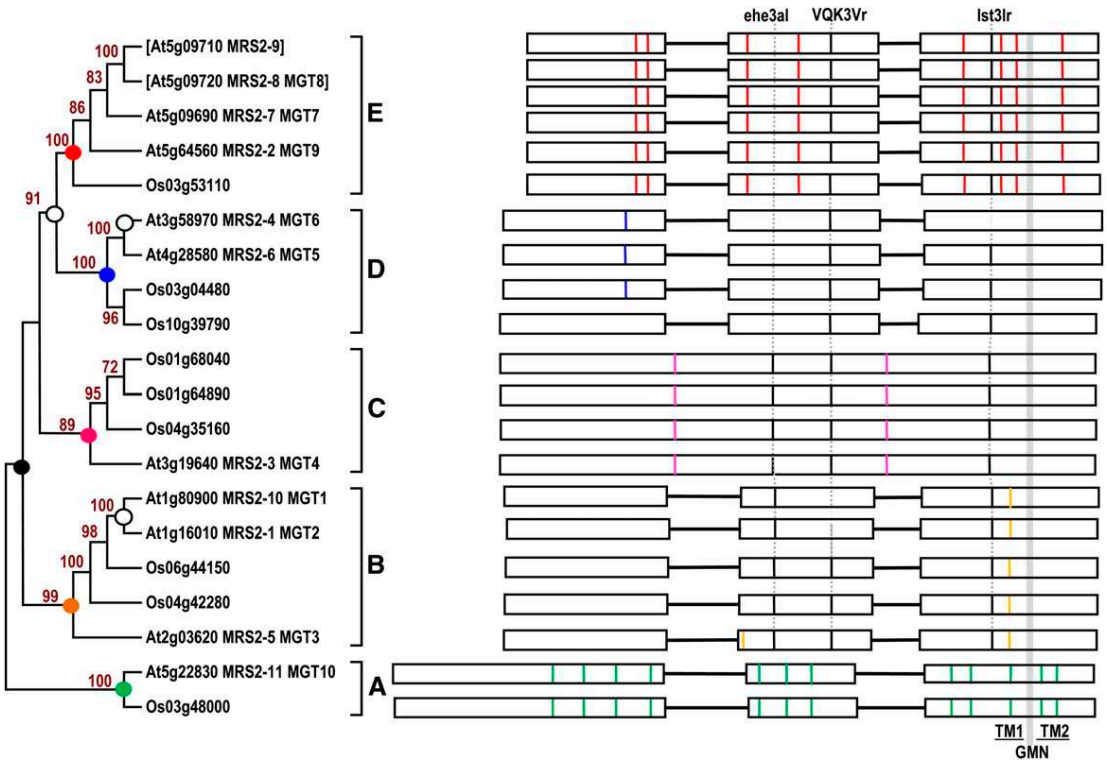

Figure 1. Phylogeny and Intron Structure of the *Arabidopsis* and *Oryza sativa* MRS2/MGT-Type Mg^{2+} Transport Protein Gene Families.

Phylogenetic relationships of family members are shown on the left side of the figure. Bootstrap node support (10,000 replicates) is shown where exceeding 70%. Standard designations for chromosomal loci and the alternatively proposed *Arabidopsis* nomenclature *MRS2* (Schock et al., 2000) and *MGT* (Li et al., 2001) are given for clarity. The pseudogenes *MRS2-8* and *MRS2-9* in *Arabidopsis* ecotype Col-0 are shown in brackets. Clades A through E of the gene family are supported by bootstrap analyses and by characteristic, ancient, and clade-specific intron patterns (vertical lines with different colors). Gains (color-filled circles) and losses (empty circles) of introns can be parsimoniously plotted onto the sequence-based tree. Intron occurrences in the respective coding sequences are shown as vertical lines in boxes on the right side of the figure. Designation of introns conserved across clades B through E (black) given on top are based on three amino acids upstream and two amino acids downstream of the insertion site (single-letter code with lower and uppercase letters reflecting low and high degrees of sequence conservation). The number in between indicates intron phase (insertion after the respective codon position of the preceding amino acid). Approximate locations of the C-terminal transmembrane domains and the conserved GMN motif between them is indicated (gray vertical line). Protein length variations are mainly due to two sequence inserts in clade C genes, which are lacking (or shorter) in the other clades (horizontal lines).

content, which reached nearly the wild-type level upon complementing the yeast mutant (Schock et al., 2000). In the meantime, a system for direct Mg^{2+} uptake measurements in yeast mitochondria has been developed using the fluorescent dye mag-fura-2, allowing a more direct confirmation of Mg^{2+} transport over biological membranes in real time, has been set up (Kolisek et al., 2003). Mag-fura-2 is a UV-excitable, Mg^{2+}-dependent fluorescent indicator that undergoes a blue shift from 380 to 340 nm upon Mg^{2+} binding. Accordingly, mitochondria were isolated from all yeast strains transformed with the *Arabidopsis MRS2* constructs to measure the magnesium uptake levels after external application of increasing Mg^{2+} concentrations in mag-fura-2–loaded mitochondria.

Mg^{2+} uptake was indeed measurable for all constructs to different extents, confirming their role as proteins mediating magnesium transport. Representative Mg^{2+} uptake recordings are shown in Figure 3. High magnesium uptake efficiencies were observed for MRS2-1, MRS2-7, and MRS2-10, whereas the other proteins proved somewhat less efficient uptake. A discrepancy was observed for MRS2-3, which appeared to complement well in the growth assay (Figure 2) but showed magnesium uptake that was not considerably higher than the background mutant level. Possibly, MRS2-3 acts as a comparatively slow transporter for Mg^{2+} (at least in the foreign yeast mitochondrial membrane environment), allowing for ion homeostasis over periods of hours as in the growth assays but not in measurable amounts over shorter time intervals, such as minutes as in the uptake experiments.

Tissue-Specific *MRS2* Gene Family Expression

To address their potential differential functions in planta, the upstream regions of all *MRS2* genes were fused to the GUS reporter gene to investigate the tissue specificities of their

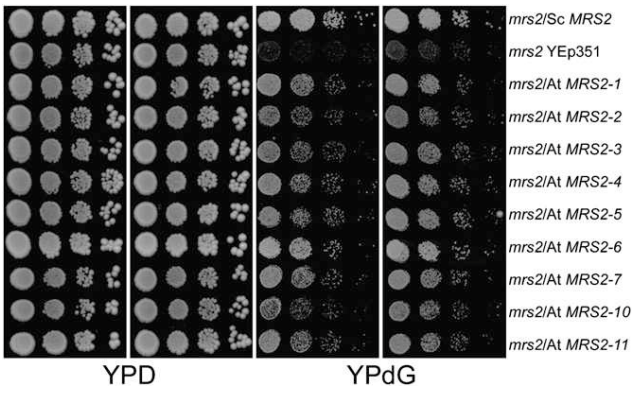

Figure 2. Complementation of the Yeast *mrs2* Mutant Strain Transformed with the *Arabidopsis MRS2* Genes.

Genes were translationally fused downstream of the native yeast MRS2 mitochondrial target sequence and were transcribed from the native yeast *MRS2* promoter. Five microliters of yeast cultures grown to an OD_{600} of 1.0 were each trickled in three dilutions (from left to right: 1.0, 0.1, 0.01, and 0.001, respectively) in parallel on nonselective YPD medium (two left panels) and on nonfermentable YPdG medium (two right panels).

promoters. We chose to clone >1000 bp of upstream noncoding regions, including the first coding exon of the *MRS2* genes, as translational fusions in front of GUS to maximize the inclusions of targets for regulatory influence on gene expression. Highly different tissue-specific patterns of gene expression during development were observed for the members of the *MRS2* gene family (Figure 4, Table 1). Several genes showed expression already at very early developmental stages of the seedlings. Nearly ubiquitous expression was observed in 3-d-old seedlings of *MRS2-1* and *MRS2-5* (Figures 4A and 4B), while expression was restricted to the radicle excluding the tip in the case of *MRS2-10* (Figure 4C).

Expression of other genes began somewhat later in development (e.g., in the case of *MRS2-3* in the central cylinder of the root; Figure 4D), interestingly with additional strong expression in the meristematic zone and in the hypocotyl (Figure 4E). Likewise, expression of *MRS2-2* was strictly restricted to the central cylinder (Figure 4F) and the veins (Figure 4G) at the early seedling stage. The absence of *MRS2-2* expression in the root tip (Figure 4F) similar to *MRS2-10* (Figure 4C) was merely complementary to the more widespread expression of *MRS2-1* in the different tissues of the root, most dominantly in the root tip (Figure 4B).

In the photosynthetic organs, the early ubiquitous expression of *MRS2-1* and *MRS2-5* (Figure 4A) became more localized to the vascular tissues of the expanded cotyledons during development, notably with a strong focus of *MRS2-5* gene expression in the early development of the first postcotyledon leaf pair (Figure 4H). This contrasted the highly localized expression of *MRS2-10* in the hydathodes of the cotyledons (Figure 4I) and the epicotyl (Figure 4J). Whereas expression of *MRS2-7* was entirely restricted to the root at the seedling stage (Figure 4K), a completely contrasting picture was observed for *MRS2-4* and *MRS2-11* with strong expression in photosynthetic tissues from the earliest stages of cotyledon development onwards (Figures 4L and 4M).

A unique particularity of *MRS2-11* was its pronounced expression in stomata guard cells (Figures 4M and 4N). Expression of *MRS2-4* in aboveground organs continued through plant development (e.g., in older leaves; Figure 4O) and the sepals of the developing flower (Figure 4P). In strong contrast, expression of the phylogenetically related *MRS2-6* gene (Figure 1) was particularly restricted and could only be observed in pollen grains (Figures 4Q and 4R). Complementary gene activities in the male flower parts were observed in the filaments for *MRS2-3* and *MRS2-10* (Figures 4S and 4T). Expression in the maturing seeds was observed for *MRS2-2* (Figures 4U and 4V). At later stages of development, pronounced gene activity was seen for *MRS2-1* in the style and coat of the silique (Figure 4W). Particularly strong overall gene expression was again observed for MRS2-4 at an early stage of silique development with the exception of the stigma (Figure 4X).

Later, in the fully developed silique, *MRS2-4* gene expression was restricted to the abscission zone, as also observed for *MRS2-11* (Figure 4Y). The focus of *MRS2-2* expression in vascular tissue in early stages of development continued later through development as, for example, in the veins during early bud development (Figure 4Z). Observation of shoot cross sections after xylem counterstaining with safranin demonstrated expression in the phloem (Figure 4Za). *MRS2-10*, phylogenetically very close to *MRS2-1*, interestingly showed a very cell type–specific expression not only in early stages of development (Figures 4C, 4I, and 4J) but also a pronounced expression in trichomes (Figure 4Zb).

Publicly available microarray data (www.genevestigator.com) so far give no indication for environmental regulation of the *MRS2* genes, and, similarly, we could not observe any obvious variability in gene expression when the *MRS2*-GUS lines were grown

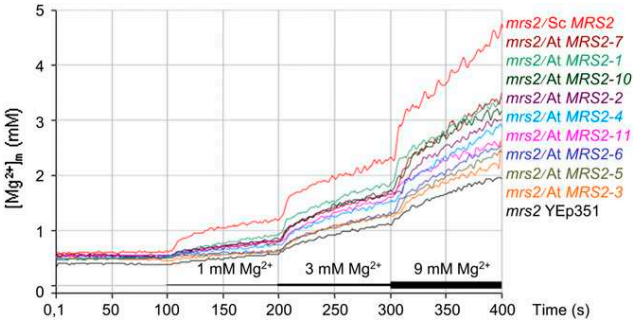

Figure 3. Measurements of Mg^{2+} Import into Isolated Mitochondria Using the Fluorescent Mag-fura-2 Dye.

Mitochondria isolated from the complemented yeast strains were exposed to stepwise increased external concentrations of magnesium (1, 3, and 9 mM $MgCl_2$) at time points of 100, 200, and 300 s of incubation, respectively. The 340/380-nm ratio of fluorescence was continuously recorded by the FL-WinLab program (v4.0; Perkin-Elmer), and the formula established by Grynkiewicz et al. (1985) was used to calculate the Mg^{2+} concentrations inside the mag-fura-2–loaded mitochondria ($[Mg^{2+}]_m$). Curves were averaged over at least two independent recordings.

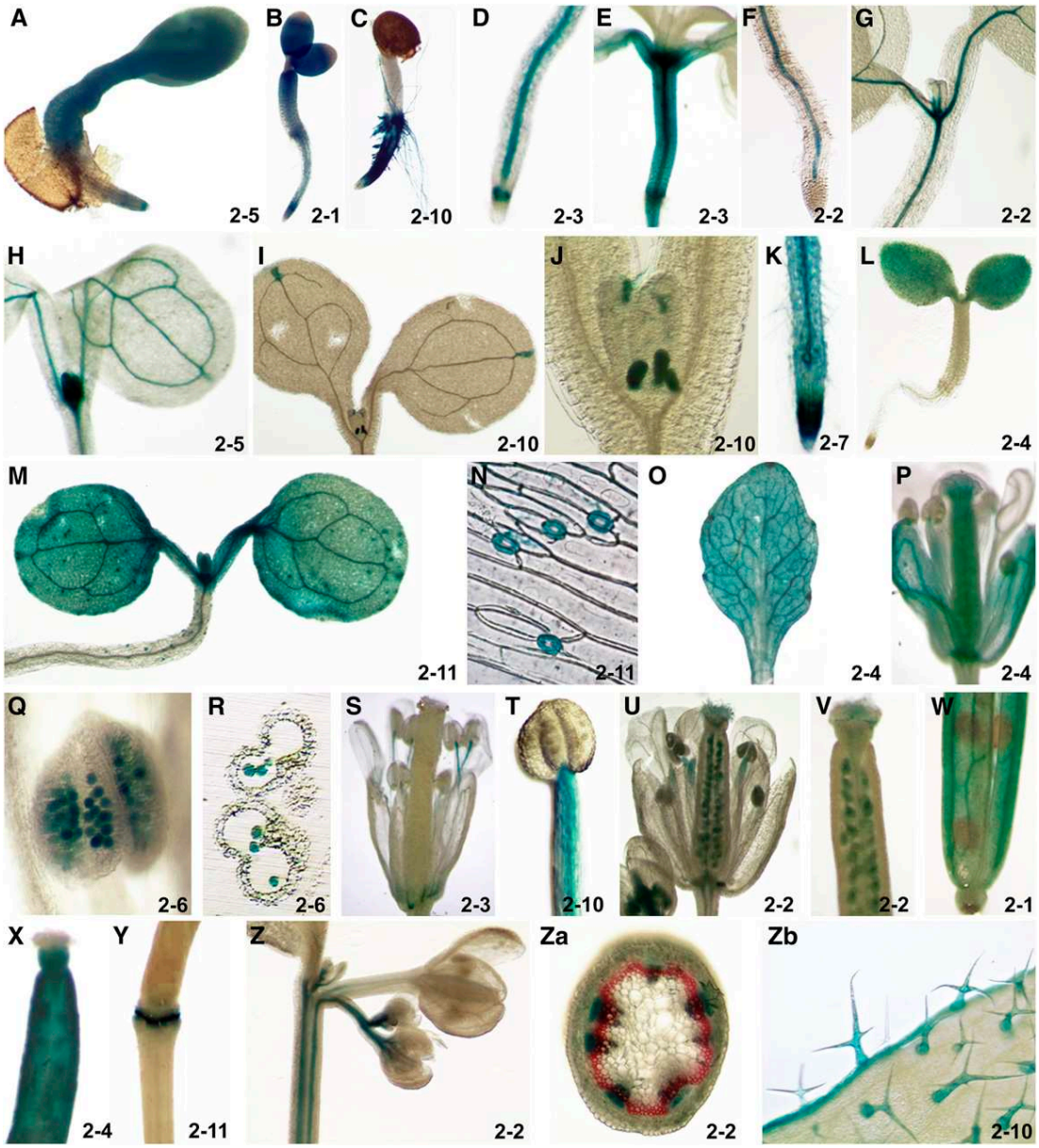

Figure 4. GUS Assays of Transgenic *Arabidopsis MRS2:GUS* Lines to Determine Tissue-Specific Transcriptional Activities in the Gene Family.

(A) and **(B)** Three-day-old seedlings of MRS2-5:GUS **(A)** and MRS2-1:GUS **(B)**.
(C) One-day-old seedling of MRS2-10:GUS.
(D) and **(E)** Three-day-old **(D)** and 10-d-old **(E)** seedlings of MRS2-3:GUS.
(F) and **(G)** Seven-day-old seedling of MRS2-2:GUS.
(H) Seven-day-old seedling of MRS2-5:GUS.
(I) and **(J)** Seven-day-old seedling of MRS2-10:GUS.
(K) Seven-day-old seedling of MRS2-7:GUS.
(L) Three-day-old seedling MRS2-4:GUS.
(M) and **(N)** Seven-day-old seedlings of MRS2-11:GUS.
(O) and **(P)** Mature MRS2-4:GUS plants in the flowering stage.
(Q) and **(R)** MRS2-6:GUS anthers **(Q)** and anther cross section showing pollen grains **(R)**.
(S) to **(U)** Anthers of MRS2-3:GUS **(S)**, MRS2-10:GUS **(T)**, and MRS2-2:GUS **(U)**.
(V) to **(Y)** Maturing siliques of MRS2-2:GUS **(V)**, MRS2-1:GUS **(W)**, MRS2-4:GUS **(X)**, and MRS2-11:GUS **(Y)**.
(Z) Flower buds of MRS2-2:GUS.
(Za) Shoot cross section of MRS2-2:GUS.
(Zb) Leaf surface with trichomes of MRS2-10:GUS.

Table 1. Summary of *MRS2/MGT* Gene Activities as Determined from GUS Activities in Transgenic Promoter-GUS Fusion Lines (Figure 4)

Tissue	*MRS2-1*	*MRS2-2*	*MRS2-3*	*MRS2-4*	*MRS2-5*	*MRS2-6*	*MRS2-7*	*MRS2-10*	*MRS2-11*
Early seedling									
Cotyledons	+	+[a]	+[a]	+	+	–	–	–	++
Hypocotyl	+	+[a]	++	–	+	–	–	–	–
Radicle	+	+[a]	+[a]	–	+	–	+[h]	++	–
Inflorescence									
Flower									
Anthers	–	+	–	–	+	++[c]	–	–	–
Filament	+	±[a]	+[a]	±[a]	–	–	–	+	–
Pistil	–	+[b]	–	+	–	–	±	–	–
Sepals	+	–	–	+	–	–	–	±	±[a]
Petals	–	–	–	–	–	–	–	–	–
Silique	+	+[b]	+[f]	++	–	–	±[f]	+[f]	+[f]
Cauline leaf	+	+[a]	+[a]	++	+	–	+[a]	±[d]	+[a]
Stem	–	+[a]	+[a]	+[a]	++[a]	–	+[a,i]	+[g]	+[i]
Rosette									
Juvenile leaf	+	+[a]	+[a]	++	+[a,e]	–	+[i]	+[d,e]	++
Adult leaf	+	±[a]	±[a]	++	+	–	+[a]	+[a,g]	++
Roots									
Lateral root	+[a]	–	+[a]	–	+[a]	–	++[a]	–	–
Root hair zone	+[a]	+[a]	+[a]	–	+[a]	–	++[a]	++	–
Elongation zone	+[a]	+[a]	+[a]	–	+[a]	–	–	++	–
Meristematic zone	++	–	+	–	++	–	++	–	–
Root tip	–	–	–	–	++	–	–	–	–

Letters indicate distinct staining in vascular tissues (a), ovules (b), pollen grains (c), hydathodes (d), leaf primordia (e), abscission zones (f), trichomes (g), quiescent centers (h), or stomata cells (i).

on different magnesium concentrations in hydroponic culture systems (see below). To address the issue of potential magnesium dependent gene regulation yet more explicitly, we performed RT-PCR analyses using *Arabidopsis* plantlets raised on 50, 500, or 1500 μM Mg^{2+} to detect potential changes in transcript amounts. No evidence for magnesium-dependent regulation for any of the *MRS2* genes was observed (see Supplemental Figure 2 online).

Gene to Function: KO Phenotypes

To further address the function of MRS2 proteins in planta, we searched for gene-specific inactivation lines to investigate mutant phenotypes. Candidates for 17 transgenic *Arabidopsis* lines with T-DNA insertions in (or close to) members of the *MRS2* gene family and potentially affecting the respective gene functions were identified in the SALK (and GABI-KAT) collections (http://signal.salk.edu/cgi-bin/tdnaexpress; see Supplemental Table 1 online) for all genes except *MRS2-4*. Seeds for all insertion lines except those of the pseudogenes *MRS2-8* and *MRS2-9* were ordered, and the progeny were investigated to first verify the genomic insertion through a PCR-based strategy.

Subsequently, we tried to raise homozygous insertion lines and confirm the knockout of transcription. Among the insertion lines, one could not be verified as harboring the insertion, and among the remaining lines, five could only be obtained in the heterozygous state. A transcriptional knockout was not observed for any of the other lines having insertions outside of the coding regions but could be confirmed for a total of six lines with insertions within the coding regions of four genes in the family (see Supplemental Figure 3 online): one each for *MRS2-1*, *MRS2-5*, and *MRS2-10* and three independent KO lines for *MRS2-7*. Furthermore, double KO mutant lines of *MRS2-1* + *MRS2-5* and *MRS2-5* + *MRS2-10* could be obtained via crossing and screening for progeny homozygous in both insertion alleles.

All six single-gene KO lines [*mrs2-1*, *mrs2-5*, *mrs2-7(1)*, *mrs2-7(2)*, *mrs2-7(3)*, and *mrs2-10*] and the two double KO lines *mrs2-1 mrs2-5* and *mrs2-5 mrs2-10* appeared fully vital without obvious phenotypes under standard growth conditions and went through a normal reproductive cycle, initially suggesting strong genetic redundancy in the gene family or its subclades, respectively.

To explore the possibility that a certain *mrs2*-related phenotype may be seen only in conditions of Mg^{2+} stress, we set up two different culture systems: a hydroponic and a liquid culture system. For the hydroponic culture system, we allowed plants to complete their life cycle under defined growth conditions. We found that wild-type *Arabidopsis* (ecotype Columbia [Col-0]) tolerates the full range of Mg^{2+} concentrations between 50 μM and 5 mM under the otherwise unaltered ion concentrations of the Siegenthaler culture medium (Siegenthaler and Depéry, 1976). Hence, $MgSO_4$ concentrations ranging between micro- and millimolar levels were used to scan for Mg^{2+}-dependent phenotypes among the T-DNA insertion lines. While the knockout lines *mrs2-1*, *mrs2-5*, and *mrs2-10* and the double knockouts *mrs2-1 mrs2-5* and *mrs2-5 mrs2-10* remained as unaffected by the varying Mg^{2+} concentrations as the wild type, a striking phenotype was observed for the knockout line *mrs2-7(2)*. Plantlets were severely retarded in development under 50 μM Mg^{2+} (Figure 5A). Raising the Mg^{2+} concentrations to slightly higher levels (150 μM) immediately restored this phenotype practically

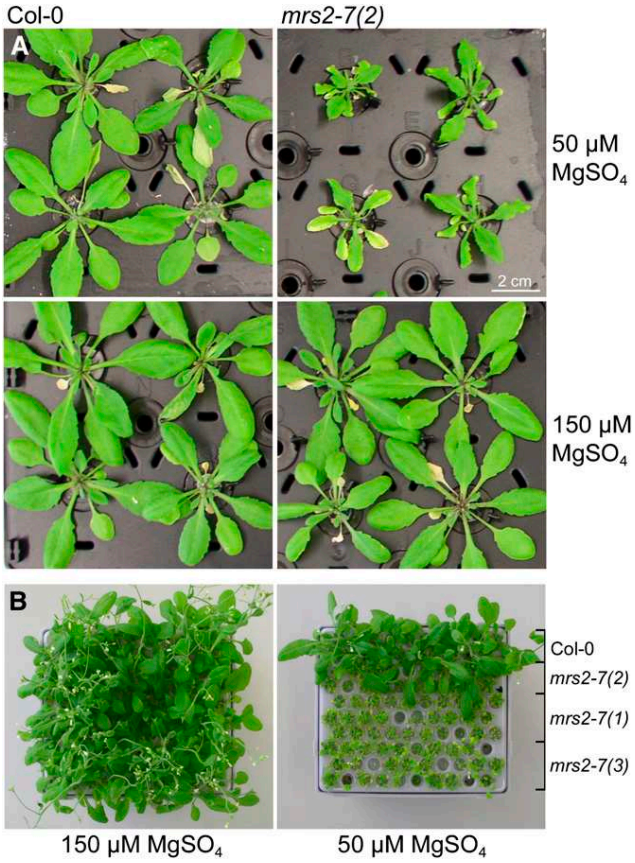

Figure 5. Hydroponic Cultivation of KO and Wild-Type Plants in Two Alternative Systems.

(A) Effect of Mg^{2+} concentration on growth of *Arabidopsis* wild type (Col-0) and the homozygous KO *mrs2-7(2)* T-DNA insertion line. Plants were grown on Siegenthaler medium with either 50 or 150 μM $MgSO_4$ and are shown 28 d after germination in the Araponics culturing system. **(B)** Twenty to thirty seedlings each of *Arabidopsis* wild-type and three independent (*1-3*) homozygous T-DNA insertion *mrs2-7* KO lines 35 d after germination in a pipette tip–based high-density hydroponic culturing system established in the laboratory.

to wild-type growth, and the mutant plants remained unaffected by yet higher magnesium concentrations.

To exclude that any additional genomic rearrangements were responsible for the low Mg^{2+} phenotype observed, we also investigated the two alternative KO lines in *MRS2-7*, which could also be obtained in the homozygous state. These lines, *mrs2-7(1)* and *mrs2-7(3)*, also carry, like the initially characterized mutant *mrs2-7(2)*, T-DNA insertions in introns of the *MRS2-7* gene. Exactly the same phenotype as for the *mrs2-7(2)* KO line was observed (Figure 5B), confirming that inactivity of *MRS2-7* indeed is the fundamental cause for the low Mg^{2+} phenotype. To determine whether KO of MRS2-7 affects ion homeostasis more globally, we used the Purdue Ionomics service (Baxter et al., 2007; Salt et al., 2008; www.ionomicshub.org), offering comprehensive ion content analyses. For all three independent *mrs2-7* KO lines, no significant imbalances in homeostasis of Mg^{2+} or any one of 17 other ions were observed under normal growth conditions in the ionomics measurements other than a possible 10 to 20% reduction of K^+ in comparison to the wild type (see Supplemental Figure 4 online).

As no similar phenotypes could be observed for the KO lines *mrs2-1*, *mrs2-5*, and *mrs2-10* and even for the double KO mutants, we tried to investigate potentially more subtle differences in these mutants using a liquid culture system containing Murashige and Skoog (MS) medium with 50 and 100 μM of $MgSO_4$. The liquid media were supplemented with sucrose to allow enhanced seedling growth, while any other complex compounds that might contribute spurious amounts of Mg^{2+} were excluded. Additionally, a stable transgenic complementation line harboring the *MRS2-7* coding sequence under control of the constitutive CaMV 35S promoter within the *mrs2-7(2)* background was investigated. As observed in the hydroponic culture, KO lines *mrs2-1*, *mrs2-5*, and *mrs2-10* never showed significant differences compared with the wild type under any condition tested (data not shown). By contrast, the *mrs2-7* KO line failed to germinate under these liquid culture conditions, whereas the *MRS2-7*–overexpressing line revealed a strong increase in biomass production under 50 μM and a slight increase under 100 μM $MgSO_4$ compared with wild-type seedlings (Figure 6). This germination phenotype of *mrs2-7* prompted us to reinvestigate the earliest stages of *MRS2-7* gene expression. Indeed, the *MRS2-7:GUS* reporter line showed very specific expression of *MRS2-7* very early in the quiescent zone of the emerging radicle (Figure 7). This finding is in full accord with the high-resolution transcriptional profiling of the *Arabidopsis* root quiescent center (Nawy et al., 2005).

Subcellular Localization of MRS2-7

Given that a first magnesium-related phenotype is now identified in planta for a member of the *MRS2/MGT* gene family, we wished to determine the subcellular localization of MRS2-7. The full-length coding sequence of MRS2-7 was cloned as a translational fusion upstream of the green fluorescent protein (GFP) under control of the CaMV 35S promoter. The construct was used for transient transformation of *Nicotiana benthamiana* leaves via *Agrobacterium tumefaciens* followed by laser scanning confocal fluorescence microscopy (Figure 8). GFP fluorescence was observed in the endomembrane system, suggesting targeting to the endoplasmatic reticulum (ER). As a control experiment, we used the ER-targeted HDEL:DsRED construct (Höfer et al., 2008) in a cotransformation assay. Nearly perfectly overlapping expression with the MRS2-7:GFP construct was observed.

DISCUSSION

We were able to raise homozygous T-DNA insertion knockout lines for four genes of the *MRS2/MGT* family: *MRS2-1*, *MRS2-5*, *MRS2-7*, and *MRS2-10*. Based on the phylogeny shown in Figure 1, this can be nicely explained, given that all four genes belong to clades B and E containing closely related homologs, which may contribute genetic redundancy, as commonly observed for

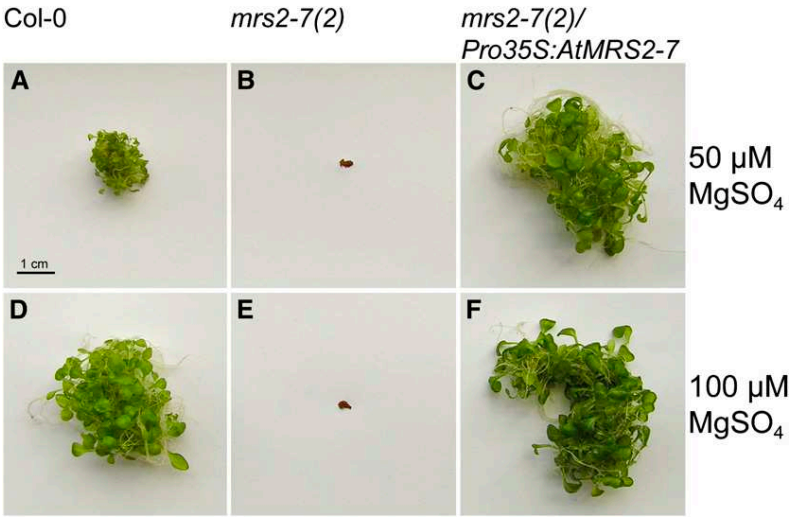

Figure 6. Biomass Accumulation of *Arabidopsis* Seedlings.

Photos were taken 14 d after incubation of ~20 seeds of each individual line in liquid shaking cultures (24°C, 16 h light long-day regime) containing 100 mL of MS medium supplemented with 1% sucrose with $MgSO_4$. Plants shown are *Arabidopsis* wild-type ecotype Col-0 (**[A]** and **[D]**), *mrs2-7(2)* KO line (**[B]** and **[E]**), and this KO line transformed with *MRS2-7* cDNA driven by the CaMV 35S promoter (**[C]** and **[F]**).
(A) to **(C)** Plants grown in 50 μM $MgSO_4$.
(D) to **(F)** Plants grown in 100 μM $MgSO_4$.

members of *Arabidopsis* gene families (Briggs et al., 2006). By contrast, we were unable to identify, raise in a homozygous state, or ultimately verify on transcriptional level any KO lines for the more isolated members of the gene family, most notably *MRS2-11/MGT10* or *MRS2-3/MGT4*, which are the respective single *Arabidopsis* members of clades A or C (Figure 1). Likewise, no KOs could be obtained for *MRS2-4/MGT6*, for *MRS2-6/MGT5* with its unique, exclusive pollen-specific expression (Figure 4), or for *MRS2-2/MGT9.* This is in full accord with recent reports finding that only heterozygous T-DNA insertion lines of *MRS2-6/MGT5* and *MRS2-2/MGT9* are viable (Li et al., 2008; Chen et al., 2009).

Here, we did not consider the pseudogenes *MRS2-8* (dysfunctional in ecotype Col-0) and *MRS2-9* (dysfunctional in ecotypes Col-0 and Landsberg) of clade E for functional studies. It should be noted, however, that the cluster of neighboring genes *MRS2-7/MRS2-8/MRS2-9* on *Arabidopsis* chromosome 5 may be an interesting object of study for ecotype variation (and possible functional evolutionary adaptation) in the future. It came as a surprise to us that just the knockout of *MRS2-7* belonging to this group of probably recently duplicated young and rapidly evolving genes resulted in the observable magnesium-dependent phenotype in planta for a member of the *MRS2/MGT* gene family. The dramatic phenotype observed under very low magnesium conditions of 50 μM is easily complemented both by a moderate increase in Mg^{2+} to 150 μM in the substrate and by ectopic overexpression of *MRS2-7* under control of the CaMV 35S promoter in the mutant background. Surprisingly, the complemented transgenic *Arabidopsis* line additionally shows a striking gain in vitality and biomass accumulation compared with wild-type plants. As a side note, we could not observe a similar effect when a genomic instead of a cDNA construct for *MRS2-7* was used. This turned out to be due to aberrant missplicing of *MRS2-7* mRNAs in that transgenic line, also including a natural splice alternative that lacks an exon and was reported previously as nonfunctional (Mao et al., 2008).

Very obviously, the overexpression of *MRS2/MGT* genes in planta may have significant influences on ion homeostasis. Three genes of the *MRS2/MGT* gene family have indeed been identified as candidate loci in a search for quantitative trait loci affecting seed mineral concentrations in general and Mg^{2+} in particular: *MRS2-2*, *MRS2-3*, and *MRS2-11* (Waters and Grusak, 2008).

Figure 7. GUS Assay for Promoter Activity of the *MRS2-7:GUS* Transgenic Line in the Earliest Stage of Seedling Development Showing Transcriptional Activity in the Tip of the Radicle at Day 1.

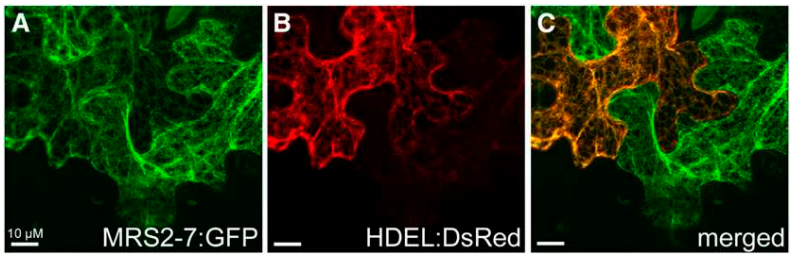

Figure 8. Subcellular Localization of MRS2-7.

(A) and **(B)** Confocal laser scanning microscopy images taken 2 d after transient *N. benthamiana* leaf transformation with the AtMRS2-7:GFP fusion construct **(A)** or the HDEL:Ds-Red construct **(B)** to visualize the ER.
(C) Overlay of **(A)** and **(B)**.

Overexpression of MRS2-11, localizing to the chloroplast envelope membrane, however, showed no difference in magnesium content, neither in whole *Arabidopsis* plants nor isolated chloroplasts (Drummond et al., 2006).

Aside from the single KO lines for the three *MRS2/MGT* genes of clade B (Figure 1), we were also able to obtain double KO lines for *mrs2-5 mrs2-1* and *mrs2-5 mrs2-10.* Like the corresponding single-gene KO lines, these lines had no detectable phenotype. This observation is somewhat surprising in the light of the strong and overlapping expression, notably of *MRS2-1* and *MRS2-5* early in seed development (Figure 4). Moreover, in the context of proteome analyses of cellular compartments, it was found that MRS2-1/MGT2 was localized to the tonoplast (Carter et al., 2004), whereas MRS2-5/MGT3 was found either in the plasma membrane (Alexandersson et al., 2004) or the tonoplast (Whiteman et al., 2008). This allows no reasonable assignment as to whether these two proteins are redundant in function or not. The magnesium-proton exchanger *MHX*, which is unrelated to the *MRS2/MGT* gene family, was also localized in the tonoplast membrane (Shaul et al., 1999). Assuming that the MRS2-1/MGT2 channel would allow Mg^{2+} flow from the positively charged, acidic vacuole into the cytosol, it is unlikely that a knockout could be functionally complemented by MHX, which transports Mg^{2+} into the vacuole in exchange for protons. On the other hand, MRS2-10/MGT1, like MRS2-5/MGT3, was also found to be localized to the plasma membrane (Li et al., 2001). Hence, the double KO line *mrs2-5 mrs2-10* described here shows that two membrane proteins of identical localization may be missing simultaneously without strongly interfering with Mg^{2+} homeostasis in the plant.

Certainly, observations and reports regarding protein localizations in the cell should not be overstated and instead should be considered carefully. At least some MRS2/MGT proteins, including MRS2-7, here found to be ER localized (Figure 8), may actually be localized to more than one membrane type (possibly in variable stoichiometries), and this is certainly very obvious for the endomembrane system extending from the ER up to the plasma membrane. Clearly set apart with respect to subcellular localizations are the MRS2/MGT family members localized to the endosymbiotic organelles: MRS2-6/MGT5 in mitochondria (Li et al., 2008) or MRS2-4/MGT6 and MRS2-11/MGT10 in chloroplasts (Froehlich et al., 2003; Drummond et al., 2006; this study).

The drastic phenotype of growth retardation in *mrs2-7* KO lines in environments of very low magnesium concentrations may, in the light of an ER localization of the protein, suggest that the endomembrane system is highly sensitive to Mg^{2+} deficiency. Notably, among the many functions of magnesium ions in the cell is the stabilization of biological membranes, which may at the same time be a possible explanation for the enhanced viability of *Arabidopsis* lines upon overexpression of MRS2-7 here observed. Alternatively, Mg^{2+} has also been shown to participate in Ca^{2+}-based signal transduction processes (Baumann et al., 1991; Wiesenberger et al., 2007), and low magnesium concentrations may become a limiting factor for functional intracellular communication.

The GUS indicator gene expression data of the *MRS2* gene family revealed partially overlapping expression for some genes but also highly specific patterns of expression for others (Figures 4 and 7). Publicly available whole-genome expression data from chip hybridization experiments are largely consistent as far as comparable; unfortunately, a probe set for *MRS2-5* is missing on the widely used *Arabidopsis* whole-genome Affymetrix probe array ATH1 (Redman et al., 2004). A gene expression map of the *Arabidopsis* root distinguishing 15 tissue stages based on data from the microarray data (Birnbaum et al., 2003) is likewise in accord (e.g., reflecting comparatively strong overall expression of *MRS2-1* and *MRS2-3* [again, *MRS2-5* is lacking] in the root). The strong stage 1 expression observed for *MRS2-7* in those experiments is fully congruent with the focused expression in the meristematic zone observed here. Available microarray expression data (www.genevestigator.com) so far give no conclusive hints on significantly divergent expression patterns of *MRS2/MGT* genes in different environmental setups, and the same can be said for GUS assays after plant cultivation on different media (data not shown).

Direct proof for channel-like Mg^{2+} transport through the yeast mitochondrial homolog Mrs2p by use of the fluorescence indicator mag-fura-2 had previously been shown (Kolisek et al., 2003). The measurements reported here of Mg^{2+} uptake into isolated *mrs2* yeast mutant mitochondria after expression of *Arabidopsis* MRS2/MGT proteins show their principal capability of magnesium transport in this nonhomologous membrane system. The complementation of mutants lacking some of their

endogenous Mg^{2+} uptake systems has previously been demonstrated for *Arabidopsis MRS2-1/MGT2* and *MRS2-11/MGT10* in yeast (Schock et al., 2000; Li et al., 2001) and for *Arabidopsis MRS2-2/MGT9*, *MRS2-6/MGT5*, *MRS2-7/MGT7*, and *MRS2-10/MGT1* in *Salmonella enterica* (Li et al., 2001, 2008; Mao et al., 2008; Chen et al., 2009). Somewhat in contrast with this apparent functional complementation across wide phylogenetic distances, only *MRS2-1*, *MRS2-10*, and *MRS2-11* but not the other members of the gene family were found to complement the *alr1 alr2* yeast mutant with a defect of plasma membrane magnesium transport (Drummond et al., 2006). Those observations may possibly be explained by mistargeting of the *Arabidopsis* MRS2/MGT proteins in the yeast cells.

Direct demonstration of Mg^{2+} transport through the yeast plasma membrane homolog ALR1 had previously also been achieved electrophysiologically (Liu et al., 2002). In an alternative approach, patch clamp experiments using giant lipid vesicles have recently demonstrated that the yeast MRS2 protein is a Mg^{2+}-regulated Mg^{2+} channel of high conductance with lower conductance for Ni^{2+} but none for Co^{2+}, Mn^{2+}, or Ca^{2+} (Schindl et al., 2007). This may be reasonably well explained by an increasing ion radius, although there is only a minor difference between the one for Ni^{2+} (0.72 Å) versus Co^{2+} (0.74 Å), compared with (0.65 Å) for Mg^{2+}. However, these findings stand in contrast with the bacterial CorA proteins obviously also transporting Co^{2+} (Niegowski and Eshaghi, 2007). Certainly, this may reflect actual differences in eukaryotic protein structure affecting ion selectivity, and it will be highly interesting to perform comparative studies.

The membrane topology of the 2-TM-GMN type of proteins has been clarified through crystallization and x-ray structural analysis of the *T. maritima* CorA homolog (Eshaghi et al., 2006; Lunin et al., 2006; Payandeh and Pai, 2006), showing the protein to form a pentamer in the membrane. It is likely that the eukaryotic homologs of the MRS2 or ALR type will assemble very similar structures in the membranes. Indeed, there is already biochemical evidence (through cross-linking) and genetic evidence using the yeast mating-based split-ubiquitin system (mbSUS; Obrdlik et al., 2004) for oligomerization of ALR1 and ALR2, the yeast cytoplasmic type of 2-TM-GMN–type membrane proteins. As a consequence, mutations in one of the two proteins can exert dominant-negative effects on magnesium transport (Wachek et al.. 2006).

METHODS

Plant Material and Growth Conditions

Arabidopsis thaliana ecotype Col-0 and T-DNA insertion lines in *MRS2/MGT* genes were obtained from the European *Arabidopsis* Stock Centre. T-DNA insertions were confirmed, homozygous lines raised, and gene knockout on the transcript level was finally confirmed for six lines in four of the *MRS2/MGT* genes (see Supplemental Table 1 and Supplemental Figure 2 online). Additionally, two double KO lines were successfully obtained via crossing: *mrs2-1 mrs2-5* and *mrs2-5 mrs2-10*. *Arabidopsis* seeds were surface sterilized (Swinburne et al., 1992) and sown on MS medium (Duchefa Biochemie) supplemented with 1% sucrose, 0.05% MES, pH 5.7 (KOH), and 0.8% bacto agar. Transgenic plants were selected in the presence of 50 μg/mL kanamycin. All plants were stratified for 2 d at 4°C and grown under 16 h of light photoperiods at 24°C and ~100 μmol/m^2/s light intensity.

Hydroponic cultivation of *Arabidopsis* plants (Norén et al., 2004) was modified, using either opaque filter tip containers or the Araponics growing system (Araponics) and nutrient solutions with varying concentrations of magnesium. Nutrient solutions were replaced every 2 weeks or immediately upon indication of emerging algal growth. Liquid cultivation of germinating *Arabidopsis* seeds was done in conical flasks incubated on a rotary shaker at 100 rpm. Liquid media were based on MS medium mentioned above, which was adjusted to different magnesium concentrations. Comprehensive ionomics measurements with inductively coupled plasma mass spectrometry were performed using the Purdue Ionomics Information Management System (Baxter et al., 2007).

Plasmid Constructs and Plant Transformation

All plasmid constructs were cloned by recombination of PCR products into destination vectors using Gateway technology (Invitrogen). GUS (*uid*A) reporter gene constructs comprised the noncoding upstream region and the first exon of each MRS2 gene cloned in frame upstream of GUS into vector pKGWFS7 (Karimi et al., 2002). The full-length *MRS2-7* (At5g09690.1) coding sequence was cloned behind the CaMV 35S promoter in vector pK7WG2D (Karimi et al., 2002) for overexpression and upstream of GFP in translational fusion into vector pMDC83 (Curtis and Grossniklaus, 2003), respectively. *Agrobacterium tumefaciens* strain GV3101 pMP90 (Koncz and Schell, 1986) was transformed with the binary vector constructs (Höfgen and Willmitzer, 1988) and used to transform developing floral tissues of 4-week-old *Arabidopsis* plants using the floral dip method (Clough and Bent, 1998).

Transcript Analyses

Total RNAs were prepared from 2-week-old *Arabidopsis* plantlets grown in liquid cultures or rosette leafs from adult plants grown on soil using the NucleoSpin RNA plant kit (Macherey-Nagel), and cDNA was synthesized with the Transcriptor High Fidelity cDNA synthesis kit (Roche Diagnostics) applying anchored-oligo $(dT)_{18}$ primer with equalized amounts of template RNA. Expression levels of the target genes were determined after 30, 35, and 40 cycles of gene-specific PCR amplification via gel electrophoresis and ethidium bromide staining.

GUS Assays, Histochemical Staining, and Microscopy

To detect GUS activity, *Arabidopsis* plant samples or entire seedlings were infiltrated with substrate solution (1 mM 5-bromo-4-chloro-3-indolyl-β-D-glucuronic acid, 100 mM sodium phosphate buffer, at pH 7.0, 10 mM EDTA, 3 mM ferrocyanide, 0.5 mM ferricyanide, and 0.1% Triton X-100) at 37°C for 16 h (Jefferson et al., 1987). After staining, chlorophyll was removed with 70% ethanol at 37°C. For sectioning before microscopy, plant samples were placed in fixation buffer (50 mM PIPES, 1.5% glutaraldehyde, and 0.5% glucose) and dehydrated through a dilution series of ethanol incubations up to absolute ethanol. Tissues were embedded in Spurr Low-Viscosity Embedding Media (Polysciences Europe) and sliced with a microtome (Ultramikrotom Om U43; Reichert Optische Werke).

Transient Expression of GFP Fusions in *Nicotiana benthamiana*

Agrobacterium strains containing the MRS2-7:GFP or a HDEL:DsRED construct (Jach et al., 2001) for ER colocalization studies (kindly provided by the cell biology department at the Institut für Zelluläre und Molekulare Botanik, Bonn) were grown overnight in 4 mL Luria-Bertani medium containing the appropriate antibiotics at 28°C to stationary phase. Bacteria were harvested by centrifugation and pellets were resuspended in 2

mL infiltration medium (10 mM $MgCl_2$, 10 mM MES, and 150 μM acetosyringone, pH 5.7) and incubated at 28°C for 3 h. The bacterial suspensions were adjusted to an optical density (OD_{600}) of 1.0 and coinfiltrated into the abaxial spaces of young but fully expanded leaves of 6- to 8-week-old *N. benthamiana* plants with a needleless syringe. Infiltrated leaves were examined after 48 h with an Olympus FV1000 confocal microscope, and serial confocal optical sections were taken. Images were analyzed using the Olympus FV1000 Viewer software.

Functional Complementation and Mg^{2+} Uptake Measurements in the Yeast *mrs2* Mutant

To express the *Arabidopsis* MRS2/MGT proteins in yeast, an upstream fragment of the yeast *MRS2* gene encoding the first 94 amino acids for mitochondrial targeting and the native promoter region was amplified by PCR from the plasmid YEp351-MRS2 (Wiesenberger et al., 1992). The amplified fragment was fused to the respective N-terminally shortened *MRS2* coding sequences at the first conserved protein motif (RDLR) of the *Arabidopsis MRS2* genes with a single hemagglutinin tag at the C termini by overlap extension PCR and cloned into vector YEp351 (Hill et al., 1986). Yeast strain DBY *mrs2-1* (Wiesenberger et al., 1992) was transformed using the LiOAc/SS Carrier DNA/PEG method (Gietz and Woods, 2002) and trickled in parallel in a 10-fold serial dilution on normal (YPD) and nonfermentable media (YPdG) to test complementation of the *mrs2* growth defect (Bui et al., 1999). Magnesium uptake was determined via the fluorescent dye mag-fura-2 (Invitrogen) in isolated mitochondria as previously described (Kolisek et al., 2003).

Phylogenetic Tree Construction

Accession numbers for protein sequences used for alignment are listed in the following section. *Arabidopsis* and rice (*Oryza sativa*) MRS2/MGTprotein sequences were aligned using the CLUSTAL algorithm (gap creation and extension penalties of 10 and 1, respectively) with minor manual adjustments in MEGA (Kumar et al., 2008). Alignments are provided in Supplemental Data Set 1 online. The protein phylogeny was inferred using the neighbor-joining method (Saitou and Nei, 1987) and Poisson-corrected amino acid distances with MEGA with the pairwise deletion option eliminating indels only in pairwise comparisons. Node reliability was determined with 10,000 bootstrap replicates.

Accession Numbers

Sequence data from this article can be found in the GenBank/EMBL or Arabidopsis Genome Initiative data libraries under the accession numbers that follow. The following nucleotide sequence accessions were used for cloning of the yeast and the *Arabidopsis* constructs: NM_101469 (*MRS2-1*, At1g16010), NM_125852 (*MRS2-2*, At5g64560), NM_112854 (*MRS2-3*, At3g19640), NM_115759 (*MRS2-4*, At3g58970), NM_126412 (*MRS2-5*, At2g03620), NM_119000 (*MRS2-6*, At4g28580), NM_121006 (*MRS2-7*, At5g09690), NM_106738 (*MRS2-10*, At1g80900), and NM_122188 (*MRS2-11*, At5g22830). The following protein sequence accessions were used for construction of the phylogenetic tree: CAC13981 (At MRS2-1), AAN73212 (At MRS2-2), AAN73213 (At MRS2-3), AAN73214 (At MRS2-4), AAN73215 (At MRS2-5), AAN73216 (At MRS2-6), NP_196531 (At MRS2-7), AAN73218 (At MRS2-8), NP_196533 (At MRS2-9), AAN73219 (At MRS2-10), AAG45213 (At MRS2-11), BAB89805 (Os01g64890), BAB92573 (Os01g68040), Os03g04480, as given in the Aramemnon database (Schwacke et al., 2003), AAR87307 (Os03g39790), AAK14424 (Os03g48000), CAE03029 (Os04g35160), CAE01634 (Os04g42280), BAD38112 (Os06g44150), and AAK20062 (N-terminally modified; Os10g39790). Accession numbers for T-DNA insertion lines are as follows: SALK_006797 (*mrs2-1*), SALK_105475 (*mrs2-5*), SALK_064741 [*mrs2-7(1)*], SALK_090559 [*mrs2-7(2)*], SALK_063452 [*mrs2-7(3)*], and SALK_100361 (*mrs2-10*).

Supplemental Data

The following materials are available in the online version of this article.

Supplemental Figure 1. Alignment of *Arabidopsis* MRS2 Proteins -11, -3, -5, -6, and -2 as Representatives of Clades A through E.

Supplemental Figure 2. Expression Levels of All Functional *MRS2/MGT* Genes Expressed in Vegetative Tissue in 2-Week-Old Plantlets Grown in Liquid Culture on Different $MgSO_4$ Concentrations.

Supplemental Figure 3. Investigation of Transcriptional Status for Homozygous T-DNA Insertion Lines.

Supplemental Figure 4. Ion Profiles of the Three *mrs2-7* KO Lines in Reference to the Col-0 Wild-Type Background.

Supplemental Table 1. List of *Arabidopsis* T-DNA Insertion Lines Investigated in the Course of This Study.

Supplemental Data Set 1. Text File of the Alignment Used for the Phylogenetic Analysis Shown in Figure 1.

ACKNOWLEDGMENTS

We thank Diedrik Menzel and coworkers at the cell biology department of the Institut für Zelluläre und Molekulare Botanik, especially Martina Beck for access to and help with confocal laser scanning microscopy, and Ursula Mettbach for help with thin sections for light microscopy. For skillfull technical assistance, we thank Monika Polsakiewicz, Johanna Schmitz, and Daniel Serwas. We are grateful for helpful comments and constructive criticisms by referees and editors on the initial version of this article. Finally, we gratefully acknowledge support of this work in an early phase through the Deutsche Forschungsgemeinschaft DFG (Kn411/4) in the framework of Schwerpunktprogramm SPP1108 on plant membrane transport.

Received August 6, 2009; revised October 28, 2009; accepted November 17, 2009; published December 4, 2009.

REFERENCES

Alexandersson, E., Saalbach, G., Larsson, C., and Kjellbom, P. (2004). *Arabidopsis* plasma membrane proteomics identifies components of transport, signal transduction and membrane trafficking. Plant Cell Physiol. **45:** 1543–1556.

Baumann, O., Walz, B., Somlyo, A.V., and Somlyo, A.P. (1991). Electron probe microanalysis of calcium release and magnesium uptake by endoplasmic reticulum in bee photoreceptors. Proc. Natl. Acad. Sci. USA **88:** 741–744.

Baxter, I., Ouzzani, M., Orcun, S., Kennedy, B., Jandhyala, S.S., and Salt, D.E. (2007). Purdue ionomics information management system. An integrated functional genomics platform. Plant Physiol. **143:** 600–611.

Birnbaum, K., Shasha, D.E., Wang, J.Y., Jung, J.W., Lambert, G.M., Galbraith, D.W., and Benfey, P.N. (2003). A gene expression map of the *Arabidopsis* root. Science **302:** 1956–1960.

Briggs, G.C., Osmont, K.S., Shindo, C., Sibout, R., and Hardtke, C.S. (2006). Unequal genetic redundancies in *Arabidopsis* - A neglected phenomenon? Trends Plant Sci. **11:** 492–498.

Bui, D.M., Gregan, J., Jarosch, E., Ragnini, A., and Schweyen, R.J. (1999). The bacterial magnesium transporter CorA can functionally

substitute for its putative homologue Mrs2p in the yeast inner mitochondrial membrane. J. Biol. Chem. **274:** 20438–20443.

Carter, C., Pan, S., Zouhar, J., Avila, E.L., Girke, T., and Raikhel, N.V. (2004). The vegetative vacuole proteome of *Arabidopsis thaliana* reveals predicted and unexpected proteins. Plant Cell **16:** 3285–3303.

Chen, J., Li, L.G., Liu, Z.H., Yuan, Y.J., Guo, L.L., Mao, D.D., Tian, L. F., Chen, L.B., Luan, S., and Li, D.P. (2009). Magnesium transporter AtMGT9 is essential for pollen development in *Arabidopsis.* Cell Res. **19:** 887–898.

Clough, S.J., and Bent, A.F. (1998). Floral dip: A simplified method for *Agrobacterium*-mediated transformation of *Arabidopsis thaliana.* Plant J. **16:** 735–743.

Curtis, M.D., and Grossniklaus, U. (2003). A gateway cloning vector set for high-throughput functional analysis of genes in planta. Plant Physiol. **133:** 462–469.

Drummond, R.S.M., Tutone, A., Li, Y.C., and Gardner, R.C. (2006). A putative magnesium transporter AtMRS2-11 is localized to the plant chloroplast envelope membrane system. Plant Sci. **170:** 78–89.

Eshaghi, S., Niegowski, D., Kohl, A., Molina, D.M., Lesley, S.A., and Nordlund, P. (2006). Crystal structure of a divalent metal ion transporter CorA at 2.9 angstrom resolution. Science **313:** 354–357.

Froehlich, J.E., Wilkerson, C.G., Ray, W.K., McAndrew, R.S., Osteryoung, K.W., Gage, D.A., and Phinney, B.S. (2003). Proteomic study of the *Arabidopsis thaliana* chloroplastic envelope membrane utilizing alternatives to traditional two-dimensional electrophoresis. J. Proteome Res. **2:** 413–425.

Gardner, R.C. (2003). Genes for magnesium transport. Curr. Opin. Plant Biol. **6:** 263–267.

Gietz, R.D., and Woods, R.A. (2002). Transformation of yeast by lithium acetate/single-stranded carrier DNA/polyethylene glycol method. Methods Enzymol. **350:** 87–96.

Graschopf, A., Stadler, J.A., Hoellerer, M.K., Eder, S., Sieghardt, M., Kohlwein, S.D., and Schweyen, R.J. (2001). The yeast plasma membrane protein Alr1 controls Mg^{2+} homeostasis and is subject to Mg^{2+}-dependent control of its synthesis and degradation. J. Biol. Chem. **276:** 16216–16222.

Gregan, J., Bui, D.M., Pillich, R., Fink, M., Zsurka, G., and Schweyen, R.J. (2001a). The mitochondrial inner membrane protein Lpe10p, a homologue of Mrs2p, is essential for magnesium homeostasis and group II intron splicing in yeast. Mol. Gen. Genet. **264:** 773–781.

Gregan, J., Kolisek, M., and Schweyen, R.J. (2001b). Mitochondrial Mg^{2+} homeostasis is critical for group II intron splicing in vivo. Genes Dev. **15:** 2229–2237.

Grynkiewicz, G., Poenie, M., and Tsien, R.Y. (1985). A new generation of Ca^{2+} indicators with greatly improved fluorescence properties. J. Biol. Chem. **260:** 3440–3450.

Hill, J.E., Myers, A.M., Koerner, T.J., and Tzagoloff, A. (1986). Yeast/*E. coli* shuttle vectors with multiple unique restriction sites. Yeast **2:** 163–167.

Höfer, R., Briesen, I., Beck, M., Pinot, F., Schreiber, L., and Franke, R. (2008). The *Arabidopsis* cytochrome P450 *CYP86A1* encodes a fatty acid ω-hydroxylase involved in suberin monomer biosynthesis. J. Exp. Bot. **59:** 2347–2360.

Höfgen, R., and Willmitzer, L. (1988). Storage of competent cells for *Agrobacterium* transformation. Nucleic Acids Res. **16:** 9877.

Jach, G., Binot, E., Frings, S., Luxa, K., and Schell, J. (2001). Use of red fluorescent protein from *Discosoma sp.* (dsRED) as a reporter for plant gene expression. Plant J. **28:** 483–491.

Jefferson, R.A., Kavanagh, T.A., and Bevan, M.W. (1987). GUS fusions: β-Glucuronidase as a sensitive and versatile gene fusion marker in higher plants. EMBO J. **6:** 3901–3907.

Karimi, M., Inze, D., and Depicker, A. (2002). GATEWAY vectors for Agrobacterium-mediated plant transformation. Trends Plant Sci. **7:** 193–195.

Kehres, D.G., Lawyer, C.H., and Maguire, M.E. (1998). The CorA magnesium transporter gene family. Microb. Comp. Genomics **3:** 151–169.

Knoop, V., Groth-Malonek, M., Gebert, M., Eifler, K., and Weyand, K. (2005). Transport of magnesium and other divalent cations: Evolution of the 2-TM-GxN proteins in the MIT superfamily. Mol. Genet. Genomics **274:** 205–216.

Kolisek, M., Zsurka, G., Samaj, J., Weghuber, J., Schweyen, R.J., and Schweigel, M. (2003). Mrs2p is an essential component of the major electrophoretic Mg^{2+} influx system in mitochondria. EMBO J. **22:** 1235–1244.

Koncz, C., and Schell, J. (1986). The promoter of Ti-DNA gene 5 controls the tissue-specific expression of chimeric genes carried by a novel type of *Agrobacterium* binary vector. Mol. Gen. Genet. **204:** 383–396.

Kumar, S., Nei, M., Dudley, J., and Tamura, K. (2008). MEGA: A biologist-centric software for evolutionary analysis of DNA and protein sequences. Brief. Bioinform. **9:** 299–306.

Lee, J.M., and Gardner, R.C. (2006). Residues of the yeast ALR1 protein that are critical for magnesium uptake. Curr. Genet. **49:** 7–20.

Li, L., Tutone, A.F., Drummond, R.S., Gardner, R.C., and Luan, S. (2001). A novel family of magnesium transport genes in *Arabidopsis*. Plant Cell **13:** 2761–2775.

Li, L.G., Sokolov, L.N., Yang, Y.H., Li, D.P., Ting, J., Pandy, G.K., and Luan, S. (2008). A mitochondrial magnesium transporter functions in *Arabidopsis* pollen development. Mol. Plant **1:** 675–685.

Lilley, R.M., Holborow, K., and Walker, D.A. (1974). Magnesium activation of photosynthetic CO_2-fixation in a reconstituted chloroplast system. New Phytol. **73:** 657–662.

Liu, G.J., Martin, D.K., Gardner, R.C., and Ryan, P.R. (2002). Large Mg^{2+}-dependent currents are associated with the increased expression of *ALR1* in *Saccharomyces cerevisiae.* FEMS Microbiol. Lett. **213:** 231–237.

Lunin, V.V., Dobrovetsky, E., Khutoreskaya, G., Zhang, R., Joachimiak, A., Doyle, D.A., Bochkarev, A., Maguire, M.E., Edwards, A.M., and Koth, C.M. (2006). Crystal structure of the CorA Mg^{2+} transporter. Nature **440:** 833–837.

MacDiarmid, C.W., and Gardner, R.C. (1998). Overexpression of the *Saccharomyces cerevisiae* magnesium transport system confers resistance to aluminum ion. J. Biol. Chem. **273:** 1727–1732.

Maguire, M.E., and Cowan, J.A. (2002). Magnesium chemistry and biochemistry. Biometals **15:** 203–210.

Mao, D.D., Tian, L.F., Li, L.G., Chen, J., Deng, P.Y., Li, D.P., and Luan, S. (2008). *AtMGT7*: An *Arabidopsis* gene encoding a low-affinity magnesium transporter. J. Integr. Plant Biol. **50:** 1530–1538.

Marschner, H. (2002). Mineral Nutrition of Higher Plants, 2nd ed. (London: Elsevier Academic Press).

Moncrief, M.B., and Maguire, M.E. (1999). Magnesium transport in prokaryotes. J. Biol. Inorg. Chem. **4:** 523–527.

Moomaw, A.S., and Maguire, M.E. (2008). The unique nature of Mg^{2+} channels. Physiology (Bethesda) **23:** 275–285.

Nawy, T., Lee, J.Y., Colinas, J., Wang, J.Y., Thongrod, S.C., Malamy, J.E., Birnbaum, K., and Benfey, P.N. (2005). Transcriptional profile of the *Arabidopsis* root quiescent center. Plant Cell **17:** 1908–1925.

Niegowski, D., and Eshaghi, S. (2007). The CorA family: Structure and function revisited. Cell. Mol. Life Sci. **64:** 2564–2574.

Norén, H., Svensson, P., and Andersson, B. (2004). A convenient and versatile hydroponic cultivation system for *Arabidopsis thaliana.* Physiol. Plant. **121:** 343–348.

Obrdlik, P., et al. (2004). K^+ channel interactions detected by a genetic

system optimized for systematic studies of membrane protein interactions. Proc. Natl. Acad. Sci. USA **101:** 12242–12247.

Payandeh, J., and Pai, E.F. (2006). A structural basis for Mg^{2+} homeostasis and the CorA translocation cycle. EMBO J. **25:** 3762–3773.

Redman, J.C., Haas, B.J., Tanimoto, G., and Town, C.D. (2004). Development and evaluation of an Arabidopsis whole genome Affymetrix probe array. Plant J. **38:** 545–561.

Saitou, N., and Nei, M. (1987). The neighbor-joining method: A new method for reconstructing phylogenetic trees. Mol. Biol. Evol. **4:** 406–425.

Salt, D.E., Baxter, I., and Lahner, B. (2008). Ionomics and the study of the plant ionome. Annu. Rev. Plant Biol. **59:** 709–733.

Schindl, R., Weghuber, J., Romanin, C., and Schweyen, R.J. (2007). Mrs2p forms a high conductance Mg^{2+} selective channel in mitochondria. Biophys. J. **93:** 3872–3883.

Schock, I., Gregan, J., Steinhauser, S., Schweyen, R., Brennicke, A., and Knoop, V. (2000). A member of a novel *Arabidopsis thaliana* gene family of candidate Mg^{2+} ion transporters complements a yeast mitochondrial group II intron-splicing mutant. Plant J. **24:** 489–501.

Schwacke, R., Schneider, A., van der Graaff, E., Fischer, K., Catoni, E., Desimone, M., Frommer, W.B., Flügge, U.I., and Kunze, R. (2003). ARAMEMNON, a novel database for Arabidopsis integral membrane proteins. Plant Physiol. **131:** 16–26.

Shaul, O. (2002). Magnesium transport and function in plants: The tip of the iceberg. Biometals **15:** 309–323.

Shaul, O., Hilgemann, D.W., Almeida-Engler, J., Van Montagu, M., Inzé, D., and Galili, G. (1999). Cloning and characterization of a novel Mg^{2+}/H^{+} exchanger. EMBO J. **18:** 3973–3980.

Siegenthaler, P.A., and Depéry, F. (1976). Influence of unsaturated fatty acids in chloroplasts - Shift of pH optimum of electron flow and relations to ΔpH, thylakoid internal pH and proton uptake. Eur. J. Biochem. **61:** 573–580.

Swinburne, J., Balcells, L., Scofield, S.R., Jones, J.D., and Coupland, G. (1992). Elevated levels of *Activator* transposase mRNA are associated with high frequencies of *Dissociation* excision in *Arabidopsis*. Plant Cell **4:** 583–595.

Wachek, M., Aichinger, M.C., Stadler, J.A., Schweyen, R.J., and Graschopf, A. (2006). Oligomerization of the Mg^{2+}-transport proteins Alr1p and Alr2p in yeast plasma membrane. FEBS J. **273:** 4236–4249.

Waters, B.M., and Grusak, M.A. (2008). Quantitative trait locus mapping for seed mineral concentrations in two *Arabidopsis thaliana* recombinant inbred populations. New Phytol. **179:** 1033–1047.

Weghuber, J., Dieterich, F., Froschauer, E.M., Svidovà, S., and Schweyen, R.J. (2006). Mutational analysis of functional domains in Mrs2p, the mitochondrial Mg^{2+} channel protein of *Saccharomyces cerevisiae.* FEBS J. **273:** 1198–1209.

Whiteman, S.A., Serazetdinova, L., Jones, A.M., Sanders, D., Rathjen, J., Peck, S.C., and Maathuis, F.J. (2008). Identification of novel proteins and phosphorylation sites in a tonoplast enriched membrane fraction of *Arabidopsis thaliana.* Proteomics **8:** 3536–3547.

Wiesenberger, G., Steinleitner, K., Malli, R., Graier, W.F., Vormann, J., Schweyen, R.J., and Stadler, J.A. (2007). Mg^{2+} deprivation elicits rapid Ca^{2+} uptake and activates Ca^{2+}/calcineurin signaling in *Saccharomyces cerevisiae*. Eukaryot. Cell **6:** 592–599.

Wiesenberger, G., Waldherr, M., and Schweyen, R.J. (1992). The nuclear gene MRS2 is essential for the excision of group II introns from yeast mitochondrial transcripts *in vivo.* J. Biol. Chem. **267:** 6963–6969.

Zsurka, G., Gregán, J., and Schweyen, R.J. (2001). The human mitochondrial Mrs2 protein functionally substitutes for its yeast homologue, a candidate magnesium transporter. Genomics **72:** 158–168.

3.6. Publication VI

Lpe10p modulates the activity of the Mrs2p-based yeast mitochondrial Mg^{2+} channel

Gerhard Sponder[1], Soňa Svidová[1], Rainer Schindl[2], Stefan Wieser[2], Rudolf J. Schweyen[1], Christoph Romanin[2], Elisabeth M. Froschauer[1,*] and Julian Weghuber[2,*]

FEBS Journal 277 (2010) 3514–3525

[1] Max F. Perutz Laboratories, Department of Microbiology, Immunology and Genetics, Vienna, Austria

[2] Institute of Biophysics, University of Linz, Austria

[*]Corresponding author

Authors' contributions to the manuscript

I designed and cloned the YGMN mutant of Lpe10, performed Mg^{2+} uptake measurements in isolated mitochondria and analyzed the data. I also participated partly in the cloning of the fusion proteins and in the preparation of the manuscript.

the FEBS Journal

Lpe10p modulates the activity of the Mrs2p-based yeast mitochondrial Mg^{2+}channel

Gerhard Sponder[1], Sona Svidova[1], Rainer Schindl[2], Stefan Wieser[2], Rudolf J. Schweyen[1], Christoph Romanin[2], Elisabeth M. Froschauer[1,*] and Julian Weghuber[2,*]

1 Max F. Perutz Laboratories, Department of Microbiology, Immunology and Genetics, Vienna, Austria
2 Institute of Biophysics, University of Linz, Austria

Keywords
membrane potential; Mg^{2+}-channel; mitochondria; oligomerization; single-channel patch clamp

Correspondence
J. Weghuber, Institute of Biophysics, University of Linz, Altenbergerstraße 69, 4040 Linz, Austria
Fax: +43 732 2468 29284
Tel: +43 732 2468 9266
E-mail: julian.weghuber@jku.at

*These authors contributed equally to this work

Note
This paper is dedicated to the memory of Rudolf Schweyen, who tragically died during the preparation of the manuscript

(Received 20 April 2010, revised 28 May 2010, accepted 1 July 2010)

doi:10.1111/j.1742-4658.2010.07761.x

Saccharomyces cerevisiae Lpe10p is a homologue of the Mg^{2+}-channel-forming protein Mrs2p in the inner mitochondrial membrane. Deletion of *MRS2*, *LPE10* or both results in a petite phenotype, which exhibits a respiratory growth defect on nonfermentable carbon sources. Only coexpression of *MRS2* and *LPE10* leads to full complementation of the *mrs2*Δ*/lpe10*Δ double disruption, indicating that these two proteins cannot substitute for each other. Here, we show that deletion of *LPE10* results in a loss of rapid Mg^{2+} influx into mitochondria, as has been reported for *MRS2* deletion. Additionally, we found a considerable loss of the mitochondrial membrane potential (ΔΨ) in the absence of Lpe10p, which was not detected in *mrs2*Δ cells. Addition of the K^+/H^+-exchanger nigericin, which artificially increases ΔΨ, led to restoration of Mg^{2+} influx into mitochondria in *lpe10*Δ cells, but not in *mrs2*Δ*/lpe10*Δ cells. Mutational analysis of Lpe10p and domain swaps between Mrs2p and Lpe10p suggested that the maintenance of ΔΨ and that of Mg^{2+} influx are functionally separated. Cross-linking and Blue native PAGE experiments indicated interaction of Lpe10p with the Mrs2p-containing channel complex. Using the patch clamp technique, we showed that Lpe10p was not able to mediate high-capacity Mg^{2+} influx into mitochondrial inner membrane vesicles without the presence of Mrs2p. Instead, coexpression of Lpe10p and Mrs2p yielded a unique, reduced conductance in comparison to that of Mrs2p channels. In summary, the data presented show that the interplay of Lpe10p and Mrs2p is of central significance for the transport of Mg^{2+} into mitochondria of *S. cerevisiae*.

Structured digital abstract

- MINT-7905005: *LPE10* (uniprotkb:Q02783) *physically interacts* (MI:0915) with *MRS2* (uniprotkb:Q01926) by *anti tag coimmunoprecipitation* (MI:0007)
- MINT-7905028: *LPE10* (uniprotkb:Q02783) and *LPE10* (uniprotkb:Q02783) *covalently bind* (MI:0195) by *cross-linking study* (MI:0030)
- MINT-7905072: *LPE10* (uniprotkb:Q02783) and *MRS2* (uniprotkb:Q01926) *covalently bind* (MI:0195) by *cross-linking study* (MI:0030)

Abbreviations
BN-PAGE, Blue native PAGE; HA, haemagglutinin; JC-1, 5,5′,6,6′-tetrachloro-1,1′,3,3′-tetraethylbenzimidazolocarbocyanine iodide; $[Mg^{2+}]_e$, external Mg^{2+} concentration; $[Mg^{2+}]_m$, inner mitochondrial Mg^{2+} concentration; WT, wild-type; ΔΨ, mitochondrial membrane potential.

Introduction

The inner mitochondrial membrane forms a tight barrier to the passage of cations. Their movement across this barrier requires the action of transporters and ion channels. Physiological studies suggest that uptake of cations is driven by the inside-negative membrane potential of the organelle, whereas extrusion from mitochondria occurs against the electrochemical gradient by the influx of protons [1,2]. Mrs2p was the first molecularly identified cation channel of mitochondria [3]. It forms an oligomeric, Mg^{2+}-selective channel of high conductance in the inner mitochondrial membrane, whose probability of being open is controlled by the Mg^{2+} concentration inside the organelle [4,5].

Mrs2p is distantly related to the bacterial Mg^{2+} transport protein CorA [6] and to the Mg^{2+} transport protein Alr1p in the plasma membrane of fungi [7]. Proteins of this superfamily are characterized by two adjacent transmembrane domains (TM1 and TM2) in their C-terminal part, an F/YGMN motif at the end of TM1, a short loop with a surplus of negative charges connecting TM1 and TM2 [8], and a series of helical structures in the long N-terminal protein part. Crystallization and X-ray diffraction analysis of the *Thermotoga maritima* transporter CorA, determined in a closed state, have revealed a homopentamer with a membrane pore formed by five TM1 helices and a funnel-shaped structure composed of the N-terminal extension of TM1 in the cytoplasm [9,10].

Vertebrates express only a single *MRS2* gene in their mitochondria, whereas plant genomes contain at least 10 *MRS2*-related genes, whose products are not restricted to mitochondria [11,12]. The genome of *Saccharomyces cerevisiae* encodes not only Mrs2p but also a homologue with 32% sequence identity, which has been named Lpe10p. Like Mrs2p, it is located in the inner mitochondrial membrane with an N_{in}–C_{in} orientation, and it has been reported to be involved in Mg^{2+} uptake as well, but the mode of action remains undefined [13]. Notably, disruption of only one of *mrs2*Δ or *lpe10*Δ has been shown to cause a growth defect on nonfermentable carbon sources (petite phenotype) and a reduction in mitochondrial Mg^{2+} content [13,14].

Here, we found that deletion of *LPE10* led to a loss of Mg^{2+} influx, comparable to what is seen with *MRS2* deletion, but also resulted in a prominent decrease in the mitochondrial membrane potential ($\Delta\Psi$). To obtain further insights into the diverse functions of Lpe10p and Mrs2p, we constructed Mrs2-Lpe10p fusion proteins and investigated their ability to transport Mg^{2+} and to oligomerize. The results presented indicate an influence of Lpe10p on the size of Mrs2p-containing complexes, and show a direct interaction between Lpe10p and Mrs2p. Furthermore, single-channel recordings of giant lipid vesicles with fused inner mitochondrial membranes revealed a significantly decreased conductance for the Mrs2p channel if Lpe10p was coexpressed. On the basis of these results, we assume that Lpe10p has the potential to interact with the Mrs2p-based Mg^{2+} channel and, in addition, modulates its activity.

Results

Secondary structure prediction of Lpe10p

Full-length secondary structure prediction of *S. cerevisiae* Lpe10p and Mrs2p [5,13,15] reveals similarities to *Arabidopsis thaliana* Mrs2–7 [11], and *T. maritima* CorA [16]. As shown in Fig. S1, secondary structure similarity is particularly high in the α-helical regions N-terminal to TM1, which appear to be homologous to helices α5, α6 and α7 (highlighted in blue, yellow and green) of *T. maritima* CorA, whose tertiary structure has been solved [10]. A unique feature of Mrs2p is the extended C-terminus containing a box of positively charged amino acids [15], which is absent in Lpe10p and other members of the Mrs2p family.

Complementation of *mrs2*Δ and *lpe10*Δ mutants as well as the *mrs2*Δ/*lpe10*Δ double mutant with Mrs2p and Lpe10p

Chromosomal deletion of *LPE10* (*lpe10*Δ mutant) results in growth reduction on nonfermentable substrates (petite phenotype), which is less pronounced than that resulting from *MRS2* disruption [13]. We analysed the complementation of strains with deleted *MRS2* and/or *LPE10* by Mrs2p or Lpe10p expressed from episomal high copy number (H) or low copy number (L) vectors (Fig. 1). In the cross-wise combinations, $(MRS2)_L$ and $(MRS2)_H$ partly complemented *lpe10*Δ, whereas Lpe10p did not detectably restore growth of *mrs2*Δ cells. The double disruption *mrs2*Δ/*lpe10*Δ was only partly complemented by $(MRS2)_H$. Interestingly, coexpression of $(MRS2)_H$ and $(LPE10)_L$ fully restored growth of double-disruption cells, whereas the presence of $(MRS2)_H$ and $(LPE10)_H$ led to only weak complementation. These data suggest

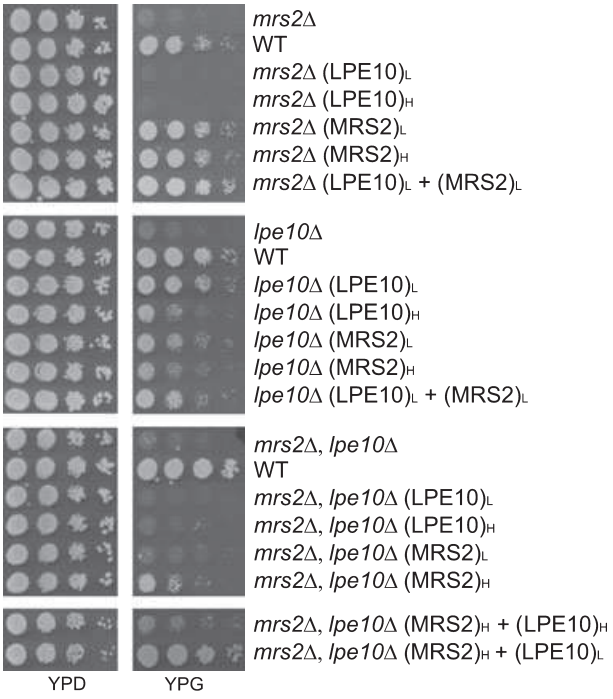

Fig. 1. Growth phenotypes of yeast strains with deleted *MRS2* and/or *LPE10*. Serial dilutions of DBY 747 *mrs2*Δ, DBY747 *lpe10*Δ and the double-deletion strain DBY747 *mrs2*Δ/*lpe10*Δ expressing MRS2 or LPE10 from high (H) or low (L) copy number vectors were spotted on fermentable (YPD) or nonfermentable (YPG) plates and incubated at 28 °C for 3 or 6 days, respectively.

that mitochondrial Mg^{2+} homeostasis in yeast may be dependent on the relative expression levels of Mrs2p and Lpe10p, with the latter playing an inhibitory role if overexpressed. Consistently, high copy number expression of Lpe10p reduced growth.

To determine whether parts of Mrs2p and Lpe10p are exchangeable, we created Mrs2-Lpe10p and Lpe10p-Mrs2p fusion proteins in an attempt to examine respective domain functions (Fig. 2A). Secondary structure prediction data revealed two coiled-coil domains for Mrs2p [15], which turned out to be helical structures homologous to helices α5/α6 and α7 of *T. maritima* CorA [10]. We chose the fusion site between α6 and α7. The chimeric proteins were expressed at similar levels (Fig. 2B), but only weakly restored growth of *mrs2*Δ and also *lpe10*Δ mutant cells. We detected slightly better complementation on expression of Lpe10-Mrs2p fusion proteins, which contained the pore of Mrs2p (Fig. 2C). It is noteworthy that complementation with Lpe10-Mrs2p was more pronounced in both single disruption backgrounds. However, neither of the chimeras could restore growth of *mrs2*Δ/*lpe10*Δ mutant cells.

Loss of high-capacity Mg^{2+} influx in *lpe10*Δ mitochondria is partly restored by Mrs2-Lpe10p fusion proteins

Our previous studies with Eriochrome blue as an indicator to measure Mg^{2+} concentration in mitochondrial extracts have revealed that mitochondria from *LPE10* disruptants contain lower steady-state concentrations of Mg^{2+} than mitochondria from wild-type (WT) cells [13]. Alternatively, we used the Mg^{2+}-sensitive dye mag-fura 2 to determine changes in free ionized inner mitochondrial Mg^{2+} ($[Mg^{2+}]_m$) [4], with the aim of examining whether disruption of *LPE10* affects Mg^{2+} influx into mitochondria isolated from these mutant cells (Fig. 3A). The resting $[Mg^{2+}]_m$ of *lpe10*Δ mitochondria was slightly reduced (to 0.4–0.5 mM) as compared with that of mitochondria overexpressing Lpe10p (0.8 mM) in nominally Mg^{2+}-free buffer. When the external Mg^{2+} concentration $[Mg^{2+}]_e$ was increased stepwise to final concentrations of 1 and 3 mM, *lpe10*Δ mitochondria lacked the rapid, Mg^{2+}-dependent influx. High copy number expression of Lpe10p led to an increased rate of uptake of Mg^{2+} upon addition of 1 and 3 mM $[Mg^{2+}]_e$. Expression of Mrs2–Lpe10p or Lpe10–Mrs2p chimeric proteins partially restored Mg^{2+} influx in *lpe10*Δ mitochondria. In particular, the presence of the Lpe10-Mrs2p chimeric protein resulted in almost complete restoration of Mg^{2+} influx.

In *mrs2*Δ mitochondria expressing the Mrs2-Lpe10p fusion protein, Mg^{2+} influx was similar to that in *lpe10*Δ, with both mutants restoring the influx to a considerable degree (Fig. 3B). We did not find influx of Mg^{2+} into mitochondria isolated from *mrs2*Δ/*lpe10*Δ cells expressing the Mrs2-Lpe10p chimeric proteins (data not shown).

We conclude that the presence of endogenous Lpe10p or Mrs2p in combination with expression of Mrs2-Lpe10p chimeric proteins is sufficient to restore moderate influx of Mg^{2+} into mitochondria.

Deletion of *LPE10* causes reduction of mitochondrial membrane potential (ΔΨ)

We have shown that Mg^{2+} influx of Mrs2p channels is dependent on ΔΨ as a driving force [4]. Using the ΔΨ-sensitive dye 5,5′,6,6′-tetrachloro-1,1′,3,3′-tetraethylbenzimidazolocarbocyanine iodide (JC-1), we analysed ΔΨ of *lpe10*Δ and *lpe10*Δ/*mrs2*Δ mitochondria, and observed a pronounced loss of relative ΔΨ as compared with WT or *mrs2*Δ mitochondria. Expression of $(LPE10)_H$ in *lpe10*Δ or *mrs2*Δ/*lpe10*Δ cells restored ΔΨ close to WT levels, meaning that the loss of

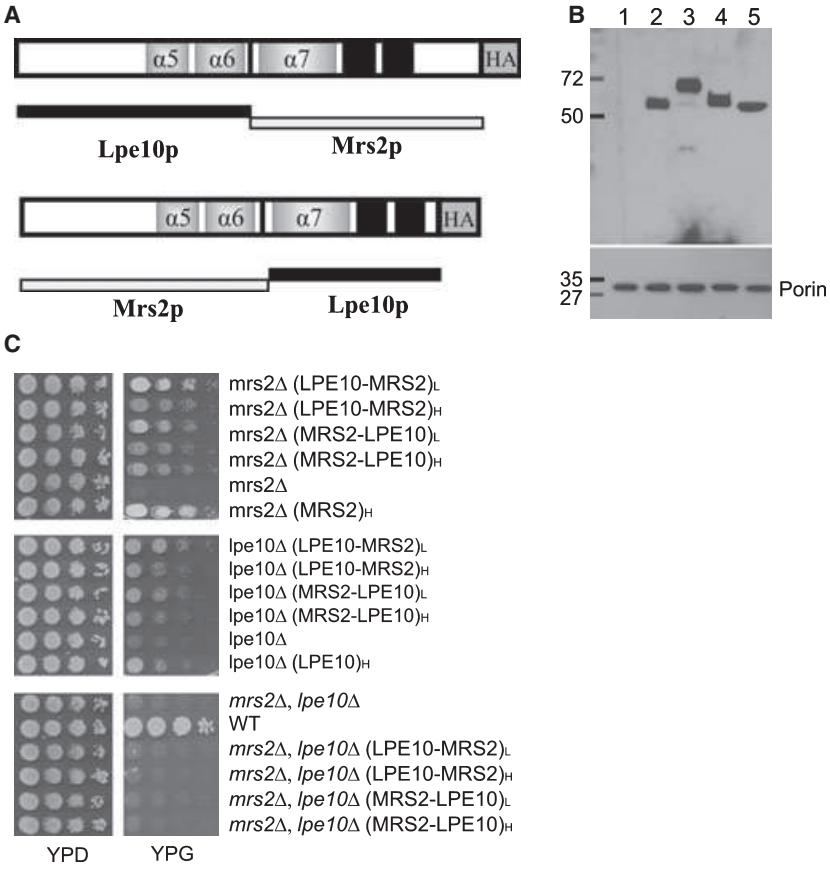

Fig. 2. Characterization of Lpe10-Mrs2p chimeric proteins. (A) Schematic representation of two chimeric proteins with indicated transmembrane (black boxes) and helical regions (α5–α7). (B) Western blot analysis of isolated mitochondria from *mrs2Δ/lpe10Δ* cells transformed with an empty plasmid (lane 1) or a high copy number vector expressing MRS2–HA (lane 2), LPE10–HA (lane 3), LPE10–MRS2–HA (lane 4) or MRS2–LPE10–HA (lane 5). The samples were separated by SDS/PAGE, and proteins were visualized by immunoblotting with an antiserum against HA. The porin protein was used as a loading control. (C) Serial dilutions of DBY 747 *mrs2Δ*, DBY747 *lpe10Δ* and the double-deletion strain DBY747 *mrs2Δ/lpe10Δ* expressing Lpe10-Mrs2p or Mrs2-Lpe10p fusion proteins from high (H) or low (L) copy number vectors were spotted onto fermentable (YPD) or nonfermentable (YPG) plates and incubated at 28 °C for 3 or 6 days, respectively.

ΔΨ was dependent on the *lpe10Δ* deletion. Consistently, $(MRS2)_H$ failed to restore ΔΨ (Fig. 4A).

Expression of $(LPE10–MRS2)_L$ in the *mrs2Δ/lpe10Δ* background led to restoration of ΔΨ up to levels comparable to those detected with full-length Lpe10p present, whereas $(MRS2–LPE10)_L$ was less efficient (Fig. 4A). This is in good agreement with the better complementation and Mg^{2+} influx restoration in *lpe10Δ* cells by the Lpe10-Mrs2p chimeric protein.

We assume that deletion of *LPE10* caused a disturbance in the maintenance of ΔΨ, which could be a major cause of the substantial reduction in Mg^{2+} influx. To further test this hypothesis, we repolarized *lpe10Δ* mitochondria to determine whether Mg^{2+} influx could be restored. Addition of nigericin, an Na^+, K^+/H^+ ionophore, to the growth medium or to isolated mitochondria is known to restore ΔΨ in yeast mutants [17]. Thus, we used mag-fura 2 to measure Mg^{2+} influx into mitochondria isolated from *lpe10Δ* cells pretreated with nigericin. We found Mg^{2+} influx to be restored nearly to WT levels, whereas no significant Mg^{2+} influx could be detected in repolarized mitochondria from *mrs2Δ/lpe10Δ* cells (Fig. 4B). Addition of nigericin did not have an effect on Mg^{2+} influx into mitochondria isolated from WT cells (data not shown). These experiments clearly showed that Lpe10p has a key regulatory role by maintaining ΔΨ. However, mitochondria with deleted Lpe10p still retained 30% of WT ΔΨ. The remaining level might explain why high copy number expression of Mrs2p in *mrs2Δ/lpe10Δ* cells led to weak growth restoration in the absence of Lpe10p.

The F/YGMN motif is essential for the Mg^{2+} transport activity of Lpe10p

The conserved F/YGMN motif in TM1 of CorA-like proteins cannot be varied without loss of Mg^{2+} uptake [4,18]. We performed site-directed mutagenesis, replacing the F/YGMN motif of Lpe10p with ASSV, resulting in the mutant Lpe10-J1. These amino acid substitutions were chosen to create a nonfunctional pore, without substantially affecting the charge or polarity of the protein in this region, which could lead to incorrect folding. Growth of mutant *lpe10Δ* or *mrs2Δ* cells expressing $(LPE10–J1)_H$ was only

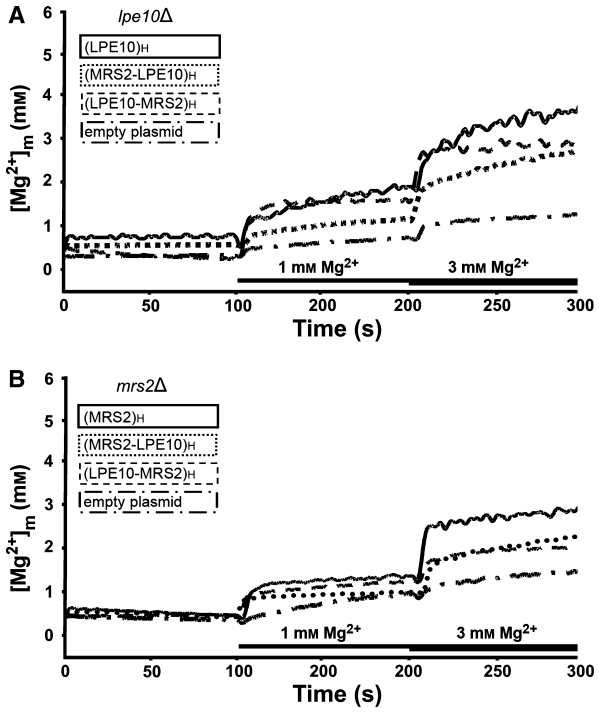

Fig. 3. Expression of Lpe10-Mrs2p chimeric proteins restores Mg^{2+} influx into isolated mitochondria from *lpe10*Δ or *mrs2*Δ cells. $[Mg^{2+}]_e$-dependent changes in $[Mg^{2+}]_m$ in *lpe10*Δ (A) or *mrs2*Δ (B) mitochondria isolated from cells expressing either Lpe10p, Mrs2p or Lpe10-Mrs2p chimeric proteins from a high copy number vector. Mitochondria were loaded with the Mg^{2+}-sensitive fluorescent dye mag-fura 2, and $[Mg^{2+}]_m$ values were determined in nominally Mg^{2+}-free buffer or upon addition of Mg^{2+} to the level of $[Mg^{2+}]_e$, as indicated in the figure. Note that the framing of the different samples (solid, dotted, dashed or dash–dotted lines, respectively) matches the style of the individual traces (identical description in Figs 4B and 5B). Representative curve traces of four individual measurements are shown.

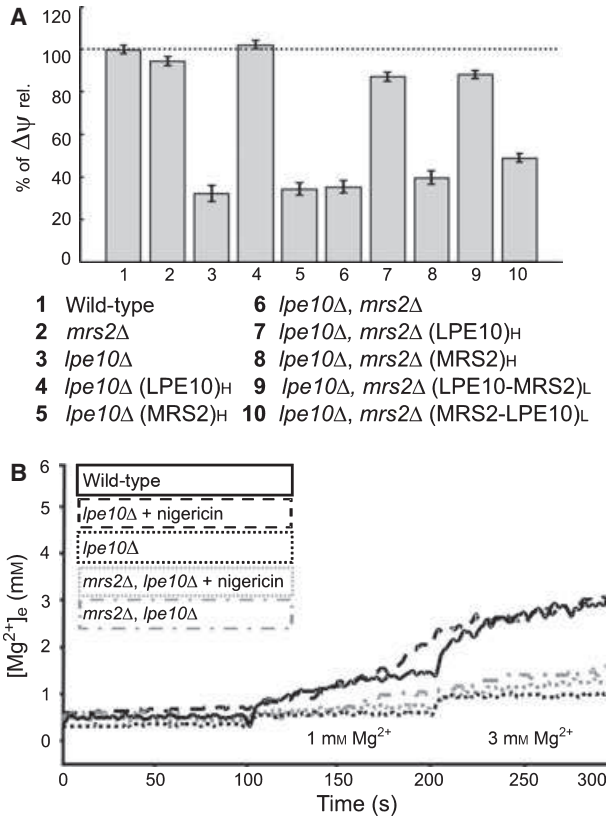

Fig. 4. Chromosomal deletion of *LPE10* leads to loss of ΔΨ. Mitochondria isolated from *mrs2*Δ, WT, *lpe10*Δ or *mrs2*Δ/*lpe10*Δ yeast cells transformed with various *MRS2*-containing or *LPE10*-containing high (H) or low (L) copy number plasmids were incubated with JC-1, and the intensity changes of the monomeric and multimeric forms were recorded (A). Relative ΔΨ was determined as described in Experimental procedures. (B) $[Mg^{2+}]_e$-dependent changes in $[Mg^{2+}]_m$ in WT, *lpe10*Δ or *mrs2*Δ/*lpe10*Δ mitochondria. As indicated in some experiments, 1 μM nigericin was added prior to measurements. Representative curve traces of four individual measurements are shown.

minimally restored, and the double-deletion mutant failed to grow (Fig. 5A). $(LPE10–J1)_H$ led to only a minor decrease in ΔΨ (~ 10%) as compared with the level of WT mitochondria, but Mg^{2+} influx could not be detected (Fig. 5B) if this mutant was present in *lpe10*Δ cells. These data suggest that the F/YGMN motif of Lpe10p is critical for restoration of Mg^{2+} influx, possibly in conjunction with Mrs2p. By contrast, mutations in this motif did not affect the ability of the protein to maintain ΔΨ.

Homo-oligomerization and hetero-oligomerization of Mrs2p and Lpe10p

For a better understanding of how expression of Lpe10p influences the assembly of the Mrs2p channel, we performed cross-linking, Blue native (BN)-PAGE and coimmunoprecipitation experiments. Initially, we tested for the potential of Lpe10p to homo-oligomerize. Mitochondria were isolated from *mrs2*Δ/*lpe10*Δ double-disruption cells expressing [LPE10–haemagglutinin (HA)]$_H$, and treated with the chemical cross-linker oPDM. We found that the anti-HA serum reacted with a major product representing the Lpe10p-HA monomer (50.4 kDa), and upon addition of the cross-linker, additional bands of higher molecular mass of ~ 110 kDa and ~ 160 kDa, as expected for an Lpe10p-HA dimer and possibly trimer, respectively, were obtained (Fig. 6A). Accordingly, Lpe10p was apparently able to form homo-oligomers, as previously shown for Mrs2p [4]. However, we cannot exclude the presence of an undefined protein interacting with

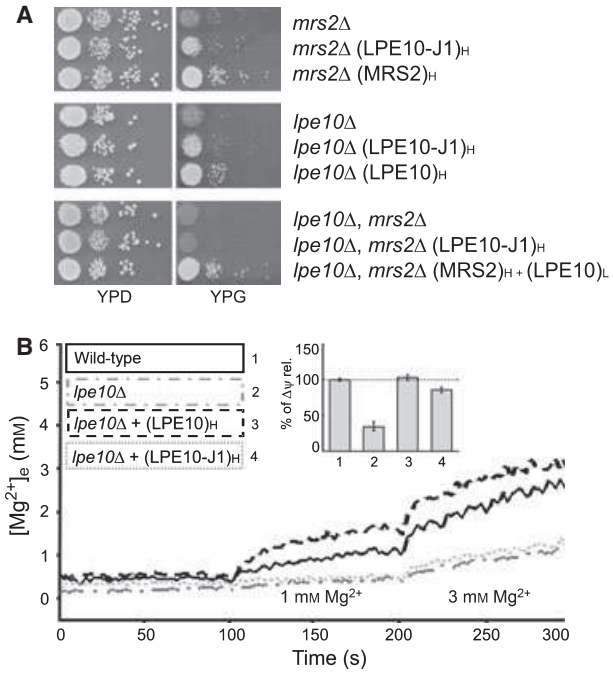

Fig. 5. The highly conserved F/YGMN motif is essential for the Mg^{2+} influx mediated by Lpe10p. (A) Serial dilutions of *mrs2*Δ or *lpe10*Δ or the double-deletion strain *mrs2*Δ/*lpe10*Δ transformed with high (H) or low (L) copy number plasmids expressing MRS2, LPE10 or the mutant variant LPE10–J1, were spotted on fermentable (YPD) or nonfermentable (YPG) plates and incubated at 28 °C for 3 or 6 days, respectively. (B) $[Mg^{2+}]_e$-dependent changes in $[Mg^{2+}]_m$ in WT or *lpe10*Δ mitochondria expressing WT LPE10 or the mutant variant LPE10–J1 from a high copy number plasmid. Representative curve traces of three individual measurements are shown. Mitochondrial membrane potential was determined as described in Experimental procedures for wild-type (1) and *lpe10*Δ (2) cells, as well as for *lpe10*Δ cells expressing LPE10 (3) or the mutant version LPE10–J1 (4) from high copy number plasmids.

Lpe10p on addition of the cross-linking reagent. We did not detect Lpe10p complexes as large as Mrs2p oligomers, which were shown to be homopentameric [4]. When we coexpressed $(LPE10–HA)_H$ and $(MRS2\text{-}Myc)_H$ and added oPDM, anti-HA serum recognized Lpe10p-HA-containing complexes, which were increased in size as compared with those detected without coexpression of Mrs2p-Myc (Fig. 6B, upper picture). Incubation of the same blot with anti-myc serum resulted in identification of Mrs2p-Myc-containing complexes of high molecular mass, which were of similar size as the largest complexes found with the anti-HA serum (Fig. 6B, lower picture). Interestingly, no intermediate dimeric or trimeric assemblies were detected in Mrs2p-cross-linking experiments in the absence of Lpe10p [4].

We continued with BN-PAGE experiments, and transformed *mrs2*Δ/*lpe10*Δ cells with different combinations of Mrs2p-Myc, Mrs2p-HA or Lpe10p-HA (64, 57.5 and 50.4 kDa, respectively). Proteins from isolated mitochondria were separated by BN-PAGE according to Schagger *et al.* [19]. As shown in Fig. 6C, expression of $(LPE10–HA)_L$ or $(LPE10–HA)_H$ resulted in a band with an apparent molecular mass of ~ 230 kDa (lanes 2 and 3). Upon coexpression of $(MRS2\text{-}Myc)_H$ and $(LPE10–HA)_L$ or $(LPE10–HA)_H$, the anti-HA serum recognized additional bands of ~ 300 and 400 kDa, and the intensity of the band at ~ 230 kDa decreased markedly (Fig. 6C, lanes 4 and 5). No bands were visible when proteins of mitochondria lacking an HA tag were immunoblotted (Fig. 6C, lane 1). These results strengthened our assumption that Lpe10p is involved in the assembly of the Mrs2p-based Mg^{2+} channel *in vivo*.

To confirm a direct interaction between Lpe10p and Mrs2p, we performed coimmunoprecipitation experiments. Mitochondria from *mrs2*Δ/*lpe10*Δ double-disruptant cells coexpressing LPE10–HA and MRS2-Myc, as well as mitochondria from cells expressing either LPE10–HA or MRS2-Myc or the empty vectors, were used. Upon coexpression of LPE10–HA and MRS2-Myc, both proteins were detected in the anti-HA immunoprecipitate (Fig. 6D, elution fractions, lanes 1 and 5). In the control experiments with mitochondria from cells expressing only LPE10–HA, the protein was found unbound (Fig. 6D, supernatant fraction, lane 3) as well as bound to HA-coated beads (Fig. 6D, elution fraction, lane 3). If mitochondria from cells expressing only MRS2-Myc were used, the respective protein was exclusively found in the unbound fraction (Fig. 6D, supernatant fraction, lane 4). These results confirm a tight interaction between the two proteins.

Lpe10p modulates the conductance of the Mrs2p channel

To initially investigate whether Lpe10p is able to generate a homomeric Mg^{2+}-permeable channel in the absence of Mrs2p, we used single-channel patch clamp recordings on giant lipid vesicles fused with inner mitochondrial membranes from $(LPE10)_H$-expressing *mrs2*Δ/*lpe10*Δ cells. We have previously used this technique to characterize the Mrs2p-based high-conductance channel with a calculated conductance of ~ 155 pS [5]. Inside-out patches were studied in a 105 mM $MgCl_2$-based pipette solution and an *N*-methyl-D-glucamine gluconate-based bath solution. Current traces at test potentials ranging from +5 to −35 mV resulted in an increase in single-channel amplitudes with decreasing potentials in four of 14 experiments, consistent with Mg^{2+}-permeable channels

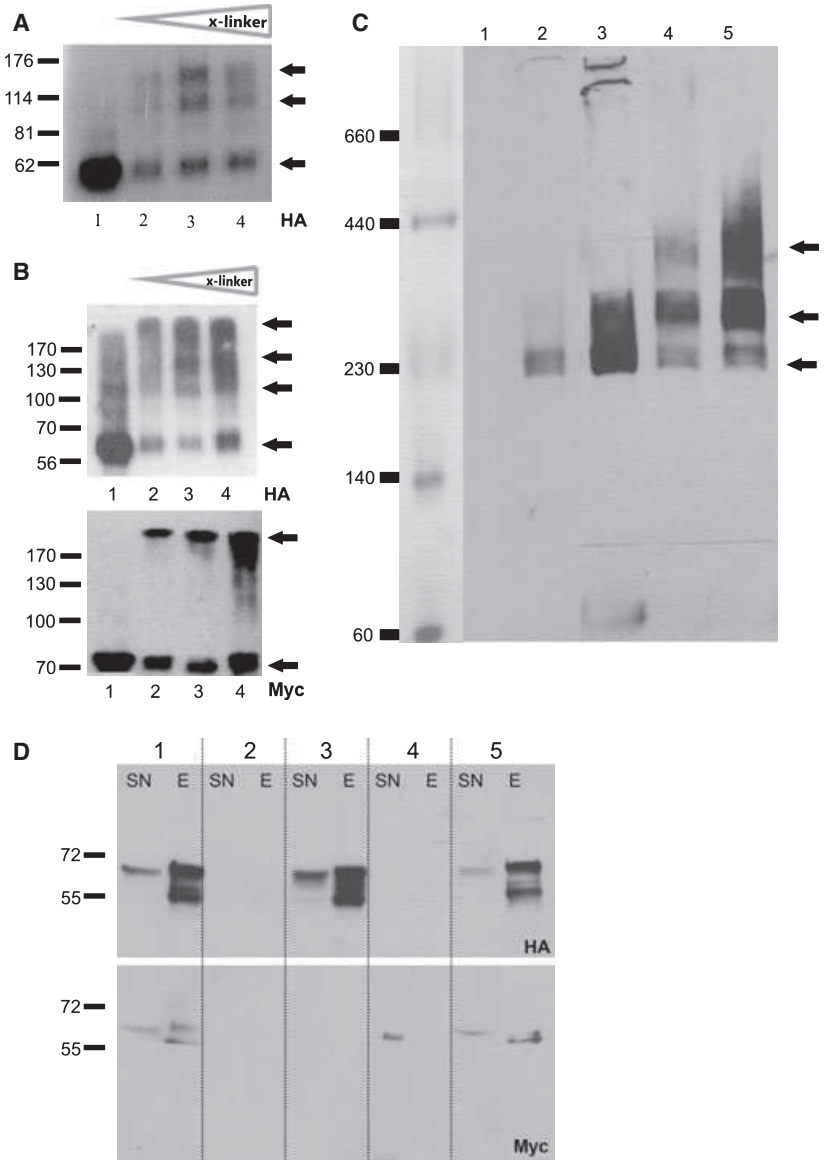

Fig. 6. Lpe10p influences the Mrs2p channel complex. (A) Isolated mitochondria of *lpe10*Δ cells transformed with LPE10–HA-expressing high copy number plasmid were incubated in sulfhydryl buffer without (lane 1) or with the chemical cross-linker oPDM at final concentrations of 30 μM (lane 2), 100 μM (lane 3) and 300 μM (lane 4), separated by SDS/PAGE, and analysed by immunoblotting with anti-HA serum. (B) Isolated mitochondria of *mrs2*Δ/*lpe10*Δ cells transformed with LPE10–HA and MRS2–Myc from multicopy plasmids were incubated in sulfhydryl buffer without (lane 1) or with the chemical cross-linker oPDM (lanes 2–4; 30, 100 or 300 μM, respectively), separated by SDS/PAGE, and analysed by immunoblotting with anti-HA serum (upper blot) or anti-Myc serum (lower blot). (C) High molecular mass complexes containing Lpe10p-HA and/or Mrs2p-Myc detected by BN-PAGE. Mitochondria of *mrs2*Δ/*lpe10*Δ cells were transformed with an empty plasmid (lane 1) or the following proteins expressed from high (H) or low (L) copy number plasmids: $(LPE10–HA)_L$ (lane 2), $(LPE10–HA)_H$ (lane 3), $(MRS2\text{-}Myc)_H$ and $(LPE10–HA)_L$ (lane 4) or $(MRS2\text{-}Myc)_H$ and $(LPE10–HA)_H$ (lane 5). Samples were solubilized in 1.2% laurylmaltoside, and products were visualized anti-HA serum. (D) Coimmunoprecipitation experiments with Lpe10p-HA and Mrs2p-Myc. Isolated mitochondria of *mrs2*Δ/*lpe10*Δ cells expressing LPE10–HA and MRS2-Myc from high copy number plasmids (lanes in blot area 1), the empty vectors (lanes in blot area 2), LPE10–HA or Mrs2-Myc alone (lanes in blot area 3 and 4, respectively) and coexpressing LPE10–HA from a low and Mrs2-Myc from a high copy number vector (lanes in blot area 5) were solubilized and incubated with anti-HA serum-coated beads. Unbound (supernatant, SN) and bound (elution, E) fractions were separated by SDS/PAGE, and analysed by immunoblotting with anti-HA serum (upper blot) or anti-Myc serum (lower blot).

(Fig. 7A). A current–voltage relationship determined at negative potentials yielded a single-channel conductance of 61 ± 5 pS (Fig. 7C). No single-channel events were recorded in the other 10 experiments. As a similar conductance of 67 ± 4 pS (in three of 15 experiments) was also observed in vesicles from *mrs2Δ/lpe10Δ* cells [5], resulting from channel activity of unknown origin, we suggest that Lpe10p is not capable of forming a detectable Mg^{2+}-permeable channel in the absence of Mrs2p.

As we found a significant effect of Lpe10p expression on the size of Mrs2p-containing complexes (Fig. 6), we examined whether the presence of Lpe10p might affect the characteristics of the Mrs2p channel (e.g. its conductance of ~ 155 pS) in giant lipid vesicles. Current traces of mitochondrial vesicles from cells expressing $(LPE10)_H$ and $(MRS2)_H$ revealed unique single-channel amplitudes at negative potentials of −15 and −35 mV as compared with *mrs2Δ/lpe10Δ* vesicles with or without expressed Lpe10p (Fig. 7B). Current–voltage relationships recorded from vesicles expressing Lpe10p and Mrs2p determined within +5 and −45 mV revealed a novel conductance of 103 ± 5 pS in four of seven experiments, with a reversal potential of +22 mV (Fig. 7B). Mrs2p channels yielded a reversal potential of > 40 mV in identical solutions [5]. The typical conductance of vesicles expressing Mrs2p only (~ 155 pS) was not observed, whereas the conductance from a channel of unknown origin (61 pS) was also observed in one of seven experiments (data not shown). We conclude that

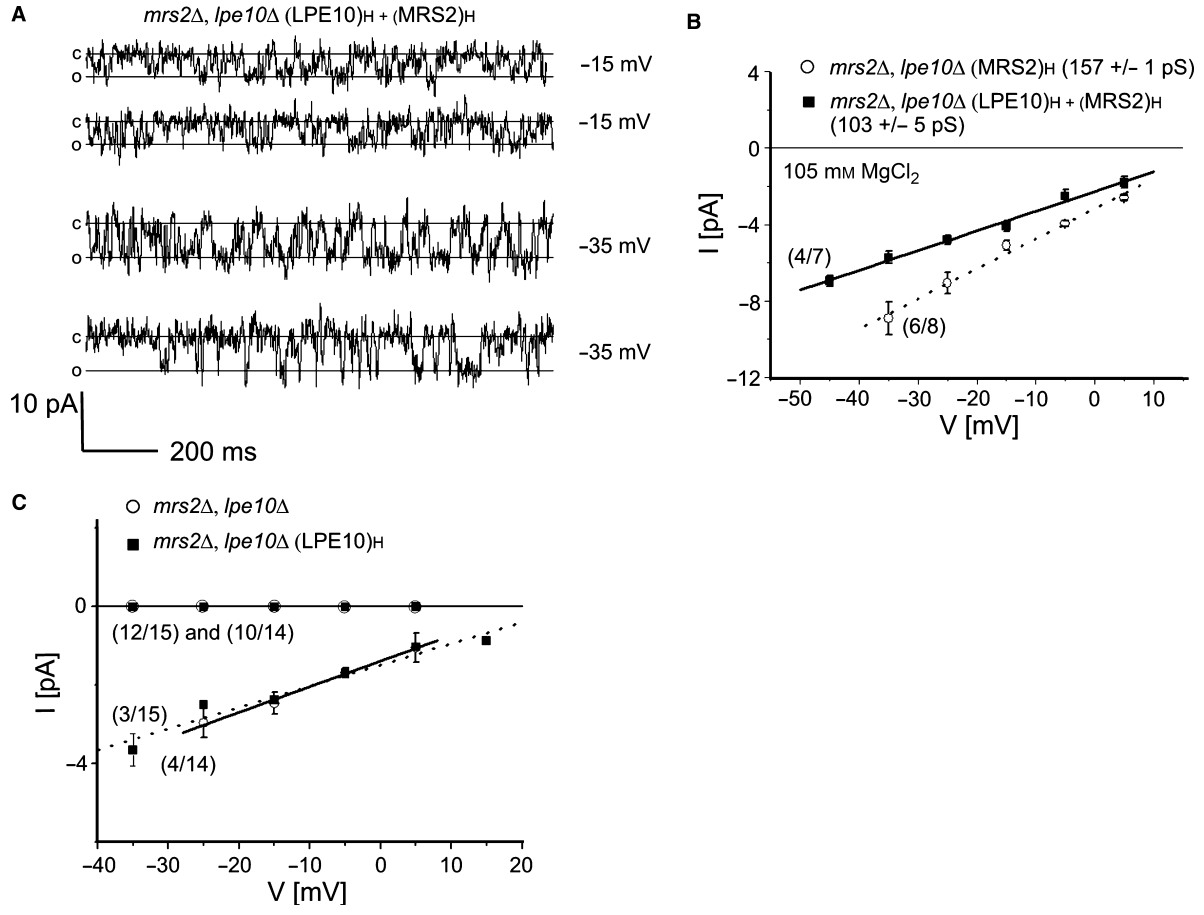

Fig. 7. Coexpression of Lpe10p and Mrs2p results in a unique single-channel conductance. Single-channel currents were obtained in an inside-out configuration from reconstituted giant vesicles fused with the inner mitochondrial membrane. (A) Recordings of vesicles overexpressing Lpe10p and Mrs2p from a multicopy plasmid were performed in the *mrs2Δ/lpe10Δ* background. Mg^{2+} (105 mM) was used as a charge carrier, and currents were recorded at −15 and −35 mV. (B) Current–voltage relationships were determined from amplitude histograms of single-channel currents at the indicated potentials, and yielded a conductance of 103 ± 5 pS (n = 4/7) for Lpe10p and Mrs2p coexpression; overexpression of Mrs2p resulted in a conductance of 157 ± 1 pS (n = 6–8). (C) Current–voltage relationships of endogenous single-channel currents of vesicles in the *mrs2Δ/lpe10Δ* background yielded a similar conductance (67 ± 4 pS, n = 3–15) as for overexpression of Lpe10p in a similar background (61 ± 5 pS, n = 4/14). In the remaining experiments, no single-channel currents were detected.

Lpe10p assembles with Mrs2p, thereby leading to a novel conductance of the Mrs2p channel.

Discussion

If the mitochondrial inner membrane protein Lpe10p and its homolog in *S. cerevisiae*, Mrs2p, fulfilled exactly the same functions, it would have been sufficient to retain one of the two proteins during evolution. In fact, the proteins cannot substitute for each other, and expression of one of the proteins in the *mrs2*Δ*/lpe10*Δ background is not sufficient to fully restore cell growth. We showed that only high copy number expression of Mrs2p weakly restored growth in the double-disruption strain, whereas Lpe10p failed to do so. In addition, Lpe10p and Mrs2p chimeric proteins were designed, and these restored Mg^{2+} influx in *mrs2*Δ as well as in *lpe10*Δ cells. Expression of a chimeric protein consisting of the N-terminal part of Lpe10p and the C-terminal region of Mrs2p, including its pore, restored growth and Mg^{2+} influx better than expression of a chimeric protein composed of the N-terminal part of Mrs2p and the C-terminal end of Lpe10p. Using mag-fura 2 for the detection of free, ionized Mg^{2+} inside mitochondria, we demonstrated that mitochondria of *lpe10*Δ cells lack the rapid Mg^{2+} influx, similar to mitochondria from *mrs2*Δ cells [4].

Interestingly, measurements of ΔΨ revealed that deletion of *LPE10* goes along with a pronounced drop in ΔΨ, which was not observed if *MRS2* was deleted. As it is necessary to use ΔΨ-dissipating (valinomycin) and ΔΨ-increasing (nigericin) chemicals for the calibration of JC-1, i.e. setting artificial minimum and maximum ΔΨ levels, it is not possible to determine absolute values of ΔΨ reduction. However, expression of Lpe10p in *lpe10*Δ or *mrs2*Δ*/lpe10*Δ cells restored ΔΨ to WT levels. Addition of nigericin, a K^+/H^+ ionophore, restored ΔΨ and, as a consequence, Mg^{2+} influx in *lpe10*Δ mitochondria. We also found that expression of the Lpe10-Mrs2p chimeric protein re-established ΔΨ to a significant degree, whereas the Mrs2-Lpe10p chimera failed to do so. Furthermore, mutation of the conserved F/YGMN motif of Lpe10p led to a strong decrease in Mg^{2+} influx, but no significant impact on ΔΨ. As Mrs2p forms an Mg^{2+} channel, the primary driving force for this system is the membrane potential, rather than pH changes in the mitochondrial matrix (ΔpH). However, we cannot fully exclude the possibility that deletion of Lpe10p also influences ΔpH, and that some of the effects of nigericin are attributable to changes in ΔpH.

Our findings led us to assume that both Mrs2p and Lpe10p physiologically contribute to the assembly of a functional Mg^{2+} channel. Moreover, Lpe10p is additionally involved in the maintenance of ΔΨ *in vivo*, a function that remains even with a mutated F/YGMN motif. It remains to be determined in what way Lpe10p has an impact on the membrane potential of yeast mitochondria, thereby setting the driving force for the influx of Mg^{2+}.

In vitro chemical cross-linking assays and BN-PAGE experiments revealed homo-oligomeric Lpe10p complexes similar to those formed by Mrs2p [4]. Thus, potential domains for oligomerization are present in the protein encoded by *LPE10*, which is not surprising, given the similarities in secondary structure between Mrs2p and Lpe10p. BN-PAGE experiments showed a size shift of the Lpe10p complex if Mrs2p was coexpressed. Finally, using coimmunoprecipitation, we were able to pull down the entire Mrs2 protein complex, and clearly identified Lpe10p as a member of this. These findings demonstrate a tight interaction of both proteins within this complex. We speculate that Lpe10p is a structural as well as modulating factor of the Mrs2p channel complex, leading to a stronger phenotype of *LPE10* deletion than the *MRS2* mutant itself. Additionally, reduction of ΔΨ may also have adverse effects on the function of other mitochondrial proteins.

Single-channel recordings on giant lipid vesicles with overexpressed Lpe10p isolated from *mrs2*Δ*/lpe10*Δ cells, as previously reported [5], did not reveal an Lpe10p-specific Mg^{2+}-permeable channel activity. However, coexpression of Lpe10p and Mrs2p decreased the Mrs2p channel conductance from ~ 155 to ~ 103 pS. Therefore, our data suggest that Lpe10p plays an important role in the physiological formation of the mitochondrial Mg^{2+} channel with a unique conductance resulting from heteromeric assembly of Mrs2p and Lpe10p. Whereas direct binding of matrix Mg^{2+} to the N-terminal domain of Mrs2p results in fast closing of the channel [8,9], the reduction of the Mrs2p channel conductance by ~ 30% (from ~ 155 to ~ 103 pS) suggests a possible regulatory role of Lpe10p in addition to its impact on ΔΨ. As compared with the Mg^{2+} conductance of 40 pS mediated by the mammalian TRPM7 channel [20,21], the conductance of 155 pS of the Mrs2p channel is surprisingly high. It is tempting to speculate that Mg^{2+} influx at strong, negative mitochondrial potentials is somewhat limited by this heteromeric Lpe10-Mrs2p channel assembly with a reduced conductance, whereas a decrease in Lpe10p expression levels leading to a reduction in mitochondrial potential might be compensated by the higher conductance of the homomeric Mrs2p channel.

In mammalian cells, only a single Mrs2p homolog has been identified [22,23]. Owing to the activity of numerous other 'modern' Mg^{2+} transporters [24], Lpe10p might be redundant in mammalian cells, whereas its presence in yeast, which lacks modern Mg^{2+} transporters, is obligatory.

Finally, we would like to propose a new name for *LPE10* (yeast ORF YPL060w), as *LPE* has only been the systematic name for many uncharacterized genes of *S. cerevisiae* [13]. We suggest calling it *MFM1* (Mrs2 function modulating factor 1), a synonym that best reflects the function of the protein.

Experimental procedures

Yeast strains, growth media and genetic procedures

The yeast *S. cerevisiae* DBY747 WT strain, the isogenic *mrs2*Δ deletion strain (DBY *mrs2-1*), the *lpe10*Δ deletion strain (DBY *lpe10-1*) and the *mrs2*Δ*/lpe10*Δ double-disruption (DBY747 *mrs2-2 lpe10-2*) have been described previously [3,13,14]. Yeast cells were grown to stationary phase in rich medium (YPD) with 2% glucose (Sigma Aldrich, Schnelldorf, Germany) as a carbon source.

Plasmid constructs

The plasmid construct YEp351 MRS2–HA [3] was digested with *Sac*I and *Sph*I and cloned into an empty YEp112 vector cut with the same restriction enzymes. The generated YEp112 MRS2–HA construct was digested with *Not*I and dephosphorylated (Antarctic Phosphatase, NEB), and a cassette coding for the myc epitope tag was cloned in frame with *MRS2* at the *Not*I site, resulting in the construct YEp112–MRS2–Myc.

To create Lpe10-Mrs2p-HA and Mrs2-Lpe10p-HA fusion proteins, a *Bcl*I restriction site was introduced at position 780 by use of overlap extension PCR according to [25]. The mutagenic forward primer 5′-AGTCTCCTAAGG A**TG**AT**CA**TTCGGACTTGGAAATGC-3′ (mismatched bases in bold) and the mutagenic reverse primer 5′-GCATTTCCAAGTCCGAA**TG**AT**CA**TCCTTAGGAG ACT-3′ were used in combination with the forward primer 5′-GTTGTCCTCCACCAAGAATAACTCTC-3′ and the reverse primer 5′-CCGCCACTGAAGTAAACCCC-3′. A double amino acid change (Asn261 to Asp and Phe262 to His) was thereby introduced, but this did not interfere with growth on nonfermentable carbon sources (data not shown). The resulting construct YEp351 MRS2–HA* *Bcl*I was digested with *Sph*I and *Bcl*I, and the isolated fragment was cloned into an *Sph*I-digested and *Bcl*I-digested YEp351 LPE10 vector [13] to generate the construct YEp351 MRS2–LPE10. The YEp351 LPE10 construct was digested with *Sph*I and *Bcl*I, and the isolated fragment was cloned into an *Sph*I-cut and *Bcl*I-cut YEp351 MRS2–HA* *Bcl*I vector to create the YEp351 LPE10–MRS2–HA construct (N-terminal 281 amino acids of Lpe10p and C-terminal 250 amino acids of Mrs2p). The YEp351 MRS2–LPE10 construct was linearized with *Not*I, and a cassette coding for the HA epitope tag was cloned in frame with the *MRS2–LPE10* fusion gene, resulting in the construct YEp351 MRS2–LPE10–HA (N-terminal 260 amino acids of Mrs2p and C-terminal 135 amino acids of Lpe10p). Both this and the YEp351 LPE10–MRS2–HA construct were cut with *Sac*I and *Sph*I, and cloned into an *Sac*I-digested and *Sph*I-digested YCp111 vector, resulting in the constructs YCp111 MRS2–LPE10–HA and YCp111 LPE10–MRS2–HA.

The plasmid construct YEp351 MRS2–HA was digested with *Sac*I and *Sph*I, and cloned into an empty YCp111 vector digested with the same restriction enzymes, resulting in the construct YCp111 MRS2–HA. The constructs YCp LPE10–HA and YEp351 LPE10–HA have been previously described [13].

In order to mutate the F/YGMN motif of Lpe10p to ASSV, overlap extension PCR was used with the mutagenic forward primer 5′-GCTCTATTCCTGTCTATCGCTAGCT CTGTTCTGGAAAGTTTCATAGAAG-3′ and the mutagenic reverse primer 5′-CTTCTATGAAACTTTCCAGA ACAGAGCTAGCGATAGAACCCAGGAATAGAGC-3′, in combination with the forward primer 5′-AAGCTTGCA TGACTGCAGGTCGACTC-3′ and the reverse primer 5′-GAATTCGAGCTCGGTACCCGGGGATAA-3′. Verification of positive clones was performed by restriction analysis with *Nhe*I, and the mutation was indicated Lpe10–J1. No additional mutations were found by sequencing.

Isolation of mitochondria and measurement of $[Mg^{2+}]_m$ by spectrofluorometry

Isolation of mitochondria and the measurement of Mg^{2+} influx into mitochondria were performed as previously dsecribed [4]. In some experiments, mitochondrial preparations equivalent to 1 mg of total mitochondrial protein were treated with 1 μM nigericin (Sigma-Aldrich, Germany) 5 min prior to the measurement.

BN-PAGE

Eighty micrograms of isolated mitochondrial protein was extracted by addition of 40 μL of extraction buffer (750 mM aminocaproic acid, 50 mM Bis–Tris/HCl, pH 7.0) and laurylmaltoside to a final concentration of 1.2%. After incubation on ice for 30 min, the samples were centrifuged at 45 000 ***g*** for 30 min, and the supernatant was supplemented with a 0.25 volume of sample buffer (500 mM aminocaproic acid, 5% Serva blue G). The solubilized protein solution was analyzed by BN-PAGE on a 5–18% linear polyacrylamide gradient [19]. The gel was blotted

onto a poly(vinylidene difluoride) membrane, which was stained with Coomassie Blue reagent or analysed by immunoblotting with an HA antiserum.

Chemical cross-linking and PAGE

Thirty micrograms of total mitochondrial protein was mixed with loading buffer containing β-mercaptoethanol, and samples were heated to 80 °C for 4 min before being loaded onto SDS/PAGE gels. HA protein-containing bands were visualized by the use of an anti-HA serum (Covance), and myc protein-containing bands by an anti-Myc serum (Sigma-Aldrich). Chemical cross-linking experiments were performed as previously reported [4], using the cross-linking reagent oPDM (Sigma Aldrich).

Coimmunoprecipitation

Five milligrams of mitochondrial protein was resuspended in solubilization buffer (500 mM NaCl, 100 mM Tris/HCl, pH 7.8), and membrane proteins were solubilized by addition of Triton X-100 to a final concentration of 1.2% and incubation for 30 min at 4 °C under gentle rotation. After centrifugation at 43 000 ***g*** for 30 min (4 °C) to remove nonsolubilized mitochondrial debris, the Triton X-100 concentration of the supernatant was reduced to 0.8%. One hundred microliters of Protein A Dynabeads (Invitrogen, Lofer, Austria) was washed with solubilization buffer + 0.8% Triton X-100. Coating of the beads was performed with an HA antibody (Covance) in the same buffer for 30 min at 4 °C under rotation. HA-coated beads were washed twice and incubated with the clarified supernatant for 1 h at 4 °C under gentle rotation. After the binding reaction, the supernatant was removed, and the beads were washed three times with solubilization buffer including 0.8% Triton X-100. Proteins were eluted from the beads by heating for 5 min at 80 °C in SDS sample buffer. The supernatant and the elution fraction were analyzed on a 10% SDS/polyacrylamide gel, and western blotting was performed as described above.

Determination of $\Delta\Psi$

Isolated yeast mitochondria equivalent to 50 μg of total mitochondrial protein were incubated with 0.5 μM JC-1 (Molecular Probes, NL) for 7 min at room temperature. The sample was spun down and resuspended in 2 mL of 0.6 M sorbitol buffer supplemented with 0.5 mM ATP, 0.2% succinate and 0.01% pyruvate. The intensity changes of the monomeric form (low energy, 540 nm) and of the multimeric form (high energy, 590 nm) were recorded with the Scan mode of a Perkin Elmer LS55 luminescence photometer. Data collection was performed with FL WINLAB4. For calibration, similar samples were treated in parallel, either with nigericin (1 μM), to determine the maximum of energization, or carbonyl cyanide p-(trifluoromethoxy)-phenylhydrazone (1 μM), to determine the minimum of energization, respectively. These datasets were used to calculate a calibration curve for every single measurement for the determination of the percentage of relative $\Delta\Psi$.

Patch clamp recordings of ion channels

Single-channel currents at various test potentials were recorded, as previously described [5], from giant lipid vesicles fused with inner mitochondrial membrane vesicles, using the patch clamp technique [26].

Computer analysis

Secondary structure analysis (prediction of transmembrane domains, helices and loops) of *S. cerevisiae* Mrs2, *S. cerevisiae* Lpe10, *A. thaliana* Mrs2-7 and *T. maritima* CorA was performed with Jpred3, a consensus method for protein secondary structure prediction at the University of Dundee.

Acknowledgements

This work was supported by the Austrian Science Fund (FWF project number 20141). We thank J. Gregan (IMP Vienna) for critically reading the manuscript.

References

1 Iwatsuki H, Lu YM, Yamaguchi K, Ichikawa N & Hashimoto T (2000) Binding of an intrinsic ATPase inhibitor to the F(1)FoATPase in phosphorylating conditions of yeast mitochondria. *J Biochem* **128**, 553–559.
2 Rodriguez-Zavala JS & Moreno-Sanchez R (1998) Modulation of oxidative phosphorylation by Mg^{2+} in rat heart mitochondria. *J Biol Chem* **273**, 7850–7855.
3 Bui DM, Gregan J, Jarosch E, Ragnini A & Schweyen RJ (1999) The bacterial magnesium transporter CorA can functionally substitute for its putative homologue Mrs2p in the yeast inner mitochondrial membrane. *J Biol Chem* **274**, 20438–20443.
4 Kolisek M, Zsurka G, Samaj J, Weghuber J, Schweyen RJ & Schweigel M (2003) Mrs2p is an essential component of the major electrophoretic Mg^{2+} influx system in mitochondria. *EMBO J* **22**, 1235–1244.
5 Schindl R, Weghuber J, Romanin C & Schweyen RJ (2007) Mrs2p forms a high conductance Mg^{2+} selective channel in mitochondria. *Biophys J* **93**, 3872–3883.
6 Niegowski D & Eshaghi S (2007) The CorA family: structure and function revisited. *Cell Mol Life Sci* **64**, 2564–2574.

7 Graschopf A, Stadler JA, Hoellerer MK, Eder S, Sieghardt M, Kohlwein SD & Schweyen RJ (2001) The yeast plasma membrane protein Alr1 controls Mg^{2+} homeostasis and is subject to Mg2+-dependent control of its synthesis and degradation. *J Biol Chem* **276**, 16216–16222.
8 Payandeh J & Pai EF (2006) A structural basis for Mg^{2+} homeostasis and the CorA translocation cycle. *EMBO J* **25**, 3762–3773.
9 Eshaghi S, Niegowski D, Kohl A, Martinez MD, Lesley SA & Nordlund P (2006) Crystal structure of a divalent metal ion transporter CorA at 2.9 angstrom resolution. *Science* **313**, 354–357.
10 Lunin VV, Dobrovetsky E, Khutoreskaya G, Zhang R, Joachimiak A, Doyle DA, Bochkarev A, Maguire ME, Edwards AM & Koth CM (2006) Crystal structure of the CorA Mg^{2+} transporter. *Nature* **440**, 833–837.
11 Gebert M, Meschenmoser K, Svidova S, Weghuber J, Schweyen R, Eifler K, Lenz H, Weyand K & Knoop V (2009) A root-expressed magnesium transporter of the MRS2/MGT gene family in Arabidopsis thaliana allows for growth in low-Mg^{2+} environments. *Plant Cell* **21**, 4018–4030.
12 Knoop V, Groth-Malonek M, Gebert M, Eifler K & Weyand K (2005) Transport of magnesium and other divalent cations: evolution of the 2-TM-GxN proteins in the MIT superfamily. *Mol Genet Genomics* **274**, 205–216.
13 Gregan J, Bui DM, Pillich R, Fink M, Zsurka G & Schweyen RJ (2001) The mitochondrial inner membrane protein Lpe10p, a homologue of Mrs2p, is essential for magnesium homeostasis and group II intron splicing in yeast. *Mol Gen Genet* **264**, 773–781.
14 Wiesenberger G, Waldherr M & Schweyen RJ (1992) The nuclear gene MRS2 is essential for the excision of group II introns from yeast mitochondrial transcripts in vivo. *J Biol Chem* **267**, 6963–6969.
15 Weghuber J, Dieterich F, Froschauer EM, Svidova S & Schweyen RJ (2006) Mutational analysis of functional domains in Mrs2p, the mitochondrial Mg^{2+} channel protein of Saccharomyces cerevisiae. *FEBS J* **273**, 1198–1209.
16 Maguire ME (2006) The structure of CorA: a Mg(2+)-selective channel. *Curr Opin Struct Biol* **16**, 432–438.
17 Nowikovsky K, Reipert S, Devenish RJ & Schweyen RJ (2007) Mdm38 protein depletion causes loss of mitochondrial K^+/H^+ exchange activity, osmotic swelling and mitophagy. *Cell Death Differ* **14**, 1647–1656.
18 Szegedy MA & Maguire ME (1999) The CorA Mg(2+) transport protein of Salmonella typhimurium. Mutagenesis of conserved residues in the second membrane domain. *J Biol Chem* **274**, 36973–36979.
19 Schagger H, Cramer WA & von Jagow G (1994) Analysis of molecular masses and oligomeric states of protein complexes by blue native electrophoresis and isolation of membrane protein complexes by two-dimensional native electrophoresis. *Anal Biochem* **217**, 220–230.
20 Monteilh-Zoller MK, Hermosura MC, Nadler MJ, Scharenberg AM, Penner R & Fleig A (2003) TRPM7 provides an ion channel mechanism for cellular entry of trace metal ions. *J Gen Physiol* **121**, 49–60.
21 Nadler MJ, Hermosura MC, Inabe K, Perraud AL, Zhu Q, Stokes AJ, Kurosaki T, Kinet JP, Penner R, Scharenberg AM *et al.* (2001) LTRPC7 is a Mg.ATP-regulated divalent cation channel required for cell viability. *Nature* **411**, 590–595.
22 Piskacek M, Zotova L, Zsurka G & Schweyen RJ (2009) Conditional knockdown of hMRS2 results in loss of mitochondrial Mg(2+) uptake and cell death. *J Cell Mol Med* **13**, 693–700.
23 Zsurka G, Gregan J & Schweyen RJ (2001) The human mitochondrial Mrs2 protein functionally substitutes for its yeast homologue, a candidate magnesium transporter. *Genomics* **72**, 158–168.
24 Quamme GA (2010) Molecular identification of ancient and modern mammalian magnesium transporters. *Am J Physiol Cell Physiol* **298**, C407–C429.
25 Pogulis RJ, Vallejo AN & Pease LR (1996) In vitro recombination and mutagenesis by overlap extension PCR. *Methods Mol Biol* **57**, 167–176.
26 Hamill OP, Marty A, Neher E, Sakmann B & Sigworth FJ (1981) Improved patch-clamp techniques for high-resolution current recording from cells and cell-free membrane patches. *Pflugers Arch* **391**, 85–100.

Supporting information

The following supplementary material is available:
Fig. S1. Secondary structure prediction of CorA and its homologues in yeast and plants.

This supplementary material can be found in the online version of this article.

Please note: As a service to our authors and readers, this journal provides supporting information supplied by the authors. Such materials are peer-reviewed and may be re-organized for online delivery, but are not copy-edited or typeset. Technical support issues arising from supporting information (other than missing files) should be addressed to the authors.

3.7. Mutational analysis of the Leu294 residue in the conserved hydrophobic gate region of TmCorA

There are several hydrophobic constrictions along the TmCorA ion conduction pathway. The narrowest one is formed by the highly conserved residues Leu294 and Met291 (Eshaghi, et al., 2006; Lunin, et al., 2006; Payandeh and Pai, 2006). They are considered to be part of the potential "hydrophobic gate" (Lunin, et al., 2006; Payandeh, et al., 2008). To verify this hypothesis our mutations targeted the Leu294 and exchange it for different amino acid residues (Tab. 2).

Table 2: List of mutants at position 294

Leu294	**Ala**
	Arg
	Asp
	Cys
	Glu
	Gly
	His
	Phe
	Ser
	Val

3.7.1. Leu294Val mutant

In the cellular complementation assay the Leu294Val mutant exhibited slightly inhibited growth on plates containing high $MgCl_2$ and IPTG concentrations, which points to a slight Mg^{2+} overdose (Fig. 2). It was also able to grow on LB amp plates without supplementation of either $MgCl_2$, or IPTG (Fig. 2). This could be explained by the fact, that the regulation of the used plasmid is not tight enough and the CorA gene is transcribed also in IPTG – free conditions. This was proved by Western blotting (results not shown).

The growth curves in liquid media more or less confirmed the results of the growth complementation assay (Fig. 3 – 5). In LB medium without any supplements we observed growth of the Leu294Val mutant caused probably by the low expression of the mutated protein (Fig. 3). In medium containing 0.05 mM IPTG the cells grew

faster than the wild-type cells (Fig. 4), whereas in media containing 0.05 mM IPTG and 5 mM $MgCl_2$ (Fig. 5), the growth was abolished completely.

Results of the recordings of Mg^{2+} uptake performed on *Salmonella typhimurium* MM281 cells transformed with the mutated CorA constructs revealed Mg^{2+} influx similar to the wild-type and the curve reached a steady state approximately at the wild-type level (Fig. 6).

3.7.2. Leu294Gly mutant

In the growth complementation assay (Fig. 2) and in liquid media (Fig. 3 - 5), the Leu294Gly mutant was even more Mg^{2+} sensitive than the Leu294Val variant. The cells did not grow on plates containing 100 mM $MgCl_2$ and 0.2 mM IPTG and growth on plates containing 100 mM $MgCl_2$ and 0.1 mM IPTG was reduced, suggesting a defect in the closing and/or in the regulation of the transporter (Fig. 2). Cells of this mutant grew also on plates without additional $MgCl_2$ or IPTG (Fig. 2), even better than cells of other mutants with similar phenotype.

The same effect was observed in liquid medium without any supplements (Fig. 3), where the Lue294Gly mutant exhibited the fastest growth of all. In liquid medium containing 0.05 mM IPTG we observed fast growth of the Leu294Gly cells, followed by a steady-state after 4 hours (Fig. 4). In medium supplemented with 0.05 mM IPTG and 5 mM $MgCl_2$ the cells did not grow at all, similarly to the Leu294Val mutant (Fig. 5).

In Mg^{2+} uptake measurements rapid Mg^{2+} influx was observed (Fig. 6), which was similar to the uptake of cells transformed with wild – type TmCorA, but it did not reach a steady-state, which indicates a defect in the closing of the transporter.

3.7.3. Leu294Ala mutant

The effect of the Leu294Ala mutation was tested in the growth complementation assay only (Fig. 2). The phenotype was similar to that of the Leu294Val mutant: the

cells were able to grow on LB plates without any supplements and growth on plates containing 100 mM $MgCl_2$ and 0.2 mM IPTG was slightly inhibited, pointing on a Mg^{2+} overdose.

3.7.4. Leu294Arg mutant

In the growth complementation assay the phenotype of this mutant was similar to the wild-type TmCorA (Fig. 7): no growth on LB plates, good growth on all plates containing IPTG alone or in combination with $MgCl_2$ and no signs for Mg^{2+} overdose.

The shapes of the growth curves in liquid media were similar to the wild-type curves: no growth in LB (Fig. 3); exponential growth in medium supplemented with 0.05 mM IPTG, which was lower than in the wild-type, suggesting lower transport activity of the Leu294Arg mutant (Fig. 4); in medium containing 5 mM $MgCl_2$ and 0.05 mM IPTG the growth curve was almost identical with the wild-type curve (Fig. 5).

Mg^{2+} uptake measurements of the Leu294Arg mutant showed slower Mg^{2+} influx and lower steady-state values (~ 80% of wild-type values) (Fig. 8) suggesting that (i) the pore of the transporter is smaller than in wild-type TmCorA; (ii) the sensitivity of CorA to Mg^{2+} or the regulation of opening and closing of the pore was affected.

3.7.5. Leu294Asp mutant

In the growth complementation assay slightly reduced growth on the plates containing 0.2 mM IPTG can be observed. On plates supplemented with 0.1 mM IPTG and 100 mM $MgCl_2$, the growth is similar to that of the wild-type cells, but at higher IPTG concentration (0.2 mM IPTG, 100 mM $MgCl_2$), severe growth defect can be observed (Fig. 2). This could be the result of a possible Mg^{2+} overdose at higher protein expression levels.

In liquid medium without $MgCl_2$ cells transformed with the Leu294Asp mutant were not able to grow (Fig. 3). In medium containing 0.05 mM IPTG we observed rapid growth but after 4 hours a steady–state phase was reached, probably due to a overdose Mg^{2+} (Fig. 4). In medium containing 0.05 mM IPTG and 5 mM $MgCl_2$ the shape of

the Leu294Asp mutant growth curve differed from that of the wild type TmCorA: the mutant cells grew significantly slower, reaching just an OD_{600} of 0.6 (~ 50% of the wild-type CorA) (Fig. 5), which also indicates a Mg^{2+} overdose.

Mg^{2+} uptake of Leu294Asp mutant increased slowly and did not reach a steady-state level within a time period of 600 seconds (Fig. 9), suggesting that the pore is neither completely open nor can it close properly, causing slow, constant Mg^{2+} uptake, leading finally to a Mg^{2+} overdose. This mutation apparently causes a defect in the regulation of opening and closing or/and in the closing process itself.

3.7.6. Leu294Glu mutant

In the growth complementation assay on plates containing 0.2 mM IPTG and 0.1 mM IPTG with 100 mM $MgCl_2$ normal growth was observed. On plates supplemented with 0.2 mM IPTG and 100 mM $MgCl_2$ this mutant exhibited reduced growth, caused possibly by Mg^{2+} overdose (Fig. 2).

In liquid LB medium we can observe moderate growth of the Leu294Glu mutant, showing that even under low expression levels of the protein a certain amount of Mg^{2+} is transported into the cells (Fig. 3). In medium supplemented with 0.05 mM IPTG the Leu294Glu mutant grew better and faster then the wild type (Fig. 4), pointing to higher Mg^{2+} uptake capacity of the mutated protein and under higher Mg^{2+} conditions (0.05 mM IPTG and 5 mM $MgCl_2$) the growth curve of this mutant was comparable with the wild type curve (Fig. 5).

In Mg^{2+} uptake measurements of the Leu294Glu mutant constant Mg^{2+} uptake was observed (Fig. 9), similar to that of the Leu294Asp mutant, but much faster, suggesting that the pore-opening is probably wider than that of Leu294Asp mutant and the closing process is disturbed.

3.7.7. Leu294Ser mutant

In this mutant we can observe sensitivity to high Mg^{2+} concentrations in 0.1 and 0.2 mM IPTG conditions on plates (Fig. 2).

In liquid LB medium the mutant exhibited fast logarithmic growth, demonstrating that the Mg^{2+} uptake capacity of the mutated transporter is sufficient even in low Mg^{2+} conditions (Fig 3). In 0.5 mM IPTG medium fast, logarithmic growth can be seen, with a steady-state already after 3 hours (Fig. 4). The growth in medium containing 0.05 mM IPTG and 5 mM $MgCl_2$ slowed down already after 2 hours with an steady-state considerably lower then that of the wild-type curve (Fig. 5). This is indicative of a possible Mg^{2+} overdose.

In Mg^{2+} uptake recordings, constant Mg^{2+} influx similar to that of the Leu294Glu mutant was observed (Fig. 9), which can be caused by a similar mechanism as in the Leu294Glu mutant.

3.7.8. Leu294Phe mutant

In this case we did not observe any sign of growth on plates containing 0.2 mM IPTG, but no growth defect was observed on plates containing IPTG and $MgCl_2$ (Fig. 10). This led us to the conclusion, that this mutation inhibits the CorA-mediated Mg^{2+} uptake, which was also proven in liquid medium (results not shown).

3.7.9. Discussion

Gating of the TmCorA magnesium transporter is a complex process, involving several events resulting in structural rearrangements of the pentamer. The gate region involves several hydrophobic residues among which leucine at position 294 plays a critical role in the gating process.

Leucine is a hydrophobic aminoacid. The side chains of the five leucines in the gate region of the pore (one for each subunit) interact with each other trough hydrophobic interactions and form a hydrophobic ring. Exchange of leucine for a similar, small hydrophobic aminoacid, like valine or alanine does not have a dramatic effect.

Valine is topologically and chemically similar to leucine, but it is smaller, which means that the side chains are reaching less into the inside of the pore and the pore can’t be closed completely. The hydrophobic interactions between the side chains of the valines are weaker and the pore becomes larger. This might be the reason for the

Mg^{2+} overdose and for the ability of this mutant to growth in low Mg^{2+} conditions. Nevertheless, the Mag-Fura measurements did not reveal a higher Mg^{2+} uptake. This might be explained by a very small difference in the Mg^{2+} uptake levels in the wild-type protein and the valine mutant, which can not be seen in the short time period of 600 seconds.

Alanine bears a smaller side chain than valine, leading to reduction of contacts between the five alanines and to a less closed pore. The diminished numbers of contacts exterted by the alanine side chain, might cause local destabilization of the structure which might be the reason for the reduced growth on high Mg^{2+} observed in the growth complementation assay (Fig. 2). This is in agreement a with the findings of Payandeh et al. (Payandeh, et al., 2008), who showed that exchange of leucine 294 to a hydrophobic amino acid with a smaller side chain (isoleucine, valine or alanine) results in an increased ability of cells to grow on media supplemented with low $MgCl_2$ concentrations.

The effect of the Leu294 mutation to glycine may be mechanistically and structurally explained by local structural changes due to introduction of a small amino acid residue with no side chain. The absence of the side chain could on one hand cause a wider opening of the pore and on the other impair its complete closing.

On the other hand the effects observed with the Leu294Arg mutant cannot only be explained by local changes. Concentration of positively charged arginine residues in this region might have two opposite effects: repulsion of the positively charged residues causing a local structural distortion, and/or repulsion of the Mg^{2+} ion and hindering its passing through the pore. Both effects can explain the slow-down of Mg^{2+} transport, but not the low steady–state values observed in Mg^{2+} uptake measurements, which indicate a change in the regulation of Mg^{2+} influx. According to Payandeh et al. a valine mutation at position 294 can alter Mg^{2+}-binding properties of the transporter (Payandeh, et al., 2008). Due to the distance of ~ 65 Å between the leucine 294 and the DCS sites a direct interaction seems impossible. Since the loss of Mg^{2+} ions from DCS sites can induce conformational rearrangements of the magnesium-binding domains, transmitted to the gate region by the α7 helices and leading to changes allowing ions to pass through (Chakrabarti, et al., 2010; Payandeh, et al., 2008), also a reverse process might be possible. Certain mutations in the gate

region may evoke structural rearrangements of the α7 helices leading to conformational changes in the DCS sites, resulting in their changed affinity to Mg^{2+} ions.

Introduction of negatively charged amino acids like aspartic or glutamic acid in place of leucine causes apparently local structural disorders. In case of aspartic acid, the negatively charged side chains coming from five monomers repulse each other, leading to the inability of the transporter to close properly and to maintain a stable magnesium concentration in the cell. Furthermore, slow magnesium uptake of this mutant indicates that Mg^{2+} ions are probably trapped in the ring of negative charges.

The side chain of the glutamic acid is longer then that of aspartic acid. Both of these mutants exhibited similar phenotypes, but in case of the glutamic acid mutant the Mg^{2+} uptake was much faster. This effect might be caused by the local structural disorder caused by the longer side chain, making the pore wider then in the case of the aspartic acid mutant, allowing faster Mg^{2+} uptake.

The oxygen atoms of the hydroxyl groups of serine can build a trap for Mg^{2+} in the middle of the pore, but this effect should be less efficient than the similar effect of aspartic acid or glutamic acid side chains. Because of the small serine side chain, there is no need of a local distortion or it is not as sever the one of aspartic acid or glutamic acid mutants. As serine is hydrophilic and smaller than leucine, the pore can’t be closed properly.

In case of phenylalanine on position 294, the loss of function effect might be caused by the bulky aromatic ring, which probably completely blocs of the pore.

Payandeh et. al investigated the hydrophobic gate region of TmCorA by mutating the leucine 294 to smaller hydrophobic residues: isoleucine, valine and alanine. In the cellular complementation assay they observed increased ability of these mutants to grow on plates with low magnesium concentrations. This effect increased with the decreasing side chain volume of the amino acids and was confirmed by fluorescence-based Mg^{2+} uptake measurements in liposomes (Payandeh, et al., 2008). From these results they conclude that not only the hydrophobic barrier, but also steric occlusion might control the passing of Mg^{2+} ion through the hydrophobic gate. In our mutational study we used two three hydrophobic amino acids: valine, alanine and phenylalanine.

Whereas the results of the Leu294Val and Leu294Ala mutants confirmed the results of Payandeh et al., the phenylalanine on position 294 inhibited the Mg^{2+} uptake completely, showing that hydrophobocity is not the only important criteria for an amino acid on this position.

The effect of a hydrophilic amino acid on position 294 was demonstrated on three mutants: Leu294Asp, Leu294Glu and Leu294Arg. The effects of these mutations are clearly different: in the Mg^{2+} uptake of the Leu294Asp mutant is very slow and the closing of the gate is impaired, the Mg^{2+} uptake of the Leu294Glu mutant is much faster, but the closing of the gate is also impaired, whereas the Mg^{2+} uptake of the Leu294Arg mutant is fast and tightly regulated.

The substitution of leucine with a small neutral amino acid like glycine or serine produced similar results: increased Mg^{2+} sensitivity caused by defect in the closing of the pore due to reduced size of the side chain.

Our results clearly showed that more important then the hydrophobic/hydrophilic character of the amino acids, are charge and structure/size of the side chain and its interactions with neighboring amino acids.

In summary, we confirmed the importance of the leucine 294 for gating of the Mg^{2+} transport. A hydrophobic residue at this position is highly conserved in the CorA protein family, but we show that also the charge and structural features of the side chain greatly influence the gating process.

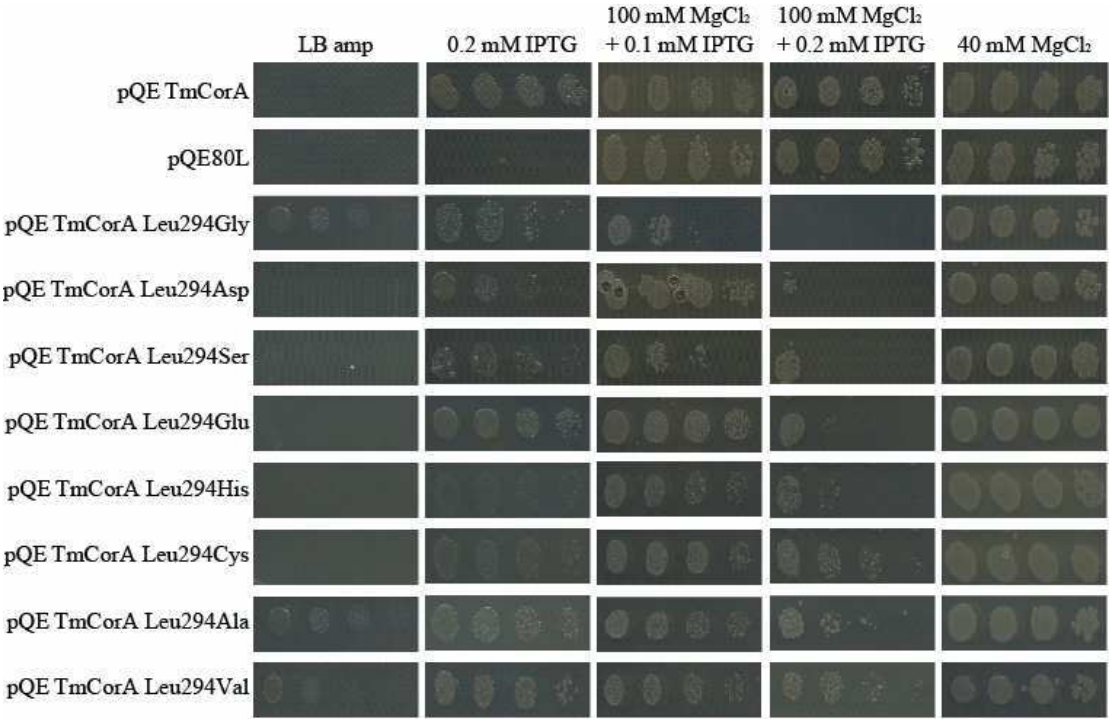

Figure 2.:Growth complementation assay of the gating mutants. *Escherichia coli* strain GS12K which lacks all three known magnesium transport systems was transformed with plasmids indicated.

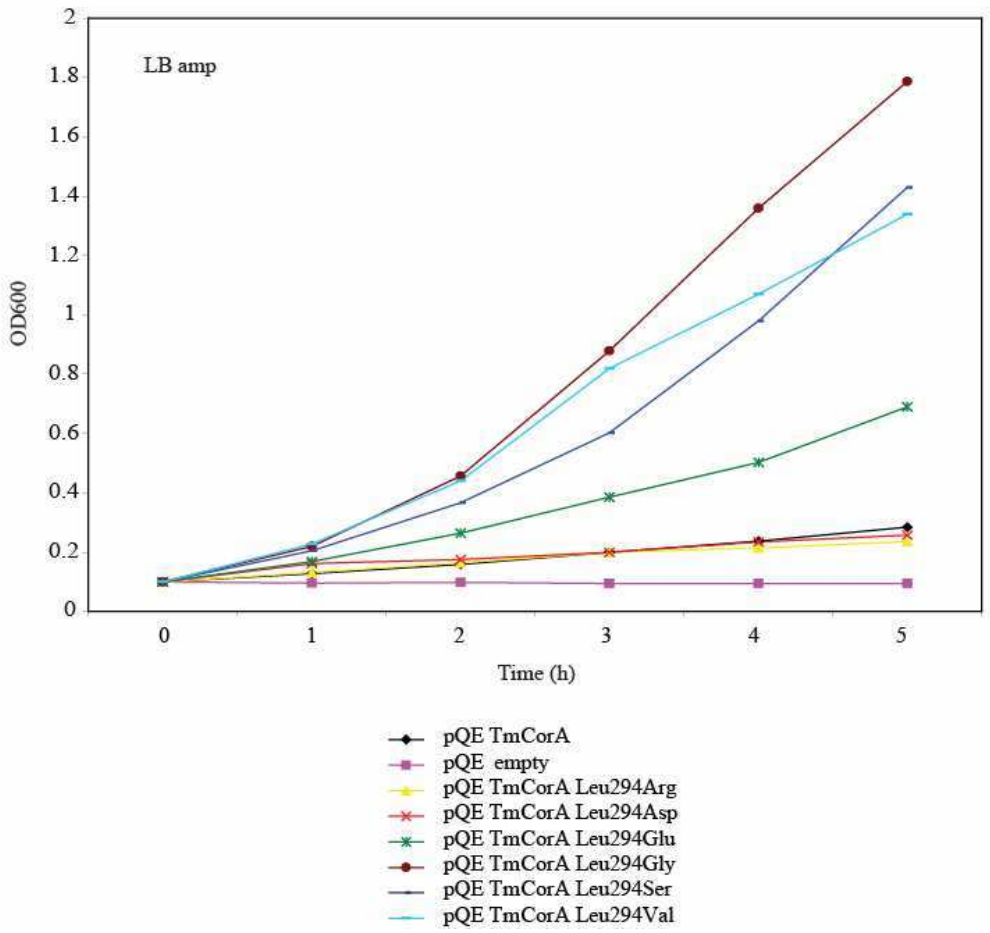

Figure 3.: Effect of gating mutantions in liquid LBamp medium. Growth curves of the *S. typhimurium* strain MM281 which lacks all three known magnesium transport systems, transformed with plasmids indicated. Cells were grown over night in LB amp medium containing 10 mM $MgCl_2$. Cultures were diluted to an OD_{600} of 0.1 and grown over 5 hours. The data were averaged from three independent experiments.

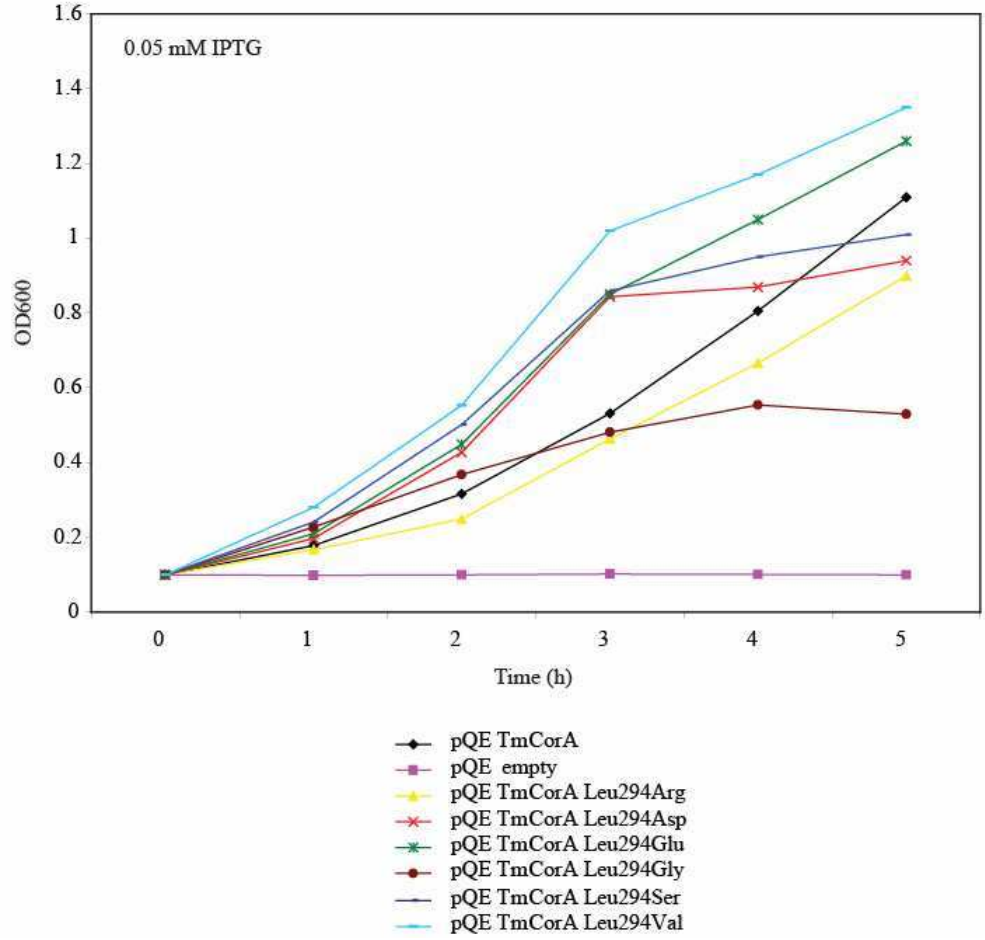

Figure 4.: Effect of gating mutantions in liquid medium containing 0.05 mM IPTG. Growth curves of the *S. typhimurium* strain MM281 which lacks all three known magnesium transport systems, transformed with plasmids indicated. Cells were grown over night in LB amp medium containing 10 mM $MgCl_2$. Cultures were diluted to an OD_{600} of 0.1 and grown over 5 hours. The data were averaged from three independent experiments.

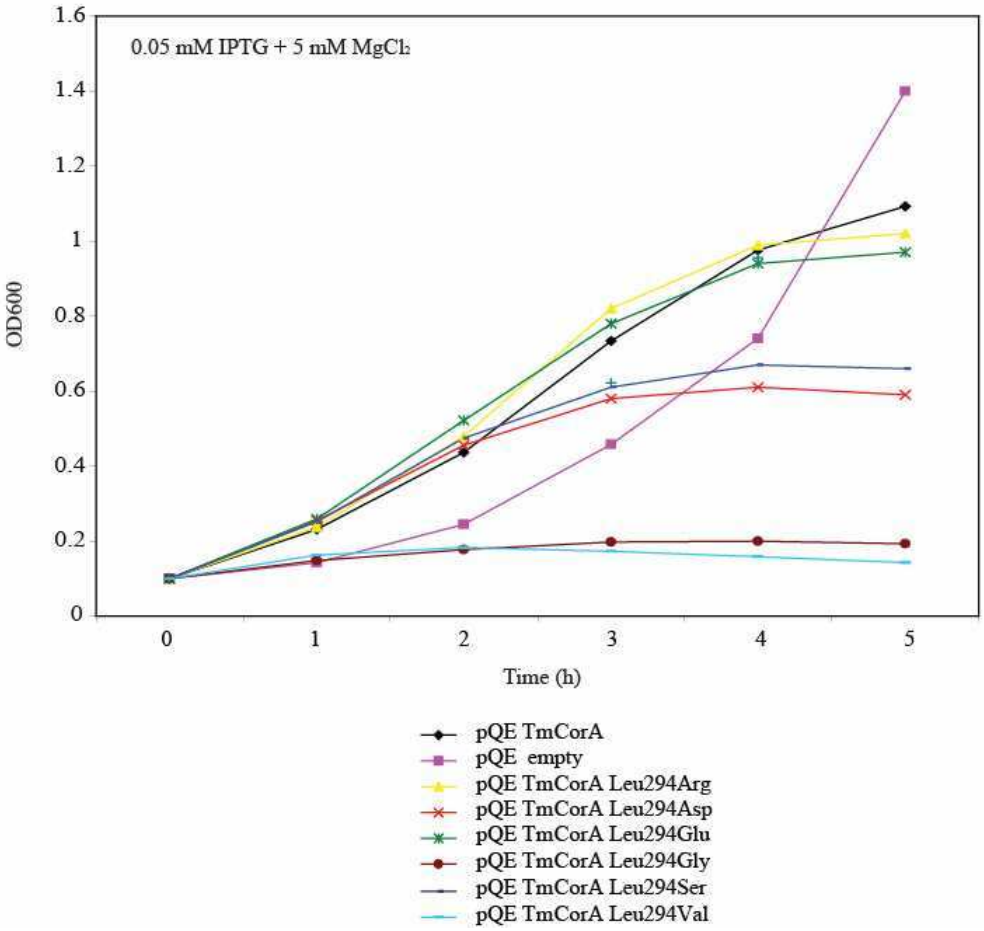

Figure 5.: Effect of gating mutantions in liquid medium containing 0.05 mM IPTG and 5 mM $MgCl_2$. Growth curves of the *S. typhimurium* strain MM281 which lacks all three known magnesium transport systems, transformed with plasmids indicated. Cells were grown over night in LB amp medium containing 10 mM $MgCl_2$. Cultures were diluted to an OD_{600} of 0.1 and grown over 5 hours. The data were averaged from three independent experiments.

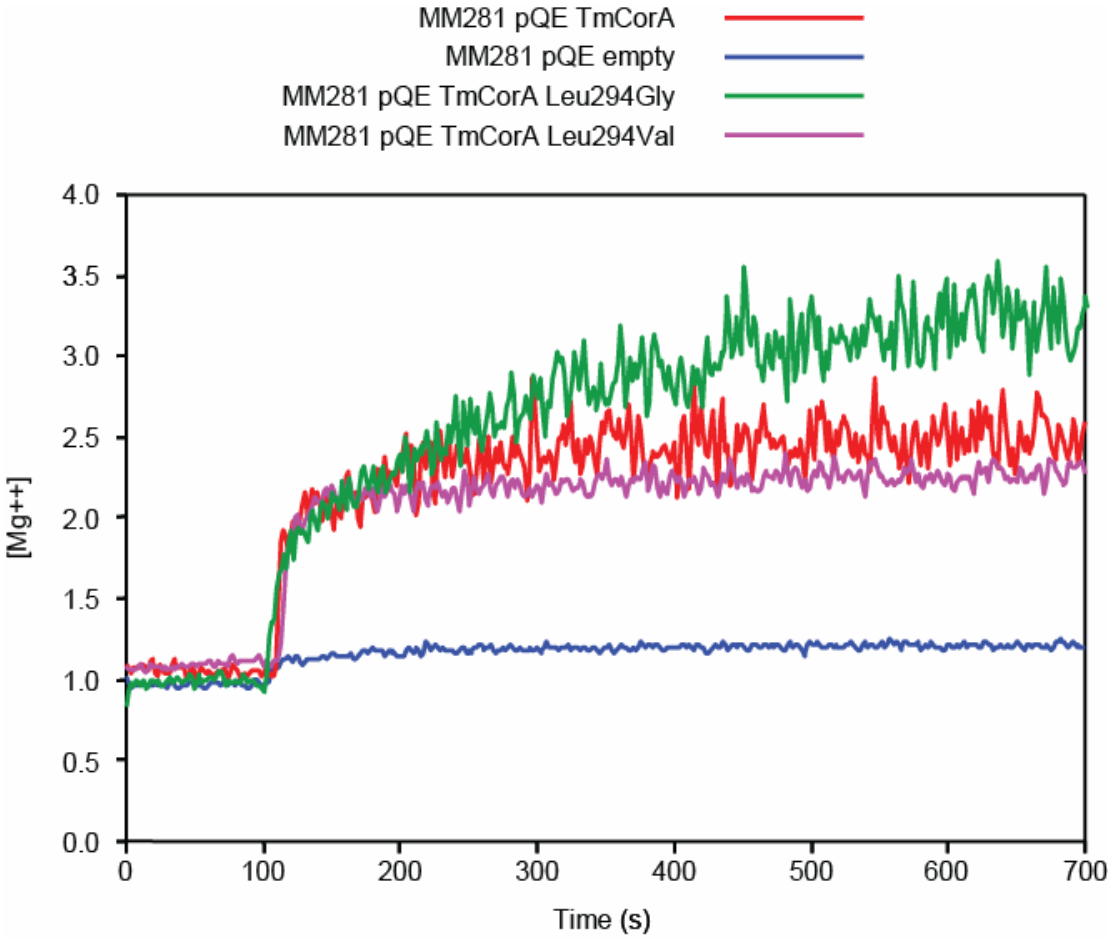

Figure 6.: Representative recordings of Mg^{2+} uptake. *S. typhimurium* strain MM281 which lacks all three known magnesium transport systems was transformed with plasmids indicated. The representative recordings show changes in fluorescence intensity of Mag-Fura-2 monitored over 10 minutes time after adding 10 mM $MgCl_2$.

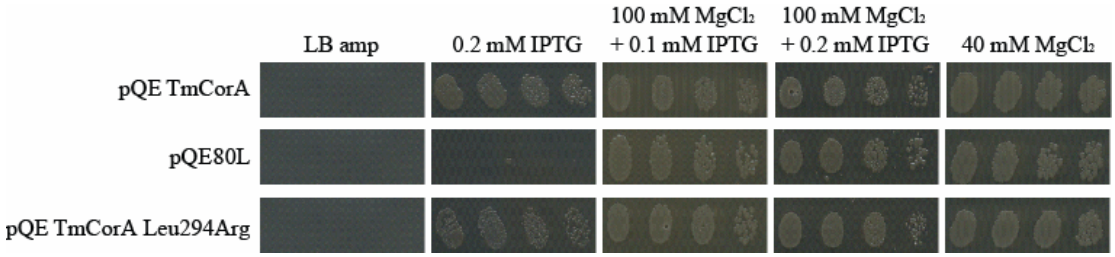

Figure 7.: Growth complementation assay of the gating mutants. *Escherichia coli* strain GS12K which lacks all three known magnesium transport systems was transformed with plasmids indicated.

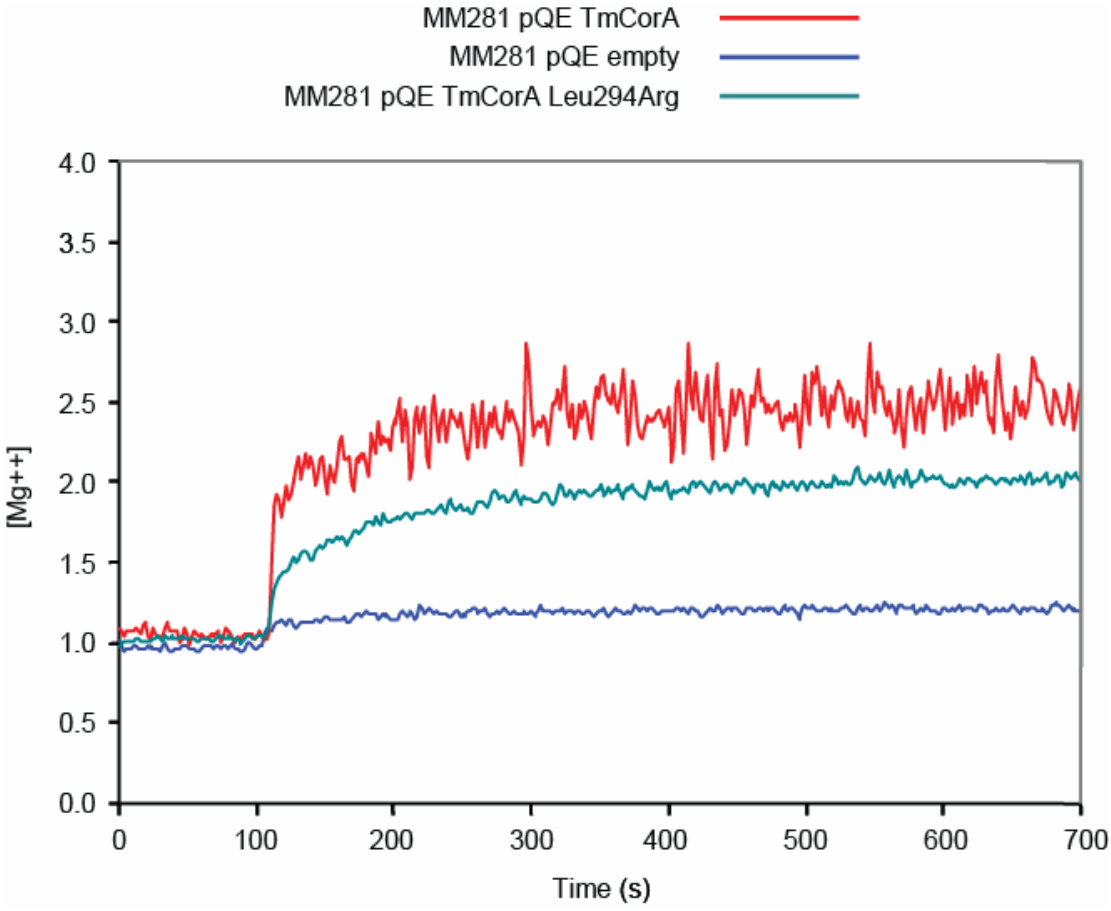

Figure 8.: Representative recordings of Mg^{2+} uptake. *S. typhimurium* strain MM281 which lacks all three known magnesium transport systems was transformed with plasmids indicated. The representative recordings show changes in fluorescence intensity of Mag-Fura-2 monitored over 10 minutes time after adding 10 mM $MgCl_2$.

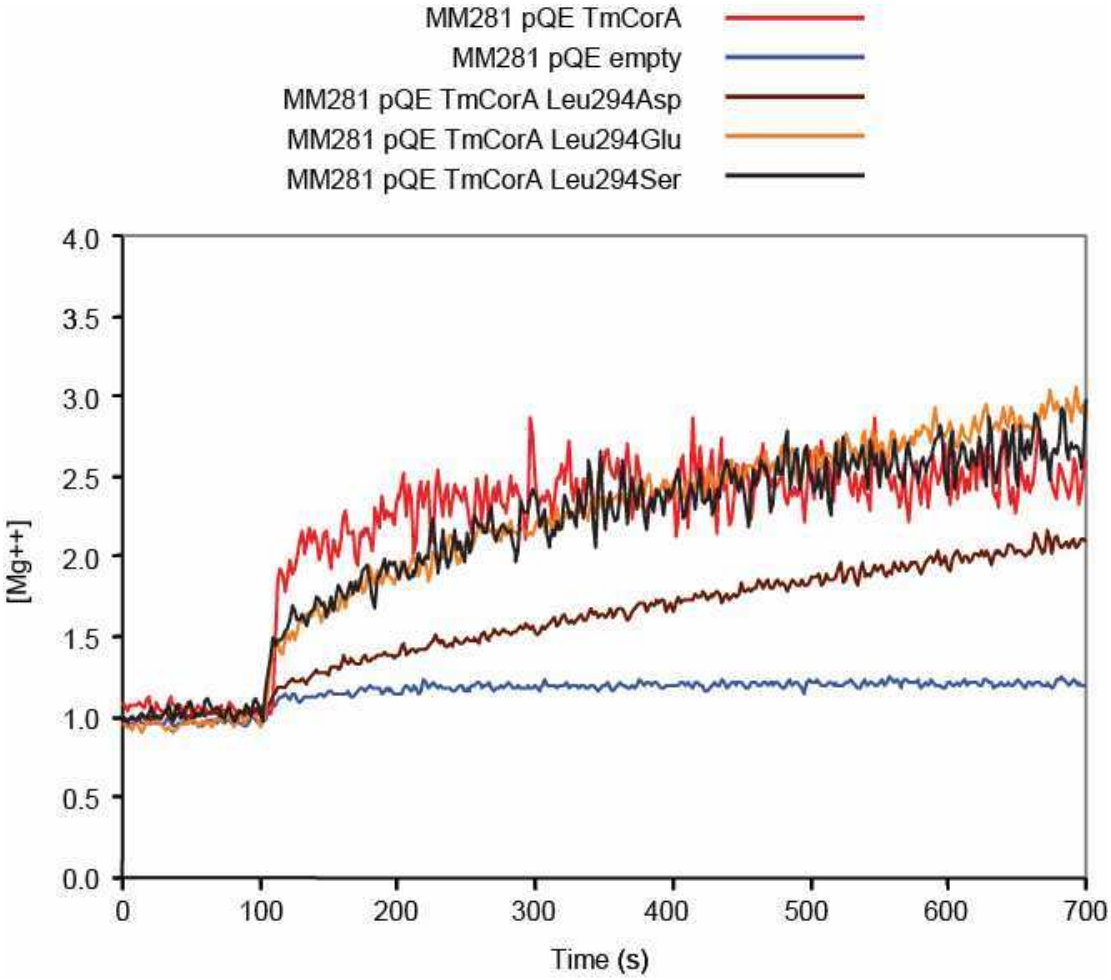

Figure 9.: Representative recordings of Mg^{2+} uptake. *S. typhimurium* strain MM281 which lacks all three known magnesium transport systems was transformed with plasmids indicated. The representative recordings show changes in fluorescence intensity of Mag-Fura-2 monitored over 10 minutes time after adding 10 mM $MgCl_2$.

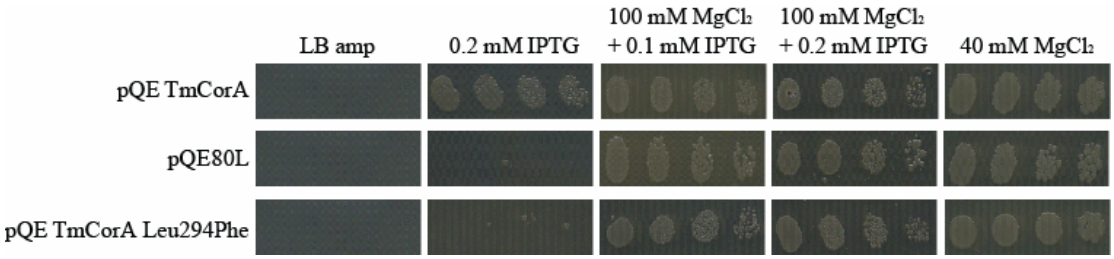

Figure 10.: Growth complementation assay of the gating mutants. *Escherichia coli* strain GS12K which lacks all three known magnesium transport systems was transformed with plasmids indicated.

4. Discussion

4.1. TmCorA

In the last years three crystal structures of *Thermotoga maritima* CorA have been published (Eshaghi, et al., 2006; Lunin, et al., 2006; Payandeh and Pai, 2006) and the mechanism of the CorA-mediated Mg^{2+} uptake has been investigated (Chakrabarti, et al., 2010; Moomaw and Maguire, 2010; Payandeh, et al., 2008; Svidova, et al., 2011). An important point of this studies is the exact gating mechanism of the TmCorA transporter, which could not been revealed before.

There are two areas considered to be the main control points in the gating mechanism of TmCorA: the ring of five aspartic acids at the pore entrance on the periplasmic side (part of the highly conserved GMN motif) (Eshaghi, et al., 2006; Lunin, et al., 2006; Payandeh and Pai, 2006) and the region known as the MM stretch – a narrow, highly hydrophobic region lying between Met291 and Met 302 (Chakrabarti, et al., 2010). Met291 and Leu294 in the narrowest part of the MM stretch are supposed to be the critical residues for Mg^{2+} gating. They create a strong energetic barrier for ion permeation and, as the pore seems to be hydrated during this process, are believed to control the movement of Mg^{2+} ions indirectly through the movement of water. According to Payandeh et al. (Payandeh, et al., 2008), not only an energetic, but also a mechanic barrier can influence the uptake of Mg^{2+} and "opening sensitivity" of the transporter.

Our mutational study was focused on Leu294 which was mutated to 8 different amino acids of different nature. The results confirmed that Leu294 is highly important for the regulation of Mg^{2+} transport. Several mutations (glycine, aspartic acid, glutamic acid, serine) caused a deregulation of Mg^{2+} transport, whereas phenylalanine mutation completely abolished the Mg^{2+} transport. These effects were caused by the charge and size of the side chains of these

amino acids, which might influence the opening/closing of the gate region by local structural distortions.

Furthermore, the lower steady-state Mg^{2+} uptake values caused by the Leu294Arg substitution indicate changes in the regulation of ion uptake. An arginine residue at position 294 might cause conformational changes not only in the hydrophobic region around this position, but also in other parts of the pore and mimic the situation, when one or both metal sensing sites are occupied. This would confirm that the gating is a complex process, involving several events which reside in distinct rearrangements of the pentamer.

4.2. ScMrs2

Unlike TmCorA, a complete crystal structure of the ScMRS2 protein has not been published yet. The only structural data existing is the structure of the N-terminal domain solved by Khan et al. (Khan, et al., submitted). Based on this structure, structure predictions and on sequence alignments between ScMrs2 and other members of the CorA/Mrs2/Alr1 protein superfamily we were able to identify certain well conserved regions, which seemed to be important for the function of the channel and we performed a series of mutational studies on them: putative Mg^{2+} sensing sites (Asp97 and Glu270), highly conserved amino acids Glu171 (named J6 in the respective study), Arg173 (J4), Glu176 (J5), Asp235 (J3), Asp244 (J2), Leu268 + Tyr272 (J9), Glu270 (J7) and Tyr272 (J8) in the N-terminal part of the protein, putative hydrophobic gate (Met309, Val315), highly conserved GMN motif (G333 + M334 + N335); negatively charged amino acids in the loop: Glu341 + Glu342 (J10, J11), putative "basic sphincter" (KRRRK), part of the so called the "arginine rich motif" (F2) and the long Mrs2 specific C-terminus.

4.2.1. Putative DCS sites

Two divalent cation binding sites were identified in TmCorA crystal structures, residing within the funnel domain (Eshaghi, et al., 2006; Lunin, et al., 2006; Payandeh and Pai, 2006). Based on structural comparison of TmCorA and the model of the Mrs248-308 funnel, Khan et al. identified amino acid residues that probably form the first divalent cation sensing site (DCS) in Mrs2: Asp97 from one subunit and Glu270 from the adjacent subunit. A sequence alignment of eukaryotic Mrs2 homologues revealed high conservation grade of this residues in the whole family of eukaryotic magnesium transporters.

Although one would expect that a mutation at one of these positions would affect the regulation of Mg^{2+} transport, after performing site-directed mutagenesis of Asp97 to alanine, phenylalanine and tryptophan, Khan et al. did not observe any growth defect of these mutants

on non-fermentable carbon sources and no significant difference between wild-type Mrs2 and the mutant proteins in Mg^{2+} uptake measurements in isolated mitochondria. As the DCS is composed of more than one proteinaceous ligand, removal of a single liganding residue (Asp97) might not abolish the capacity of Mrs2 to bind divalent ions (Khan, et al., submitted). In the study of Weghuber et al. (Weghuber, et al., 2006), several "gain of function" mutations were identified. Some of them are in the neighborhood, or are directly situated in the second part of the putative Mg^{2+} sensing site (Glu270), predicted by Khan et al. (Khan, et al., submitted). Mutations Glu270Gly (J7), Tyr272Cys (J8) and the double mutation Leu268Val and Tyr272Phe (J9) suppress the *mrs2Δ* phenotype on non-fermentable carbon source better than the wild-type Mrs2 when expressed from a low copy vector (Weghuber, et al., 2006). As no data from Mg^{2+} uptake measurements in mitochondria or growth assays with proteins expressed in high copy vector are present and the nature of used mutations is entirely different, one can not compare these results with the Asp97 mutation. Only conclusion that can be made is that the region around Glu270 seems to influence the Mrs2-mediated Mg^{2+} uptake.

4.2.2. N-terminal part of ScMrs2

Mutations of Glu171 (J6) and Glu176 (J5) to arginine resulted in "gain of function" phenotype: when expressed from a low copy vector (YCp) they showed nearly normal growth on YPdG medium (Weghuber, et al., 2006). On the other hand, another mutation in this region, Arg173Glu (J4) caused loss of complementation of the mrs2Δ phenotype when expressed from a low copy vector, but when expressed from a high copy vector (YEp), it showed a significant restoration of growth on nonfermentable YPdG medium, although not as good as the wild type Mrs2. These data are supported by the Mg^{2+} uptake measurements in isolated mitochondria, where can be clearly seen, that the Mg^{2+} uptake in this mutant is under the wild-type level, although not completely abolished (Weghuber, et al., 2006).

The change of charge, but this time from negative to positive (Asp to Lys) exhibited similar effect on positions 235 (J3) and 244 (J2) when expressed from a low copy vector. But the negative effect of the Asp244Lys (J2) mutation seemed to be more severe then in other cases, because, unlike Arg173Glu and Asp235Lys mutations, it was not able to complement the growth defect on non-fermentable substrate even when expressed from a high copy vector. Also the Mg^{2+} uptake measurements show a slow down of Mg^{2+} uptake in the Asp235Lys mutation and almost a complete loss of function in the Asp244Lys mutant (Weghuber, et al., 2006).

In the strcuture of the N-terminal regulatory domain of Mrs2 (Khan, et al., submitted), Glu171, Arg173 and Glu176 are localized in the α5 helix of Mrs2, Asp235 and Asp244 are part of the α6 helix. In the Tm-CorA structure, the long α5 and α6 helices are called 'willow' helices and harbor many glutamic and aspartic acid residues in the tip region (Lunin, et al., 2006). In contrast, the tip regions of Mrs2 α5 and α6 helices contain only 3 acidic residues (Khan, et al., submitted). Therefore we must consider the possibility, that mutations changing the charge of certain residues, especially of those, which are near to the tip of the α5 or α6 helices (in our case Asp244Lys mutation), can cause grave changes in the protein function.

4.2.3. Putative hydrophobic gate of ScMrs2

In the bacterial Mrs2 homologue, the TmCorA protein, the narrow hydrophobic constriction at the intracellular part of the membrane is considered to be one of the most important control points for ion transport. In this "hydrophobic gate" Met291 and Leu294 are supposed to be the critical residues for Mg^{2+} gating. They create a strong energetic barrier for ion permeation and probably control the movement of Mg^{2+} ions indirectly through the movement of water (Lunin, et al., 2006; Payandeh, et al., 2008). The mutational analysis of the Leu294 residue of TmCorA produced mutants with completely deregulated ion transport and clearly showed the

importance of this position for the gating process (Svidova, et al., 2011), (Svidova, unpublished results).

By superposition of the monomeric Mrs2 structure on the funnel domain of TmCorA and VpZntB and generating a model for the pentameric form of Mr2p, Khan et al. (Khan, et al., submitted) identified two potential candidates for the hydrophobic gate of Mrs2: Met309 and Val315. Met309 is highly conserved and forms the narrowest constriction in the pore of Mrs2p. Val315 forms the second narrowest constriction and it appears to be less conserved. Each of these residues was mutated to small glycine, negatively charged glutamic acid and bulky phenylalanine.

In case of Met309, all mutants exhibited growth reduction on non-fermentable media compared to cells expressing wild-type *MRS*. Results of the Mg^{2+} uptake measurements in isolated mitochondria showed changed Mg^{2+} influx in all three mutants. Met309Gly and Met309Glu mutants exhibited higher Mg^{2+} uptake then the wild-type Mrs2, especially the Met309Gly mutant, where the uptake also seemed to by deregulated (Khan, et al., submitted). Nevertheless, closing of the ion conduction pathway was never completely deregulated as we observed for the Leu294Gly and Leu294Glu mutations in TmCorA (Svidova, et al., 2011). In the case of the Met309Phe mutation we observed a decrease of the Mg^{2+} uptake into mitochondria, but again, this effect was quite different from the Leu294Phe mutation in TmCorA, which abolished the Mg^{2+} uptake completely (Svidova, unpublished results). Phenylalanine at position 309 could narrow the pore diameter and thereby reduce Mg^{2+} influx, but its bulky side chain apparently does not block the pore completely, which could suggest, that the diameter of the Mrs2 pore at this position might be wider than that of TmCorA at position 294.

In case of Val315, all three amino acid substitutions (glycine, glutamic acid and phenylalanine) were relatively well tolerated. Introduction of small glycine had again the strongest effect in growth tests on non fermentable substrate, but led only to a moderate

increase of Mg^{2+} uptake into mitochondria, whereas the uptake of other to mutants was on the same level as that of the wild-type Mrs2 (Khan, et al., submitted). These results are in line with the observed lower sequence conservation of the Val315 in the Mrs2 protein family.

Although the Met309 seems to have an influence on the gating of the Mrs2 pore, it is apparently not the only control point. As there was no other potential candidate for the hydrophobic gate of Mrs2 channel, we must conclude, that the gating mechanism of Mrs2 is more complex process then the gating of the TmCorA.

4.2.4. The G-M-N motif

The highly conserved G-M-N motif has been shown to be critical for the function of CorA and even conservative single point mutations completely abolished Mg^{2+} transport (Payandeh, et al., 2008; Szegedy and Maguire, 1999). This was also confirmed for Mrs2p where a single conservative mutation in the G-M-N motif (Gly333Ala) was introduced (Kolisek, et al., 2003). This suggests this sequence being indispensable for the function of the channel, possibly by suitably positioning the periplasmic loop implicated in initial binding of the hydrated Mg^{2+} (Lunin, et al., 2006) and in assisting in the dehydration process (Moomaw and Maguire, 2010). Regarding these facts, the necessity of the G-M-N motif was considered rather definite. Nevertheless, our mutational study comprising the whole motif at once showed that there are certain combinations of amino acids, which are still able to mediate Mg^{2+} transport, although at a considerably lower level (Svidova, et al., in revision).

In this study we took advantage of the fact that ScMrs2 is able to complement the Mg^{2+}-dependent growth defect of *S. typhimurium* strain MM281, deficient for all major bacterial Mg^{2+} transport systems (CorA, MgtA and MgtB). We performed random mutagenesis of all three amino acids and screened for mutants still able to transport Mg^{2+}.

Our study identified viable triple mutants hosting a positively charged residue primarily on the first but also on the third position. At a first glance, the presence of positively charged

residues in functional mutants might seem counterproductive, as these mutations could in fact hinder the transport of Mg^{2+} ions by electrostatic repulsion. However, since it is structurally impossible for all three amino acid residues of the motif to be in direct contact with the ion (Payandeh, et al., 2008), we can assume that these residues form a structural motif critical for ion uptake, which can be partially accomplished by different amino acid combinations, eventually leading to a functionally equivalent structure.

In order to investigate the effect of the mutations on the ion selectivity of the Mrs2 channel, we performed growth complementation assays on plates supplemented with different divalent cations (Ca^{2+}, Co^{2+}, Mn^{2+} and Zn^{2+}). The results showed that mutations in the G-M-N motif lead to reduced growth of the cells in presence of Mn^{2+} and Zn^{2+} while Ca^{2+} and Co^{2+} did not influence their viability. This can be explained in two possible ways: (i) Mn^{2+} and Zn^{2+} are transported through the pore and the growth defect is caused by Mn^{2+}/Zn^{2+} overdose, or (ii) Mn^{2+} and Zn^{2+} ions are trapped and block the channel for Mg^{2+} transport causing in this way the growth defect by Mg^{2+} deficiency.

These results clearly show that the G-M-N motif can be functionally replaced by certain combinations of amino acid residues. Our study also suggests that the G-M-N motif plays a role in ion selectivity, being therefore part of the selectivity filter together with the flanking negatively charged loop, at the entrance of the Mrs2 channel. The involvement of the G-M-N motif in the gating process and in ion selectivity as well, might be the molecular basis for its universal conservation in the CorA/Mrs2/Alr1 protein family.

4.2.5. The loop connecting trans-membrane helices in ScMrs2

As mentioned above, there is a short conformationally flexible loop of about 7–8 amino acids between the two trans-membrane helices. This is supposed to be the only part of the protein located in the inter-membrane space of yeast mitochondria (Baumann, et al., 2002; Bui, et al., 1999) and is possibly implicated in initial binding of the hydrated Mg^{2+} (Lunin, et al., 2006)

and in assisting in the dehydration process (Moomaw and Maguire, 2010). The sequence contains a cluster of negatively charged amino acids. Many members of the Mrs2 protein family (ScMrs2, HsMrs2 and AtMrs2–11) have two glutamic acid residues at position +5 and +6 relative to the G-M-N motif. Weghuber et al. (Weghuber, et al., 2006) designed two mutations at this position: Glu341Asp + Glu342Asp (J10) and Glu341Lys + Glu342Lys (J11). In growth assays on non-fermentable substrate expression of J10 fully complemented the *mrs2Δ* growth defect when expressed either from a low-copy or from a high-copy vector, but expression of J11 did not significantly complement the *mrs2Δ* phenotype when expressed from a low-copy plasmid, and when overexpressed, it restored growth only weakly. Mg^{2+} uptake measurements in isolated mitochondria confirmed these results: the change from negatively charged glutamic acids to negatively charged aspartic acids (J10) caused no difference in Mg^{2+} uptake compared to the wild-type Mrs2, whereas the change from negatively charged glutamic acids to positively charged lysines (J11) abolished the Mg^{2+} uptake almost completely (Weghuber, et al., 2006).

The loop in TmCorA appears to form the initial interaction site for hydrated Mg^{2+} ion and likely participates in the dehydration process of the ion required prior to its entrance into the channel (Moomaw and Maguire, 2010). The high conductance of Mrs2 (Schindl, et al., 2007) and TmCorA (Moomaw and Maguire, 2010) channels were proposed to be based on a mechanism which involves electrostatic interactions of the loop residues with the hydration shell of Mg^{2+} and not with the ion itself (Moomaw and Maguire, 2010). For this reason, the change of charges in the loop region can lead to abolishment of the Mg^{2+} current through the channel.

4.2.6. The long C-terminus of ScMrs2

The Mrs2 homologue Tm-CorA has a highly conserved, positively charged sequence at the C-terminus, close to the end of the second trans-membrane domain, known as the “basic sphincter”. It lies at the level of the hydrophobic gate of the pore and, in combination with the

hydrophobic constrictions formed by Leu294 and Met291, appears to be the major barrier for Mg^{2+} transport (Eshaghi, et al., 2006; Lunin, et al., 2006; Payandeh and Pai, 2006).

In contrast, ScMrs2 has a very long C-terminus, quite unique in the CorA/Mrs2/Alr1 protein family. In the C-terminal part, a sequence of positively charged amino acids can be found, but, unlike CorA, it lies about ~ 40 amino acids away from the end of the second trans-membrane helix. This region contains a surplus of arginine residues and is known as the "arginine rich motif" (ARM) (Weghuber, et al., 2006).

To investigate the importance of this motif, Weghuber et al. (Weghuber, et al., 2006) deleted a sequence of 14 amino acids: K_{400}LKRRRKWWKSTKQR$_{414}$. But this dramatic change in the amino acid sequence did not have a significant effect on the protein function: the only result was weaker Mg^{2+} influx upon low copy expression. When expressed from a high copy plasmid, the mutant exhibited no growth defect on non-fermentable carbon sources and the Mg^{2+} influx into isolated mitochondria was comparable to that of wild-type Mrs2 (Weghuber, et al., 2006).

Khan et al. used a different approach to investigate the possible role of the ARM motif for Mg^{2+} transport. They reversed the charge of the KRRRK part of the positively charged region to five glutamic acids. The resulting mutant exhibited good growth on non-fermentable media when expressed either from a low copy or from a high copy plasmid and the Mg^{2+} uptake into isolated mitochondria was moderately increased (Khan, et al., submitted).

The conclusion that might be deduced from this results is, that the positively charged ARM motif does not play a significant role in the Mrs2 mediated Mg^{2+} uptake. The weaker Mg^{2+} influx observed by Weghuber et al. (Weghuber, et al., 2006) might be more the result of structural changes caused by the deletion of 14 amino acids, than of the missing positive charge in this region and reversed of the charge done by Khan et al. (Khan, et al., submitted) showed only moderate enhancement of activity of the channel, without signs of deregulation. This higher activity might be caused by the formation of a ring of negative charges

surrounding the ion conduction pathway and stronger attraction of the positively charged Mg^{2+} ion.

In order to further investigate the function of the long C-terminus, Khan et al. (Khan, et al., submitted) prepared a truncated version of the Mrs2 protein by deleting all amino acids after residue Thr376 (deletion of 94 residues). This mutant exhibited a growth defect on non-fermentable carbon sources, comparable to the *mrs2Δ* phenotype and also strong reduction of Mg^{2+} uptake into isolated mitochondria (Khan, et al., submitted). This effect is not caused by the instability of the truncated protein, as the protein levels were even slightly higher than in a wild-type situation. As the whole C-terminus has a 26% of positively charged residues, the whole C-terminal sequence might act as an analogue of the "basic sphincter" of TmCorA and therefore influence the regulation of the Mg^{2+} transport. There is also the possibility of a direct involvement in the structural changes which take place during opening and closing of the channel.

4.3. AtMrs2

The MRS2/MGT gene family in *Arabidopsis thaliana* belongs to the CorA/Mrs2/Alr1 superfamily of proteins. They share certain similarities, like the two trans-membrane domains and the highly conserved G-M-N motif at the end of the first one. In *Arabidopsis thaliana* a gene family of 10 members has been identified and named AtMRS2 (Schock, et al., 2000) or alternatively AtMGT (Li, et al., 2001).

Gebert et al. (Gebert, et al., 2009) showed that all members of the Arabidopsis family can complement the yeast *mrs2Δ* phenotype. On non-fermentable carbon source, AtMrs2-6 reconstituted growth to the highest level among the AtMrs2 proteins, but still less efficient than ScMrs2. In Mg^{2+} uptake measurements in isolated mitochondria, all AtMrs2 proteins were able to mediate ion influx, confirming their role as magnesium transporters. The highest efficiency was observed for AtMrs2-1, AtMrs2-7 and AtMrs2-10, although none of them acted as well as the wild-type ScMrs2. For AtMrs2-3 a discrepancy was observed: it complemented well on non-fermentable media, but in the Mag-Fura-2 measurements it showed only weak Mg^{2+} uptake. A plausible explanation is that AtMrs2-3 is a slow Mg^{2+} transporter, which is able to transport enough Mg^{2+} over several hours or days, but not during the 300 second of Mg^{2+} uptake measurements (Gebert, et al., 2009).

4.4. ScLpe10

The ScLpe10 is a homologue of the ScMrs2 protein with 32% sequence identity. Both are located in the inner mitochondrial membrane and involved in the Mg^{2+} uptake into mitochondria. But, in contrast to Mrs2, the function of Lpe10 is not clear yet (Gregan, et al., 2001).

Deletion of MRS2, LPE10 or both causes a growth defect on non-fermentable media and a loss of the Mrs2-mediated rapid Mg^{2+} influx into mitochondria (Gregan, et al., 2001; Wiesenberger, et al., 1992). In an *lpe10Δ* mutant, Mrs2 can only partly complement the growth defect, whereas the expression of Lpe10 in an *mrs2Δ* background could not complement the growth defect at all. In an *mrs2Δ/lpe10Δ* double mutant, the growth defect was partly complemented only by Mrs2 expressed from a high copy plasmid and only the co-expression of Mrs2 from a high copy plasmid and Lpe10 from a low copy plasmid led to full complementation, whereas the expression of both proteins from high copy plasmids led only to a weak complementation. These results indicate that Mg^{2+} homeostasis in yeast mitochondria could be dependent on the relative expression levels of Mrs2 and Lpe10 (Sponder, et al., 2010).

Sponder et al. showed that the deletion of Lpe10 leads to the loss of Mg^{2+} influx into isolated mitochondria and loss of mitochondrial membrane potential, which is the driving force for Mg^{2+} uptake. This phenotype can be restored by adding nigericin (a K^+/H^+ exchanger) (Sponder, et al., 2010).

Like Mrs2, Lpe10 also contains the highly conserved Y/F-G-M-N motif at the end of the first trans-membrane domain. As mentioned above, it has been proposed, that even conservative mutations in this motif lead to a complete abolishment of the function (Kolisek, et al., 2003; Szegedy and Maguire, 1999). In the case of Lpe10, the Y/F-G-M-N motif was changed to A-S-S-V. As a result, the cells exhibited reduced growth non-fermentable media and almost

completely abolished Mg^{2+} uptake into isolated mitochondria, but the mutation had only a minor impact on the membrane potential (Sponder, et al., 2010), which means, that although the Y/F-G-M-N motif is important for Mg^{2+} transport, it is only of minor importance for maintenance of the membrane potential.

Mutational analysis and analysis of Mrs2-Lpe10 and Lpe10-Mrs2 fusion proteins suggest that the Mg^{2+} transport and the maintenance of the membrane potential are functionally separated. The fusion site lied between the α6 and α7 helix. Both fusion proteins restored the growth of *mrs2Δ* and *lpe10Δ* mutants only weakly, but slightly better complementation was detected by the Lpe10-Mrs2 protein, which contained the pore of Mrs2, and neither of the proteins could restore the growth defect of the *mrs2Δ/lpe10Δ* double deletion strain. Furthermore Lpe10p-Mrs2 restored the membrane potential to 80% of the wild-type level, whereas the Mrs2p-Lpe10 increased it only weakly. These results suggest that the N-terminal part of Lpe10 might be associated with maintenance of the membrane potential. This was confirmed by Mg^{2+} uptake measurements in isolated mitochondria, where the Lpe10-Mrs2 fusion protein in the *lpe10Δ* background restored the Mg^{2+} almost completely (Sponder, et al., 2010).

Crosslinking and Blue native PAGE experiments indicate an interaction between Lpe10 and Mrs2 proteins. Using the patch clamp technique, Sponder et al. showed that Lpe10 was not able to mediate Mg^{2+} influx into mitochondrial inner membrane vesicles without the presence of Mrs2 and co-expression of both proteins provided reduced conductance compared to that of Mrs2-formed channels (Sponder, et al., 2010).

On the basis of these results, we assume that Lpe10p has the potential to interact with the Mrs2p-based Mg^{2+} channel and to modulate its activity, thereby influencing the mitochondrial membrane potential.

5. References

Baumann, F., Neupert, W. and Herrmann, J. M. (2002). Insertion of bitopic membrane proteins into the inner membrane of mitochondria involves an export step from the matrix. *J Biol Chem* **277,** 21405-13.

Beeler, T., Bruce, K. and Dunn, T. (1997). Regulation of cellular Mg2+ by Saccharomyces cerevisiae. *Biochim Biophys Acta* **1323,** 310-8.

Beeler, T., Gable, K., Zhao, C. and Dunn, T. (1994). A novel protein, CSG2p, is required for Ca2+ regulation in Saccharomyces cerevisiae. *J Biol Chem* **269,** 7279-84.

Bui, D. M., Gregan, J., Jarosch, E., Ragnini, A. and Schweyen, R. J. (1999). The bacterial magnesium transporter CorA can functionally substitute for its putative homologue Mrs2p in the yeast inner mitochondrial membrane. *J Biol Chem* **274,** 20438-43.

Dai, L. J., Ritchie, G., Kerstan, D., Kang, H. S., Cole, D. E. and Quamme, G. A. (2001). Magnesium transport in the renal distal convoluted tubule. *Physiol Rev* **81,** 51-84.

Doyle, D. A., Morais Cabral, J., Pfuetzner, R. A., Kuo, A., Gulbis, J. M., Cohen, S. L., Chait, B. T. and MacKinnon, R. (1998). The structure of the potassium channel: molecular basis of K+ conduction and selectivity. *Science* **280,** 69-77.

Eshaghi, S., Niegowski, D., Kohl, A., Martinez Molina, D., Lesley, S. A. and Nordlund, P. (2006). Crystal structure of a divalent metal ion transporter CorA at 2.9 angstrom resolution. *Science* **313,** 354-7.

Froschauer, E. M., Kolisek, M., Dieterich, F., Schweigel, M. and Schweyen, R. J. (2004). Fluorescence measurements of free [Mg^{2+}] by use of mag-fura 2 in Salmonella enterica. *FEMS Microbiol Lett* **237,** 49-55.

Gardner, R. C. (2003). Genes for magnesium transport. *Curr Opin Plant Biol* **6,** 263-7.

Gebert, M., Meschenmoser, K., Svidova, S., Weghuber, J., Schweyen, R., Eifler, K., Lenz, H., Weyand, K. and Knoop, V. (2009). A root-expressed magnesium transporter of the MRS2/MGT gene family in Arabidopsis thaliana allows for growth in low-Mg^{2+} environments. *Plant Cell* **21,** 4018-30.

Gibson, M. M., Bagga, D. A., Miller, C. G. and Maguire, M. E. (1991). Magnesium transport in Salmonella typhimurium: the influence of new mutations conferring Co2+ resistance on the CorA Mg^{2+} transport system. *Mol Microbiol* **5,** 2753-62.

Graschopf, A., Stadler, J. A., Hoellerer, M. K., Eder, S., Sieghardt, M., Kohlwein, S. D. and Schweyen, R. J. (2001). The yeast plasma membrane protein Alr1 controls Mg^{2+}

homeostasis and is subject to Mg^{2+}-dependent control of its synthesis and degradation. *J Biol Chem* **276,** 16216-22.

Gregan, J., Bui, D. M., Pillich, R., Fink, M., Zsurka, G. and Schweyen, R. J. (2001a). The mitochondrial inner membrane protein Lpe10p, a homologue of Mrs2p, is essential for magnesium homeostasis and group II intron splicing in yeast. *Mol Gen Genet* **264,** 773-81.

Gregan, J., Kolisek, M. and Schweyen, R. J. (2001b). Mitochondrial $Mg^{(2+)}$ homeostasis is critical for group II intron splicing in vivo. *Genes Dev* **15,** 2229-37.

Grubbs, R. D., Snavely, M. D., Hmiel, S. P. and Maguire, M. E. (1989). Magnesium transport in eukaryotic and prokaryotic cells using magnesium-28 ion. *Methods Enzymol* **173,** 546-63.

Gunther, T. (1993). Mechanisms and regulation of Mg^{2+} efflux and Mg^{2+} influx. *Miner Electrolyte Metab* **19,** 259-65.

Hmiel, S. P., Snavely, M. D., Miller, C. G. and Maguire, M. E. (1986). Magnesium transport in Salmonella typhimurium: characterization of magnesium influx and cloning of a transport gene. *J Bacteriol* **168,** 1444-50.

Huang, H. W., Li, D. and Cowan, J. A. (1995). Biostructural chemistry of magnesium. regulation of mithramycin-DNA interactions by Mg^{2+} coordination. *Biochimie* **77,** 729-38.

Chakrabarti, N., Neale, C., Payandeh, J., Pai, E. F. and Pomes, R. (2010). An iris-like mechanism of pore dilation in the CorA magnesium transport system. *Biophys J* **98,** 784-92.

Kehres, D. G., Lawyer, C. H. and Maguire, M. E. (1998). The CorA magnesium transporter gene family. *Microb Comp Genomics* **3,** 151-69.

Khan, M. B., Sponder, G., Sjoeblo, B., Svidova, S., Carugo, O., Schweyen, R. J. and Djinovic-Carugo, K. (submitted). Structural and functionla characterization of the N-terminal domain of Mrs2 - the Mg^{2+} transporter of the yeast inner mitochondrial membrane. *The Journal of Biological Chemistry*.

Knoop, V., Groth-Malonek, M., Gebert, M., Eifler, K. and Weyand, K. (2005). Transport of magnesium and other divalent cations: evolution of the 2-TM-GxN proteins in the MIT superfamily. *Mol Genet Genomics* **274,** 205-16.

Kolisek, M., Zsurka, G., Samaj, J., Weghuber, J., Schweyen, R. J. and Schweigel, M. (2003). Mrs2p is an essential component of the major electrophoretic Mg^{2+} influx system in mitochondria. *Embo J* **22,** 1235-44.

Koll, H., Schmidt, C., Wiesenberger, G. and Schmelzer, C. (1987). Three nuclear genes suppress a yeast mitochondrial splice defect when present in high copy number. *Curr Genet* **12,** 503-9.

Kucharski, L. M., Lubbe, W. J. and Maguire, M. E. (2000). Cation hexaammines are selective and potent inhibitors of the CorA magnesium transport system. *J Biol Chem* **275,** 16767-73.

Li, L., Tutone, A. F., Drummond, R. S., Gardner, R. C. and Luan, S. (2001). A novel family of magnesium transport genes in Arabidopsis. *Plant Cell* **13,** 2761-75.

Lunin, V. V., Dobrovetsky, E., Khutoreskaya, G., Zhang, R., Joachimiak, A., Doyle, D. A., Bochkarev, A., Maguire, M. E., Edwards, A. M. and Koth, C. M. (2006). Crystal structure of the CorA Mg^{2+} transporter. *Nature* **440,** 833-7.

Maguire, M. E. (2006). Magnesium transporters: properties, regulation and structure. *Front Biosci* **11,** 3149-63.

Maguire, M. E. and Cowan, J. A. (2002). Magnesium chemistry and biochemistry. *Biometals* **15,** 203-10.

Moomaw, A. S. and Maguire, M. E. Cation selectivity by the CorA Mg^{2+} channel requires a fully hydrated cation. *Biochemistry* **49,** 5998-6008.

Moomaw, A. S. and Maguire, M. E. (2010). Cation selectivity by the CorA Mg^{2+} channel requires a fully hydrated cation. *Biochemistry* **49,** 5998-6008.

Nowikovsky, K., Reipert, S., Devenish, R. J. and Schweyen, R. J. (2007). Mdm38 protein depletion causes loss of mitochondrial K^+/H^+ exchange activity, osmotic swelling and mitophagy. *Cell Death Differ* **14,** 1647-56.

Ostersetzer, O., Cooke, A. M., Watkins, K. P. and Barkan, A. (2005). CRS1, a chloroplast group II intron splicing factor, promotes intron folding through specific interactions with two intron domains. *Plant Cell* **17,** 241-55.

Payandeh, J., Li, C., Ramjeesingh, M., Poduch, E., Bear, C. E. and Pai, E. F. (2008). Probing structure-function relationships and gating mechanisms in the CorA Mg^{2+} transport system. *J Biol Chem* **283,** 11721-33.

Payandeh, J. and Pai, E. F. (2006). A structural basis for Mg^{2+} homeostasis and the CorA translocation cycle. *EMBO J* **25,** 3762-73.

Romani, A. (2007). Regulation of magnesium homeostasis and transport in mammalian cells. *Arch Biochem Biophys* **458,** 90-102.

Romani, A. and Scarpa, A. (1992). Regulation of cell magnesium. *Arch Biochem Biophys* **298,** 1-12.

Romani, A. M. and Scarpa, A. (2000). Regulation of cellular magnesium. *Front Biosci* **5,** D720-34.

Schindl, R., Weghuber, J., Romanin, C. and Schweyen, R. J. (2007). Mrs2p forms a high conductance Mg^{2+} selective channel in mitochondria. *Biophys J* **93,** 3872-83.

Schlingmann, K. P. and Gudermann, T. (2005). A critical role of TRPM channel-kinase for human magnesium transport. *J Physiol* **566,** 301-8.

Schmitz, C., Perraud, A. L., Johnson, C. O., Inabe, K., Smith, M. K., Penner, R., Kurosaki, T., Fleig, A. and Scharenberg, A. M. (2003). Regulation of vertebrate cellular Mg2+ homeostasis by TRPM7. *Cell* **114,** 191-200.

Schock, I., Gregan, J., Steinhauser, S., Schweyen, R., Brennicke, A. and Knoop, V. (2000). A member of a novel Arabidopsis thaliana gene family of candidate Mg^{2+} ion transporters complements a yeast mitochondrial group II intron-splicing mutant. *Plant J* **24,** 489-501.

Smith, R. L., Banks, J. L., Snavely, M. D. and Maguire, M. E. (1993). Sequence and topology of the CorA magnesium transport systems of Salmonella typhimurium and Escherichia coli. Identification of a new class of transport protein. *J Biol Chem* **268,** 14071-80.

Smith, R. L. and Maguire, M. E. (1998). Microbial magnesium transport: unusual transporters searching for identity. *Mol Microbiol* **28,** 217-26.

Snavely, M. D., Florer, J. B., Miller, C. G. and Maguire, M. E. (1989). Magnesium transport in Salmonella typhimurium: $28Mg^{2+}$ transport by the CorA, MgtA, and MgtB systems. *J Bacteriol* **171,** 4761-6.

Sperrazza, J. M. and Spremulli, L. L. (1983). Quantitation of cation binding to wheat germ ribosomes: influences on subunit association equilibria and ribosome activity. *Nucleic Acids Res* **11,** 2665-79.

Sponder, G., Svidova, S., Schindl, R., Wieser, S., Schweyen, R. J., Romanin, C., Froschauer, E. M. and Weghuber, J. (2010). Lpe10p modulates the activity of the Mrs2p-based yeast mitochondrial Mg^{2+} channel. *Febs J* **277,** 3514-25.

Sternberg, P. W., Lesa, G., Lee, J., Katz, W. S., Yoon, C., Clandinin, T. R., Huang, L. S., Chamberlin, H. M. and Jongeward, G. (1995). LET-23-mediated signal transduction during Caenorhabditis elegans development. *Mol Reprod Dev* **42,** 523-8.

Svidova, S. (unpublished results).

Svidova, S., Sponder, G., Khan, M. B., Schweyen, R. J., Carugo, O. and Djinovic-Carugo, K. (in revision). Effect of mutations in the conserved GMN motif on ion transport and selectivity in the yeast magnesium transporter Mrs2p

Biochim Biophys Acta.

Svidova, S., Sponder, G., Schweyen, R. J. and Djinovic-Carugo, K. (2011). Functional analysis of the conserved hydrophobic gate region of the magnesium transporter CorA. *Biochim Biophys Acta* **1808,** 1587-91.

Szegedy, M. A. and Maguire, M. E. (1999). The CorA $Mg^{(2+)}$ transport protein of Salmonella typhimurium. Mutagenesis of conserved residues in the second membrane domain. *J Biol Chem* **274,** 36973-9.

Touyz, R. M. (2006). Magnesium and hypertension. *Curr Opin Nephrol Hypertens* **15,** 141-4.

Wachek, M., Aichinger, M. C., Stadler, J. A., Schweyen, R. J. and Graschopf, A. (2006). Oligomerization of the Mg^{2+}-transport proteins Alr1p and Alr2p in yeast plasma membrane. *Febs J* **273,** 4236-49.

Warren, M. A., Kucharski, L. M., Veenstra, A., Shi, L., Grulich, P. F. and Maguire, M. E. (2004). The CorA Mg^{2+} transporter is a homotetramer. *J Bacteriol* **186,** 4605-12.

Webb, M. (1966). The utilization of magnesium by certain Gram-positive and Gram-negative bacteria. *J Gen Microbiol* **43,** 401-9.

Weghuber, J., Dieterich, F., Froschauer, E. M., Svidova, S. and Schweyen, R. J. (2006). Mutational analysis of functional domains in Mrs2p, the mitochondrial Mg^{2+} channel protein of Saccharomyces cerevisiae. *Febs J* **273,** 1198-209.

Whelton, P. K. and Klag, M. J. (1989). Magnesium and blood pressure: review of the epidemiologic and clinical trial experience. *Am J Cardiol* **63,** 26G-30G.

Wiesenberger, G., Waldherr, M. and Schweyen, R. J. (1992). The nuclear gene MRS2 is essential for the excision of group II introns from yeast mitochondrial transcripts in vivo. *J Biol Chem* **267,** 6963-9.

Acknowledgements

First of all I would like to thank Professor Rudolf Schweyen, who gave me the chance to work in his lab and thereby changed my whole life and also my attitude to science.
I would also like to thank Professor Kristina Djinović-Carugo, who took over my supervision after Rudolf′s death and did everything possible (and sometimes almost impossible) to help me finish my experiments, publish my results and finally write this thesis.
I am very thankful to all my colleagues and friends from the Schweyen group for their help, advises and the great atmosphere in the lab. Special thank goes to Julian Weghuber, who guided me through the first months of my lab work, to Lisi Froschauer-Neuhauser, my first and best friend in Vienna, who was always ready to help me and give me a good advise (and not just about yeast mitochondria) and to Gerhard Sponder for excellent cooperation, interesting discussions and good nerves by helping me to solve my countless problems.
I am also grateful to Oliviero Carugo and Muhammad Bashir Khan from the Djinović-Carugo group for their considerable help and fruitful discussions and to Professor Christoph Romanin and Rainer Schindl (University of Linz) for the valuable cooperation.

Curriculum vitae

Name:	Soňa Svidová
Date of birth:	10th February, 1980
Place of birth:	Bratislava, Slovakia
Nationality:	Slovak
Maritual status:	single
Private address:	Keplergasse 9/1/24 1100Wien Austria
Phone number:	+43 (0) 681 10861083
Email:	sona.svidova@univie.ac.at

Education

1986 – 1994	Basic School, study direction: German language; Rajčianska 3, 821 07 Bratislava, Slovak Republic
1994 – 1998	Ivan Horváth High School, study direction: German language; ul. Ivana Horvátha 14, 821 03 Bratislava, Slovak Republic
1998 – 2003	Studies at the Comenius University, Faculty of Natural Sciences, in Bratislava, study direction: **Biology /Genetics**; Mlynska dolina 1, Bratislava, Slovakia
23. Mai 2003	Diploma thesis Title: **Potential antimutagenic effects of glucomannan.** State exam: Genetics Molecular biology Molecular biology and Genetics of Microorganisms
October 2003 – September 2005	PhD thesis at the Comenius University, Faculty of Natural Sciences, in Bratislava study direction: **Biology/Genetics**; Mlynska dolina 1, Bratislava, Slovakia
September 2005 - June 2011	PhD thesis in the lab of **Prof. Dr. Rudolf J. Schweyen** Thesis**: Functional Analysis of Conserved Motifs in Two Mg^{2+} Transporting Channels: ScMrs2p and TmCorA**

study direction: Genetics;
Department of Microbiology, Immunobiology and Genetics,
Max F. Perutz Laboratories,
University of Vienna,
Dr. Bohrgasse 9, 1030 Vienna, Austria

After the death of **Prof. Dr. Rudolf J. Schweyen** (February 2009) PhD supervision was taken over by **Prof. Dr. Kristina Djinovic – Carugo**
Department for Structural and Computational Biology,
Max F. Perutz Laboratories,
University of Vienna,
Dr. Bohrgasse 9, 1030 Vienna, Austria
kristina.djinovic@univie.ac.at

Language skills

Slovak	native language
English	fluently
German	fluently

Publications

- Muhammad Bashir Khan, Gerhard Sponder, Björn Sjöblom, **Soňa Svidová**, Rudolf J. Schweyen, Oliviero Carugo, and Kristina Djinović-Carugo
  Structural and Functional Characterization of the N-Terminal Moiety of Yeast Mg^{2+} Transporter Mrs2
  JBC - submitted

- **Svidová S**., Sponder G., Khan M.B., Schweyen R.J., Carugo O., Djinović-Carugo K.
  Effect of mutations in the conserved GMN motif on ion transport and selectivity in the yeast magnesium transporter Mrs2p
  Biochim Biophys Acta – in revision

- **Svidová S**, Sponder G, Schweyen R J, Djinović-Carugo K.
  Functional analysis in the conserved hydrophobic gate region of the magnesium transporter CorA.
  Biochim Biophys Acta. 2011 Jun;1808(6):1587-91. Epub 2010 Nov 11.

- Sponder G, **Svidova S**, Schweigel M, Vormann J, Kolisek M
  Splice-variant 1 of the ancient domain protein 2 (ACDP2) complements the magnesium-deficient growth phenotype of Salmonella enterica sv. typhimurium strain MM281.
  Magnes Res. 2010 Jun;23(2):105-14. Epub 2010 Jun 2.

- Sponder G, **Svidova S**, Schindl R, Wieser S, Schweyen R, Romanin C, Froschauer E, Weghuber J.
  Lpe10p modulates the activity of the Mrs2-based yeast mitochondrial Mg^{2+}-channel
  FEBS J. 2010 Sep;277(17):3514-25. Epub 2010 Jul 23.

- Gebert M, Meschenmoser K, **Svidová S**, Weghuber J, Schweyen R, Eifler K, Lenz H, Weyand K, Knoop V.
  A root-expressed magnesium transporter of the MRS2/MGT gene family in Arabidopsis thaliana allows for growth in low-Mg2+ environments.
  Plant Cell. 2009 Dec;21(12):4018-30. Epub 2009 Dec 4.

- Weghuber J, Dieterich F, Froschauer EM, **Svidova S**, Schweyen RJ.
  Mutational analysis of functional domains in Mrs2p, the mitochondrial Mg2+ channel protein of Saccharomyces cerevisiae.
  FEBS J. 2006 Mar;273(6):1198-209.

- Miadokova E, **Svidova S**, Vlckova V, Duhova V, Nad'ova S, Rauko P, Kogan G.
  Diverse biomodulatory effects of glucomannan from Candida utilis.
  Toxicol In Vitro. 2006 Aug;20(5):649-57. Epub 2006 Jan 18.

- Miadokova E, **Svidova S**, Vlckova V, Duhova V, Prazmariova E, Tothova K, Nad'ova S, Kogan G, Rauko P.
  The role of natural biopolymers in genotoxicity of mutagens/carcinogens elimination.
  Biomed Pap Med Fac Univ Palacky Olomouc Czech Repub. 2005 Dec;149(2):493-6.

- Trebatická, M., **Svidová, S.**, Grolmus, J., Rauko, P., Kogan, G., Miadoková, E.
  Sulphoethyl glucan – a biological active polysacharide.
  Biologi*a* (2005) 60: Suppl. 17: 121-123.

- Vlckova V, Duhova V**, Svidova S**, Farkassova A, Kamasova S, Vlcek D, Kogan G, Rauko P, Miadokova E.
  Antigenotoxic potential of glucomannan on four model test systems.
  Cell Biol Toxicol. 2004 Nov;20(6):325-32.

- Miadoková, E., **Svidová, S.**, Vlčková, V., Kogan, G., Rauko, P.
  The role of microbial polysaccharides in cancer prevention and therapy.
  J. Canc. Integrat. Med. (2004). 2: 173-178.

- Vlčková, V., Dúhová, V., **Svidová, S.**, Farkašová, A., Kamasová, S., Vlček, D., Kogan, G., Rauko, P., Miadoková, E.
  Antigenotoxic potential of glucomannan on four model test systems.
  Cell Biol.Toxicol. (2004) 20: 325-332

- Miadoková, E., **Svidová, S**., Šubjaková, I., Kogan, G.
  Detection of antimutagenic potential of glucomannan in unicellular green algae and bacteria.
  Biologia (2003). 58: 627-631

Posters

- Miadoková, E., **Svidová, S.**, Šubjaková, I., Vlček, D.
  Detection of antimutagenic potential of glucomannan in unicellular green alga and bacteria.
  Biology and taxonomy of green algae IV, International symposium, Smolenice, Slovac republic. 24.-28. 6. 2002

- Miadoková, E., **Svidová, S.**, Šubjaková, Dúhová, V., Kamasová, S., Liszeková, D., Kogan, G., Rauko, P.
  Potential bioprotective effect of fungal polysaccharides against genotoxic agents.
  23rd International symposium „*Industrial toxicology 2003*“, Faculty of Chemical and Food Technology, Slovak University of Technology, Bratislava, Slovak Republic. 06. 2003

- Miadoková, E., **Svidová, S.**, Vlčková, V., Moráňová, Z., Dúhová, V., Vráblová, I., Nováková, J., Kogan, G., Rauko, P.
  Utilization of biologically active compounds in genetic toxicology.
  Autumn Workdays of the Czech and Slovak Association of Environmental Mutagenicity: Genetic toxicology and cancer prevention, Cancer Research Institute, Slovak Academy of Science, Bratislava, Slovak Republic. 18. 10. 2004

- Miadoková, E., **Svidová, S.**, Vlčková, V., Moráňová, Z., Dúhová, V., Vráblová, I., Nováková, J., Kogan, G., Rauko, P.
  Detection of antimutagenic potential of glucans in unicellular green alga and bacteria.
  Central & Eastern European Environmental Health Conference, Prague, Czech Republic. 24.- 26. 10. 2004

Talks

- **Has glucomannan bioprotective effect?**
  Autumn Workdays of the Czech and Slovak Association of Environmental Mutagenicity: Genetic toxicology and cancer prevention. Cancer Research Institute, Slovak Academy of Science, Bratislava, Slovak Republic**.** 21.-23. 10. 2002

- **Evaluation of the effect of glucomannan.**
  Environmental Changes and their Bioindication, Department of Biology and Ecology, Faculty of Natural Sciences in Ostrava, Bartošovice, Czech Republic. 16.-17. 10. 2003

- **Potential bioprotective effect of fungal polysaccharides.**
  24th International symposium „*Industrial toxicology 2004*“,Faculty of Chemical and Food Technology, Slovak University of Technology, Spišská Nová Ves, Slovak Republic. 02.-04. 06. 2004

Appendix

Reviewers' comments

Manuscript No.: BBAMEM-11-130

Title: **Effect of mutations in the conserved GMN motif on ion transport and selectivity in the yeast magnesium transporter Mrs2p**

Article Type: Regular Paper

BBA Section: BBA - Biomembranes

Corresponding Author: Dr. Kristina Djinovic-Carugo

All Authors: Sona Svidová; Gerhard Sponder; Muhammad Bashir Khan; Rudolf J Schweyen; Oliviero Carugo; Kristina Djinovic-Carugo

Submit Date: Apr 17, 2011

Reviewer #1: Dr. Djinovic´-Carugo and her research team submitted a manuscript presenting follow-up research of the work on Mrs2p, the mitochondrial Mg^{2+}-conducting channel, which has been previously well characterized by Dr. Rudolf J. Schweyen (deceased) and his team and for which his laboratory is highly reputable in the field of molecular transport physiology of magnesium. The F/Y-GMN motif, known to be well conserved across the whole CorA-Alr1-Mrs2 family of Mg^{2+} transporters, has been identified as to be crucial for Mg^{2+} binding and its conductance by channels in this family. Early work of Dr. Gregan demonstrated, that exchange of a single aa of this motif is sufficient to suspend the Mrs2p-mediated Mg^{2+} transport/conductance.

Assumption that a single aa substitution in this motif leads to inevitable block of Mrs2p transport function has been undertaken rather dogmatic and definite. As work of researchers around Dr. Djinovic´-Carugo shows now, certain combinations of aa substitutions in GMN motif do not lead to the expected functional block but only to "mild" attenuation of efficacy of the Mg^{2+} transport conducted by Mrs2p (most frequently a positively charged residue in the first and a hydrophobic residue in the third position). Therefore, mutational vulnerability of F/Y-GMN in relation to the process of Mg^{2+} binding and Mg^{2+} via Mrs2p (and other channels from CorA-Alr1-Mrs2p family) will have to be reconsidered. From the larger point of view, this finding may have rather fundamental impact on our thinking about evolution and

evolutionary conservation of magnesium (or any other cation) binding motifs among various Mg^{2+} transporters in general.

Their study further suggests that the GMN motif plays a crucial role in ion selectivity (binding and also process of ion stripping) demonstrated by negative impact of both, manganese and zinc (but not of Co^{2+} and Ca^{2+}) on growth of the cells carrying mutated GMN motif (as described) in complementation assays. Authors speculate two possibilities: (1) that both Mn^{2+} and Zn^{2+} cross the channel due to mutations introduced to Mrs2p GMN motif, therefore, growth-retarding phenotype results from the intracellular intoxication by these metal ions; and (2) that both ions simply block the entrance of the pore, stopping the flux of Mg^{2+}. Authors conclude, that both explanations are rather equally coherent with the experimental observation that increasing cation concentrations correlate with negative effects on cell growth. Here I must slightly disagree in regard of equal feasibility of both explanations. I would recommend considering stereochemistry/coordination of solvated/hydrated Mg^{2+}, Mn^{2+} and Zn^{2+} in discussion, before drawing any conclusion on action of Mn^{2+} and/or Zn^{2+} on Mrs2p functionality.

Taken together the findings presented in this paper, were acquired with appropriate techniques and are presented clearly in concise English. I believe, that this manuscript will be a valuable information resource for the broad spectrum of BBAMEM readers, and that it would also promote further research of Mrs2p and of Mg^{2+} transport in general.

Reviewer #2: The paper selects random mutants in the GMN motif of MRS2 that are still able to transport magnesium at some level. The results show that a diverse range of mutants allow growth of E. coli, and that five such mutants function to transport magnesium into mitochondria. They also present evidence of changes to growth on Zn and Mn of E. coli cells expressing the mutants.

I am not convinced that the data presented are sufficient as they stand for publication. I accept that the demonstration that there alternative motifs that allow some Mg uptake is of interest and publishable, given that even conservative single amino acid changes to GMN block uptake completely. However, I think that some quantification of the rates of uptake of some of these mutants is needed before this can be published, and that this quantification should include a direct comparison of these new mutants with an inactive point mutation. The evidence for altered cation response is also not convincing (see below).

The major shortcoming of the work is the lack of quantification of the rates of transport of the mutants. It is simply not possible to conclude anything about rates of uptake from the data presented, other than that there is some.

In addition, there is the lack of appropriate negative controls in the data presented. A negative control must be included in the data in Table 1, for comparison purposes. Ideally this would be a completely inactive mutant, such as AMN, to allow assessment of the effect of expressing the protein on the *E. coli* cell, and possible interference with other transporters or ion metabolism. However, even an empty vector would help readers assess the data. Expression of an inactive mutant would also be a much more preferable negative control in the Mg uptake measurements, in case expression of the MRS2 protein itself causes some change in the phenotype.

Finally, the Mn and Zn growth data are extremely difficult to interpret, because they are so indirect. The authors present two interpretations, either direct transport of these ions or blockage of Mg uptake, which they are unable to distinguish. In fact there is a third explanation, that the reduced uptake of Mg by the mutants, in and of itself changes sensitivity of the cells to Mn and Zn, and that there is no direct effect of either ion on the MRS2 transporter. It is known that cation sensitivity of cells varies with the cellular availability of Mg and K, in particular. As they stand, the data provide a simple observation of altered tolerance. I do not believe that any conclusion should be made from these data about either MRS2 selectivity or changes in Mg uptake rates, without direct evidence of an effect on the protein.

In the written ms, the authors further over-interpret these Zn and Mn data by concluding that the "ion selectivity" of the protein is changed (abstract), despite the fact that the second of their two options given in the body of the text does not necessarily imply any change in selectivity. Mention is also made in the abstract of "the flanking negatively charged loop", but no data is presented on this at all, as far as I can see.

In note that the genetic screen used should not be referred to as an "unbiased" one, because it selects for mutants with residual Mg activity. (It may be unbiased with respect to amino acid changes across the tri-peptide, but it is not completely unbiased).

Reviewer #3: In this paper Svidova S and coworkers investigated the impact of conserved G-M-N motif on the selectivity of mrs2p mitochondrial magnesium transporter in S. thyphimurium MM281 by transfecting random mutated mrs2 of *S. cerevisiae*. The Authors show that the G-M-N motif can be partially replaced by certain combinations of amino acids

and demonstrate that this conserved motif plays a role in flanking negatively charged loop at the entrance of the channel that serves not only to bind and de-hidrate Mg but also serves as ion selectivity filter for other similar divalent cations. This paper is well done and very clearly presented.

Minor comments:

Does Nature (...not meaning the journal) need a capital letter? Par 3.3, lines 368-371 and corresponding comments on par. 4, lines 444.448: The competitivity among Mg and Mn for channel uptake could be investigated by measuring the relative levels of the two cations with AA or ICP-MS. There would be a good possibility that Mn would be taken up and compete with Mg for its binding sites rather than block the channel.